Cyclin F: Roles in Genome Stability and Oncogenic Pathways

Shahd Fouad

St Catherine's College



Supervisors: Associate Professor Vincenzo D'Angiolella (Primary)

Professor Francesca Buffa (Secondary)

A thesis submitted to the University of Oxford for the degree of Doctor of Philosophy

Trinity Term 2022

MRC Oxford Institute for Radiation Oncology
Department of Oncology
University of Oxford







Table of Contents

Acknowledgements ..... **Error! Bookmark not defined.**

Declaration ..... **Error! Bookmark not defined.**

Abstract 8

List of Figures 9

List of Abbreviations 11

1. Introduction 14

I. Ubiquitylation 14

a. The Ubiquitylation Process 14

b. E1 Ubiquitin-Activating Enzymes 16

c. E2 Ubiquitin-Conjugating Enzymes 17

d. E3 Ubiquitin Ligases 19

i. E3 Families: RING and U-Box, HECT, RBR and RCRs 19

ii. CRLs 21

iii. F-box Domain 24

iv. NEDD8-Mediated Cullin Regulation 27

v. SCF Substrate-Recognition Mechanisms 28

vi. Cyclin F 34

vii. EXO1 and DNA Repair 40

II. Ubiquitylation: in Sickness and in Health 41

a. The Ubiquitin Code: Cellular Roles 41

b. Ubiquitylation in Cancer 43

i. CRL1 Complexes 43

ii. Other CRL Complexes 47

c. The UPS and RAS Dysregulation in Cancer 49

i. RAS and Tumorigenesis 49

RAS Ubiquitylation 51

ii. 51

iii. Targeting RAS for Therapy 53

d. UPS-based Therapies: PROTACs 55

Project Aims 58

2. Materials and Methods 60

I. Materials 60

I.1 General laboratory buffers 60

I.2 General laboratory and cull culture reagents 61

II.2.a Table: General laboratory reagents 61

II.2.b Table: Cell culture reagents 62
I.3 Antibodies 63
I.4 Antibiotics 64
I.5 Kinase inhibitors 64
I.6 STING inhibitor 65
I.7 EGFR inhibitors 65
I.8 Primers 65
I.9 Software 66
II. Methods 67
II.1 Cell Culture 67
II.1.a Cell line maintenance 67
II.1.b Cryopreservation of cell lines 68
II.1.c Transient plasmid transfection 68
II.1.c.i Plasmids 69
II.1.d Transient siRNA transfection 69
II.1.d.i Table: siRNA list 70
II.1.e CRISPR-Cas9 generated stable cell lines 70
II.2.a Cell lysis and protein sample preparation 71
II.2.b Co-immunoprecipitation 72
II.2.c GTP-RAS activity assay 72
II.2.d *In vivo* ubiquitylation assay 72
II.2.e Protein half-life (Cycloheximide) assay 73
II.2.f Cell cycle profile 73
II.2.g *In vitro* phosphorylation assay 74
II.2.g.i *Full length proteins* 74
II.2.g.ii *Biotinylated peptides* 74
II.2.h SDS-PAGE and Western blotting 75
II.2.i Protein purification using ÄKTA start 76
II.3 Molecular and cellular biology techniques 77
II.3.a Preparation of media and agar plates 77
II.3.b Transformation of bacteria 77
II.3.c Agarose gel electrophoresis 78
II.3.d Small- and large-scale preparation of plasmid DNA 78
II.3.e Site-directed mutagenesis 79
II.3.f Determination of DNA purity and concentration 80
II.3.g DNA fiber combing assay 80

II.3.h Resazurin cell viability assay 81
II.3.i Exposure to γ-irradiation 82
II.3.j Clonogenic survival assay 82
II.4 Liquid chromatography-tandem mass spectrometry 83
II.5 UbiFast 84
II.6 Statistical analysis 85
3. Results Chapter I: *CCNF-EXO1* Axis Governs Cell Survival Post IR 86
a. Cyclin F Regulation of EXO1 is Crucial for Post-IR DNA Repair 86
b. Mechanism of EXO1 Recognition by Cyclin F 94
c. Refinement of Cyclin F Degron 114
4. Results Chapter II: The KRAS-Cyclin F Regulatory Network 121
a. Investigating Cyclin F Regulation by KRAS 121
i. KRAS Promotes the Degradation of Cyclin F Substrates RRM2 and E2F1 121
b. Investigating KRAS regulation by Cyclin F 124
i. Cyclin F Loss Decreases RAS Activity in KRAS Mutant Cells 124
ii. Decreased RAS Activity is Reflected in Decreased Resistance of KRAS Mutant Cells to EGFRi 125
a. Optimising Mass Spectrometry Data Acquisition Method for Deep Proteomic Study in LIM1215 Cells: DDA, DIA and TMT 128
5. Results Chapter III: Exploring Proteome Changes Induced by Cyclin F's E3 Ligase Activity and the KRAS-Cyclin F Regulatory Network 147
a. Cyclin F Potential Neo-substrates Identification (Mut and Ctrl ±*CCNF*) 151
b. KRAS-Dependent Proteome Alterations (Mut vs Ctrl) 158
c. Combined KRAS and Cyclin F-Dependent Proteome Alterations (*CCNF* K/O ±*KRAS* mutation) 161
.....Results Chapter IV: Role of the Cyclin F-KRAS Regulatory Network in the RTKi Response 166
6. 166
a. Interferon Pathway and the RTKi Response 166
b. MAP2K6, p38 MAPK and the RTKi Response 168
7. Discussion and Future Work 172
I. Overview 172
II. Cyclin F as a novel target in multiple malignancies 173
III. Cyclin F recognises a novel degron not shared with other cyclins . 178
IV. KRAS-Cyclin F regulatory loop 184
V. Mechanisms of proteome variation dependent on the KRAS-Cyclin F axis 186

8. Supplementary Figures 191
9. References 197

Acknowledgements

I dedicate this thesis to my parents and my friends who I count as family back home. Your unwavering support is worth much more than I can express in writing.

This D.Phil project would not have been possible without the help of some – it truly does take a village, so I would like to take this opportunity to thank them.

Vincenzo, from being my academic advisor, to my career coach, to my in-lab supervisor and even my lab-bench neighbour at times – you have genuinely offered me support in more ways than I can ever fully thank you for. Most importantly, thank you for your trust. You have welcomed me into your lab when I had no formal biology training – let alone molecular biology! The steep learning curve has made this simultaneously my most challenging and most rewarding experience, and having your guidance and reassurance every step of the way is something I am eternally grateful for.

Hongbin, I count myself exceptionally lucky to have had you as my lab mentor the whole time I was here – I honestly would not have had it any other way. Your infinite scientific knowledge, of which the entire department speaks, as well as your patience and kindness made you come to my rescue far more times than I can count. For everything, thank you.

Rafa, thank you for keeping me company during late lab nights when we were both stuck in there because of our poor tissue-culture time-planning. Also thank you for helping me work on my language skills by teaching me vocabulary, in two new languages not one, that I absolutely *cannot* use publicly.

Paul, thank you for the constant insightful input for my project over Friday's fish and chips. Irene, Miriam, Katherine, Beatrice and Sara, thank you for making the lab the colourful space it is today.

In addition to my own lab members, thank you to Susan, Kay, YC, Tiffany, Pauline, Ashwin and Letitia for making those past 4 years in Oxford the most memorable.

My S.H. crew, thank you for giving me a community I have truly longed for. It only took me 4 years to find you, so good luck getting rid of me now.

Nounie, thank you for saving me from my self-inflicted thesis colour co-ordination demise. You made, and continue to make, everything pretty.

Stine, four years ago in my M.Phil acknowledgements I thanked you for making a strange little English city feel like home. Today I thank you for the same, only tenfold.

Leo, thank you for all the support, especially keeping me well-fed when I was in survival mode this last stretch of thesis writing.

I also want to thank my collaborators from the Kessler group at the Target Discovery Institute for the highest quality mass spectrometry data collection and analysis, especially the brilliant Iolanda Vendrell.

Lastly, I gratefully acknowledge the funding received towards this D.Phil from the Oxford Institute for Radiation Oncology, Al Alfi Foundation and St. Catherine's college.

Declaration

I declare that the work presented in this thesis is my own except where explicitly stated otherwise, and that this work has not been submitted for any other degree at this or any other university.

Abstract

F-box proteins are a family of substrate recruitment factors that assemble into multi-subunit complexes known as SCFs to ubiquitylate their substrates and thereby alter their fate, ex. by directing them to the proteasome for degradation. Cyclin F is the founding member of this family, and it has been identified by our lab to be protecting cells against ionising radiation (IR). This discovery is the result of a CRISPR screen focused on the ubiquitin system in cells treated with IR. Data from my affinity purification and mass spectrometry studies revealed that EXO1 is the Cyclin F substrate responsible for this phenotype. EXO1 is an exonuclease whose upregulation has been shown to drive DNA hyper-resection which impedes DNA repair. I report that $SCF^{Cyclin\ F}$ targets EXO1 for proteasomal degradation in the G_2/M phases of the cell cycle and upon challenging the cells with IR, and that this is dependent on a phosphorylation event by the kinase CDK2. Using cell survival assays I prove that IR-sensitivity in cells lacking Cyclin F can be fully rescued by EXO1 depletion, underlining the IR-sensitising effects of EXO1 accumulation.

I also demonstrate that Cyclin F is involved in a regulatory loop with the most frequently mutated oncoprotein, RAS. Using affinity purification to pull-down active RAS, I show that Cyclin F loss contributes to suppressing RAS activity. This effect is reflected in the cellular response to RTK inhibitor therapy, whereby the signature RTK inhibitor resistance of RAS mutant cells is attenuated in Cyclin F depleted settings. Results from a deep proteomic study of the Cyclin F-KRAS axis present valuable insights into the implicated pathways and demonstrate clinically-exploitable weaknesses of this axis.

Together, results from both projects highlight novel roles for Cyclin F in genome stability maintenance and oncogenic pathways.

List of Figures

Introduction

Figure 1i. The ubiquitin code **16**
Figure 1ii. Cullin Ring Ubiquitin Ligases **23**
Figure 1iii. F-box protein sub-families **26**
Figure 1iv. NEDD8, CSN and CAND1-mediated cullin regulation **27**
Figure 1v. SCF substrate-recognition mechanisms **30**
Figure 1vi. Cyclin F is a unique cyclin **35**
Figure 1vii. Cyclin F-E2F1 axis in DNA replication stress **37**
Figure 1viii. Mechanisms of DNA DSB repair **39**
Table 1. F-box proteins in cancer **45**
Figure 1ix. RAS signalling cascade **52**

Results Chapter I: CCNF-EXO1 Axis Governs Cell Survival Post IR

Figure 3i. *CCNF* loss sensitises cells to IR and EXO1 is identified as the top interactor under these conditions **90**
Figure 3ii. EXO1 is targeted for ubiquitylation by Cyclin F in unperturbed cells and is even more strongly targeted after IR **94**
Figure 3iii. Cyclin F binds to EXO1 through its RAI 842-844 degron site following priming phosphorylation on T824A **97**
Figure 3iv. R842I EXO1 mutation in GBM completely prevents EXO1 binding to Cyclin F **100**
Figure 3v. Cyclin F binds to EXO1's through its RxI 842-844 degron site, and phosphorylation hinders the Cyclin F binding to short EXO1 peptides **102**
Figure 3vi. Proposed Cyclin F-EXO1's binding mechanism primed by the T824 phosphorylation on EXO1 **104**
Figure 3vii. CDK2 is the kinase responsible for the priming phosphorylation on T824 of EXO1 *in vivo* **108**
Figure 3viii. Cyclin A/E-CDK2 is the kinase responsible for the priming phosphorylation on T824 of EXO1 *in vitro* **111**
Figure 3ix. PIN1 is not a co-factor of Cyclin F for EXO1 binding **114**
Figure 3x. Degron refinement of Cyclin F substrates EXO1 and RRM2 to be RxIF and not RxI only **116**
Figure 3xi. Cyclin F degron refinement search by cross-checking previous mass spectrometry experiments with *Scansite 4.0* sequence match results **119**

Results Chapter II: The KRAS-Cyclin F Regulatory Network

Figure 4i. KRAS and Cyclin F are in a reciprocal regulation loop **123**
Figure 4ii. Cyclin F loss reduces the resistance of *KRAS* mutant cells to EGFRi treatment **128**
Figure 4iii. Planned proteome analysis of the 4 LIM1215 cell lines **129**
Figure 4iv. Cyclin F loss results in multiple forms of DNA replication stress **131**
Figure 4v. Data acquisition methods tested: DDA LFQ, TMT and DIA **133**
Figure 4vi. Density scatter plots representing total proteome data quality check: DDA vs DIA vs TMT **137**
Figure 4vii. Density scatter plots representing diGly data quality check: DDA vs DIA **139**
Figure 4viii. Missing values comparison: DDA vs DIA vs TMT **140**
Figure 4ix. Hit overlap and cost breakdown for DDA, DIA and TMT **142**
Figure 4x. Initial short-listing of Cyclin F neo-substrates from DIA and TMT total proteome data **144**

Results Chapter III: Exploring Proteome Changes Induced by Cyclin F's E3 Ligase Activity and the KRAS-Cyclin F Regulatory Network
Figure 5i. Principal component analysis (PCA) plot for the 4 LIM1215 samples ran in triplicates **149**
Figure 5ii. Hierarchical clustering of total proteome data filtered by Anova q-value (5% FDR) with Z-score presented as intensity **151**
Figure 5iii. Volcano plots of comparative samples and western blot validation **153**
Figure 5iv. Volcano plots highlighting interferon response proteins (blue) in comparative samples **154**
Figure 5v. Illustration of the observed activation of the interferon response pathway **155**
Figure 5v. Refined list of likely Cyclin F substrates from total proteome data **157**
Figure 5vi. Enrichr-identified significant pathway alterations of proteins enriched in Mut *CCNF* K/O vs Mut **159**
Figure 5vii. Volcano plots highlighting KRAS-dependent proteome differences in Ctrl vs Mut samples **161**
Figure 5viii. Enrichr-identified significant pathway alterations of proteins enriched in both: *CCNF* K/O vs Ctrl, and Mut vs Mut *CCNF* K/O **164**
Figure 5ix. Protein levels of members of the signalling pathways altered the most between *CCNF* K/O and Mut *CCNF* K/O samples **165**

Results Chapter IV: Role of the Cyclin F-KRAS Regulatory Network in the RTKi Response
Figure 6i. Effect of STING inhibition on the EGFRi response of LIM1215 cell **169**
Figure 6ii. Effect of p38 MAPK inhibition on the EGFRi response of LIM1215 cells **171**
Figure 6iii. Effect of MAP2K6 overexpression on the EGFRi response of LIM1215 cells **172**

Supplementary Figures
Supplementary Figure 1. *CCNF* loss sensitises cells to IR due to EXO1 accumulation which is rescued by si*EXO1* depletion **193**
Supplementary Figure 2. Cyclin F targets EXO1 for ubiquitylation in G_2/M **194**
Supplementary Figure 3. Specificity testing of EXO1 pT824 primary antibody **195**
Supplementary Figure 4. Cell cycle profile of LIM1215 cells. **196**
Supplementary Figure 5. Missing values across samples, N = 3 **197**
Supplementary Figure 6. Enrichr-identified significant pathway alterations of proteins enriched in *CCNF* K/O vs Ctrl **198**

List of Abbreviations

aa	Amino acid
Alt-EJ	Alternative end joining
AMPK	AMP-Activated Protein Kinase
APC/C	Anaphase Promoting Complex/Cyclosome
BORA	Protein Aurora Borealis
BRAT1	BRCA1 Associated ATM Activator 1
BTB	Broad complex, Tramtrack and Bric-à-Brac
BTN	Biotin(-ylated)
CAND1	Cullin-Associated and NEDDylation-Dissociated 1
CCNF	Cyclin F
CCP110	Centriolar Coiled-Coil Protein 110
CDC6	Cell Division Cycle 6
CDKs	Cyclin-dependent kinases
CDT1/2	Chromatin Licensing and DNA Replication Factor 1/2
CHK1	Checkpoint Kinase 1
CHX	Cycloheximide
CK1α	Casein Kinase Iα
CKII	Casein kinase II
CKS1	CDK Subunit 1
CldU	5-chloro-2′-deoxyuridine
CNS	Central nervous system
CoREST	Corepressor of RE1 Silencing Transcription Factor
CPT	Camptothecin
CRBN	Cereblon
CRC	Colorectal cancer
CRL	Cullin-Ring Ubiquitin Ligase
CRY	Cryptochrome Circadian Regulator
CSN	COP9 Signalosome
Ctrl	Control
DCAF	DDB1 and CUL4 Associated Factor
DDA	Data-dependent acquisition
DDB1	DNA Damage-Binding Protein 1
DDR	DNA-damage response
dHJ	double Holliday junction
DIA	Data-independent acquisition
DNA PK	DNA-Dependent Protein Kinase
DSBs	Double strand breaks
DT block	Double-thymidine block
DUB	De-ubiquitylating enzyme
E1	E1 ubiquitin-activating enzyme
E2	E2 ubiquitin-conjugating enzyme
E3	E3 ubiquitin ligase
EGFR	Epidermal Growth Factor Receptor
EGFRi	Epidermal Growth Factor Receptor inhibitor
EMT	Epithelial-mesenchymal transition
EST	Expressed sequence tag
EV	Empty vector
EXO1	Exonuclease 1
FACS	Fluorescence-Activated Cell Sorting
FAD	Flavin adenine dinucleotide
FAT1	FAT Tumour Suppressor Atypical Cadherin 1
FBA domain	F-box associated domain
FDR	False-discovery rate
FOXO1	Forkhead Box O1
GAP	GTPase Activating Protein

GBM	Glioblastoma multiforme
GEF	Guanine Nucleotide Exchange Factor
GG	Gly-Gly
GIN	Genomic instability
GSK3	Glycogen Synthase Kinase 3
HCD site	Higher-energy collision dissociation site
H.E	Higher exposure
HECT	Homologous to the E6AP Carboxyl Terminus
HELLS/LSH	Lymphoid-Specific Helicase
HIF-1	Hypoxia-Inducible Factor 1
HLTF	Helicase Like Transcription Factor
HR	Homologous recombination
HU	Hydroxyurea
IdU	5-iodo-2′-deoxyuridine
IMiDs	Immunomodulatory drugs
iBAQ	Intensity Based Absolute Quantification
IP	Immunoprecipitation
IR	Ionising radiation
JAK-STAT	Janus Kinase – Signal Transducer and Activator of Transcription
K/O	Knock-out
KBTBD4	Kelch Repeat and BTB Domain-Containing Protein 4
KEAP1	Kelch Like ECH Associated Protein 1
LAS1L	LAS1 Like Ribosome Biogenesis Factor
LB broth	Luria-Bertani broth
LC/MS	Liquid chromatography – mass spectrometry
LFQ	Label-free quantification
LRR	Leucine-rich repeats
LZTR1	Leucine Zipper Like Transcription Regulator 1
m/z	Mass-to-charge ratio
MAP2K6	Mitogen-Activated Protein Kinase Kinase 6
MAPK	Mitogen-Activated Protein Kinase
mAU	Milli absorbance units
MCL1	Myeloid Cell Leukaemia 1
MDC1	Mediator of DNA Damage Checkpoint 1
MGMT	O^6-methyl-guanine-DNA methyltransferase
mTOR	Mechanistic Target of Rapamycin Kinase
Mut	Mutant
MYCBP2	MYC Binding Protein 2
NEDD8	Neural Precursor Cell Expressed Developmentally Down-regulated Protein 8
NEK9	NIMA Related Kinase 9
NF-κB	Nuclear Factor-Kappa B
NHEJ	Non-homologous end joining
NLS	Nuclear localisation signal
NRF2	Nf-E2-Related Factor 2
NSCLC	Non-small cell lung cancer
NUSAP1	Nucleolar and Spindle Associated Protein 1
O/N	Overnight
ODD domain	Oxygen-dependent degradation domain
ORC2	Origin Recognition Complex Subunit 2
PBS	Phosphate-buffered saline
PCA	Principal component analysis
PCNA	Proliferating Cell Nuclear Antigen
PEI	Polyethylenimine
PIN motif	PAR interaction motif
PIN1	Peptidylprolyl Cis/Trans Isomerase, NIMA-Interacting 1
PIP box	PCNA-interacting protein box

PIP2	Phosphatidylinositol-4,5-biphosphate
PIP3	Phosphatidylinositol-3,4,5-triphosphate
PLK1	Polo Like Kinase 1
PRC1	Protein Regulator of Cytokinesis 1
PROTACs	Proteolysis Targeting Chimeras
PTEN	Phosphatase and Tensin Homolog
RB	Retinoblastoma
RBL2	Retinoblastoma-Like Protein 2
RBR	RING–in-between–RING
RBX1/2	RING-Box protein 1/2
RCR	RING-cys-Relay
RING	Really Interesting New Gene
RMI1	RecQ Mediated Genome Instability 1
RNR	Ribonucleotide Reductase
ROS	Reactive oxygen species
RRM2	Ribonucleotide Reductase Subunit M2
RTK	Receptor tyrosine Kinase
RTKi	Receptor tyrosine Kinase inhibitor
SCF	SKP1–CUL1–F-box
SDM	Site-directed mutagenesis
SDS-PAGE	Sodium dodecyl-sulfate (SDS)-Polyacrylamide Gel Electrophoresis
SHH	Sonic Hedgehog
ssDNA	Single-stranded DNA
siRNA	Small interfering RNA
SKP1	S-phase Kinase Associated Protein 1
SLBP	Stem-Loop Binding Protein
SLC7A5/SLC38A2/SLC1A5	Solute Carrier Family 7 Member 5/ Family 38 Member 2/ Family 1 Member 5
SOCS	Suppressor of Cytokine Signalling
SOS	Son of Sevenless
SPINT2	Serine Peptidase Inhibitor, Kunitz Type 2
ST14	Suppressor of Tumorigenicity 14
STAT1	Signal Transducer and Activator of Transcription 1
STING	Stimulator of Interferon Response CGAMP Interactor
STT3A/ITM1	STT3 Oligosaccharyltransferase Complex Catalytic Subunit A/ Integral Transmembrane Protein 1
TAF7/TAFII55	TATA-Box Binding Protein Associated Factor 7/ Transcription Initiation Factor TFIID 55 KDa Subunit
TCGA	The Cancer Genome Atlas
TFA	Trifluoroacetic acid
TMEJ	Theta-mediated end joining
TMT	Tandem mass tag
TMZ	Temozolomide
TOP2A	DNA Topoisomerase II Alpha
TP53	Tumour Protein P53
U2AF1	U2 Small Nuclear RNA Auxiliary Factor 1
Ub	Ubiquitin
UBC	Ubiquitin-conjugating domain
UBD	Ubiquitin-binding domain
UPS	Ubiquitin-proteasome system
VHL	von Hippel-Lindau
WNT	Wingless/Integrated
WT	Wild type
ZMAT3	Zinc Finger Matrin-Type 3
β-TrCP	Beta-Transducin Repeat Containing Protein
λPP	Lambda Protein Phosphatase

1. Introduction

I. Ubiquitylation

a. The Ubiquitylation Process

The ubiquitin-proteasome system (UPS) is the major proteolytic system in eukaryotes and, as such, maintains protein homeostasis (Rock et al., 1994). Ubiquitylation is a versatile post-translational modification that plays critical roles in various cellular processes. Ubiquitin (Ub), a 76-residue protein highly conserved among all eukaryotes, is covalently conjugated to the lysine (K) residues of substrate proteins through an enzyme cascade involving a ubiquitin-activating enzyme (E1), a ubiquitin-conjugating enzyme (E2), and a ubiquitin ligase (E3) (Figure 1i). Substrates can be mono- or poly-ubiquitylated, where the latter involves different ubiquitin chain topologies that are determined by the combinatorial specificity of E2s and E3s (Ye and Rape, 2009).

This large repertoire of ubiquitin chain types along with the various possible combinations of its components, from substrates to E2s to E3s, is the core of the high diversity of the ubiquitin system. The fact that ubiquitylation is a modification that can be removed by highly specific de-ubiquitylating enzymes (DUBs) adds a further layer of regulation to this system (Reyes-Turcu et al., 2009). The different ubiquitin chains signal for a variety of fates for modified substrates, and such fates include proteolysis, trafficking, and changes in localisation or activity (Figure 1i) (Komander and Rape, 2012, Yau and Rape, 2016). Proteins with ubiquitin-binding domains (UBDs) are capable of receiving and transducing these transmitted signals in order to mediate the intended output. Such proteins are known as ubiquitin code readers, and they can carry out their

function owing to their specialised capacity to differentiate between the chains. This differentiation is carried out based on multiple distinguishing factors between ubiquitin chains – one of which is ubiquitin spacing

Enzymes encoded by the human genome that are responsible for the ubiquitylation process include 2 E1s, ~40 E2s, more than 700 E3s, and almost 100 DUBs (Stewart et al., 2016, Zheng and Shabek, 2017). An E1 hydrolyses ATP to activate the C-terminal glycine of a ubiquitin molecule through an adenylation reaction resulting in a ubiquitin-AMP intermediate, after which the E1's active-site cysteine attacks the activated C-terminus of ubiquitin forming a thioester bond. The E1-bound (active) ubiquitin is then passed onto the E2 following a trans-thiolation reaction where a thioester is formed between the C-terminal glycine residue of ubiquitin and the E2 cysteine active site, and subsequently deposited onto the substrate by forming an isopeptide bond between the carboxyl group on its C-terminal glycine and the ε-amino group of a lysine residue on the substrate in a process mediated by E3 ligases.

The E3s dictate substrate specificity – they simultaneously interact with an E2~Ub conjugate and a specific substrate, thereby enhancing the proximity between both parties and mediating the ubiquitin transfer. DUBs can either remove a ubiquitin molecule directly from the substrate (ubiquitin-substrate bond cleavage) or from a poly-ubiquitin chain (ubiquitin-ubiquitin bond cleavage), and play major parts in critical cellular functions owing to their roles in switching off ubiquitin-mediated signalling and in ubiquitin recycling (Nicassio et al., 2007, Yao and Cohen, 2002, Clague et al., 2013). It is worth noting that the E1, E2, E3 and DUB enzymes collectively make up close to 1.3% of the total number of proteins within our cells (Kulak et al., 2014).

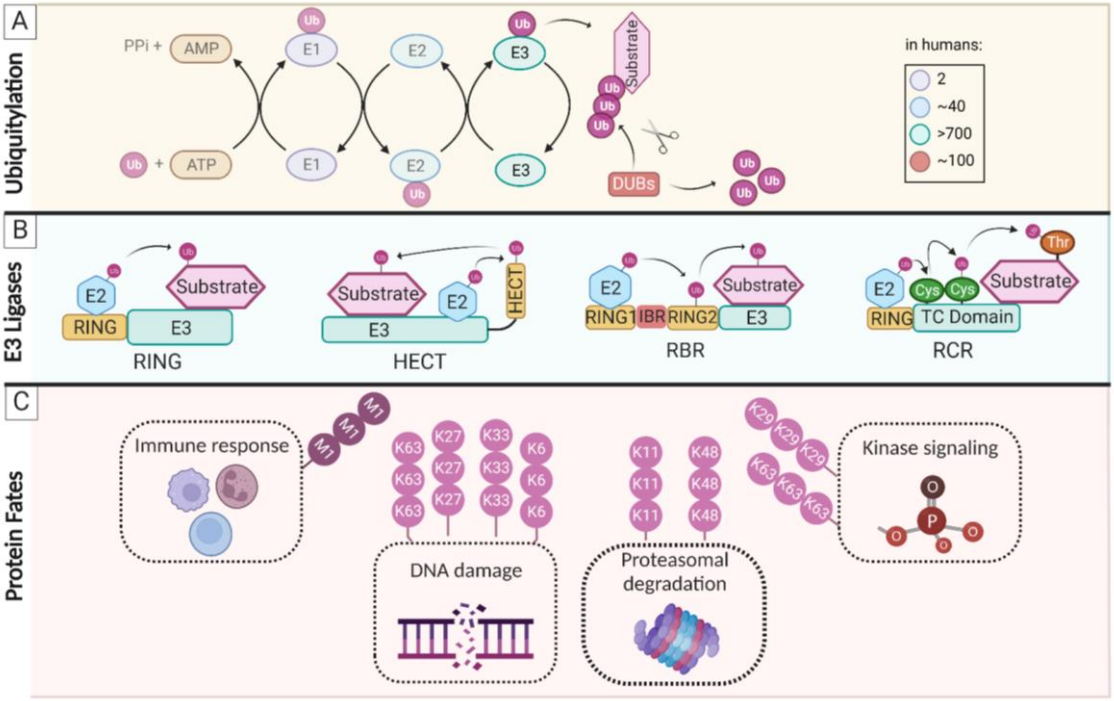


Figure 1i. The ubiquitin code.

a. The ubiquitylation process involving E1, E2, E3 and DUB enzymes.
b. Families of E3 ligases: RING (and U-Box), HECT, RBR and RCRs
c. Ubiquitin chain topology-dependent protein fates.

b. E1 Ubiquitin-Activating Enzymes

The two E1 enzymes encoded in the human genome are *UBA1* and *UBA6*, and they share only 40% sequence homology (Jin et al., 2007). Despite there being only two of such ubiquitin-activating enzymes in humans, they are present at substantially high concentrations within cells (Clague et al., 2015). Given that the two E1s are distantly related (< 50% identical), they behave differently on certain levels. In an assay that measures the degree of ubiquitin-loading on different E2s, it was shown that all UBA1 molecules in proliferating HEK293T cells are charged with ubiquitin whereas only half of the UBA6 population is Ub-loaded (Jin et al., 2007). One plausible reason for this is that UBA1 is specifically a ubiquitin-activating enzyme, while UBA6 activates both ubiquitin and FAT10 –

a ubiquitin-like modifier strongly associated with the immune system and inflammatory pathways (Chiu et al., 2007, Liu et al., 1999, Lukasiak et al., 2008). The two E1 enzymes also appear to have different affinities for the various E2 enzymes (Jin et al., 2007).

c. E2 Ubiquitin-Conjugating Enzymes

There are ~40 E2 enzymes encoded by the human genome, and virtually all of them are conjugated to ubiquitin at any given moment (Jin et al., 2007). This is because E2s that have not yet bound a ubiquitin molecule (unloaded E2s) have a very high affinity for ubiquitin-conjugated E1s, which is even higher than their affinity for E3s. This lower affinity enables the dissociation of the E2 from the E3 following ubiquitin transfer, which then allows the E2 to become re-loaded by Ub-charged E1s and simultaneously allows E3s to bind other E2s that are Ub-conjugated (Gundogdu and Walden, 2019). One example of such different affinities between E2~Ub conjugates and isolated E2s to E3 ligase complexes is demonstrated by the E2 enzyme CDC34/UBCH3; RBX1 – the protein bridging cullin scaffolds to E2s in CRL complexes – shows 50-fold higher affinity to UBCH3~Ub than to UBCH3 alone (Spratt et al., 2012).

Although there exists a pyramid structure with regards to the numbers of E1s, E2s and E3s in humans – where the E1 family is at the apex and shows the least diversity with only 2 members, and the E3 one is at the bottom of the pyramid and has the highest diversity with around 700 members – this does not correspond to the actual concentration of these enzymes within the cell. While cellular concentrations are still lowest for E1s, they are 3 times higher for E2s and only 2 times higher for E3s (Kulak et al., 2014). Besides the number of encoded enzymes and their cellular concentration, an additional factor that needs

to be considered is the activity level of such enzymes – particularly at an individual level and relating to the specialised function(s) of each.

E2s have a subset of functions; some of them can only deposit one ubiquitin molecule onto the substrate (chain initiators) whereas others can deposit ubiquitin molecules onto other ubiquitin molecules that are already on the substrate (chain extenders), and a subset of them can even do both (Stewart et al., 2016). One example of task distribution between a chain initiator and an extender is demonstrated by the E2s for Anaphase Promoting Complex/Cyclosome (APC/C), a major cell cycle regulating E3 ligase that comprises close to 20 subunits and is believed to be a distant relative of SCFs owing to the cullin and RING-finger domains of its APC2 and APC11 subunits, respectively (Chang et al., 2014, Ohta et al., 1999, Yu et al., 1998, Zachariae et al., 1998, Chang et al., 2015). The E2 UBE2C is responsible for relaying the priming ubiquitin molecule onto the APC/C substrate, after which the E2 UBE2S starts building the poly-ubiquitin chain which marks the substrate for proteasomal degradation (Williamson et al., 2009, Wu et al., 2010).

Such E2 functional diversity likely evolves from E2 structural variations. Despite the majority of E2s having only one domain, a ubiquitin-conjugating (UBC) domain, a significant number have additional N- or C-terminus extensions that are believed to contribute to differential E2 abilities to shape ubiquitin chains (summarised in (Stewart et al., 2016)). Utilising their one UBC domain, E2s are tasked with two critical reactions for the ubiquitylation process: an E1-E2 trans-thiolation to receive the ubiquitin from the E1, and an E2-substrate aminolysis to deposit the ubiquitin onto the target protein. Given their abundance and central

roles in ubiquitylation, E2 ubiquitin-conjugating enzymes have been established as the main regulators of ubiquitin chain assembly.

d. E3 Ubiquitin Ligases

i. E3 Families: RING and U-Box, HECT, RBR and RCRs

Over 700 E3 ubiquitin ligases have been identified to date and, although members of the same family share some common features, their mechanism of action differs significantly. Overall, E3s fulfil key roles in important cellular process, including ones at the basis of cell survival, which renders them promising candidates for anti-cancer approaches.

Based on differences in their specialised domains and their mechanisms of Ub transfer, E3s are classified into 4 major types: the Really Interesting New Gene and U-box (RING and U-box) E3s, the Homologous to the E6AP Carboxyl Terminus (HECT) E3s, the RING–in-between–RING (RBR) E3s and the recently identified type: the RING-Cys-Relay (RCR) E3s (Figure 1i).

RING E3s are the largest class of E3s and get their name from their characteristic zinc-bound RING domain, which is responsible for recruiting the E2 enzyme along with its conjugated ubiquitin molecule. This recruitment results in the E2~Ub conjugate being in close proximity to the substrate that the E3 has also recruited, and enables the transfer of the Ub from the E2 directly onto the substrate (Deshaies and Joazeiro, 2009). It has been shown that multiple RING E3s are capable of catalysing the ubiquitin transfer from E2~Ub onto the substrate through a conserved positively charged “linchpin” arginine residue that interacts with both the E2 and the Ub to alter their conformations relative to one another. This conformational change is from a state where the Ub is further apart

from the E2 (open conformation; flexible and dynamic) towards a state where the Ub is more tightly assembled with the E2 (closed conformation; firmly tethered). This shift in conformational equilibrium leaves the thioester bond of the E2~Ub more susceptible to nucleophilic attack from the substrate's lysine and is therefore a shift that is linked to an accelerated rate of Ub transfer activity from E2s onto substrates (Pruneda et al., 2012, Pruneda et al., 2011, Saha et al., 2011).

With more than 200 members, the Cullin-Ring Ubiquitin Ligase (CRL) family stands as the largest among RING E3s (Sarikas et al., 2011). The structurally similar U-box E3 ligases employ a very similar Ub-transfer mechanism, and are even referred to as 'modified RING ligases'. Their main difference is that the U-box stabilisation is derived from a combination of salt-bridges and hydrogen bonds *in lieu* of the zinc ions that stabilise the RING domain (Aravind and Koonin, 2000).

Instead of allowing the direct transfer of Ub onto substrates, HECT E3s transiently bind the Ub themselves as a result of a catalytic cysteine-dependent trans-thiolation reaction with the E2~Ub before passing it on to the substrate (Rotin and Kumar, 2009). RBR E3s are a hybrid between RBR and HECT E3s in terms of mediating Ub transfer. In similar fashion to RING E3s, the first of the two RING domains recruits the E2~Ub conjugate and thereby positions it close enough to the second RING domain to allow Ub transfer onto it. In similar fashion to HECT E3s, the second RING domain in the RBR E3 ligases transiently binds the Ub molecule thanks to its conserved cysteine that allows the formation of a reversible thioester intermediate with Ub, before passing on the Ub to the substrate (Wenzel et al., 2011, Spratt et al., 2014).

Four years ago the RCR class of E3s was first described, and its identification is recent enough that there is only one known member to date: the E3 ligase MYC Binding Protein 2 (MYCBP2). The Ub transfer mechanism of this type of E3s involves a tandem cysteine domain including two catalytic cysteines that relay the Ub molecule between themselves before the Ub is eventually deposited onto the substrate (Pao et al., 2018).

ii. CRLs

Given their position as the largest family of RING E3s, and the fact that their activity accounts for ~20% of all proteasomal degradation, CRLs are the subject of attention of many researchers (Sarikas et al., 2011, Soucy et al., 2009). CRLs employ a cullin family member as their central scaffold to form a multi-subunit E3 (Figure 1ii). The cullin subunit bridges a RING-Box protein (RBX1/2) through its C-terminus and an adaptor-subunit–substrate-recruitment-subunit complex through its N-terminus (Sarikas et al., 2011). CRL1s are multi-subunit E3 ligases that use Cullin 1 as their scaffold, F-box proteins as their substrate recruitment subunits and S-phase Kinase Associated Protein 1 (SKP1) as their substrate adaptor that bridges the cullin to the F-box protein. For this reason, CRL1s are more commonly known as SKP1–CUL1–F-box (SCF) complexes, and they represent the prototypical CRLs (Sarikas et al., 2011). With around 70 F-box proteins at their disposal, SCFs have quite the range of substrate recruiters to choose from. Similarly to CRL1s with F-box proteins, other CRLs have their own specific toolboxes of substrate receptors to choose from (which I summarised in (Fouad et al., 2019)).

Research using the roundworm *C. elegans* as a model organism identified a family of cullin genes that share significant similarity with Cullin 1. Using Cullin

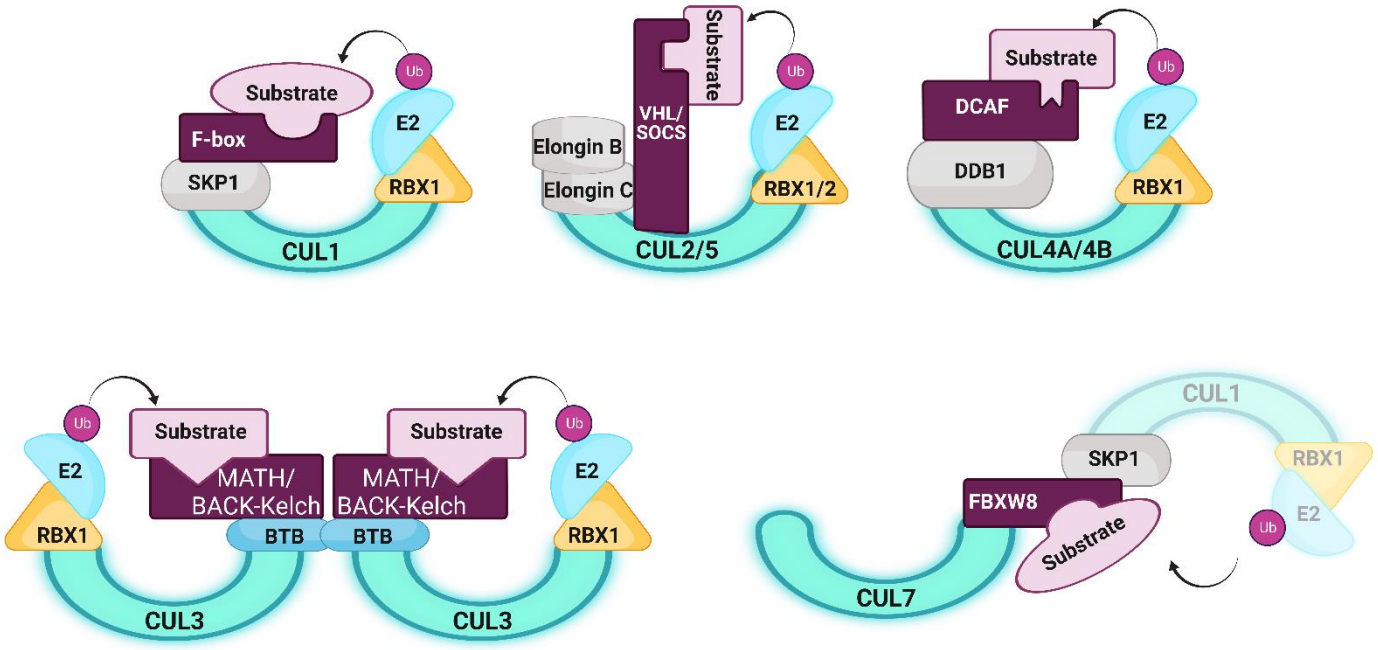
1 as reference, an expressed sequence tag (EST) search in the *H. sapiens* database revealed the human equivalent of this family: the genes Cullin 1, 2, 3, 4A, 4B and 5 (Kipreos et al., 1996). Since CRL1s are the archetypal CRLs, the rest of the CRL complexes mostly follow suit when it comes to their general structure. Despite this similarity, the complexes show considerable differences in assembly and subunit selection according to structural studies. These differences possibly stem from distinct mechanisms of ubiquitylation and modes of substrate engagement, but the required research into the comparative kinetics of action among these complexes is lacking.

Cullins 2 and 5 have high structural similarity and utilise the same adaptor complex Elongin B/C. However, they employ different substrate recognition subunits: CRL2s use von Hippel-Lindau (VHL)-box proteins whereas CRL5s use Suppressor of Cytokine Signalling (SOCS)-box proteins (Kamura et al., 2004) (Figure 1ii).

CRL3 complexes differ from CRLs 1, 2 and 5 in terms of their scaffold's N-terminal subunits: instead of having both a substrate recruitment subunit and an adapter that connects it to the cullin scaffold, CRL3s use Broad complex, Tramtrack and Bric-à-Brac (BTB)-domain proteins to fulfil both of these functions (Pintard et al., 2004, Xu et al., 2003). Another unique characteristic of CRL3s has to do with their assembly: they possess an intrinsic capacity to homo-dimerise through their BTB domains (Stogios et al., 2005) (Figure 1ii). A tightly regulated

quality control system of this dimerisation process has been described in recent years and relies on the F-box protein FBXL17 (Mena et al., 2018).

Figure 1ii. Cullin Ring Ubiquitin Ligases. CUL1-5 scaffold proteins recruit a RING-Box protein through their C-terminus and an adaptor-subunit–



substrate-recruitment-subunit complex through their N-terminus. Employed adapters include SKP1 (CUL1), Elongins B and C (CUL2/5), DDB1 (CUL4) and BTB-MATH/Kelch-domain proteins which simultaneously act as adaptors and substrate receptors (CUL3). Other utilised substrate receptors include F-box proteins (CUL1), VHL/SOCS-box proteins (CUL2/5) and DCAFs (CUL4). CRL3 has the capacity to homo-dimerise through its BTB domain, whereas CRL1 has the capacity to hetero-dimerise with CUL7 through the F-box protein FBXW8, and this forms an active CRL1/CRL7 complex through which CRL7 is able to induce ubiquitylation by sharing CRL1's E2~Ub.

Similarly to CRL3 complexes, CRL4s have unique aspects that separate them from the other previously described CRLs. CRL4 complexes use one of two closely related paralogs, Cullin 4A or Cullin 4B, as scaffolds. The 2 proteins share 82% sequence homology but Cullin 4B has an additional nuclear localisation signal (NLS) (Zou et al., 2009). Both of these Cullin 4 scaffolds use the adaptor protein DNA Damage-Binding Protein 1 (DDB1) to bind to a large class of proteins

known as DDB1 and CUL4 Associated Factors (DCAFs) which fulfil the role of substrate receptors (Jin et al., 2006) (Figure 1ii).

Cullin 7 is quite similar to Cullin 1 since it also uses SKP1 as its adaptor, although the binding is indirect in the case of Cullin 7 (Hopf et al., 2022), and an F-box protein as its substrate recruiter. However, Cullin 7 uses only one specific F-box protein, which is FBXW8, unlike Cullin 1 which has a lot of options within the sizeable selection of ~70 F-box proteins to choose from (Dias et al., 2002). This FBXW8 exclusivity has been recently explained (Hopf et al., 2022). On its own, the CRL7 complex is unable to induce ubiquitylation. This is due to its orientation restraints, which render it unable to bind E2. Instead, it binds SKP1 through FBXW8, and together they bind the active CUL1-RBX1 complex, which in turn mediates the FBXW8-recruited substrate ubiquitylation (Figure 1ii). Through this mechanism, CRL7 acts as a substrate receptor in its CRL1/CRL7 complex (Hopf et al., 2022).

Cullin 9 is the most recently identified family member and hence the least well studied; CRL9 assembly features remain poorly elucidated. Cullin 7 and 9 form the largest complexes among CRLs and have the least in common with the other family members (Dias et al., 2002, Marín, 2009).

iii. F-box Domain

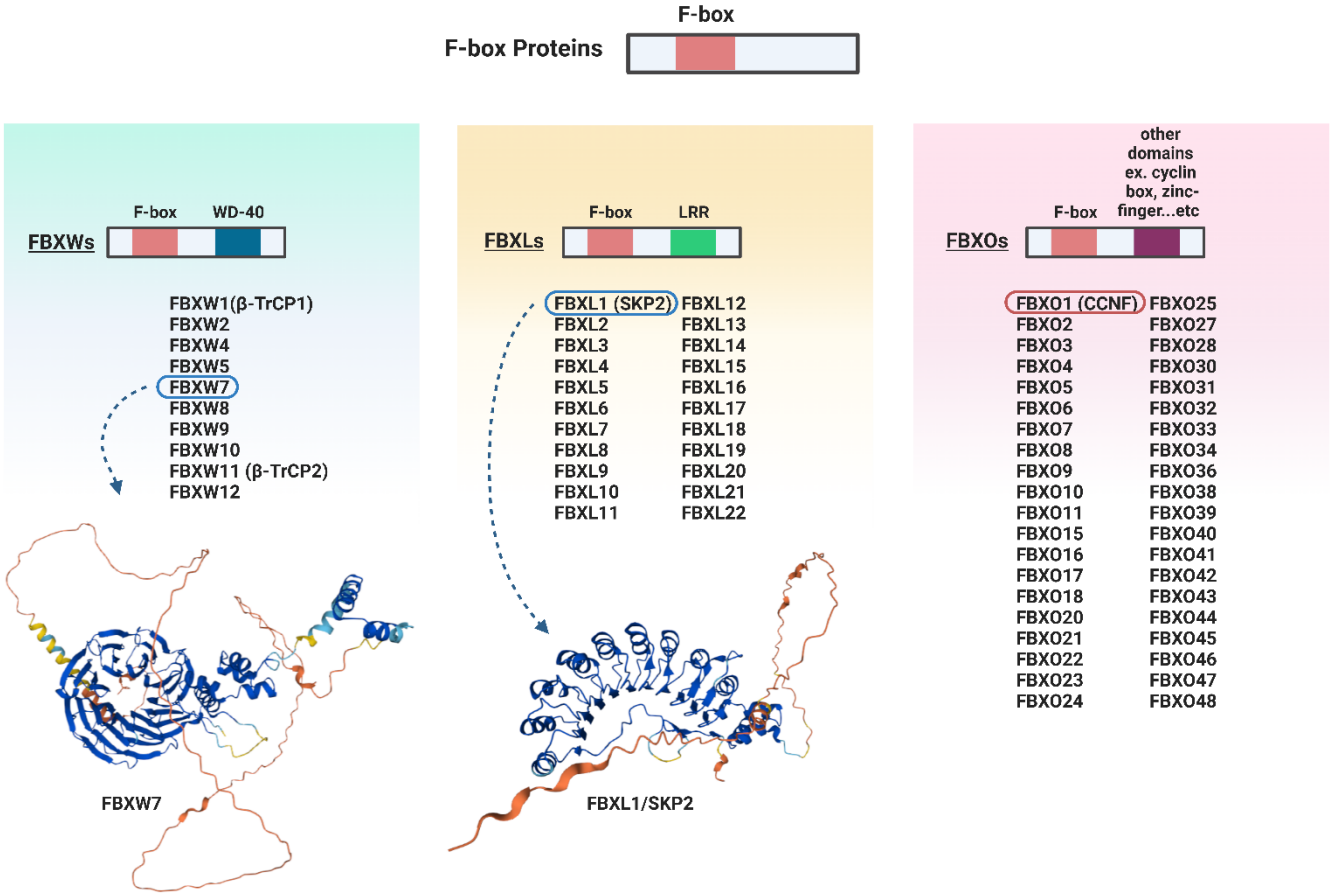
Cyclin F (also known as FBXO1) is the protein in which the 40-amino-acid F-box domain was first discovered, and the one after which this family of proteins was named (Bai et al., 1996). The F-box domain is responsible for SKP1 binding and this interaction with SKP1 was used to identify other F-box proteins through a yeast two-hybrid screening system; SKP1 was fused to the DNA-binding

domain of the transcription factor GAL4 in yeast cells and thereby used as bait to search for interactors by transforming the same yeast strain with a cDNA library expressed as proteins fused to the GAL4-activation domain. Reporter assays showing the successful reconstitution of GAL4 as a functional transcription factor – by measuring its transcriptional activity on reporter genes – were used to identify 6 novel F-box proteins. The conserved residues of the F-box domain in these proteins were used for a database sequence-matching search, which revealed another 19 novel F-box proteins (Cenciarelli et al., 1999, Winston et al., 1999a).

Although around 70 F-box proteins have been discovered to date, a large fraction of them remain orphan proteins since their substrates, and therefore cellular functions, are yet to be unveiled. However, the number of F-box proteins whose functions have been extensively elucidated, often times in the context of tumorigenesis, appear to have integral roles in regulating essential cellular processes (reviewed in (Nguyen and Busino, 2020, Tekcham et al., 2020)). Mammalian F-box proteins are split into 3 major subgroups based on the distinct domains they utilise to fulfil substrate recruitment roles: FBXWs engage their WD-40 domain whose WD-40 repeats exhibit a β-propeller architecture (Smith et al., 1999), FBXLs rely on their leucine zipper whose leucine-rich repeats (LRR) assume a horse-shoe structure constituted by β-sheets together with a variety of possible helix structures (Enkhbayar et al., 2004), and FBXOs use other variable domains and were formerly known as F-box only proteins as they were initially mistakenly thought to have no recognisable domains beyond the F-box one (Jin et al., 2004) (Figure 1iii). A little over half of F-box proteins are FBXOs, most likely owing to the large variation in the nature of domains used by this subgroup. Such

additional domains include: cyclin box, zinc-finger domains, TRAF domain-like motifs and carbohydrate-interacting domains, among others (Nguyen and Busino, 2020).

Figure 1iii. F-box protein sub-families. In addition to their F-box



domains, FBXWs have WD-40 domains which exist in a β-propeller structure and FBXLs have leucine-rich repeats whose structural organisation resembles a horse-shoe owing to the β-sheets as well as helices constituting this architecture. The structures of FBXW7 and FBXL1 are included as representative examples of FBXWs and FBXLs, respectively, and were acquired from AlphaFold. FBXOs, like Cyclin F (circled in red), do not have an additional characteristic domain besides their F-box one. However, different FBXOs have been shown to have a variety of extra domains such as cyclin boxes, zinc-finger domains, TRAF domain-like motifs and carbohydrate-interacting domains. *Figure generated using BioRender.*

iv. NEDD8-Mediated Cullin Regulation

CRL1 through CRL5 complexes are regulated by Neural Precursor Cell Expressed Developmentally Down-regulated Protein 8 (NEDD8) (Jones et al., 2008). NEDD8 is a small ubiquitin-like molecule that has its own distinct E1, E2 and E3 enzyme cascade which is similar to that of ubiquitylation (Dye and Schulman, 2007). It also tethers itself covalently to its target, in this case the cullin component of CRL complexes, which results in a significant conformational change at the C-terminus of the cullin scaffold, thereby releasing RBX1/2 on a flexible tether which allows it to adopt the necessary repositioning to bridge the gap between the ubiquitin-conjugated E2 enzyme and the recruited substrate for the eventual ubiquitin transfer to occur (Figure 1iv) (Duda et al., 2008, Baek et al., 2020).

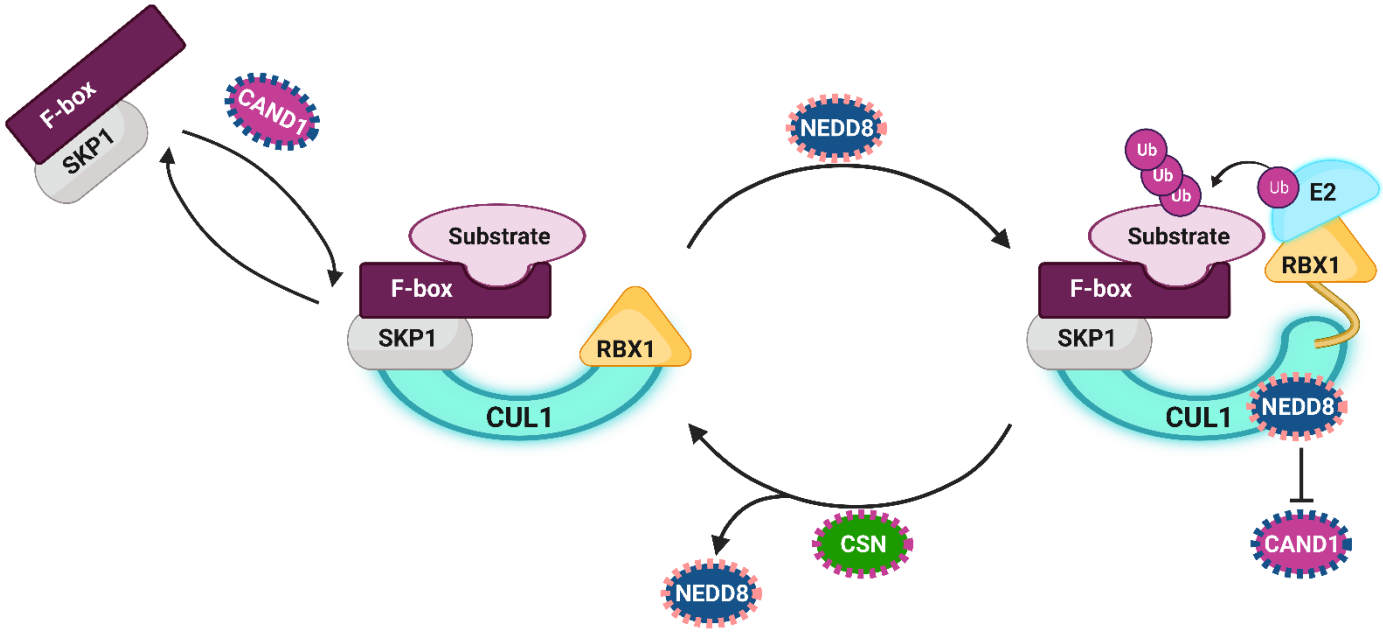


Figure 1iv. NEDD8, CSN and CAND1-mediated cullin regulation. The small modifier NEDD8 covalently binds to the C-terminus of the cullin scaffold in CRL complexes, thereby resulting in the RING-box protein adapting a more loosely attached conformation instead of its initial compact one with the cullin,

and this allows it the necessary flexibility to engage both the E2 and the substrate for Ub transfer. NEDDylation can be reversed by the CSN, and this leaves the CRL complex susceptible to CAND1 activity which promotes the substitution of the substrate recruitment subunit – in this case, F-box proteins. *Figure adapted from (Mohanty et al., 2021, Reitsma et al., 2017) and generated using BioRender.*

Depositing NEDD8 onto Cullin 1 prevents its interaction with Cullin-Associated and NEDDylation-Dissociated 1 (CAND1), a NEDDylation inhibitor and also the protein responsible for F-box protein exchange (only on non-NEDDylated cullins) (Pierce et al., 2013). For CAND1 to bind to a NEDD8-activated Cullin 1, allowing a substitution of its substrate recruitment subunit, Cullin 1 requires de-NEDDylation (and thereby de-activation) first (Figure 1iv). This is carried out through proteolytic cleavage by the multi-subunit COP9 Signalosome (CSN) (Cavadini et al., 2016). Altogether, NEDD8, CAND1 and CSN create a tight regulatory loop for CRL1 complex assembly (Figure 1iv).

v. SCF Substrate-Recognition Mechanisms

CRL1 complexes bind their substrates following different ‘stimuli’, the most common of which are summarised below and in Figure 1v. Well-characterised examples of such stimuli include post-translational modifications or priming by co-factors. In the canonical model, SCF complexes recognise their targets through binding a minimal element which consists of a short sequence of degradation motifs known as a degron (Varshavsky, 1991).

1. Phosphorylation

Phospho-Degrons

Degron phosphorylation is a common mechanism of substrate recognition by E3s. This phospho-degron is often required to mediate efficient substrate-ligase interaction. For example, the substrate receptor Beta-Transducin Repeat Containing Protein (β-TrCP)/FBXW1/11 recognises the degron DSGXXS (or closely-related variants where a phosphorylation-prone amino acid is substituted by another or by a phospho-mimicking one) where X represents any amino acid and both serine resides are phosphorylated (Winston et al., 1999b, Frescas and Pagano, 2008). Examples of proteins targeted by this F-box protein through their DSGXXS degron include the cell cycle regulator EMI1/FBXO5 and the inhibitor of the innate immunity modulator NF-κB's transcriptional activity IκBα, among others (Margottin-Goguet et al., 2003, Winston et al., 1999b). Similarly, the tumour suppressive F-box protein FBXW7 recognises the sequence (T/S)PXX(S/T/E) where both phosphorylation sites are modified by kinases (Welcker and Clurman, 2008).

In some cases, degrons are activated by degron-kinases that specifically phosphorylate essential residues within the degron. In other cases, they are activated as a result of the sequential action of a 'priming' kinase acting outside of – or on binding-non-essential amino acids within – the degradation-motif area, followed by the action of a degron-targeting kinase. This is the case for the β-TrCP substrate β-Catenin where Casein Kinase Iα (CK1α) phosphorylates the S45 residue, which then allows Glycogen Synthase Kinase 3 (GSK3) to phosphorylate S33 and S37 – both of which are essential for β-TrCP recognition of β-Catenin and the substrate-ligase binding (Liu et al., 2002). Similarly,

phosphorylation of CDC25A by the Checkpoint Kinase 1 (CHK1) at S76 primes it for further phosphorylation on S82 by CK1α, and this finally enables β-TrCP-CDC25A binding which marks CDC25A for proteasomal degradation (Busino et al., 2003, Donzelli et al., 2004).

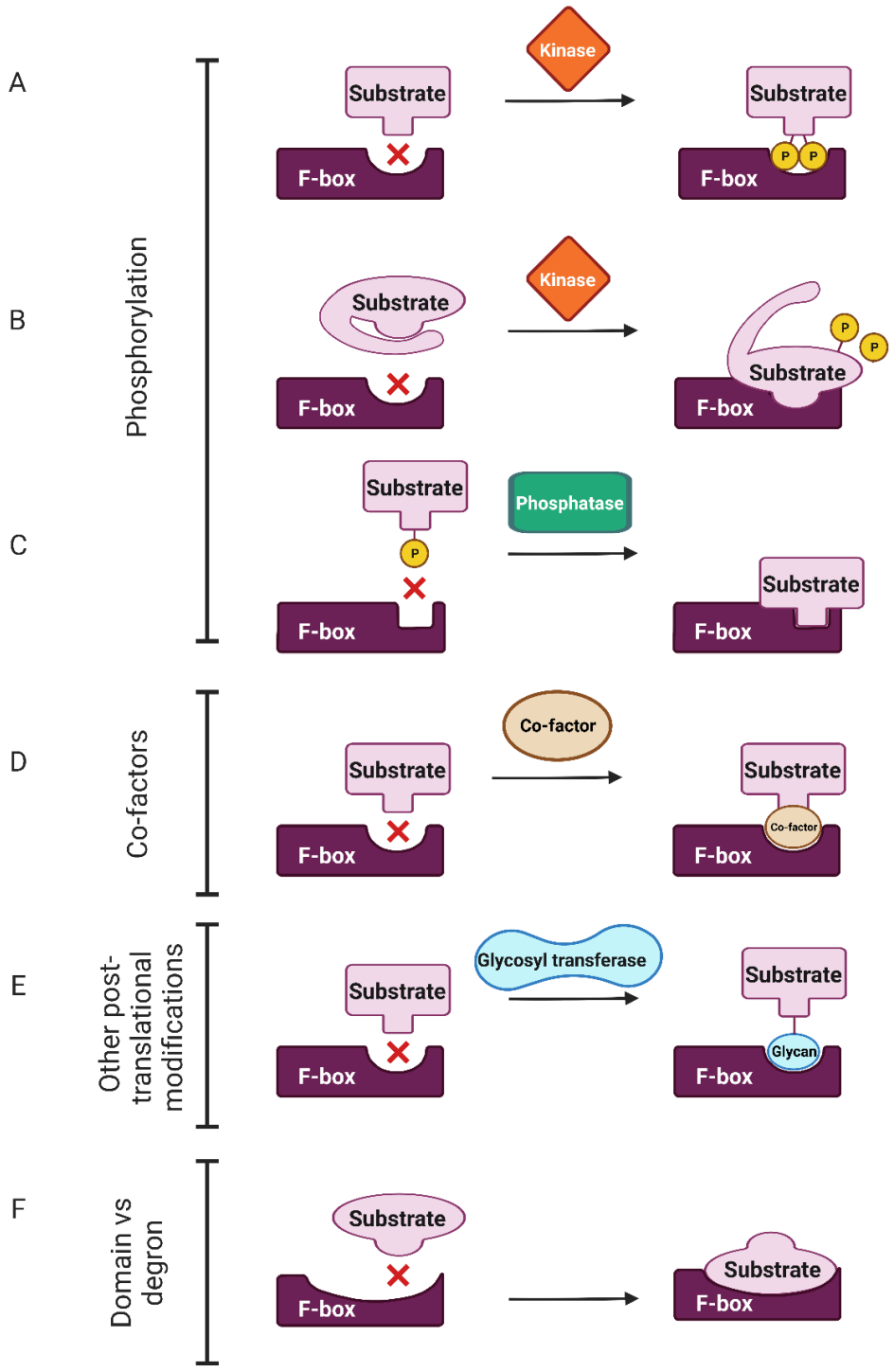


Figure 1v. SCF substrate-recognition mechanisms.

A. Phospho-degrons, B. Phosphorylation-driven degron access, C. Degron phospho-inhibition, D. Co-factor-mediated substrate recognition, E. Other post-translational modifications than phosphorylation (ex. glycosylation), F. Domain-based (as opposed to degron-based) recognition. *Figure adapted from (Skaar et al., 2013) and generated using BioRender.*

Phosphorylation-Driven Degron Access

Priming kinases can also induce a conformational change in the substrate which results in exposure of a previously obscure degron. This is the case for the Cyclin F substrate Ribonucleotide Reductase Subunit M2 (RRM2), which requires priming phosphorylation by cyclin-dependent kinases (CDKs) prior to a conformational change that enables Cyclin F's physical access to its degron and thereby the substrate's eventual proteolysis. This is a reliable mechanism to temporally restrict RRM2 degradation. RRM2, the regulatory subunit of Ribonucleotide Reductase (RNR), is essential for making deoxyribonucleotides (dNTPs, the building blocks of DNA) from ribonucleotides (Kunz et al., 1994, Nordlund and Reichard, 2006). Given its critical role in DNA synthesis and repair, RRM2 needs to be expressed at the earlier phases of the cell cycle (G_1/S) but its persistent expression at later phases (G_2/M) promotes dNTP pool imbalances and consequently DNA replication/repair infidelity (D'Angiolella et al., 2012). This is why RRM2 is targeted for degradation at G_2/M by Cyclin F, which is where levels of the required CDKs are high, hence allowing the priming phosphorylation, degron reveal and eventual RRM2 degradation to occur in this specific cell cycle phase (D'Angiolella et al., 2012).

Degron Phospho-Inhibition

Despite phosphorylation being a major post-translational modification that facilitates substrate-ligase binding, it can also lead to the inverse of that in some

cases by inhibiting the binding instead. Phosphorylation has the ability to mask the degron of an F-box protein's target, thereby hindering substrate recognition by the E3 ligase, unless a phosphatase is involved and mediates degron exposure. One example of this is the blocking of FBXO11 binding to Chromatin Licensing and DNA Replication Factor 2 (CDT2), a key regulator of cell cycle progression due to its control of the proteolysis of the replication licensing factor CDT1. CDKs phosphorylate CDT2 within its degron region, which in turn protects it against proteasomal degradation in cycling cells (Rossi et al., 2013). Having a constitutively phosphorylated CDT2 was shown to interfere with the cell cycle by hindering mitotic exit, which – similarly to RRM2 phosphorylation by CDKs – emphasises the importance of cell cycle-coordinated ubiquitylation events for the purpose of maintaining healthy cellular functions (D'Angiolella et al., 2012, Rossi et al., 2013).

2. Co-factors

Given the large size of the F-box protein family, it is tantalising to speculate that they use diverse stimuli to help them bind their substrates. It has been shown that multiple stimuli work for one SCF complex to bind its target. Besides phosphorylation, this family of substrate recruitment subunits also relies on co-factors to help ubiquitylate their target proteins. FBXL1/SKP2 requires the chaperone protein CDK Subunit 1 (CKS1) to bind both itself and its substrate p27 after CDK-mediated p27 phosphorylation, and this results in a significantly increased affinity of phosphorylated p27 for SKP2 (Ganoth et al., 2001, Spruck et al., 2001). The resulting degradation of the CDK inhibitor p27 is essential in G1 in order to allow S-phase entry, and it is believed that the requirement for the

accessory protein CKS1 limits this degradation to G_1/S where CKS1 levels are highest (Spruck et al., 2001). Once again, the need for priming phosphorylation by CDKs ensures well-timed ubiquitin-mediated degradation, which highlights the importance of this collaboration of the two post-translational modifications.

3. Other Stimuli

While phosphorylation and co-factor chaperoning make up a considerable number of cases when it comes to events inducing SCF complex binding to substrates, there is a sizeable number of alternative stimuli at work. One example is non-phosphorylation-based post-translational modifications, such as glycosylation. FBXO2, FBXO6, FBXO17, FBXO27 and FBXO44 all have F-box-associated (FBA) domains that have been shown, at least for FBXO2 and FBXO6, to recognise glycosylation on a substrate which thereby allows substrate binding and SCF-mediated ubiquitylation (Glenn et al., 2008). This glycosylation is believed to serve as a marker for incorrectly folded proteins and hence a signal for their UPS-mediated proteolysis, however, such studies on glycosylation as a stimulus for SCF binding and UPS-mediated degradation have not been followed up since, and therefore their importance to the field of ubiquitylation remains unclear.

Another alternative mode of substrate recognition is domain-based, as opposed to degron-based. In contrast to detecting the short sequences that make up the degradation motifs, some F-box proteins detect larger domains instead. This is exemplified by FBXL3 and its substrates Cryptochrome Circadian Regulator 1 and 2 (CRY1/2, see Table 1). These 2 substrates, both essential for a functional circadian clock, have leucine-rich repeats that FBXL3 recognises and

binds to before marking the proteins for proteasomal degradation (Busino et al., 2007, Siepka et al., 2007, Xing et al., 2013). In line with the fact that multiple stimuli often work in tandem to facilitate substrate recruitment, it was shown that the metabolic redox co-factor flavin adenine dinucleotide (FAD) regulates this CRY-FBXL3 interaction (Xing et al., 2013).

vi. Cyclin F

Cycling cells initiate a cascade of kinase activity mediated by cyclins in complex with their CDKs, which directs DNA replication and cell division. In each cell cycle, tight regulation of DNA replication prevents over- or under replication. Unlike other cyclins, Cyclin F does not bind to or activate any CDKs (D'Angiolella et al., 2010, Fung et al., 2002). Instead, Cyclin F has an F-box domain which is essential for its activity as an E3 ligase and is in fact the founding member of the F-box family of substrate recruitment factors (Bai et al., 1996) (Figure 1vi.A). Cyclin F levels fluctuate throughout the cell cycle; they start to build up in G_1/S, peak in G2, and drop in mitosis and the subsequent G_1 following Cyclin F's ubiquitin-mediated degradation by the E3 ligases $SCF^{\beta\text{-}TrCP}$ and APC/C^{Cdh1} (Choudhury et al., 2016, Mavrommati et al., 2018). Through its contribution to the UPS, Cyclin F has important roles in both DNA replication and DNA damage pathways (see Table 1).

Cyclin F and DNA Replication Stress

Through its $SCF^{Cyclin\ F}$ complex, Cyclin F promotes the ubiquitylation of the dNTP-synthesis catalyst RRM2 (D'Angiolella et al., 2012), the centrosomal-duplication protein Centriolar Coiled-Coil Protein 110 (CCP110) (D'Angiolella et al., 2010), the spindle-assembly protein Nucleolar and Spindle Associated Protein 1 (NUSAP1) (Emanuele et al., 2011), the origin licensing protein Cell

Division Cycle 6 (CDC6) (Walter et al., 2016), the exonuclease EXO1 (Elia et al., 2015), the transcriptional activators E2F1, E2F2 and E2F3 (Clijsters et al., 2019, Burdova et al., 2019b) and the transcriptional repressors E2F7 and E2F8 (Yuan et al., 2019).

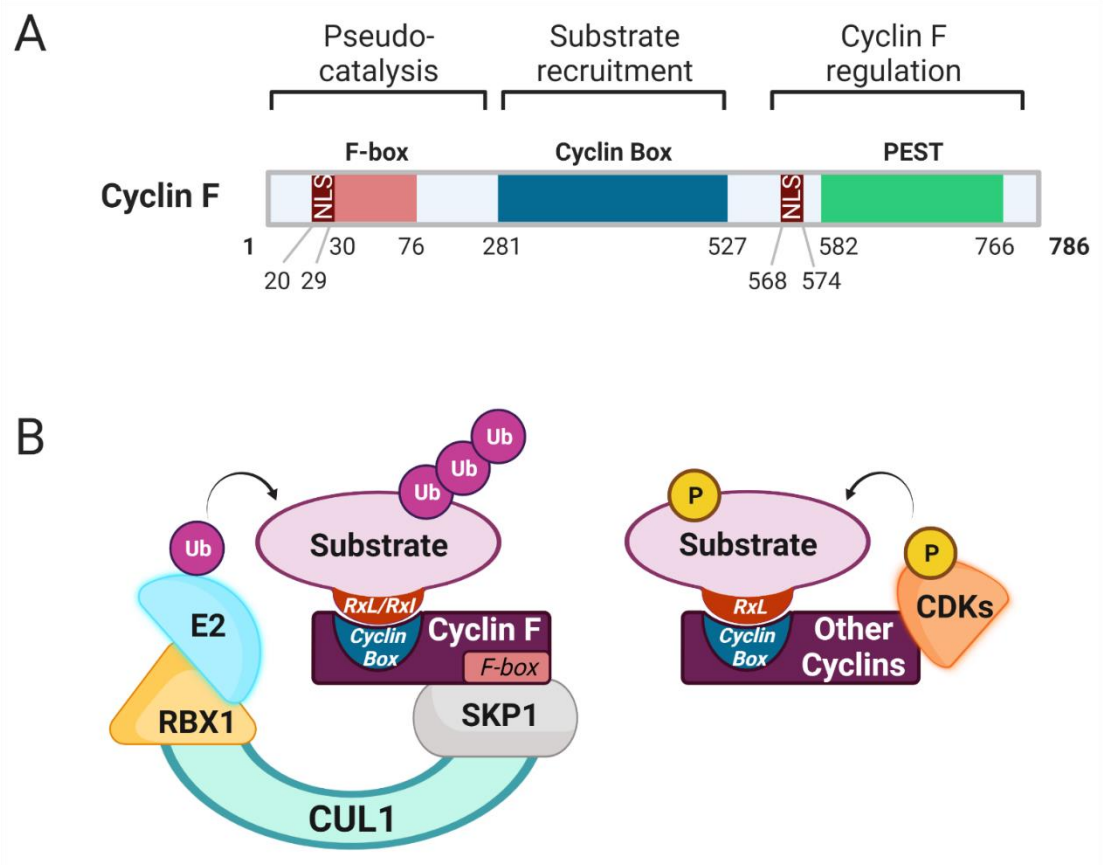


Figure 1vi. Cyclin F is a unique cyclin.

A. Functional domains of Cyclin F, including those essential for its function as an E3 ligase (ex. F-box and Cyclin Box). NLS = nuclear localisation signal.
B. Comparison between Cyclin F and other cyclins in terms of substrate binding mechanism and substrate modification type. *Figure adapted from (D'Angiolella et al., 2013) and generated using BioRender.*

In contrast, Cyclins A to E phosphorylate target substrates rather than ubiquitylate them. Despite the differences in the nature of the post-translational

modification relayed onto the substrates, Cyclin F does share some similarity with the other cyclins. It binds its substrates the same way most of the cyclins bind CDKs; through a hydrophobic patch in the cyclin domain which binds a CY motif Rx(L/I) in the target protein where x represents any amino acid residue (Figure 1vi) (D'Angiolella et al., 2013). In addition to its F-box domain that mediates its binding to SKP1 and its cyclin box through which it binds its substrates, Cyclin F has a PEST domain which is believed to regulate its stability (Figure 1vi).

The regulation of cyclins is mediated by the E2F family of transcriptional activators and repressors. Since E2F1, one of the family's 3 canonical activators, is the archetypal member, it is the most extensively studied (Kent and Leone, 2019). Although E2F1 has been shown to transcriptionally activate (transactivate) multiple genes in various pathways such as checkpoint control, apoptosis and differentiation, its best-established function is promoting cell cycle progression by transactivating genes required for DNA synthesis (Polager and Ginsberg, 2008). In line with this, failure to degrade E2F1 constitutes a plausible source for an accumulation of DNA replication stress (Fouad et al., 2020).

Expectedly, a significant number of oncogenic pathways converge on aberrant E2F1 functioning, most commonly in ways that encourage constitutive proliferation independently of the external stimuli that usually signal for cell cycle progression (Fouad et al., 2020). Accordingly, E2F1 is dysregulated in numerous cancers such as hepatocellular carcinoma, non-small cell lung cancer (NSCLC), glioblastoma multiforme (GBM), ovarian, cervical, breast, pancreatic and renal cancers (Chen et al., 2009).

Cyclin F has also been recently found to target the Retinoblastoma (RB)-family tumour suppressor Retinoblastoma-Like Protein 2 (RBL2)/p130 (Enrico et

al., 2021). Since the tumour suppressor RB is the major repressor of E2F activity, and RBL1/p107 and RBL2/p130 are its 2 closely related family members, $SCF^{Cyclin\ F}$ ubiquitylation of multiple E2Fs in addition to p130 together adds a new layer of complexity and intricacy to the regulation of the cyclin/E2F/RB axis (Dyson, 1998, Stengel et al., 2009). Cyclin F's involvement in this axis could be clinically exploitable for cancer therapy since it has been shown that Cyclin F, RB and the checkpoint kinase CHK1 form a triad that tightly regulates E2F1 post-translationally, whereby if at least 2 of its components are defective synthetic lethality ensues (Figure 1vii) (Burdova et al., 2019a, Fouad et al., 2020, Witkiewicz et al., 2018).

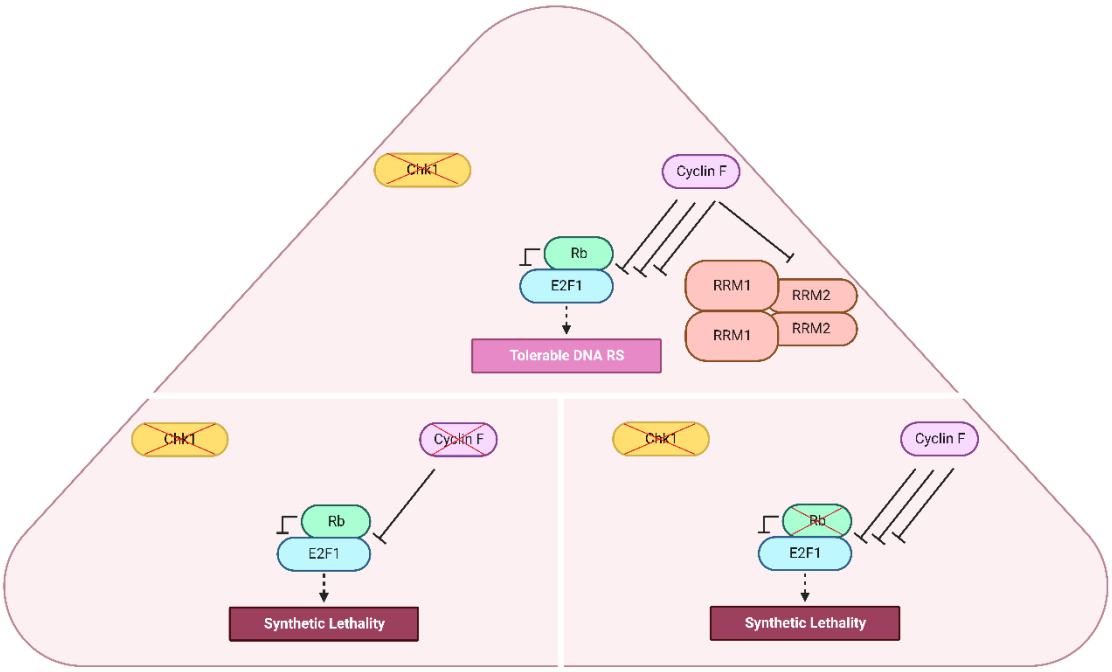


Figure 1vii. Cyclin F-E2F1 axis in DNA replication stress. Cyclin F, RB and CHK1 converge on E2F1 regulation whereby defective control of this transcriptional activator by 2 or more of these regulators results in synthetic lethality. *Figure adapted from (Fouad et al., 2020) and generated using BioRender.*

Cyclin F and DNA-Damage Response

$CRL1^{Cyclin\ F}$ has important roles in the DNA-damage response (DDR) through a number of its substrates, which is not unexpected since CRLs are responsible for 10% of all DNA-damage-induced ubiquitylation events (Elia et al., 2015). Cyclin F has been reported to prevent mitotic entry post treatment with ionising radiation (IR) through competitively inhibiting b-MYB, thereby resulting in an enforcement of the G_2 checkpoint. B-Myb transactivates multiple genes necessary for mitotic entry, hence through inhibiting its activity Cyclin F controls mitotic entry after IR (Klein et al., 2015a).

Imbalances in dNTP levels have been linked to genomic instability and cancer progression (Kunz et al., 1994). Mirroring this, abnormally high levels of the Cyclin F substrate RRM2 have been directly linked to tumorigenesis in mice and an overall poor prognosis for a variety of cancers in humans (Jones et al., 2011, Morikawa et al., 2010, Xu et al., 2008). One explanation for this deleterious effect is the increase in the rate of spontaneous mutations, which was proven to arise from dysregulated RRM2 levels (D'Angiolella et al., 2012).

DNA damage in the form of double strand breaks (DSBs) is repaired by 2 main pathways: the first involves ligating the broken ends together by the error-prone non-homologous end joining (NHEJ) method, which is active throughout the entirety of the cell cycle (Burma et al., 2006). The other major repair pathway involves the use of a second copy of DNA as a template by the error-free process of homologous recombination (HR), which is only active in S- and G_2-phases where the undamaged sister chromatid is available and can therefore be used as a template (Figure 1viii) (Heyer et al., 2010). RRM2 silencing has been shown to massively attenuate DSB repair, since a 90% drop in functional HR has been

observed following *RRM2* knock-down using an siRNA approach (Gustafsson et al., 2018). As a main RRM2 regulator, this is one way Cyclin F contributes to DNA-damage repair fidelity.

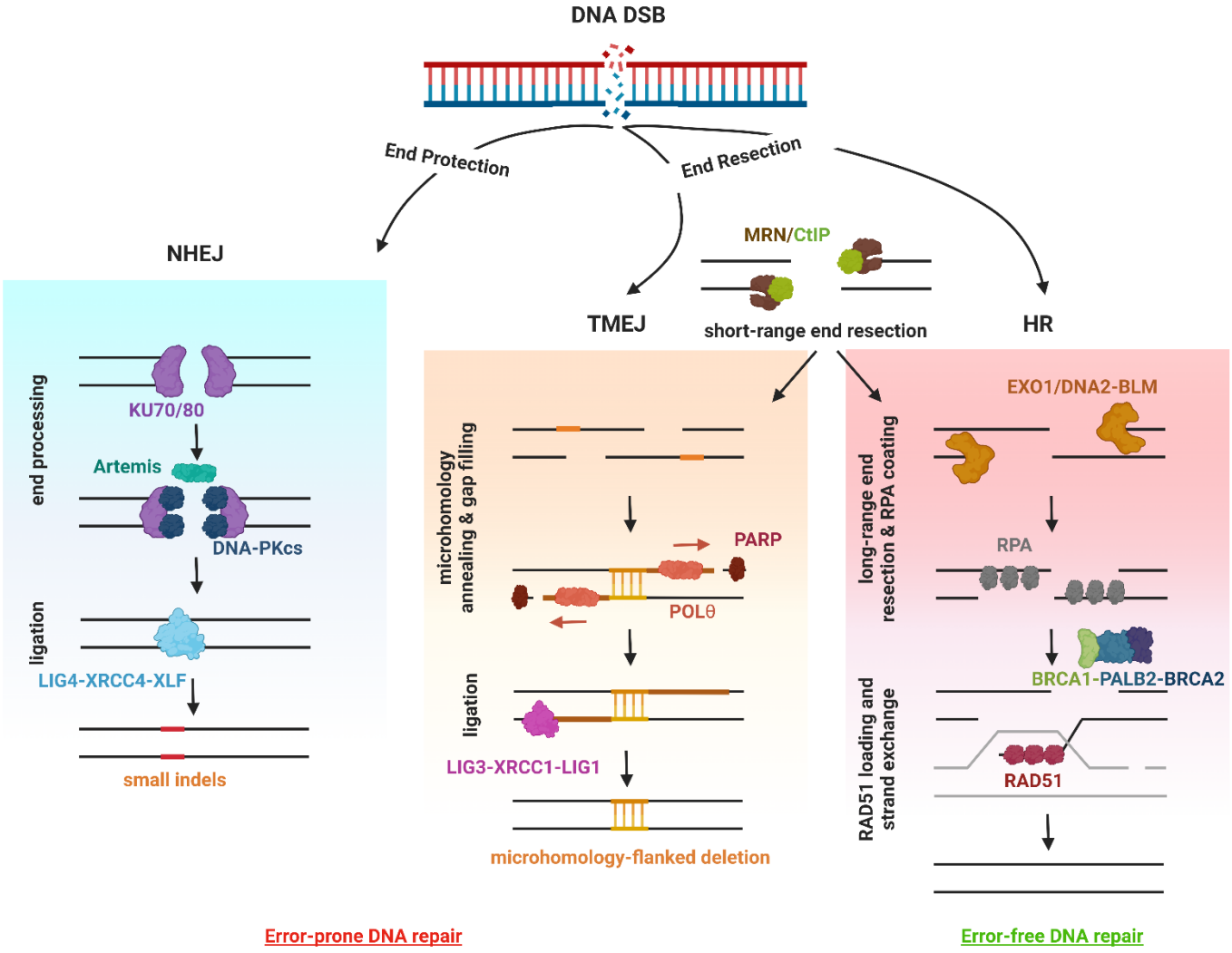


Figure 1viii. Mechanisms of DNA DSB repair. NHEJ repair pathway involves the protection of the damaged DNA ends, whereas TMEJ (Alt-EJ) and HR both require end processing prior to repair process initiation. Both NHEJ and TMEJ are error-prone repair processes whereas HR is error free. NHEJ relies on KU70/80, DNA-PKcs, Artemis, DNA ligase 4, XRCC4 and XLF whereas HR requires MRN/CtIP, EXO1/DNA2-BLM, RPA, BRCA1/2-PALB2 and RAD51, and TMEJ utilises PARP, POLθ, DNA ligase 3/1 and XRCC1 in addition to the MRN/CtIP complex. *Figure adapted from (Schrempf et al., 2021, Trenner and Sartori, 2019) and generated using BioRender.*

vii. EXO1 and DNA Repair

EXO1 is a 5' to 3' exonuclease which is required for DNA repair after damage via DSBs (Elia et al., 2015). In the cell cycle phases where either NHEJ or HR can be engaged (S and G_2), a necessary step that commits the cells to HR as the chosen DNA repair method is the resection of broken ends of DNA to enable strand invasion of the homologous template, and this is carried out largely by EXO1 and DNA2 owing to their ability to conduct long-range resection at DSBs (Figure 1viii). This is because the KU70/80 complex, which is essential for NHEJ, is efficient in mediating re-ligation and end joining only when the DNA overhangs resulting from the strand breaks are blunt – which is not the case following DNA long-range resection by EXO1 upon IR, especially upon EXO1 dysregulation and a subsequent increase in its levels and/or activity (Figure 1viii) (Ma et al., 2003).

Similarly to HR, yet in contrast to NHEJ, theta-mediated end joining ('TMEJ', also known as alternative end joining 'Alt-EJ') is initiated by end resection, but involves a set of proteins (PARP, POLθ, the CtIP/MRN complex and DNA ligase 3) very different from the classical NHEJ ones (KU70/80, DNA-PKcs and DNA ligase 4) (Ahrabi et al., 2016, Ghezraoui et al., 2014, Soni et al., 2014). TMEJ/Alt-EJ does not require a donor strand, and depends on microhomology regions at both sides of the DSB site instead (Figure 1viii) (Ahrabi et al., 2016). TMEJ/Alt-EJ is engaged when HR essential proteins are defective or when NHEJ essential proteins (like KU or the DNA ligase complex) are lacking, and is even more error-prone than classic NHEJ (Ceccaldi et al., 2015).

Given how delicate this process is, it requires tight regulation to prevent erroneous hyper- or hypo-resection of the DNA – an event known to give rise to genomic instability (Tomimatsu et al., 2017). Consistent with this, EXO1 levels

are regulated by both phosphorylation and ubiquitylation after DNA damage induced directly by IR or indirectly by the topoisomerase inhibitor Camptothecin (CPT) – two DNA-damaging agents that result in the formation DSBs – and were also shown to drop in a UPS-mediated manner following replication fork stalling upon treatment with the RNR inhibitor hydroxyurea (HU) (Tomimatsu et al., 2017, El-Shemerly et al., 2005, El-Shemerly et al., 2008).

SCF complexes were implicated in the UPS-mediated regulation of EXO1 after treatment with multiple DNA-damaging agents, while $SCF^{Cyclin\ F}$ specifically was implicated in EXO1 targeting after treatment with the UV-mimetic drug 4NQO (Elia et al., 2015, Tomimatsu et al., 2017). However, it remains unclear whether the regulation of EXO1 by Cyclin F also extends to the other forms of DNA damage described, and whether this regulation is functionally important for DNA repair after these forms of DNA damage.

II. Ubiquitylation: in Sickness and in Health

a. The Ubiquitin Code: Cellular Roles

In humans and other multicellular organisms, the highly conserved ubiquitin protein is encoded by 4 genes: *UBA52/RPL40*, *UBA80/RPS27A*, *UBB* and *UBC* (Finley et al., 1987). Both *UBA52/RPL40* and *UBA80/RPS27A* generate ubiquitin as a single molecule fused to the ribosomal protein L40 or S27A, respectively, from which the ubiquitin is released following post-translational processing. *UBB* and *UBC*, on the other hand, generate ubiquitin cassettes – head-to-tail-linked ubiquitin multimers – that can be processed into ubiquitin monomers by DUBs (Amerik and Hochstrasser, 2004).

Proteins modified with ubiquitin are either mono- or poly-ubiquitylated, where the latter involves a chain made up of 2 or more ubiquitin molecules conjugated to one another. This polymerisation of ubiquitin-ubiquitin is enzymatically directed by the different E2-E3 complexes and utilises one ubiquitin molecule's N-terminal methionine (M1) or any of its seven lysine residues (K6, K11, K27, K29, K33, K48 or K63) and the C-terminus glycine residue of the other ubiquitin molecule (reviewed in (Rape, 2018)). Another layer of complexity to this ubiquitin chain topology is whether it is homotypic (formed of one type of linkage, ex. a K48 chain) or heterotypic (consists of a mix of linkages, ex. a K11/K48 hybrid chain), and in the latter case the chain can either be linear or branched. Such chains can also be post-translationally modified, for example by phosphorylation or acetylation, among other small-molecule modifiers, which can further regulate the signalling output of the substrate's ubiquitylation (Kane et al., 2014, Ohtake et al., 2015). These various levels of intricacy of the ubiquitin chains make up a code that is read by the cells to execute important cellular functions and prevent the accumulation of unwanted protein products.

Altogether, the diverse functions of ubiquitylation are known as the ubiquitin code (Komander and Rape, 2012). The simplest of all ubiquitylation patterns is mono-ubiquitylation, and it serves important roles in protein-protein, protein-lipid and protein-DNA interactions, which can result in both degradative and non-degradative fates for the involved substrates (reviewed in (Magits and Sablina, 2022)). With regards to poly-ubiquitylation, chains that signal for proteasomal degradation are the most thoroughly studied. This is not unexpected, since the UPS is responsible for the degradation of most intracellular proteins (Rock et al., 1994).

K48, K11 and K11/48-hybrid chains signal for the proteasomal degradation of their ubiquitylated protein (Chau et al., 1989, Jin et al., 2008, Meyer and Rape, 2014). After K48, K63 is the most abundant chain linkage and together the 2 linkages account for almost 80% of ubiquitin linkages in cells (Ohtake et al., 2016). K63 chains usually have proteasome-independent roles and instead are involved in complex assembly in the DDR and signal transduction (Chan and Hill, 2001, Stewart et al., 2009). K6, K27 and K33 are also involved in the DDR (Elia et al., 2015, Gatti et al., 2015), K29 is involved in kinase (Wingless/Integrated 'WNT') signalling (Fei et al., 2013), and M1 chains have been shown to be directly linked to the immune response via Nuclear Factor-Kappa B (NF-κB) signalling (Aalto et al., 2022, Aalto et al., 2019). Considering the multitude of functions carried out by the various ubiquitin modifications, ubiquitylation controls a rich communication system of signals that regulate the significant functions required for healthy development.

b. Ubiquitylation in Cancer

i. CRL1 Complexes

Given the major cellular pathways regulated by E3 ligase complexes, it comes as no surprise that E3s are just as heavily engaged when the regular functioning of these pathways goes awry – for example during tumorigenesis.

F-box proteins, the substrate recruitment subunits of SCF/CRL1 complexes, are heavily involved in tumour development (summarised in Table 1 below). These roles are a result of the F-box proteins' ubiquitylation abilities through their respective E3 ligase complexes, and their substrates comprise members of hallmark cancer pathways such as cell cycle progression/arrest, epithelial-mesenchymal transition (EMT), programmed cell death and genomic

instability (GIN). F-box proteins implicated in tumorigenesis also target major oncogenic signalling pathways such as those involving Mechanistic Target of Rapamycin Kinase (mTOR), central tumour suppressor p53, NF-κB and the transcription factor Nf-E2-Related Factor 2 (NRF2) – all of which contribute to malignant phenotypes in such ways as proliferation, metastasis and invasion.

In some cases this involvement is quite direct as the F-box protein targets an oncoprotein for ubiquitin-mediated degradation, or stabilises a tumour suppressor by targeting its E3 ligase instead. Examples include the most characterised oncogenic F-box protein SKP2/FBXL1, which degrades the CDK inhibitors p21 and p27 – both recognised as key cell cycle suppressors (Bornstein et al., 2003, Carrano et al., 1999). Additionally, SKP2 has been identified as an E3 ligase for Forkhead Box O1 (FOXO1) – a transcription factor with major roles in tumour suppression owing to its ability to induce growth arrest and apoptosis (Huang et al., 2005).

On the other hand, FBXW7 is a well-studied tumour suppressor. FBXW7 is heavily involved in oncoprotein degradation as Cyclin E, mTOR, c-MYC and c-JUN are among its substrates (Mao et al., 2008, Nateri et al., 2004, Strohmaier et al., 2001, Yada et al., 2004). FBXO4 has a similar function as it plays important roles in cell cycle arrest and apoptosis induction through its substrates Cyclin D and the pro-survival protein Myeloid Cell Leukaemia 1 (MCL1), however, the lack of mutations of this F-box protein in cancer raises some doubts on the tumour suppressive nature of its reported functions. Further examples are briefly described in Table 1 below.

Table 1. F-box proteins in cancer. Tumorigenic roles of FBXLs, FBXWs and FBXOs. *Adapted from (Tekcham et al., 2020).*

F-box Protein	***Substrate(s)***	***Function(s) (respectively to the substrates)***
FBXL1 (SKP2)	P21 (Bornstein et al., 2003) P27 (Carrano et al., 1999) P130 (Bhattacharya et al., 2003) c-MYC (von der Lehr et al., 2003) Cyclin E (Yeh et al., 2001) YAP1 (Yao et al., 2018) AKT (Clement et al., 2018) FOXO1 (Huang et al., 2005) PDCD4 (Li et al., 2019)	Cell cycle progression, transcription, signalling pathways (AKT and FOXO) and inhibition of apoptosis
FBXL2	Cyclin D (Chen et al., 2012a, Chen et al., 2012b) AURKB (Chen et al., 2013) FOXM1 (Li et al., 2016) P85β (Kuchay et al., 2013)	Cell cycle arrest and suppressing PI3K/AKT signalling pathway
FBXL3	CRY1/2 (Busino et al., 2007) c-MYC (Huber et al., 2016)	Stabilising tumour suppressors PER1/2 and c-MYC oncoprotein degradation
FBXL4	KDM4A (Van Rechem et al., 2011)	Regulation of chromatin modifiers
FBXL5	SNAIL1 (Viñas-Castells et al., 2014) hSSB1 (Chen et al., 2014) P150 (Zhang et al., 2007)	Metastatic factor degradation, modulating DNA-damage response and chromosome stability
FBXL7	AURKA (Coon et al., 2012)	Cell cycle progression
FBXL13	CEP192 (Fung et al., 2018)	Centrosome duplication
FBXL14	c-MYC (Fang et al., 2017) SNAIL1 (Viñas-Castells et al., 2010) TWIST1 (Lander et al., 2011) CDCP1 (Cui et al., 2018)	Oncoprotein and metastatic factor degradation and suppression of breast cancer progression
FBXL17	SUFU (Raducu et al., 2016) BACH1 (Tan et al., 2013)	Hedgehog signalling and NFR2 oxidative stress pathway
FBXL18	AKT (Zhang et al., 2017) FBXL7 (Liu et al., 2015)	AKT signalling pathway and cell cycle arrest

FBXL19	RAC3 (Dong et al., 2014) RhoA (Wei et al., 2013)	Oncoprotein degradation, attenuation of cell proliferation and cytoskeleton rearrangement
FBXL20	E-cadherin (Zhu et al., 2012) VPS34 (Xiao et al., 2015)	WNT signalling pathway and autophagy
FBXW1/11 (β-TrCP)	IκBα (Winston et al., 1999b) CDC25A (Busino et al., 2003) c-MYC (Popov et al., 2010) P53 (Xia et al., 2009) BimEL (Dehan et al., 2009) PDCD4 (Dorrello et al., 2006) Cyclin F (Mavrommati et al., 2018) β-Catenin (Hart et al., 1999) WEE1 (Watanabe et al., 2004) YAP (Zhao et al., 2010) REST (Guardavaccaro et al., 2008) MCL1 (Ding et al., 2007) ZNF281 (Zhu et al., 2017) NRF2 (Rada et al., 2011)	NF-κB pathway activation, cell cycle progression, regulating cell viability, chromosome stability, apoptosis and the NFR2 oxidative stress pathway
FBXW2	FBXL1 (SKP2) (Xu et al., 2017) β-Catenin (Yang and Sun, 2019)	Oncoprotein degradation and regulating cell viability
FBXW7	Cyclin E (Strohmaier et al., 2001) mTOR (Mao et al., 2008) NOTCH1 (Close et al., 2019) c-JUN (Nateri et al., 2004) c-MYC (Yada et al., 2004) MCL1 (Mori et al., 2018)	Oncoprotein degradation
FBXO1 (CCNF)	E2F1-3 and 7 (Burdova et al., 2019a, Clijsters et al., 2019, Yuan et al., 2019) p130/RBL2 (Enrico et al., 2021) RRM2 (D'Angiolella et al., 2012) CCP110 (D'Angiolella et al., 2010) NUSAP1 (Emanuele et al., 2011) CDC6 (Walter et al., 2016)	Transcriptional regulation, DNA replication and repair, centrosome duplication, chromosome assembly and cell cycle progression

	CDH1 (Choudhury et al., 2016)	
FBXO4	Cyclin D1 (Lin et al., 2006) MCL1 (Feng et al., 2017) ICAM1 (Kang et al., 2017)	Cell cycle arrest, apoptosis and suppressing malignant transformation
FBXO7	cIAP1 (Chang et al., 2006)	Inhibition of apoptosis
FBXO10	BCL1 (Chiorazzi et al., 2013)	Apoptosis
FBXO11	BCL6 (Duan et al., 2012) HIF-1α (Ju et al., 2015) SNAIL (Zheng et al., 2014)	Oncoprotein and metastatic factor degradation
FBXO31	SNAIL1 (Zou et al., 2018) MDM2 (Malonia et al., 2015) Cyclin D1 (Santra et al., 2009) MKK6 (Liu et al., 2014)	Metastatic factor degradation, p53 tumour suppressor stabilisation, cell cycle arrest and suppressing MAPK signalling pathway
FBXO38	PD-1 (Meng et al., 2018)	Regulation of anti-tumour T-cell mediated immunity

ii. Other CRL Complexes

In addition to CRL1 complexes, numerous other CRL family members are implicated in controlling cancer development. One such example is CRL2 and its substrate the alpha subunit of Hypoxia-Inducible Factor 1 (HIF-1). HIF-1 is a transcription factor that tumour cells express in hypoxic conditions and also as a result of IR-induced oxidative stress – but the latter case involves only transient expression (Semenza, 1999). HIF-1 is responsible for the transcriptional activation of a plethora of hypoxia-responsive genes in oncogenic pathways, thereby promoting tumorigenesis through processes like apoptotic resistance, enhanced tumour growth and proliferation, invasion, metastasis, angiogenesis and resistance to radiotherapy (Gorski et al., 1999, Moeller et al., 2004, Semenza, 2003). HIF-1α, subunit of the heterodimer HIF-1 which consists of both α and β subunits, has an oxygen-dependent degradation (ODD) domain that controls its binding to, and thereby consequent degradation by, $CRL2^{VHL}$ (Huang et al., 1998). Proline hydroxylation within the ODD signals for VHL binding, which

is why the responsible hydroyxylases are inhibited in hypoxia to enable HIF-1 induced hypoxic signalling (Bruick and McKnight, 2001, Epstein et al., 2001, Maxwell et al., 1999).

Kelch Like ECH Associated Protein 1 (KEAP1), a CRL3 substrate adapter, is known to regulate NRF2 – a master transcriptional activator of the anti-oxidation response against reactive oxygen species (ROS) (Cullinan et al., 2004, Kobayashi et al., 2004, Zhang et al., 2004). ROS mediate the covalent modification of two cysteine residues in KEAP1, which hinders its ability to ubiquitylate NRF2 through its CRL3 complex, and thereby stabilises it by allowing it to evade its proteasomal degradation (Kobayashi et al., 2006). Since high levels of ROS are a common event in cancer, the KEAP1-NRF2 axis serves a tumour suppressive role. Expectedly, this axis is commonly hijacked by cancer cells to acquire a survival advantage in conditions of oxidative stress (Chen and Chen, 2016). In line with this, the KEAP1-NRF2 axis is quite frequently defective in cancers and this normally is in the form of KEAP1 loss-of-function mutations, NRF2 gain-of-function mutations, or NRF2 mutations that abrogate KEAP1 binding (Shibata et al., 2008, Konstantinopoulos et al., 2011, Ohta et al., 2008, Singh et al., 2006, Yoo et al., 2012, Shibata et al., 2011, Tong et al., 2006).

Another direct link between a CRL3 complex and cancer was quite recently uncovered by some of our lab members, and follows a study of the CRL3 ligase adaptor Kelch Repeat and BTB Domain-Containing Protein 4 (KBTBD4) (Chen et al., 2022). The research was focused on the more elusive medulloblastoma groups that lack pathogenic alterations in the well-studied WNT or Sonic Hedgehog (SHH) pathways; medulloblastoma groups 3 and 4. In-frame insertion mutations in KBTBD4 were shown to be a frequent event in these 2

medulloblastoma groups, which formed the basis for this study (Northcott et al., 2017, Wong et al., 2020). Investigating this E3 ligase adaptor has shown that the reported mutations, which occur in the Kelch domain, are neo-morphic mutations (like IDH1 (Dang et al., 2009, Mardis et al., 2009, Ward et al., 2010)) and result in the recruitment of Corepressor of RE1 Silencing Transcription Factor (CoREST) as a neo-substrate to mark it for UPS-mediated degradation. CoREST acts as a major scaffold for chromatin-modifying complexes (Lee et al., 2005, Shi et al., 2004) and results show that its degradation has oncogenic potential since it results in altered transcription in a way that favours stemness and therefore cancer development in medulloblastoma (Chen et al., 2022, Selvadurai et al., 2020).

c. The UPS and RAS Dysregulation in Cancer

i. RAS and Tumorigenesis

RAS is the most mutated oncoprotein as it is estimated that 18.7% of patients with cancer harbour RAS mutations (Prior et al., 2020). The RAS superfamily consists of around 39 small GTPases which are encoded by approximately 36 genes (Murugan et al., 2019). The 3 best-characterised are the ubiquitously expressed RAS proto-oncogenes *HRAS*, *KRAS* (comprising the 2 splice variants *KRAS4A* and *KRAS4B* where the latter is the more predominant variant), and *NRAS*. Its drastically high mutation rate in cancer has earned *RAS* the title of a “hallmark cancer gene” and made it one of the most sought-after therapeutic targets (Simanshu et al., 2017, Haigis, 2017). Of this mutated ~19%, KRAS accounts for 14.3%, NRAS for 3.1% and HRAS for the remaining 1.3% (Prior et al., 2020). The 3 most mutated amino acid residues in these oncoproteins are G12, G13 and Q61 (Prior et al., 2020).

These mutations inhibit the GTPase Activating Proteins (GAPs)-catalysed hydrolysis of GTP (which produces inactive RAS-GDP), resulting in constitutively active RAS that is constantly bound to GTP. In healthy cells, the activity of RAS is tightly regulated by the activating Guanine Nucleotide Exchange Factors (GEFs) and the de-activating GAPs (Bos et al., 2007). RAS proteins are involved in important signalling pathways that sustain normal cellular functions in healthy cells, however, when they are dysregulated through mutations they become constitutively activated and proceed to aberrantly activate the signalling pathways that control proliferation, growth, differentiation, migration and survival (Murugan et al., 2019).

Downstream of active RAS are 2 major pathways involved in tumorigenesis: the Mitogen-Activated Protein Kinase 'MAPK' (RAF/MEK/ERK) and the PI3K/AKT/mTOR pathways (Figure 1ix). Upon RAS-mediated activation, PI3K converts Phosphatidylinositol-4,5-biphosphate (PIP2) to Phosphatidylinositol-3,4,5-triphosphate (PIP3), a reaction which is reversed by the tumour suppressor Phosphatase and Tensin Homolog (PTEN) (Zhao and Vogt, 2008). PIP3 then mediates the activating phosphorylation on AKT at T308 by the kinase PDK1 (Alessi et al., 1997), and activated AKT in turn initiates protein synthesis via its downstream effectors such as NF-κB and mTOR (mTOR2 endows even further activation to AKT by additionally phosphorylating it at S473) (Alessi et al., 1997, Sarbassov et al., 2005). AKT has been shown to suppress the pro-apoptotic activity of the Cyclin F target E2F1, whereas E2F1 has been shown to regulate AKT by transactivating its positive regulator GRB2-Associated Binder 2 (GAB2) (Chaussepied and Ginsberg, 2004, Hallstrom and Nevins, 2003). Similarly to its role in the PI3K pathway, GTP-bound RAS is known

to activate MAPK pathway components such as ERK. ERK relays an activating phosphorylation on Cyclin D, and the hyperactivity of this cyclin (in complex with CDK4/6) releases E2F1 from its RB suppressive complex by directly phosphorylating RB (Lavoie et al., 1996, von Willebrand et al., 2003).

ii. RAS Ubiquitylation

Owing to its significant oncogenic role, there is a strong interest in investigating the regulatory mechanisms of RAS. Post-translational modifications on RAS have been shown to contribute to its regulation and one such modification is ubiquitylation. Research has shown that CRLs once again play an important role in the regulation of an oncoprotein as data suggested that the CRL3 adapter Leucine Zipper Like Transcription Regulator 1 (LZTR1) promotes the mono- and di-ubiquitylation of the 3 RAS isoforms, which weakens their membrane association and hence attenuates their signalling (Bigenzahn et al., 2018, Steklov et al., 2018). A later study clarified this role further by showing that LZTR1 ubiquitylates the RAS-related protein RIT1 rather than RAS itself (Castel et al., 2019).

CRL1s also contribute to RAS regulation, and this is through $SCF^{\beta\text{-TrCP}}$ which reportedly poly-ubiquitylates HRAS and mediates its proteolysis – an event that is counteracted by the aberrant activation of WNT/β-Catenin signalling that stabilises HRAS instead (Jeong et al., 2012, Kim et al., 2009). The $CRL1^{FBXL2}$ complex controls signalling downstream of RAS through the F-box protein FBXL2, which ubiquitylates and hence degrades the PI3K regulatory subunit p85, and thereby regulates the PI3K/AKT signalling cascade (Kuchay et al., 2013).

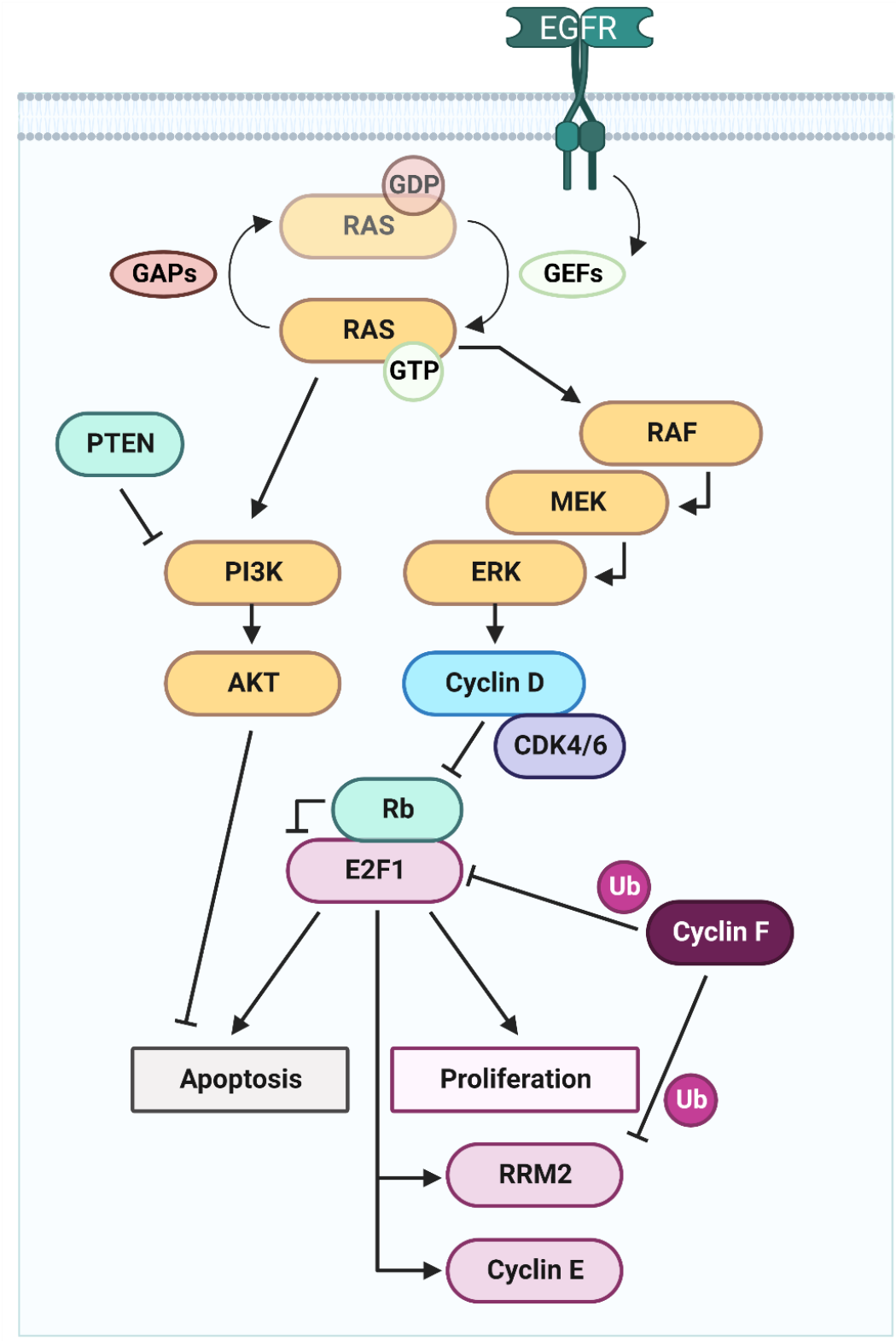


Figure 1ix. RAS signalling cascade.

RAS is upstream of 2 major signalling pathways: PI3K/AKT and MAPK (RAF/MEK/ERK). Both of these pathways are heavily implicated in tumour development and progression. *Figure adapted from (Fouad et al., 2020) and generated using BioRender.*

iii. Targeting RAS for Therapy

Since *KRAS* accounts for 76% of *RAS* mutations, multiple efforts converge on inhibiting the oncogenic effects of this mutation, for example by developing targeted chemical inhibitors which specifically exploit the mutation site to lock the KRAS protein in an inactive state (Prior et al., 2020). Indeed, approaches to target the KRAS G12C mutation, which is the most common KRAS mutation in lung cancer, the second most common in colorectal cancer (CRC) and the third most common KRAS mutation overall, have been rendered fruitful in recent years (Moore et al., 2020). The nature of this mutation has been exploited via a small-molecule inhibitor known as AMG510 (Sotorasib/Lumakras™) that covalently binds the reactive cysteine in the protein's active site when KRAS is in its inactive GDP-bound state, thereby constricting it to this inactive conformation and inhibiting its activation by GEFs (Ostrem et al., 2013). Clinical trials using AMG510 were promising in NSCLC (54% partial response and 46% stable disease rates) but less so in CRC (8% partial response and 83% stable disease rates) (AMGEN, 2019). This constituted the first milestone in the drug's journey towards FDA approval, which was granted in 2021 for the treatment of KRAS G12C NSCLC patients who have received at least one prior systemic therapy (FDA, 2021).

Other frequent KRAS mutations like G12D and G12V require different approaches for their inhibition due to the absence of a relatively easily-targetable reactive cysteine from the protein's active site. One such approach has been shown as proof-of-concept quite recently by two groups who generated specific KRAS G12D inhibitors. These inhibitors bind the aspartic acid residue of KRAS G12D and form non-classical hydrogen bonding and ion pair interactions (i.e. salt

bridges), eventually resulting in the disruption of KRAS' downstream activation cascade (Mao et al., 2022, Hallin et al., 2022). Cell-based and *in vivo* tumour models showed promising results for these inhibitors and expectations for clinical trials are set for later in 2023.

Less direct approaches have targeted proteins both downstream and upstream of RAS to inhibit its oncogenic signalling. The 2 main RAS downstream pathways, RAF/MEK/ERK and PI3K/AKT/mTOR have had inhibitors developed against each of these pathway members (Moore et al., 2020). For example, the following 4 inhibitors of the PI3K catalytic subunit p110α have been developed and are FDA-approved for the treatment of different cancers and other diseases: Alpelisib (for PIK3CA-related overgrowth spectrum), Copanlisib (for relapsed follicular lymphoma), Duvelisib (for chronic lymphocytic leukaemia and small lymphocytic lymphoma) and Idelalisib (for chronic lymphocytic leukaemia) (Moore et al., 2020).

As for targets upstream of RAS, there have also been notable efforts to inhibit the main GEF Son of Sevenless (SOS) and, even further upstream, the epidermal growth factor receptors (EGFR) (Moore et al., 2020). FDA-approved EGFR inhibitors include Cetuximab & Panitumumab (both monoclonal antibodies approved for the treatment of metastatic KRAS wild type 'WT' CRCs), and Erlotinib & Gefitinib (both small-molecule inhibitors approved for the treatment of EGFR-mutant NSCLC) (Moore et al., 2020). Given the high resistance of *KRAS* mutant cancers to these EGFR inhibitors, and the fact that ~90% of pancreatic ductal adenocarcinoma, 40% of CRC and 30% of lung adenocarcinoma are driven by *KRAS* mutations, clinics are in dire need of novel approaches that can help sensitise *RAS*-mutant cancers to EGFR inhibitors (Network, 2012, Network,

2014, Network, 2017). One system that researchers have been increasingly exploiting for the generation of novel targeted anti-cancer therapy is the UPS, and the emerging technology behind that is the development of Proteolysis Targeting Chimeras (PROTACs).

d. UPS-based Therapies: PROTACs

PROTACs are rapidly gaining more interest from the pharmaceutical industry, and many companies are racing to expand the targeted-therapy toolbox through this promising addition. Among these companies are ones established mainly – or even solely – for the purpose of PROTAC development, such as Arvinas, C4 Therapeutics, Kymera Therapeutics and Captor Therapeutics – all founded between the years 2013 and 2017 (Sasso et al., 2022). Other players in the PROTAC field are big pharmaceutical companies that are newly investing in this technology through major collaborations, such as Pfizer's collaboration with Arvinas.

The molecules in question are hetero-bifunctional ones made up of two different ligands and a linker. One ligand of the PROTAC binds the protein in need of degradation, and the other one is degron mimicking and therefore binds to an E3 ligase that will mediate said degradation. Once the three-membered E3–PROTAC–protein complex is formed, E2 enzymes proceed to transfer ubiquitin molecules onto the substrate, and thereby mark it for proteolysis via the UPS. Through this process, PROTACs bring the desired protein and the hijacked E3 ligase within close proximity to one another, and thereby acts catalytically to induce the proteasomal degradation of its target.

PROTACs were first introduced in 2001 through proof-of-concept experiments involving the successful recruitment of the CRL1 E3 ligase $SCF^{\beta TrCP}$ (Sakamoto et al., 2001). With the 2015 discovery that VHL and Cereblon (CRBN) – a CRL2 and a CRL4 E3 substrate receptor, respectively – can be recruited using PROTACs, the number of reported PROTACs boomed (Bondeson et al., 2015, Lu et al., 2015b, Winter et al., 2015, Zengerle et al., 2015). It was found that $CRL4^{CRBN}$ was prone to hijacking by the immunomodulatory drugs (IMiDs) Thalidomide, Lenalidomide, and Pomalidomide, which lead to the development of PROTACs with IMiD-based CRBN-binding ligands (Lai et al., 2016, Lu et al., 2015b, Winter et al., 2015).

PROTACs were designed with the aim of overcoming many of the limitations that hindered the progress of their predecessors, small-molecule inhibitors. Given that the basis of the PROTAC's activity is a ubiquitin transfer, it is a transient and reversible process. This by default renders them less prone than small-molecule inhibitors to drug resistance arising from mutations at the target's active site. Also owing to the nature of their reactions, PROTACs are recyclable. PROTACs are only needed in sub-stoichiometric ratios to the substrate since they undergo multiple rounds of ubiquitylation, in contrast to small-molecule inhibitors that act in a 1:1 ratio to the substrate and are therefore required at much higher concentrations that can trigger off-target effects (Bondeson et al., 2015, Lu et al., 2015a, Olson et al., 2018). Additionally, PROTACs utilise degron-mimicking ligands to bind their targets and this has two outcomes that make them more practical than traditional small-molecule inhibitors. The first is that PROTACs do not need to rely on active sites (such as those of enzymes) which the proteome largely lacks, and the second is that this

process exploits the UPS to degrade the entire protein rather than inhibiting one of its domains and leaving the rest of it functional (Toure and Crews, 2016).

As of last year, there are 13 PROTACs currently in the clinic (summarised in (Mullard, 2021)). A few examples include Arvinas' androgen receptor degraders ARV-110 and ARV-766, which are in phase II and I clinical trials in prostate cancer, respectively, and oestrogen receptor degrader ARV-471, which is in phase II clinical trials in breast cancer (Mullard, 2021). Despite the promise of PROTACs, their high molecular weight raises questions on permeability as well as absorption and hence represents a major reason why they do not follow Lipinski's 'Rule of 5', a set of drug-design principles defined by molecular properties that correlate with predicted efficiency of oral absorption of a drug – although it is worth noting that there are reports of successful exceptions that violate this rule (Doak et al., 2014, Lipinski et al., 2001). Molecular glues are much smaller entities that promote protein-protein (E3 and target of interest) interaction through proximity-induced protein degradation. In contrast to PROTACs, molecular glues are not engineered to have a certain degradative function but instead are screened for with the hopes of an opportunistic discovery of a degrader for a sought-after therapeutic target (Békés et al., 2022).

PROTACs and molecular glues are quite promising therapeutic candidates owing to their massive contribution in increasing, at an accelerated pace, the targetable-protein space. For example, such molecules can induce the degradation of proteins lacking enzymatic activity, like transcription factors, thereby making the previously non-targetable now targetable. However, to maximise the capabilities of these degraders, we need to fully understand the function of many more E3 ligases coded in the human genome.

Project Aims

Research in the D'Angiolella lab focuses on identifying functions of E3s in cancer pathogenesis as well as in cancer treatment. Despite continuous advances in the field's understanding of glioblastoma, 5-year survival remains at a bleak 5% (Hegi et al., 2005). The current treatment paradigm is limited, and includes maximal surgical resection, followed by concomitant radiotherapy and chemotherapy (Stupp et al., 2005). Temozolomide is one of very few chemotherapeutic options available, and it is met with drug resistance in almost 50% of glioblastoma cases, indicating a pressing need for additional treatments that synergise with ionising radiation.

To address this therapeutic need, our lab conducted a focused CRISPR screen of the ubiquitin system coupled with ionising radiation. Cyclin F scored as one of the top hits, further highlighting its role in tumorigenesis and cancer therapy. My objectives have been to characterise substrates of Cyclin F involved in the ionising radiation response observed, and to investigate the ubiquitylation mechanism operated by $SCF^{Cyclin\ F}$ in these settings.

While this project was underway, I serendipitously discovered a novel feedback mechanism between Cyclin F and the oncoprotein KRAS. My aim for this project has been to gain insights into this regulation and how it establishes a novel connection between MAP kinases and the G_2-phase of the cell cycle. My objectives were to evaluate the effects of Cyclin F loss on the proteome when KRAS is constitutively active to understand how Cyclin F regulates KRAS, to evaluate the effect of *KRAS* mutational status on the proteome to understand how KRAS regulates Cyclin F, and to use this generated data to search for

clinically exploitable weaknesses within this system to treat *KRAS* mutant cancers.

The underlying questions I initially addressed were focused on understanding Cyclin F substrates and the Cyclin F substrate-recognition mechanism. These questions were soon expanded to more broadly-relevant questions on *KRAS* and cancer thanks to the techniques developed in the laboratory during my studies.

2. Materials and Methods

I. Materials

I.1 General laboratory buffers

Concentrations expressed as percentages in this chapter are all in volume per volume (v/v) unless specified otherwise, in which case it is highlighted that the percentage is in weight per volume (w/v).

- **NP-40-based (general) lysis buffer:** 50 mM Tris-HCl, 150 mM NaCl, 10% glycerol, 1 mM EDTA, 5 mM $MgCl_2$, 0.1% NP-40)
- **1 x TAE:** 40 mM Tris, 20 mM acetic acid, 1 mM EDTA.
- **10x Resazurin stock solution:** for 1L, 100 mg Resazurin salt (R7017, Sigma-Aldrich) was dissolved in 1L 1xPBS to make up a 100 µg/mL solution, filtered using a 0.22 µm membrane and stored at 4°C away from light.
- ***In vivo* ubiquitylation assay buffers:**
  - **Ubiquitin lysis buffer:** 10 mM Tris-HCl pH 7.4, 150 mM NaCl, 2% (w/v) SDS
  - **Ubiquitin dilution buffer:** 10 mM Tris-HCl pH 7.4, 150 mM NaCl, 2 mM EDTA, 1% Triton-X100
  - **Ubiquitin wash buffer:** 10 mM Tris-HCl pH 7.4, 1 M NaCl, 1 mM EDTA, 1% NP-40
- ***In vitro* phosphorylation assay (using biotinylated peptides) buffers:**
  - **Low-salt Tris buffer:** 25 mM Tris, pH7.2, 150 mM NaCl, 1% Triton X-100
  - **High-salt Tris buffer:** 25 mM Tris, pH7.2, 500 mM NaCl, 1% Triton X-100

- **Protein purification lysis buffer:** 150 mM NaCl, 50 mM Tris HCl , 2 mM EDTA, 1% Triton X-100, 1 mM PMSF, 0.5 mg/mL Lysozyme, 10% glycerol. pH 8.0 (pH was guided by the pI of the expressed protein, which was estimated using the Expasy pI/Mw online tool. Ideally the lysis buffer's pH should be +1/-1 of the protein's pI to make sure it's charged).
- **ÄKTA Start solutions:**
  - **Wash buffer (Solution A):** 20 mM Tris/HCl, 200 mM NaCl, 10 mM imidazole.
  - **Elution buffer (Solution B):** 20 mM Tris/HCl, 200 mM NaCl, 500 mM imidazole.
- **Crystal violet staining solution:** for 100 mL, 0.5 g crystal violet powder was dissolved in 80 mL water and 20 mL methanol.
- **1× HBS:** For 1L, 8.76 g NaCl was dissolved into 900 mL double distilled water, 20 mL 1 M HEPES solution was added, pH was adjusted to 7.4 and then volume was brought up to 1L by adding double distilled water. Solution was filtered using a 0.22 µm membrane and stored at 4°C.

I.2 General laboratory and cull culture reagents

II.2.a Table: General laboratory reagents

Name	Producer or UK distributor
Acetic acid	Sigma-Aldrich
Agarose	Invitrogen/Life Technologies
β-mercaptoethanol	Sigma-Aldrich
BSA (bovine serum albumin)	Sigma-Aldrich
Ethanol	Sigma-Aldrich
Laemmli buffer	Invitrogen/Life Technologies

LB (Luria-Bertani broth)	Sigma-Aldrich
Methanol	Thermo Fisher Scientific
NEM (N-ethylmaleimide)	Sigma-Aldrich
Nocodazole	Cayman Chemicals
Nonidet P-40 (NP-40)	Sigma-Aldrich
Paraformaldehyde	VWR
10x Dulbecco's Phosphate-Buffered Saline (DPBS)	Thermo Fisher Scientific
PMSF (phenylmethylsulfonyl fluoride)	Sigma-Aldrich
Protease inhibitor cocktail (mammalian)	Roche
SDS (sodium dodecyl sulphate)	BioRad
SYBR® Green	Applied Biosystems
thymidine	Sigma-Aldrich
Triton X-100	Sigma-Aldrich
Tween 20	Thermo Fisher Scientific

II.2.b Table: Cell culture reagents

Name	Manufacturer
DMEM (Dulbecco's modified Eagle medium)	Corning
RPMI 1640	Corning
DMSO (dimethylsulphoxide)	Sigma-Aldrich
FBS (foetal bovine serum)	Sigma-Aldrich
HiPerfect	Qiagen
Lipofectamine 2000	Invitrogen/Life Technologies
PBS, pH 7.4	Thermo Fisher Scientific
PEI (Polyethylenimine HCl) Max	Polysciences
X-tremeGENE HP	Roche
Tissue culture disposables/plastics	Greiner Bio-One

I.3 Antibodies

Primary Antibodies used for Western blotting

**dilution = 1:1,000, unless specified otherwise in the product manual*

Name	Species	Reference
FLAG	Rabbit	Sigma-Aldrich, F7425
GAPDH	Mouse	Invitrogen/Life Technologies, MA5-15738
HA-HRP		Roche, 12013819001
RRM2 (A-5)	Mouse	Santa Cruz, sc-398294
pThr33 RRM2	Rabbit	Custom generated for work by (D'Angiolella et al., 2012)
EXO1	Rabbit	Bethyl, A302-639A
EXO1 (recognize only the long isoform)	Rabbit	Bethyl,A302-640A
CCNF	Rabbit	Bethyl,A303-406A
GFP (FL)	Rabbit	Santa Cruz, sc-8334
α- TUBULIN (B-5-1-2)	Rabbit	Santa Cruz, sc-23948
CUL1	Mouse	Thermo Fisher Scientific, 32-2400
SKP1	Rabbit	Cell Signalling Technology, 2156
Cyclin A2 (E1D9T)	Rabbit	Cell Signalling Technology, 91500
PRC1 (C-1)	Mouse	Santa Cruz, sc-376983
TAF II p55 (SQ-8)	Mouse	Santa Cruz, sc-101167
MDC1	Rabbit	Abcam, ab11171
ITM1 (A-2)	Mouse	Santa Cruz, sc-390227
AKAP9	Rabbit	Abcam, ab237752
LAS1L	Rabbit	Bethyl, A304-438A
ORC2	Rabbit	Generated in house by (Chou et al., 2021)
NEK9 (3907)	Mouse	Santa Cruz, sc-100401
BRAT1	Rabbit	Atlas, HPA029455
HELLS/LSH (H-4)	Mouse	Santa Cruz, sc-46665
Cdt1	Rabbit	Santa Cruz, sc-28262
BORA (H-4)	Mouse	Santa Cruz, sc-393741
pan-RAS	Mouse	Sigma-Aldrich, 05-516
ISG15	Mouse	Santa Cruz, sc-166755

MAP2K6	Mouse	Atlas, HPA031134
pSTAT1 (Y701) clone 58D6	Rabbit	Cell Signalling Technology, 9167S
RMI1/BLAP75	Rabbit	Bethyl, A300-631A
Topo IIα (TOP2A)	Mouse	Santa Cruz, sc-365916
HLTF	Mouse	Santa Cruz, sc-398357

Secondary Antibodies used for Western blotting

Name	Dilution	Reference
HRP Goat Anti-Mouse IgG (H+L)	1:10,000	Invitrogen/Life Technologies, 62-6520
HRP Goat Anti-Rabbit IgG (H+L)	1:10,000	Invitrogen/Life Technologies, 65-6120

I.4 Antibiotics

Ampicillin and Kanamycin (Sigma-Aldrich) were made up as 1000x stock solutions of 50 mg/mL in sterile, double distilled water. Stocks were filtered using a 0.22 µm filter, then aliquoted and stored at -20°C. Ampicillin and Kanamycin were used at the final concentrations of 50 µg/mL.

G 418 (analog of neomycin sulfate) disulfate salt solution (Sigma-Aldrich, 50 mg/mL in H_2O, 0.1 µm filtered) was used at a final concentration of 0.8 mg/mL for LIM1215 G12V$^{+/-}$ (both *CCNF* WT and *CCNF* K/O) cell culturing.

I.5 Kinase inhibitors

LY2603618 (CHK1i), BML-277 (CHK2i), RO-3306 (CDK1i), KO3861 (CDK2i), VE-821 (ATRi), KU55933 (ATMi), MLN8237 (Aurora Ai), AZD1152-HQPA (Aurora Bi), NU7026 (DNA PKi), BI 6727 (PLKi), PHA-767491 (CDC7i), CKIIi VIII (CKIIi), SB202190 (p38α/β MAPKi) and TAK-715 (p38α MAPKi) were purchased from Selleck Chemicals and used at 5 µM (except for CDK1i and DNA

PKi which were used at 10 µM) according to the literature in the kinase inhibitor screen.

I.6 STING inhibitor

The STING inhibitor H151 (InvivoGen, Cat # inh-h151) was used at 15 µM and kept in culture for the duration of the cell viability experiments (3 or 5 days, as indicated).

I.7 EGFR inhibitors

Gefitinib (ZD1839) (Cat #S1025) and Cetuximab (Cat #A2000) were purchased from Selleck Chemicals, and Erlotinib hydrochloride (Cat #ab141930) was purchased from Abcam.

I.8 Primers

Primers for SDM experiments were designed using the NEB Base Changer online tool and their sequences are listed in the table below:

Table: Primers used for SDM

Primer name	Sequence (5' to 3')
EXO1-S815A-Forward	GAAACCCCTGgccCCAGTCAGAG
EXO1-S815A-Reverse	TTACAAGGAGGAAGCTTTTCAGAATCTTTTTTAAATC
EXO1-T824A-Forward	CATCCAACTAgctCCAGAAGCGG
EXO1-T824A-Reverse	TTATCTCTGACTGGGGACAG
EXO1-R842A-Forward	CCGTGTTCAAgcaGCAATATTCCAG
EXO1-R842I-Forward	CCGTGTTCAAataGCAATATTCC
EXO1-R842A-Reverse	CCACATTCAGGTTTGTTAAATATATC
EXO1-RXI/AAA-Forward (using R/A as template)	TCAAGCAGCAgcaTTCCAGTAAGGATCC
EXO1-RXI/AAA-Reverse (using R/A as template)	ACACGGCCACATTCAGGT
EXO1-I844A-Forward	TCAAAGAGCAgcaTTCCAGTAAGGATCCAC

EXO1-I844A-Reverse	ACACGGCCACATTCAGGT
EXO1-F845A-Forward	AAGAGCAATAgccCAGTAAGGATCCAC
EXO1-F845A-Reverse	TGAACACGGCCACATTCA
EXO1-Q846A-Forward	AGCAATATTCgcgTAAGGATCCACCATG
EXO1-Q846A-Reverse	CTTTGAACACGGCCACAT
EXO1-P825A-Forward	CCAACTAACTgcaGAAGCGGAAG
EXO1-P825C-Forward	CCAACTAACTtgtGAAGCGGAAGAG
EXO1-P825A-Reverse	ATGTTATCTCTGACTGGGG
EXO1-TP/AA-Forward (using T/A as template)	CCAACTAGCTgcaGAAGCGGAAG
EXO1-TP/AC-Forward (using T/A as template)	CCAACTAGCTtgtGAAGCGGAAG
EXO1-TP/AA-Reverse	ATGTTATCTCTGACTGGGGAC
RRM2-F52A-Forward	GAGGAGGATCGCCCAGGAGCCCACG
RRM2-F52A-Reverse	GCGGTCTTGCTGGCCAGG
RRM2-Q53A-Forward	GAGGATCTTCgcgGAGCCCACGGAGCC
RRM2-Q53A-Reverse	CTCGCGGTCTTGCTGGCC
RRM2-R49A-Forward	CAAGACCGCGgcgAGGATCTTCCAGGAGCC
RRM2-R49A-Reverse	CTGGCCAGGACGCGGGTC
RRM2-I51A-Forward	CGCGAGGAGGgccTTCCAGGAGC
RRM2-I51A-Reverse	GTCTTGCTGGCCAGGACG

I.9 Software

Mass spectrometry files were analysed using MaxQuant (by Iolanda Vendrell). Quantified data was further analysed using Perseus software version 1.6.2.2 (by Iolanda Vendrell and additionally by myself). Enrichr, a comprehensive gene set enrichment analysis web server, was used to look for the most impacted pathways in the total proteome mass spectrometry samples. The sequence matching website *Scansite 4.0* was used to match the newly refined Cyclin F degron [S/T]Px(2,20)RxIF to potential Cyclin F substrates. cBioPortal was used to scan the 10,967 samples in its TCGA PanCancer Atlas Studies dataset for *EXO1* mutations in cancer. The Venn diagram generating

online tool Venny (https://www.stefanjol.nl/venny) was used to visualise protein and GG peptide overlap when comparing the data quality for DIA, DDA and TMT data acquisition and labelling methods. GraphPad Prism software version 8.0.2.263 was used for clonogenics and cell survival assay data visualisation and figure generation. MARS data analysis software (BMG Labtech) was used for measuring protein and DNA concentration and for Resazurin-based cell viability assays. iBright™ FL1500 Imaging System (Thermo Fisher Scientific) was used for membrane developments and protein quantification for Western blots. FiberVision® (Genomic Vision) coverslip scanner was used for visualising DNA fibers and identifying as well as quantifying replication events for the DNA fiber combing experiment. The online figure generator tool BioRender was used for making illustrations for this thesis where indicated.

II. Methods

II.1 Cell Culture

II.1.a Cell line maintenance

Human HEK293T and HeLa cells were obtained from ATCC, and LIM1215 KRAS WT and KRAS G12V$^{+/-}$ were purchased from Horizon Discovery (HD 116-006). All cell lines were cultured in media containing 10% FBS, 100 U/mL Penicillin and 100 mg/mL Streptomycin (Millipore), and passaged when 60-90% confluent (every 2-4 days). HEK293T and HeLa cell lines were cultured in DMEM media and LIM1215 cell lines were cultured in RPMI1640 media. All cell lines were regularly screened for mycoplasma using a MycoAlert™ Mycoplasma Detection Kit (Lonza).

II.1.b Cryopreservation of cell lines

Cells at 70-90% confluency were trypsinised, resuspended in 5 mL of fresh media, and centrifuged at 180 rcf for 3 min at room temperature. The pellet was then resuspended in 1 mL of freezing media (10% DMSO in FBS), and transferred to a 2 mL cryovial (Thermo Fisher Scientific). The cryovial was immediately placed on dry ice, and then transferred to liquid nitrogen for long-term storage.

To defrost cells from liquid nitrogen, cryovials were quickly thawed in a 37°C water bath.The thawed cell solution was transferred to 9 mL of pre-warmed fresh media, gently mixed by falcon tube inversion and centrifuged at 180 rcf for 3 min. The pelleted cells were resuspended in fresh media and plated in a T-175 flask. The media was changed the following day, and cells were typically ready to be split after 48-72 h.

II.1.c Transient plasmid transfection

Cells were seeded the previous day prior to transfection. HEK293T cells were transfected using the reagent Polyethylenimine (PEI) Max (Polysciences, Cat #23966). PEI solution was prepared by dissolving 125 mg PEI powder (bought from Polysciences, Cat #23966) in 50 mL of 1×HBS (see general laboratory buffers). Solution was filtered using a 0.22 µm membrane and aliquots were stored at -80°C.

LIM1215 cells were transfected using Lipofectamine Stem Transfection Reagent (Thermo Fisher Scientific). 3 µL of PEI solution or 5 µL Lipofectamine reagent was used per 1 µg of DNA and mixed in DMEM (without any supplement) or Opti-MEM I Reduced Serum Medium (Thermo Fisher Scientific), respectively, in a total volume of 200 µL for a well in a 6-well plate or 400 µL for a 10-cm dish.

The transfection mixture was vortexed and incubated for 15 min at room temperature before adding dropwise to cells. Cells were harvested 24-48 h post-transfection.

II.1.c.i Plasmids

Transient transfection plasmids were constructed using the pcDNA3.1(+) or pEGFP-C1 vectors from Invitrogen or Clontech, respectively, and many of them have derivative plasmids that harbour engineered mutations (mutations are not listed in the table below) brought about by SDM experiments carried out by me. Plasmids used are listed below:

Recombinant DNA
pCDNA3.1 *CCNF* - FLAG
pCDNA3.1 *RRM2* - FLAG
pCDNA3.1 *EXO1* - FLAG
pCDNA3.1 *MAP2K6* - FLAG
pEGFP-C1 *EXO1*
pEGFP-C1 *CCNF*
pCDNA3.1-Ubiquitin -HA

II.1.d Transient siRNA transfection

HEK293T or LIM1215 cells were seeded at 24 h before transfection at a density that warrants 60-80% confluence at the time of transfection. HEK293T or LIM1215 cells were transfected for 24 h using HiPerfect Transfection Reagent (Qiagen) or Lipofectamine RNAiMAX Transfection Reagent in Opti-MEM I Reduced Serum Medium (Thermo Fisher Scientific) according to the manufacturer's instructions. For combination siRNA/cDNA transfections, HEK293T cells were transfected first with the siRNA for 24 h after which they were transfected additionally with the cDNA for a further 24 h, and harvested after the 48 h total. The siRNAs used in this study were all purchased from Ambion,

and their catalogue numbers are listed in the table below along with their working concentrations.

II.1.d.i Table: siRNA list

Name	Working conc.	Manufacturer and cat. number
si*CCNF*	15 nM	Ambion, s2527
si*PIN1*	15 nM	Ambion, s10545
si*NTC*	15 nM	Ambion, 4390843

II.1.e CRISPR-Cas9 generated stable cell lines

Cyclin F knock-out in LIM1215 cells was carried out using a plasmid (pX458, Addgene, Cat #48138) containing the sgRNA targeting exon 2 of *CCNF* (CTCAAGATGGTCAGGTTTCG), Cas9, and a C-terminal GFP tag was purchased from Addgene. The plasmid was transfected into LIM1215 *KRAS* WT and LIM1215 *KRAS* G12V$^{+/-}$ cells using Lipofectamine Stem Transfection Reagent (Thermo Fisher Scientific) in a ratio of 5 µL transfection reagent to 1 µg DNA . Transfection success was confirmed 24 h post-transfection using a fluorescence microscope (to visualise GFP signals), cells were trypsinised into single cells, resuspended in PBS and sent for Fluorescence-Activated Cell Sorting (FACS) analysis to sort out the GFP-positive cells and seed them individually into a 96-well plate (1 cell/well) in order to generate a population of cells derived from a single clone.

Cyclin F protein expression in the LIM1215 selected clones was analysed by immunoblotting. For each cell line (LIM1215 *KRAS* WT *CCNF* K/O and LIM1215 *KRAS* G12V *CCNF* K/O), clones with no visible Cyclin F expression were selected and aliquots were cryogenically saved as stocks. Of these clones,

at least one for each cell line was used for further experiments (mainly clone #1 for LIM1215 *KRAS* WT *CCNF* K/O and clone #8 for LIM1215 *KRAS* G12V *CCNF* K/O.

EXO1 CRISPR knock-out in HeLa cells was generated using the Synthego multi-guide method. The sequence of the sgRNA guides is detailed below:

EXO1 + guide_#0: C*C*U*AUCAGUAGGUUCACCUU (+ Synthego modified EZ scaffold)

EXO1 + guide_#1: U*G*U*GAGGAAGUAUAAAGGGC (+ Synthego modified EZ scaffold)

EXO1 + guide_#2: U*U*U*GGCACCAUGGGGAUACA (+ Synthego modified EZ scaffold)

II.2 Protein analysis and biochemistry techniques

II.2.a Cell lysis and protein sample preparation

Cells were collected in 1x PBS and harvested by centrifugation at 180 rcf. Cells were lysed in roughly 5x the pellet volume with NP-40 based lysis buffer supplemented with β-glycerophosphate, phenylmethylsulfonyl fluoride (PMSF), protease inhibitor cocktail (PIN) (Sigma-Aldrich, P8340) and okadaic acid, and incubated on ice for 30 min. After centrifugation, protein concentration for cell lysates was quantified using the Lowry protein kit (Bio-Rad) in a 96-well format. The 96-well plate was then read with the SPECTROstar Nano spectrometer (BMG Labtech) at 650-750 nm using MARS data analysis software (BMG Labtech). Protein concentrations were interpolated from a BSA standard curve and the appropriate volume of lysate was added to 4x Laemmli buffer

(NuPAGE™ lithium dodecyl sulfate sample loading buffer), Thermo Fisher Scientific) supplemented with β-mercaptoethanol and diluted to 1x, then finally boiled for 10 min at 95°C.

II.2.b Co-immunoprecipitation

Cell lysates were incubated with 10 µL bead slurry (per 1 mg lysate) of FLAG M2 agarose beads (Sigma-Aldrich), GFP-trap agarose beads (ChromoTek) or Pierce anti-HA agarose beads (Thermo Fisher Scientific) for 2 h at 4°C. The samples were then washed 3 times in lysis buffer, and resuspended then boiled in 30 µL of 1x Laemmli buffer.

II.2.c GTP-RAS activity assay

RAS can be present in both the active GTP-bound state or the inactive GDP-bound state. Downstream effectors of RAS proteins recognise the GTP-bound form with high specificity, which is why the RAS-binding domain of the RAS effector c-RAF is used in this assay to pull-down active RAS. This RAF domain is conjugated to agarose beads which are used as the resin for this pull-down assay. For each sample, 780 µg lysate was incubated with 10 µL of conjugated beads for 50 min at 4°C with gentle agitation. Following bead washes, samples were boiled in the correct dilution of Laemmli buffer to get 1x Laemmli final concentration then immunoblotted, after which RAS levels were detected using a pan-RAS antibody (recognising all 3 RAS isoforms) included in the kit.

II.2.d *In vivo* ubiquitylation assay

HEK293T cells were plated in 10-cm dishes to be 60-70% confluent the following day for transfection. Cells were then transfected using the indicated

plasmids for 24 h. Cells were treated with 5 µM MG132, a 26S proteasome inhibitor, for 4 h prior to harvest. Cells were then lysed in ubiquitylation lysis buffer. Ubiquitylated proteins were immunoprecipitated using resins against their tag (FLAG/GFP) by incubation at 4°C for 4 h in ubiquitin dilution buffer (to dilute SDS in samples so that the antibody on the beads is not denatured by the highly concentrated SDS). After 3 rounds of washes using the ubiquitin wash buffer, beads were resuspended then boiled in 30 µL of 1x Laemmli buffer. Poly-ubiquitylated forms of the proteins were detected by immunoblotting using antibodies against their tags.

II.2.e Protein half-life (Cycloheximide) assay

Cells were transfected as indicated. After 48 h, cells were treated with 50 µg/mL Cycloheximide to inhibit further protein synthesis. Samples were collected at the indicated time points over a 5 h period, and protein levels were detected by Western blot.

II.2.f Cell cycle profile

LIM1215 cells were labelled with 10 nM EdU 30 min before harvesting. Cells were then trypsinised into singlets, collected by centrifugation and resuspended in 4% PFA in PBS (Santa Cruz, sc-281692) and incubated for 15 min at room temperature away from light. After PBS washes, cells were blocked with 1% (w/v) BSA + 0.5% Triton X-100 in PBS for 1 h at room temperature. A click reaction was prepared in the following order: 0.1 M Tris-HCl, 0.1 M Sodium Ascorbate, $CuSO_4$ and Alexa-fluor 647 (Thermo Fisher Scientific, A10277). Following cell washes with PBS, this reaction solution was added to the cells and allowed to react for 1 h at room temperature away from light. Click reaction was

quenched using 1% (w/v) BSA in PBS to exhaust the Cu^{2+} ions, cells were washed, resuspended in 5 µg/mL DAPI and sent for FACS analysis.

II.2.g *In vitro* phosphorylation assay

II.2.g.i *Full length proteins*

In a total volume of 50 µL of 1x kinase buffer (Cell Signalling Technology, Cat #9802S), 2 µg of purified His-MBP-TEV-EXO1 WT or His-MBP-TEV-EXO1 T824A (negative phosphorylation control) was mixed with 400 ng of either Cyclin A-CDK2 (Cat #PV6289) kinase or Cyclin E-CDK2 kinase (Thermo Fisher Scientific, Cat #PV6295) and 200 µM ATP (Cell Signalling Technology, Cat #9804S). After mixing, the solution was incubated for 30 min at 30˚C after which the reaction was stopped by boiling in Laemmli buffer, then samples were immunoblotted.

II.2.g.ii *Biotinylated peptides*

Biotinylated peptides were custom ordered from LifeTein and dissolved to make up 1 mM stock solutions according to the manufacturer's instructions which take into account the polarity of the peptide (https://www.lifetein.com/handling_and_storage_of_synthetic_peptides.html). 6x 10-cm dishes of HEK293T cells harvested at 80% confluence were used for this experiment.

For binding assays, 50 µL streptavidin beads slurry (Strep-Tactin® Sepharose® 50% suspension, IBA, Cat # 2-1201-002) /sample were washed 3x with low-salt Tris buffer and pre-incubated with 20 µM peptides in a total of 400

µL low-salt Tris buffer for 2 h at 4°C. For this step, peptides were dissolved in low salt buffer at 2x their final concentration first, then their pH was adjusted (using 10x dilute ammonia/acetic acid, 3-5 µL at a time) to neutrality using pH paper, after which they were diluted 2x into the Eppendorf tube containing the 50 µL bead slurry. Following this, the beads were washed 3x with low salt Tris buffer and incubated with 250 ug cell lysate in a total of 400 µL at 4°C for 2 h. After the 2 h incubation, beads were briefly spun down and washed 3x with high-salt Tris buffer. 40 mL of 1x Laemmli buffer was added to the beads and they were boiled for 5-10 mins, after which they were ready for immunoblotting.

II.2.h SDS-PAGE and Western blotting

For SDS-Polyacrylamide Gel Electrophoresis (SDS-PAGE), proteins were resolved using Bolt™ 4-12% Bis-Tris Plus gels (Invitrogen/Life Technologies), alongside a PageRuler protein ladder (Thermo Fisher Scientific, 026616) for molecular weight reference. Gels were run using Invitrogen gel tanks at 170 V for 30 min, using MOPS-SDS or MES-SDS Running Buffers (Invitrogen/Life Technologies) for high or low molecular weight proteins, respectively. Gels were then transferred onto nitrocellulose membranes (Millipore) using a wet transfer system run for 1 h at 20 volts. Membranes were then washed once in 1 x PBS-T and blocked in 5% (w/v) milk in 1x PBS-T for 1 h at room temperature.

Primary antibodies against the protein of interest were diluted in 5% (w/v) milk (or 3% (w/v) BSA for antibodies detecting phosphorylated proteins) in 1x PBS-T and supplemented with 0.02% (w/v) sodium azide, and incubated with the membrane overnight 4°C. The next day, membranes were washed three times in 1 x PBS-T (5 mins/wash) and incubated with the appropriate HRP-conjugated

secondary antibody (diluted in 5% (w/v) milk in TBS-T) for 1 h at room temperature. Membranes were then washed three times in 1 x PBS-T (10 mins/wash), drained, and incubated with enhanced chemiluminescent substrate detection reagent (Thermo Fisher Scientific Fisher) for 2 mins. Proteins were visualised using double-sided X-ray films (Scientific Labs) and in more recent experiments via digital development using the iBright™ FL1500 Imaging System (Thermo Fisher Scientific).

II.2.i Protein purification using ÄKTA start

Recombinant EXO1 constructs were transformed into *E. coli* BL21 (DE3) cells. Single colonies were picked into 15 mL LB supplemented with 50 µg/µL Ampicillin and incubated overnight at 37°C with shaking. This starter culture was then diluted 1:100 into 1 L of Terrific Broth (TB, Sigma-Aldrich) supplemented with Ampicillin, and incubated at 37°C with shaking until an OD600 of 0.5 was reached. Protein production was then induced with 0.4 mM isopropyl β-D-1-thiogalactopyranoside (IPTG). Induced flasks were incubated overnight in a 16°C shaker.

Cells were then pelleted at 6,000 rcf for 15 min, and resuspended in 20 mL lysis buffer per 1 L of culture, then lysed for 30 min on ice. Lysates were sonicated for 6 x 15 sec with 15 sec breaks, then cleared by centrifugation for 10 min at 20,000 rcf.

Lysates were then purified using the ÄKTA Start system (GE Healthcare) using a His 1 mL column (GE Healthcare) through an Affinity AC run (Column vol. = 1 mL, column flow rate = 1 mL/min, pressure = 0.5 MPa, collection vol. = 1.8 mL). Fractions were analysed by SDS-PAGE followed by Coomassie

blue staining, and were then dialysed overnight using SnakeSkin™ Dialysis Tubing (Thermo Fisher Scientific). The next day an Amicron Ultra-15 30K centrifugal filter (Merck, UFC903024) was used to concentrate the solution and eliminate contaminants that are less than 30 kDa in size. Protein concentrations were determined using the NanoDrop's Protein A280 reading (Thermo Fisher Scientific).

II.3 Molecular and cellular biology techniques

II.3.a Preparation of media and agar plates

Bacteria was cultured in Luria-Bertani (LB) broth. This was prepared by dissolving 25 g of LB powder (Sigma-Aldrich) in 1 L of sterile, double distilled water, which was then autoclaved. LB agar was prepared by dissolving 35 g of LB agar in 1 L of double distilled water and sterilised by autoclaving. LB agar was then supplemented with the appropriate antibiotic (only after it has cooled down to 50°C) before pouring the agar into sterile 10-cm Petri dishes in a sterile environment (~20 mL/plate). Plates were allowed to set at room temperature and left on the bench overnight to test for contamination, then moved to 4°C storage the next day.

II.3.b Transformation of bacteria

Bacterial transformations for plasmid production were carried out using Gold Efficiency α-Select Competent Cells (Bioline, 85027), an *E. coli* competent strain DH5α with recA1 and endA1 mutations to prevent recombination and digestion. 50 µL of competent cells were thawed on ice prior to addition of 1 µg of DNA, and incubated on ice for 30 min. The bacteria were then heat shocked at

42°C for 1 min, followed by an additional 5 min incubation on ice. 500 µL of LB was then added to the bacteria, and bacteria was allowed to grow for 30 min at 37°C with shaking on an Eppendorf Thermo Fisher Scientific mixer. Bacteria was then plated on agar containing the right antibody, and the plating was done at 2 densities: low and high. Colony growth was allowed to take place overnight in a 37°C incubator, and the next morning single bacterial colonies were picked from the LB agar plates. Each picked colony was added to 5 mL of LB supplemented with antibiotics in a 15 mL Falcon tube, and allowed to grow at 37°C overnight in a shaking incubator. The next day, the plasmid was extracted using the Qiagen Miniprep kit (Qiagen) and sent for Sanger sequencing (Eurofins or Source BioScience).

II.3.c Agarose gel electrophoresis

DNA analysis was performed using 1% (w/v) agarose gels. Gels were prepared by dissolving 1 g of agarose in 100 mL 1x TAE buffer. The mixture was heated to boiling point, and then allowed to cool to approximately 50°C prior to the addition of 10 µL SYBR Safe DNA Gel Stain (Stratech Scientific Ltd) per 100 mL of agarose mixture. DNA samples were diluted with 6x DNA Gel Loading Dye (Thermo Fisher Scientific) prior to loading, and run alongside a Generuler 1 kb DNA molecular weight marker (Thermo Fisher Scientific). Gel electrophoresis was carried out in 1x TAE buffer at 120V.

II.3.d Small- and large-scale preparation of plasmid DNA

Mini- (small-scale) or Maxi- (large-scale) preparation of DNA was

performed using Qiagen kits according to the manufacturer's instructions. This method is based on alkaline lysis. In brief, a bacterial cell pellet is lysed in a solution containing sodium hydroxide and SDS. The alkaline sodium hydroxide denatures bacterial DNA – both genomic and plasmid. Upon neutralisation using a buffer containing acetate, only plasmid DNA can re-anneal due to its much smaller size. Genomic DNA remains precipitated, and can therefore be removed via centrifugation. The plasmid DNA remains in solution, and can be purified using a cation exchange column which binds DNA in low-salt, and is eluted with high salt.

II.3.e Site-directed mutagenesis

Site directed mutagenesis was carried out using the SDM primers detailed previously along with the high-fidelity polymerase 'Q5 Hot Start High-Fidelity 2x Master Mix' (New England BioLabs). The PCR mix contained 15 ng of template, 10 µM of each forward and reverse primer and 1 U of polymerase provided in the kit. The PCR mix was placed into a Thermo Fisher Scientific cycler programmed for an initial denaturation at 98°C for 30 sec, followed by 25 cycles of 98°C for 10 sec, then primer annealing temperature (50-72°C) for 20 sec, then 72°C for 30 sec per kb of template and then a final extension at 72°C for 2 min after which the reaction mixture was kept at 4°C until further use. The PCRproduct was then treated with 1 U KLD Enzyme Mix (DpnI, New England BioLabs) in 1x KLD Reaction Buffer from the same kit, and incubated at room temperature for 30 min to digest the parental template. The digest product was then directly transformed into competent DH5α bacteria as outlined previously,and plated onto LB agar plates containing the appropriate antibiotics. The antibiotic-resistant clones were picked and expanded into 5 mL LB supplemented with antibiotics overnight. The

plasmid was extracted using the Qiagen Miniprep kit and sent for Sanger sequencing (Eurofins or Source BioScience).

II.3.f Determination of DNA purity and concentration

DNA concentration was determined by measuring the optical density (OD) at A_{260} using the SPECTROstar Nano spectrophotometer (BMG LabTech). Generally, a dsDNA sample of 1 µg/µl has an A_{260} of 50. An A_{260}/A_{280} ratio of ≥1.8 was used to confirm that the DNA was free from protein contamination.

II.3.g DNA fiber combing assay

For the replication combing assay (RCA), Hela and HeLa *CCNF* K/O cells were seeded at 120,000 cells/dish into 10-cm dishes 1 day before labelling with the nucleotide analogues (5-chloro-2′-deoxyuridine 'CldU', 60 µM, 30 min then 5-iodo-2′-deoxyuridine 'IdU', 762 µM, 30 min).

Using FiberPrep DNA Extraction Kit (http://www.genomicvision.com/wp-content/uploads/User-Manual_FiberPrep-EXT-001_version-3_September-2017.pdf), agarose-plugs were prepared (50,000 cells/plug) and proteins were digested in proteinase K-containing buffer for 16 h at 50°C. Plugs were then treated with agarase for 16 h at 42°C. Solution was then poured into a DNA reservoir and combing was done on silanised CombiCoverslips using FiberComb® Molecular Combing System (http://www.genomicvision.com/wp-content/uploads/IFU-MCS-05__English.pdf).

Coverslips were dehydrated at 60°C for 2 h, then denatured in 0.5 M NaOH + 1 M NaCl for 8 min at room temperature, and dehydrated once more. Coverslips were saturated using Block Aid solution for 30 min at 37°C, and then probed for

IdU and CldU with primary antibodies (2 µL mouse anti-BrdU + 1 µL rat anti-BrdU in 22 µL Block Aid/coverslip) for 2 h at 37°C followed by secondary antibodies (1 µL goat anti-mouse Cy3.5 + 1 µL goat anti-rat Cy5 in 23 µL Block Aid/coverslip) for 1.5 h at 37°C. Coverslips were then probed for ssDNA with primary antibody (4 µL mouse anti-ssDNA in 21 µL Block Aid/coverslip) for 2 h at 37°C followed by secondary antibody (2 µL goat anti-mouse BV480 in 23 µL Block Aid/coverslip) for 45 min at 37°C.

Finally, coverslips were mounted on FiberVision sample holders and the RCA Green First AFIs programme was run using the FiberVision automated scanner. Scans were visualised using FiberStudio software.

II.3.h Resazurin cell viability assay

LIM1215 cells were seeded in triplicates in 96-well plates and allowed 16-24 h to attach, following which they were treated with the indicated drugs (EGFRi, p38 MAPKi, STINGi) by adding a volume (50 µL) of the 2x final concentration drug solution to an equal volume (50 µL) of the media of seeded cells (to avoid LIM1215 cells detaching upon decanting) to make up a 1x final drug concentration. After 3 days (or 5 days in the case of STINGi) of drug treatment, 10x Resazurin stock solution was diluted in complete media to 2x its final concentration and once again added in equal volume (100 µL) to the volume of media already in the wells (100 µL) to make up a final 1x Resazurin working solution. Plates were incubated for 2 h (up to 4 h) at 37°C, after which fluorescence was measured using the POLARstar OMEGA plate reader (excitation: 544 nm, emission 590-610 nm) and recorded using the MARS data analysis software (BMG Labtech).

II.3.i Exposure to γ-irradiation

All irradiations were carried out in 10-cm dishes using a Gamma Service® GSR D1 irradiation containing a Cs^{137} source. The dose rates of the system, as determined by the supplier, was 1.938 Gy/min and 1.233 Gy/min based on the distance from the source. Samples were positioned on shelf 1 and the exposure times were calculated based on these dose rates for each indicated sample.

II.3.j Clonogenic survival assay

HeLa parental and HeLa *CCNF* K/O cells were seeded in triplicates in 6-well plates and allowed to attach for 24 h. Cells were then treated with the indicated doses of ionising radiation (0-6 Gy), after which they were left to recover in an incubator (37°C, 5% CO_2) for 14 days. During the 14-day period the media was changed every 5 days for the untreated controls, and after the 14 days the media was removed, the wells carefully washed 2 mL of 1xPBS each, then stained with 2 mL crystal violet solution for 1 h on a rocker set to very low speed. Crystal violet was decanted afterwards, wells were carefully rinsed in H_2O and left to dry, and finally colonies were manually counted. The surviving fraction was calculated as the number of colonies in the treated plate divided by the number of colonies in the untreated control plate (while normalising for plating efficiency) using the below equations.

Plating efficiency = 100x (# of colonies formed/# of cells seeded)

Surviving fraction = 100x (# of colonies formed after IR/# of cells seeded x plating efficiency)

The surviving fractions were then fitted to a linear quadratic equation (below) using GraphPad Prism software version 8.0.2.263 (Brenner, 2008),

Where α and β are constants determined in GraphPad Prism that represent two survival response rates to DNA damage (Brenner, 2008).

$$\text{Surviving fraction} = e^{-(\alpha \times \text{IR dose in Gy}) + \beta \times (\text{IR dose in Gy})^2}$$

II.4 Liquid chromatography-tandem mass spectrometry

For the FLAG-*RRM2* and GFP-*EXO1* LC/MS, both cDNA constructs were transfected in HEK293T cells for 48 h. The HEK293T cells were then lysed, and the FLAG-*RRM2* and GFP-*EXO1* separately purified using Anti-FLAG M2 affinity gel beads (Sigma-Aldrich) and GFP trap agarose beads (ChromoTek), respectively. The co-immunopurified material was then eluted by competition using 1x FLAG peptide (Sigma-Aldrich), or just by 10 mM Tris 2% (w/v) SDS in the case of the GFP pull-down. Supernatant material was processed in collaboration with Professor Benedikt M Kessler's group, specifically Iolanda Vendrell (Target Discovery Institute, University of Oxford). There, the eluted material was subject to two rounds of chloroform-methanol precipitation. Samples were then resuspended in 6 M urea, 100 mM ammonium acetate pH ~8 and subjected to in-solution trypsin digestion. The digested peptides were analysed using a Nano-Acquity-UPLC (Waters) coupled to an Orbitrap Velos tandem mass spectrometer (Thermo Fisher Scientific Scientific) as described (Raducu et al., 2016). The LC/MS data were processed using published guidelines and the spectra compared against the SwissProt database (UniProt_SwissProt, human 20,353 sequences).

The resulting LC/MS data were then processed in-house by subtracting

agarose binding proteins downloaded from the Contaminant Repository for Affinity Purification (http://www.crapome.org/).

II.5 UbiFast

This experiment was done in collaboration with Professor Benedikt M Kessler and Iolanda Vendrell. Samples of the 4 LIM1215 cell lines were prepared according to the instructions described in depth in the protocol 'PTMScan® HS Ubiquitin/SUMO Remnant Motif (K- ε-GG) Kit' from Cell Signalling Technology, Cat #59322). In brief, cells were lysed using the lysis buffer suggested in the kit (250 mg SDS + 250 µL of 1 M TEAB + 4.75 mL water/ sample), reduced and alkylated, then trypsinised overnight to digest the proteins into peptide fragments. The next day the digested peptides were eluted and dried, and the day after they were resuspended in the binding buffer supplied by the kit and then used for a pull-down assay using magnetic beads conjugated to the highly specific anti K-ε-GG antibody. Aliquots were saved as input prior to the pull-down to enable total proteome analysis alongside the IP analysis.

Data was collected using both the Data-Independent Acquisition method (DIA) and Data-Dependent Acquisition method (DDA). For the DDA, 2 approaches were attempted: label-free quantification (LFQ) and TMT-labelling. On-bead TMT-labelling was followed based on the study by Udeshi *et al* (Udeshi et al., 2020). TMTpro-16plex kit was used and the following steps were followed: labels were split in 2 (half for the total proteome and half for GG IP samples), resuspended in acetonitrile and incubated for 10 min at room temperature on a shaker. 5% (w/v) hydroxylamine was used to quench the reaction, and after extensive washing the beads were eluted using 0.15% TFA.

TMT samples were imagined to be complex, owing to the fact that it required all 4 samples to be combined in one, so high-performance liquid chromatography (HPLC) was used to fractionate the samples. Samples were fractionated into 50 fractions that were concatenated into 10, and then ran on the Orbitrap Velos tandem mass spectrometer (Thermo Fisher Scientific Scientific).

II.6 Statistical analysis

Statistical analysis was carried out using GraphPad Prism6 (GraphPad Software Inc.). Differences between groups were compared using unpaired Student's t-test. Statistically insignificant results are indicated by a missing asterisk for $P>0.05$. Statistically significant results are indicated as * for $P\leq0.05$, ** for $P\leq0.01$, *** for $P\leq0.001$ and **** for $P\leq0.0001$.

For the total proteome analyses, Analysis of Variance (ANOVA) and student's t-test were both applied using Perseus software version 1.6.2.2 (mostly by Iolanda Vendrell) where described in the figures.

3. Results Chapter I: *CCNF-EXO1* Axis Governs Cell Survival Post IR

a. Cyclin F Regulation of EXO1 is Crucial for Post-IR DNA Repair

GBM is the most common malignant primary central nervous system (CNS) tumour in adults (around 15% of all primary CNS tumours, half of all primary malignant brain tumours and 60% of all gliomas) (Ostrom et al., 2019, Ostrom et al., 2022). GBM's 5-year survival rate of 6.8% is the lowest compared to the rest of malignant CNS tumours for which the average is 35.8% (Ostrom et al., 2019).

GBM treatment consists of maximal surgical resection, followed by radiotherapy and chemotherapy. The alkylating agent Temozolomide (TMZ), approved by the FDA for newly-diagnosed GBM patients in 2005, is the gold standard for GBM treatment when administered in combination with radiotherapy and has been shown to improve the dismal GBM prognosis of only 12.1-month (radiotherapy only) to 14.6-month (radiotherapy with TMZ) median survival (Stupp et al., 2005). TMZ works by methylating the DNA at the N^7 and O^6 sites on guanines and the O^3 site on adenines, and its cytotoxicity is mainly attributed to its O^6 guanine methylation which is resolved by the O^6-methyl-guanine-DNA methyltransferase (MGMT) – a DNA repair enzyme (Esteller et al., 2000).

Owing to its role, widespread TMZ resistance in GBM can be largely attributed to MGMT activity, to the extent that the hypermethylation of its promoter (present in around 50% of GBM cases) became a prognostic biomarker for treatment with alkylating agents such as TMZ (Rivera et al., 2010). Indeed,

patients without MGMT methylation show an increase in median overall survival from 14 to 21.2 months (Gilbert et al., 2013, Wick et al., 2014).

Given the inadequate response rates to the main line of GBM therapy – comprised of TMZ and radiation – arising from tumour resistance to TMZ, there is a dire need for novel targets and compounds to synergise with radiotherapy with the mission of improving patient survival. To meet this clinical need, the D'Angiolella lab has conducted 2 sets of IR-coupled CRISPR screens in the GBM cell lines DBTRG (p53 WT) and LN229 (p53 mutant) using a ubiquitin-focused sgRNA library targeting around 600 genes in the ubiquitin system ('*Edit-R Ubiquitin Conjugation sgRNA Pooled Library'*). This commercial library included all E1s, E2s and more than half of CRL E3s – but was missing CRL3s, DCAFs and DUBs. The library was imperfect but it was the most comprehensive of its kind at the time the screening was conducted.

The first of the two was an enrichment screen in the IR-sensitive cell line DBTRG. Following sgRNA-based gene knock-out (10 guides/gene), IR treatment, DNA extraction and sequencing, analysis of the sequencing results showed the change in relative abundance of each sgRNA and hence outlined the loss of which genes has enabled the cells to survive and multiply after DNA damage by IR, thereby enriching these sgRNA-containing cells. Such genes are classified as IR-sensitising, as their loss conferred resistance when the cells were treated with IR.

Contrastingly, the drop-out screen was carried out in the IR-resistant cell line LN229. The sequencing results from this screen showed the loss of which genes led to cell death and hence the drop-out of these sgRNA-containing cells

from the population. These genes are classified as IR-resisting, as their loss conferred sensitivity when the cells were treated with IR.

I chose to focus on the hits from the drop-out screen since the therapeutic approach for following up the hits from this screen seemed more straightforward than that for the enrichment one. Hits from the drop-out screen were mediating resistance to radiotherapy, so the aim would be to deplete them within cells – a strategy our lab is interested in, particularly with regards to PROTAC technology. On the other hand, the therapeutic approach for the enrichment screen would necessitate stabilising the hits to sustain their radio-sensitising activity – an approach that would require the indirect and therefore more complex route of targeting the hits' degraders. For these reasons, data from this screen is not presented in this thesis.

Results from the drop-out screen show Cyclin F to be one of the highest ranking hits among genes protecting cells from IR (Figure 3i.A). The statistical analysis of the hits from this screen was conducted using the online tool CRISPRAnalyzeR – a GitHub-based interactive analysis, annotation and documentation tool for pooled CRISPR screens (https://github.com/boutroslab/CRISPRAnalyzeR).

This finding was validated using a clonogenics assay where the effect of Cyclin F loss on survival ability was observed (Figure 3i.B). Cells without Cyclin F were more sensitive to IR, and this sensitivity increased in an IR dose-dependent manner.

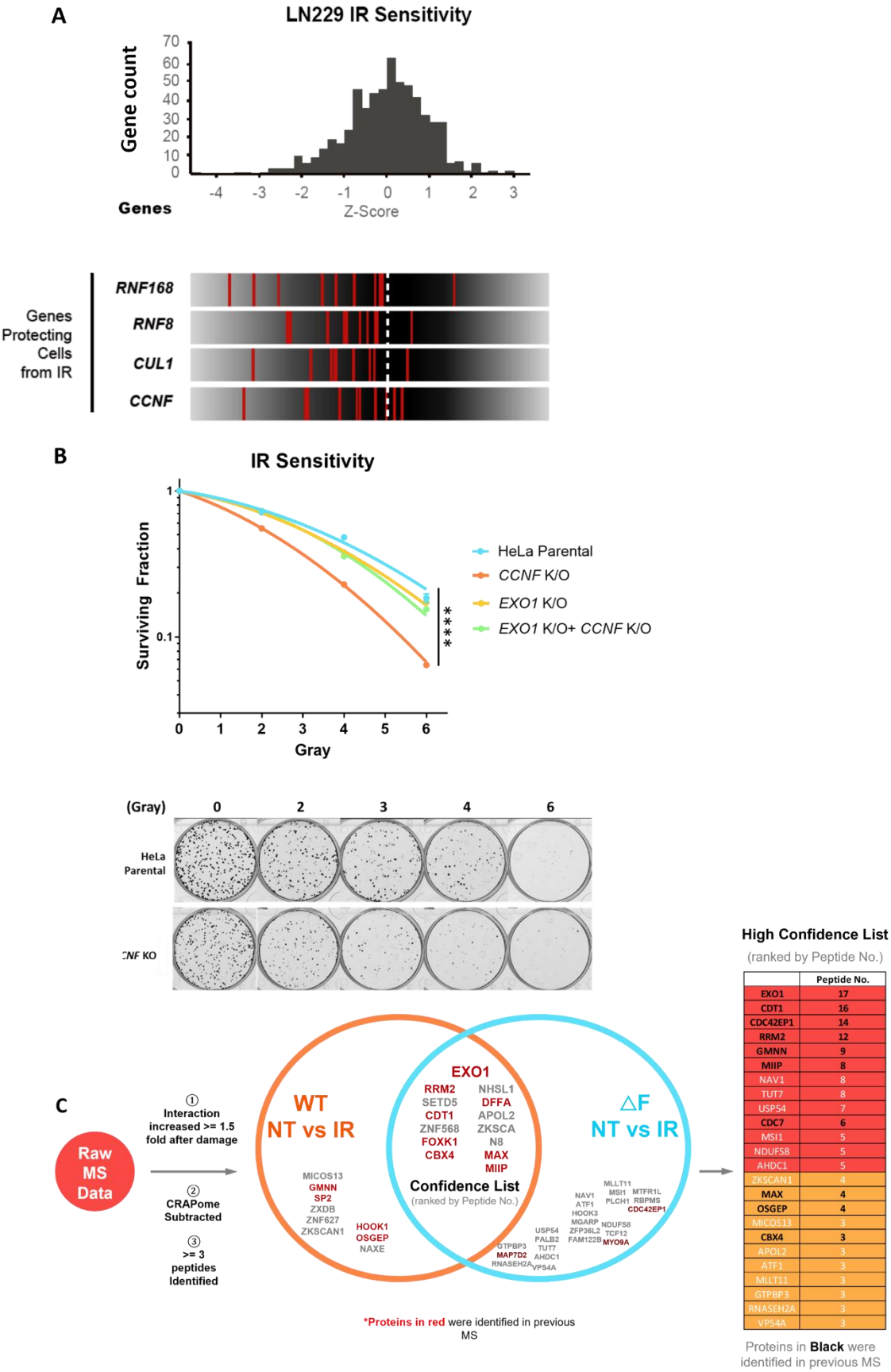


Figure 3i. *CCNF* loss sensitises cells to IR and EXO1 is identified as the top interactor under these conditions.

A. Barcode plot of the data from a drop-out IR CRISPR screen using the E3 ubiquitin library *Edit-R* (Horizon, Cat #VSGH11110) and conducted in the glioblastoma cell line LN229 to search for IR-sensitising genes. Library genes were knocked-out using sgRNA transduction followed by a 7-day puromycin selection, then treated with IR (4 Gy) and allowed a 20-day recovery period. DNA was then extracted, PCR amplified and submitted for next-generation sequencing. Z-scores of one of the top genes, *CCNF*, as well as the positive controls RNF168 and RNF8 are presented in the figure.

B. HeLa, HeLa *CCNF* K/O, HeLa *EXO1* K/O and double K/O cells were treated with IR at the indicated doses (0-6 Gy) and left to recover for 14 days after which surviving colonies (examples from 2 samples shown below) were quantified then plotted.

C. LN229 cells transfected with FLAG-tagged Cyclin F (WT or the non-degrading/non-ubiquitylating mutant ΔF) were IR-treated (12 Gy, 1 h). FLAG-*CCNF* was immunoprecipitated with an anti-FLAG resin and then sent for LC/MS analysis to search for substrates of Cyclin F after IR-induced DNA DSBs. Hits were filtered using a cut-off score of ≥ 1.5 fold increase in interaction in treated samples compared to untreated controls, and peptide number of ≥ 3.

**This figure was made using Hongbin Yang's data.*

To identify the Cyclin F substrates that are relevant for IR-mediated DNA repair, immunoprecipitation followed by a mass spectrometry experiment was conducted to discover the IR-specific interactors of Cyclin F. To this end, two variants of Cyclin F were used as bait: Cyclin F WT and Cyclin F ΔF which lacks the F-box motif required for SCF assembly and E2 recruitment. The Cyclin FΔF is an ideal mutant to capture substrates as it allows the binding of Cyclin F to its substrates yet not the degradation of said substrates. Cells were challenged with IR treatment to identify the Cyclin F interactome that is induced by IR.

Analysis of the liquid chromatography – mass spectrometry (LC/MS) data involved comparing the hits common to both Cyclin F WT and the ΔF mutant, then identifying which of them are enriched at least 1.5x more in the ΔF compared to the WT sample – this was to detect Cyclin F substrates in untreated conditions. The second part of the analysis involved identifying proteins that were enriched

at least 1.5x more in the Cyclin F WT IR-treated sample compared to its untreated control – this was to detect IR-specific substrates of Cyclin F. The reason the ΔF mutant was not used for this IR analysis is that it already is saturated with Cyclin F substrates since it is unable to degrade them, so further stimulation of substrate binding does not alter the amount of bound substrate since the binding is already at capacity and therefore no significant differences would be detected.

This analysis showed EXO1 to be the top hit in terms of increased interaction with Cyclin F following IR damage, as well as enriched interaction with the non-degrading/non-ubiquitylating mutant of Cyclin F (*CCNF* ΔF) (Figure 3i.C). This supported the idea that EXO1 is a potential substrate of Cyclin F after IR. Interestingly the LC/MS analysis identified other hits including the following known Cyclin F substrate and novel interactors: RRM2 (D'Angiolella et al., 2012), CDT1, GMNN and CDC7.

To investigate whether EXO1 accumulation was responsible for the observed sensitisation to IR in cells lacking Cyclin F, stable HeLa cell lines were generated with an *EXO1* knock-out and these cell lines were used for a clonogenics assay (Figure 3i.B). Cells lacking Cyclin F that were previously shown to be significantly more sensitive to IR than their *CCNF* WT counterparts showed a complete rescue upon EXO1 loss in the double knock-out cells lacking both Cyclin F and EXO1 (Figure 3i.B). Results from an earlier experiment prior to *EXO1* K/O generation in which si*EXO1* was used instead were very similar to these generated from the K/O experiment (Supplementary Figure 1). This confirmed that failure to degrade EXO1 resulting in abnormally high levels of this protein is indeed behind the IR-induced drop in cell survival observed in *CCNF* K/O cells.

To validate EXO1 as a substrate of Cyclin F, a ubiquitylation experiment was carried out where tagged versions of the E3 ligase (Cyclin F, both WT and ΔF), the substrate being tested (EXO1) and ubiquitin were all co-expressed. This co-expression took place in the presence of the proteasome inhibitor MG132 which prevents the activity of the proteasome and thus protein degradation, enabling the accumulation of any ubiquitylated substrate. Ubiquitylated substrates appear typically in the form of a ladder/smear in immunoblots, and this ladder corresponds to the molecules of ubiquitin added to the substrates.

In the sample with *CCNF* WT, *EXO1* and Ub co-expression, an intense laddering of EXO1 corresponding to the Cyclin F-mediated ubiquitylated forms of the EXO1 protein can be observed. In contrast, EXO1 is not ubiquitylated when a mutant of Cyclin F (ΔF) lacking catalytic activity is expressed. Accordingly, levels of EXO1 in the blot of the input are reduced due to ubiquitylation only in the presence of Cyclin F WT (Figure 3ii.A).

An additional way to validate that EXO1 is a substrate of Cyclin F is through a Cycloheximide (CHX) chase assay where the half-life of the protein is monitored after blocking protein translation with CHX. In this case I compared the half-life of EXO1 in HeLa cells lacking Cyclin F (*CCNF* K/O) to HeLa parental cells. Data shows that the stability of EXO1 is markedly increased in the *CCNF* K/O cells, similarly to that of published substrates RRM2 and E2F1, providing strong evidence that EXO1 is indeed a ubiquitylation substrate of Cyclin F (Figure 3ii.B). Evidence from further experiments that involved cell synchronisation using a double-thymidine (DT) block narrowed down the window of Cyclin F-mediated degradation of EXO1 to G_2/M, which is expected since this is when Cyclin F levels

are at their peak, and have also shown that failure to carry out EXO1's timely degradation results in its accumulation in mitosis (Supplementary Figure 2).

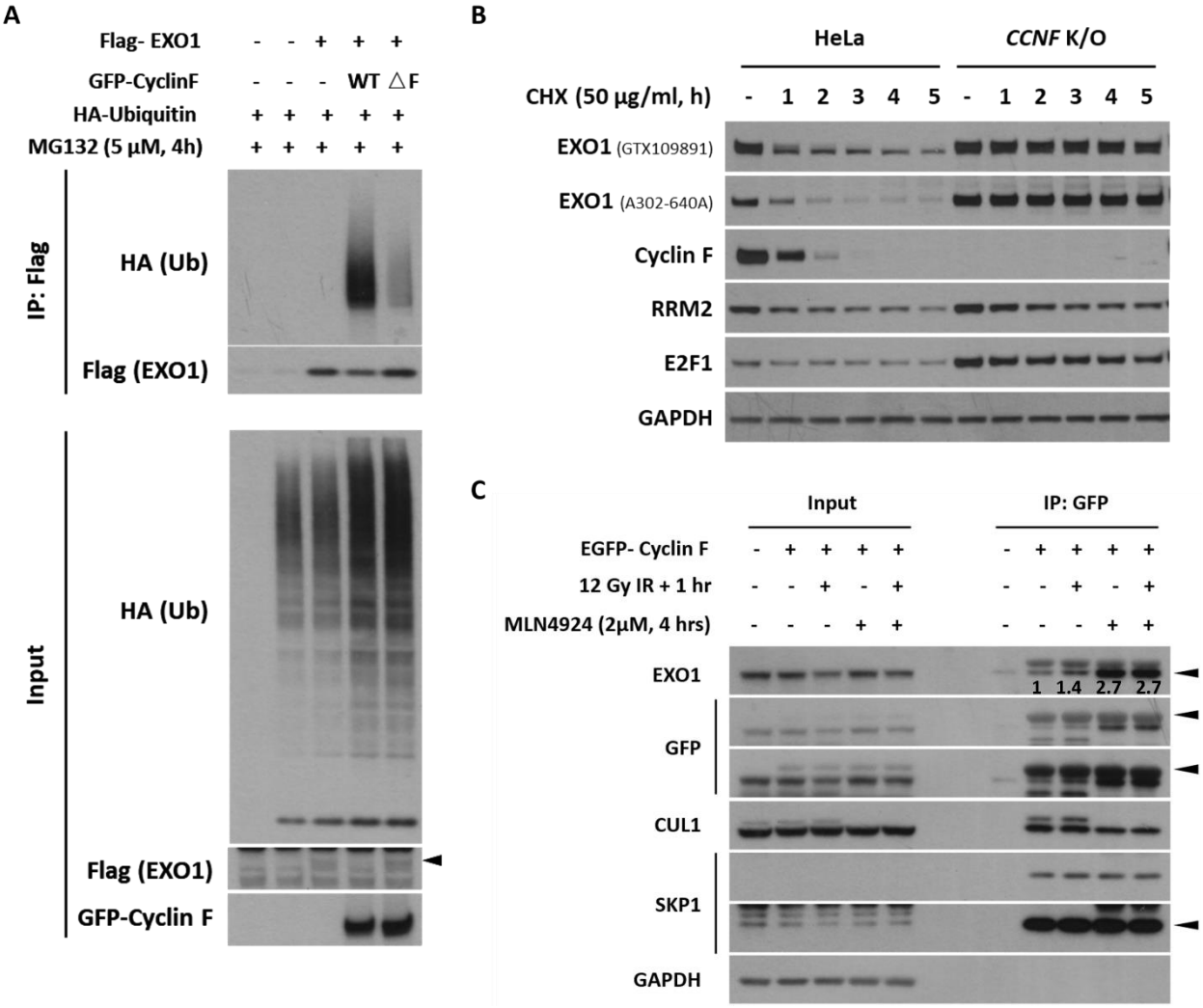


Figure 3ii. EXO1 is targeted for ubiquitylation by Cyclin F in unperturbed cells and is even more strongly targeted after IR.

A. HEK293T cells were co-transfected with GFP-tagged Cyclin F (WT and ΔF), FLAG-*EXO1* and HA-ubiquitin in the presence of the proteasome inhibitor MG132 (5 µM, 4 h). FLAG-*EXO1* was immunoprecipitated with an anti-FLAG resin under denaturing conditions and immunoblotted. Two different EXO1 primary antibodies were used for this blot.

B. HeLa and HeLa *CCNF* K/O cells were treated with Cycloheximide (CHX – 50 µg/mL) for the indicated duration, harvested and lysed using SDS. Indicated proteins were immunoblotted.

C. HEK293T cells were transfected with EGFP-*CCNF* in the absence or presence of the NEDDylation inhibitor MLN4924 as indicated (+). Cells were treated with

IR (12 Gy) where indicated and harvested after 1 h of IR treatment. Tagged Cyclin F was immunoprecipitated with an anti-GFP resin and immunoblotted. *This figure was produced in collaboration with Hongbin Yang.*

Following the validation of EXO1 as a substrate of Cyclin F in untreated cells, I also tested whether EXO1 is targeted by Cyclin F following DNA damage by IR. To examine this, an immunoprecipitation experiment was carried out in cells treated with IR and with the NEDDylation inhibitor (thus indirect inhibitor of CRLs via blocking their activation) MLN4924. As expected, in untreated cells (2nd and 4th lanes) the levels of EXO1 pulled-down with Cyclin F are higher in MLN4924-treated samples (Figure 3ii.C). This is because Cyclin F is still able to bind its substrates yet not able to degrade them as MLN4924 blocks the activity of all CRLs, including CRL1/SCF complexes. This reinforcement of Cyclin F-EXO1 interaction by MLN4924 confirms that EXO1 is a substrate of Cyclin F.

In IR-challenged cells, a similar observation is made where MLN4924 treated cells bind more EXO1 with the pulled-down Cyclin F than in cells with active NEDDylation (3rd and 5th lanes). Most importantly, when comparing cells treated with IR to their untreated controls, an increase in Cyclin F-EXO1 binding (2nd and 3rd lanes) pointing to increased EXO1 targeting by Cyclin F following IR treatment can be seen. This is also reflected in the decreased levels of EXO1 in the input of IR treated cells (3rd lane) which is mostly, yet not completely, rescued by MLN4924 treatment (5th lane).

b. Mechanism of EXO1 Recognition by Cyclin F

Based on the results above it is possible to conclude that EXO1 is a ubiquitylation target of Cyclin F following IR, however, the mechanism used by

Cyclin F to interact with EXO1 had yet to be elucidated. EXO1 has important roles in HR mediated repair and mismatch repair. In line with this, the protein possesses interaction domains to recruit multiple mismatch repair proteins such as MSH2, MSH3 and MLH1 (Figure 3iii.A). Other significant EXO1 domains include the C-terminal PCNA-interacting protein (PIP box) used for PCNA binding and the N-terminal PAR interaction (PIN) motif used for PARP1 binding. To test whether any of these domains are involved in Cyclin F binding, GFP-tagged EXO1 was truncated to generate mutants that lack one or more of these important domains at a time. Data from immunoprecipitation experiments using the generated GFP-tagged EXO1 mutants as bait showed that the C-terminal, more specifically aa 786-846, is the region responsible for Cyclin F binding (Figure 3iii.B).

Upon closer inspection, it was observed that this region had 2 possible phosphorylation sites (SP 815-816 & TP 824-825) and one possible RxI Cyclin F degron site (RAI 842-844) – both highly reminiscent of recognition sites present in Cyclin F's established substrate, RRM2. To examine the possible contribution of each of these sites to Cyclin F binding, site-directed mutagenesis (SDM) experiments were carried out where the relevant amino acids at these sites were mutated to alanines to abrogate their function (Figure 3iii.C). Using the GFP-tagged EXO1 mutants as bait, pull-down experiments showed that the T824A and ΔRxI mutants completely failed to bind Cyclin F, whereas the S815A mutant successfully bound Cyclin F just as strongly as the *EXO1* WT control. This experiment demonstrates that any potential phosphorylation on S815 is dispensable for Cyclin F binding, while TP 824-825 and RAI 842-844 are both essential sites for the binding to occur (Figure 3iii.D).

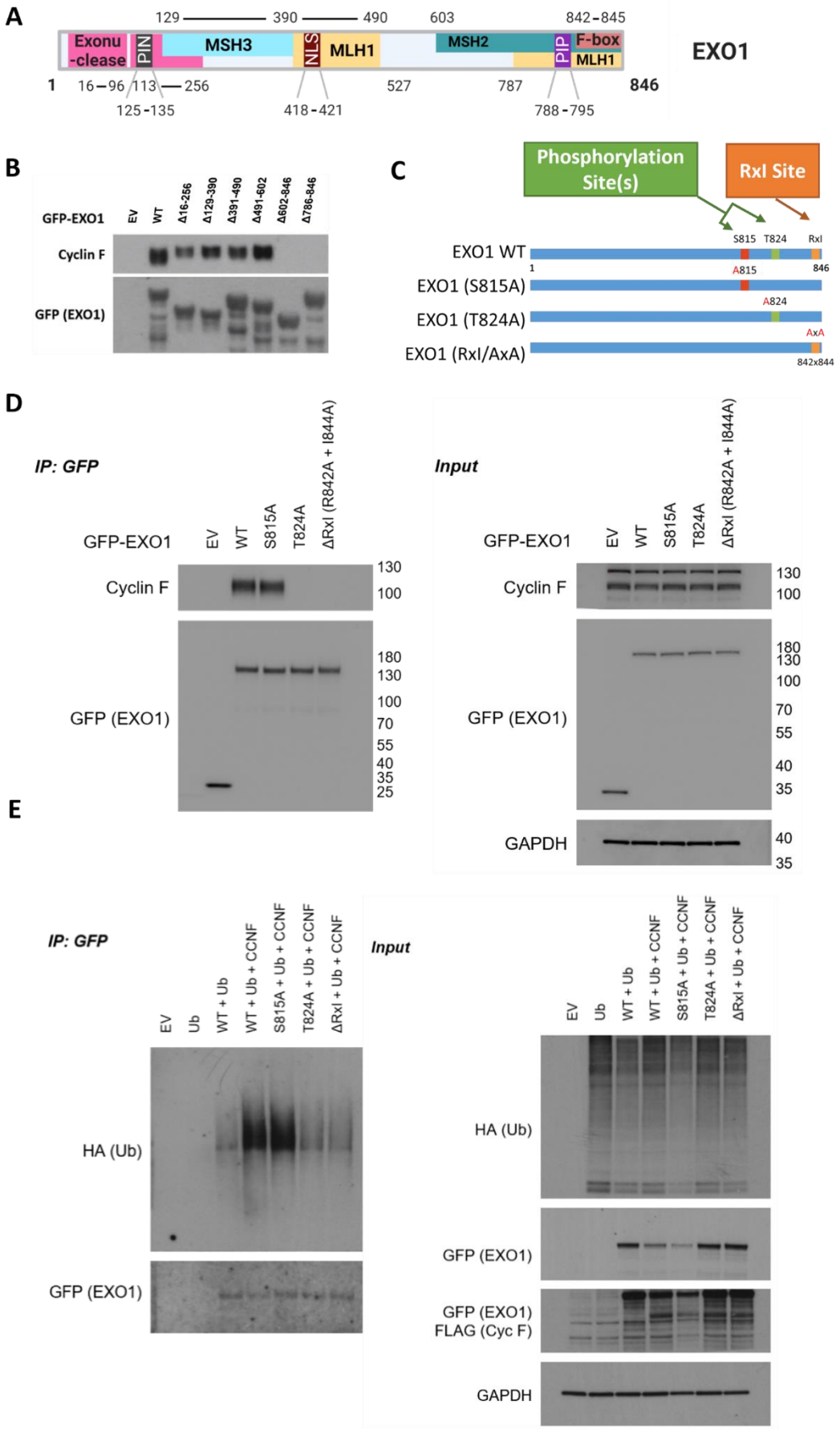


Figure 3iii. Cyclin F binds to EXO1 through its RAI 842-844 degron site following priming phosphorylation on T824A.

A. Schematic of EXO1's significant interaction domains including binding sites to MSH2, MSH3, MLH1, PCNA and PARP1. *Figure adapted from (Keijzers et al., 2018) and generated using BioRender.*

B. HEK293T cells were transfected with GFP-*EXO1* truncation mutants (as shown in A) and immunoprecipitated using a GFP resin after which Cyclin F binding to each of the mutants was visualised via immunoblots.

C. Schematic of EXO1's potential phosphorylation sites and Cyclin F degron site tested through aa mutations to alanines using SDM.

D. HEK293T cells were transfected with GFP-*EXO1* mutants (shown in C) and immunoprecipitated using a GFP resin after which Cyclin F binding to each of the mutants was visualised via immunoblots.

E. HEK293T cells were co-transfected with GFP-*EXO1* mutants (shown in C), FLAG-*CCNF* and HA-ubiquitin in the presence of the proteasome inhibitor MG132 (5 μM, 4 h). GFP-*EXO1* was immunoprecipitated with an anti-GFP resin under denaturing conditions and immunoblotted.

To further investigate this, the ubiquitylation of *EXO1* WT and *EXO1* mutants was tested in the presence of Cyclin F WT. Compared to the intense ubiquitin smear visualised above the EXO1 protein in both the WT and S815A samples, the T824A and ΔrxI mutations prevented EXO1's ubiquitylation by Cyclin F as only background ubiquitylation appears (identical to that which appears in the negative control sample without *CCNF* overexpression) (Figure 3iii.E). This data further confirms that TP 824-825 and RAI 842-844 are both essential sites for Cyclin F binding and subsequent ubiquitylation by $SCF^{Cyclin\ F}$. Based on this evidence, it is safe to speculate that the T824 is a priming phosphorylation site which allows Cyclin F binding to the RAI 842-844, similarly to RRM2.

Using the Cancer Genome Atlas (TCGA) PanCancer Atlas Studies dataset comprised of 10,967 samples from 32 studies on cBioPortal, I have queried the *EXO1* gene to screen for mutations within the 2 newly identified EXO1 regions

essential for Cyclin F binding. I found a diploid missense mutation in the RxI degron region of EXO1 protein in GBM and the mutation was R842I (Figure 3iv.A).

The search also indicated that *EXO1* is mutated in 1% of all GBM patients within the TCGA dataset. Curious as to whether this R/I mutation phenocopies the loss of EXO1-Cyclin F binding seen in my R/A mutation, I carried out SDM on GFP-*EXO1* to produce the same GFP-*EXO1* R842I mutation seen in the GBM patient and compared it to the positive control GFP-*EXO1* R842A in an immunoprecipitation study. Indeed, the R842I completely abrogated the binding of EXO1 to Cyclin F (Figure 3iv.B). This proves that cancer cells can modify this pathway to increase their survival. However, the incidence of this mutation is quite low, so the clinical relevance of the EXO1-Cyclin F axis should be further investigated in GBM. One way to further test this axis is to examine whether more common mutations, such as the 24 truncating mutations outlined in Figure 3iv, have a similar effect on Cyclin F binding.

After confirming the essential EXO1 regions for Cyclin F binding *in vivo* using overexpression experiments coupled with SDM, I aimed to reconstitute the same reaction using isolated proteins and whole cell lysates. By this means I could unequivocally establish the necessity of the T824 phosphorylation. For this purpose, I ordered custom-synthesised short biotinylated (BTN-) EXO1 peptides encompassing the degron region with or without the phosphorylation site, including peptides with function-disrupting mutations in those 2 regions (Figure 3v.A). The biotin-tagged peptides were used in immunoprecipitation experiments

where the peptides were conjugated to streptavidin beads and used to pull-down interactors (including Cyclin F) from the whole cell lysate.

A

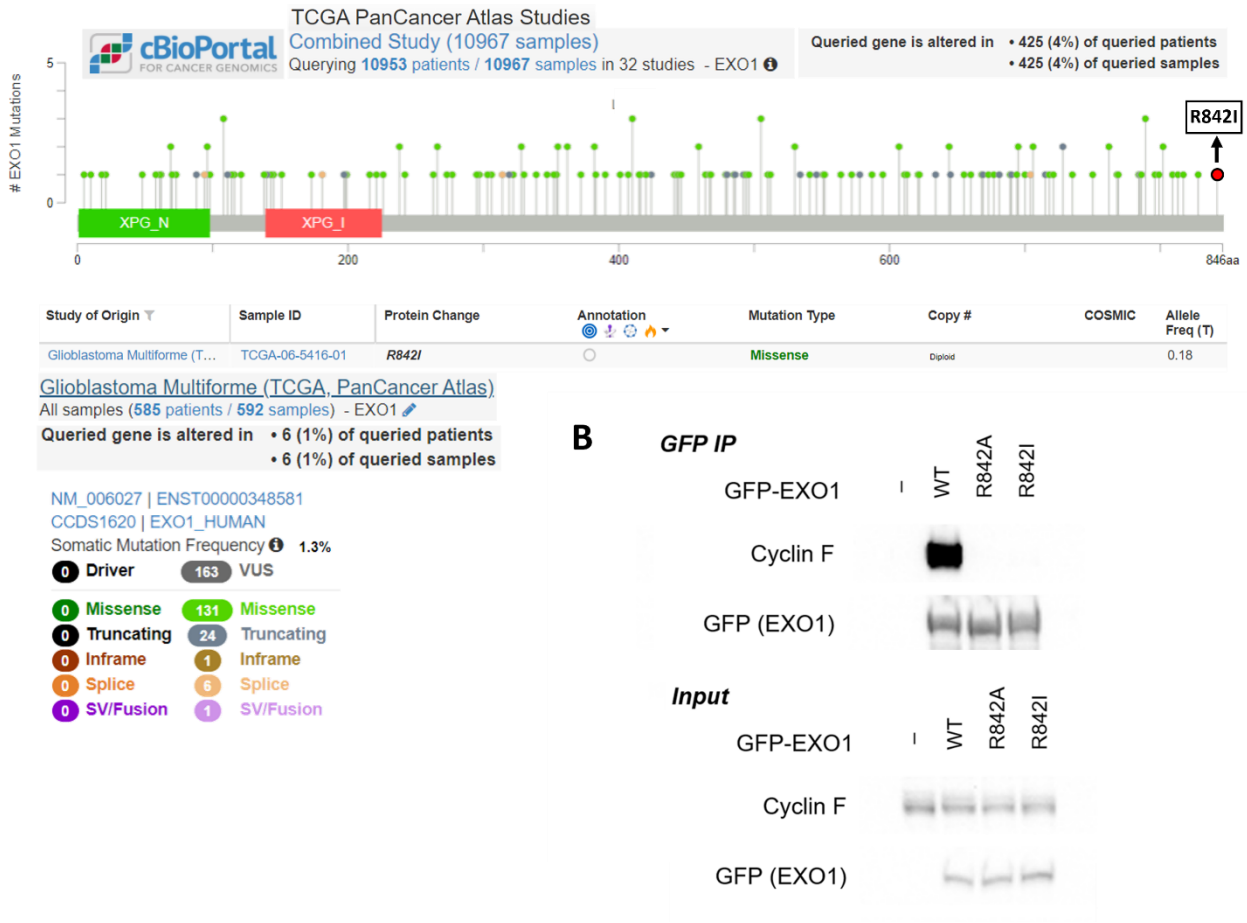


Figure 3iv. R842I EXO1 mutation in GBM completely prevents EXO1 binding to Cyclin F.

A. cBioPortal results for TCGA PanCancer Atlas Studies dataset queried for *EXO1*. The figure shows details of the R842I mutation, *EXO1* mutation frequency in GBM (1%), and *EXO1* mutation frequency in cancer (4%).

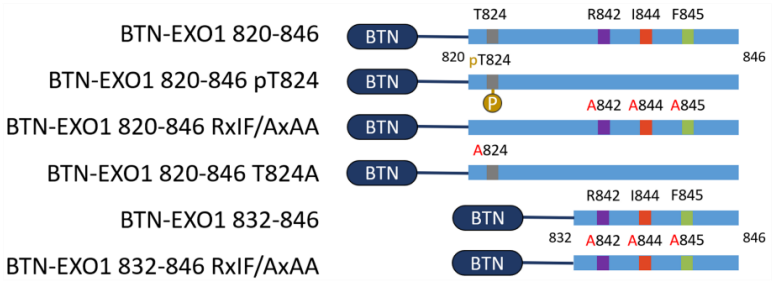
B. HEK293T cells were transfected with GFP-*EXO1* mutants R842I or R842A (positive control) alongside the GFP-*EXO1* WT or EGFP-EV negative controls. Immunoprecipitation using a GFP resin followed, after which Cyclin F binding to each of the mutants was visualised via immunoblotting.

The shortest peptide containing only the degron region (BTN-EXO1 832-846) bound Cyclin F the most strongly (5th IP lane, Figure 3v.B). This binding was completely abolished upon RxIF/AxAA degron mutation (6th IP lane). As for the

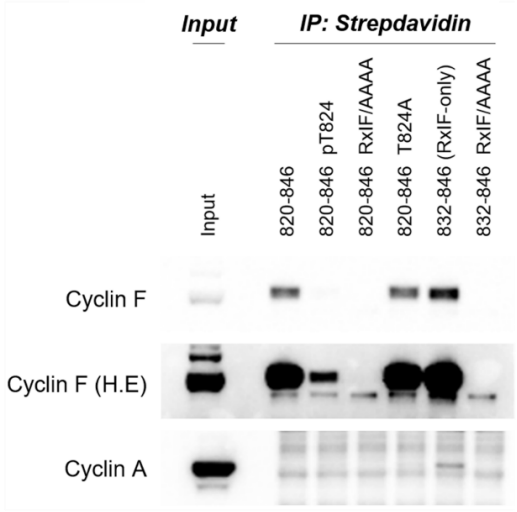
longer peptides, the one without any modifications or mutations bound Cyclin F strongly (1st IP lane), although not as strongly as its shorter counterpart that's missing the phosphorylation site, and that binding was once again completely blocked following an RxIF/AxAA degron mutation (3rd IP lane). Interestingly, the longer peptide with a constitutive priming phosphorylation (BTN-EXO1 820-846 pT824) largely lost its binding to Cyclin F, whereas the Cyclin F binding of its counterpart with a mutated phosphorylation site (BTN-EXO1 820-846 T824A) was completely unaffected by this loss of priming phosphorylation (4th IP lane).

The first takeaway from this data is the confirmation of RxI EXO1 as the Cyclin F binding site using peptides and whole cell lysates, similarly to the *in vivo* result, with high specificity to Cyclin F over other cyclins like Cyclin A. The second is that the shorter EXO1 peptide (aa 832-846) binds Cyclin F more strongly than its longer counterpart (aa 820-846), although with slightly less specificity as the shorter peptide also very weakly binds Cyclin A – the cyclin most similar to Cyclin F. It appears that when only the C-terminus of EXO1 is used for the pull-down, as in the case with the synthetic peptides, the previously identified priming phosphorylation site plays less of a role in Cyclin F binding. One explanation for this could be that the peptides are short enough to linearise and be unstructured, so the degron is presumably already exposed, hence no priming is needed prior to Cyclin F's recognition of EXO1's degron. This is backed up by the unaffected EXO1-Cyclin F binding upon T/A mutation.

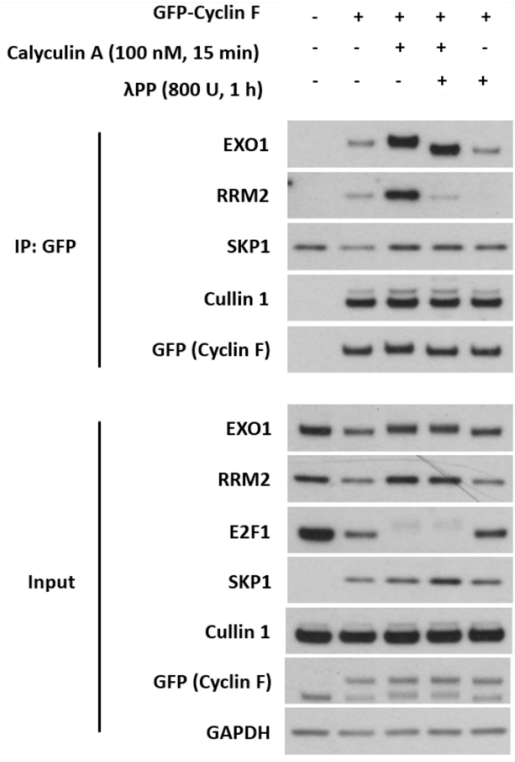
A



B



C



D

					Unique peptides / sample			Relative Protein Abundace			Fold Change (iBAQ)
Protein IDs	Protein names	Gene names	Mol. weight [kDa]	Unique peptides	Unique peptides _EV	Unique peptides _RRM2 peptide	Unique peptides _pRRM2 peptide	iBAQ _EV	iBAQ _RRM2 peptide	iBAQ _pRRM2 peptide	Fold Change: pRRM2/RRM2 peptides
P41002	Cyclin F	CCNF	87.639	27	0	8	16	0	2281000	64148000	28.12



Figure 3v. Cyclin F binds to EXO1's through its RxI 842-844 degron site, and phosphorylation hinders the Cyclin F binding to short EXO1 peptides.

A. Schematic of the synthesised biotin-tagged EXO1 peptides purchased from Lifetein.

B. HEK293T cells were lysed and 250 µg protein from the lysate was incubated with streptavidin beads (50 µL beads/sample, 2 h in low-salt Tris buffer at 4˚C) that have been conjugated to the biotinylated peptides in an earlier step (20 µM, 2 h in low-salt Tris buffer at 4˚C). Following bead washes in high-salt Tris buffer,

samples were boiled in Laemmli buffer then immunoblotted. Binding to Cyclin F (both at low and high exposure) and Cyclin A was assessed. *H.E = higher exposure (of the X-Ray film).*
C. HEK293T cells were transfected with GFP-*CCNF* and treated with the phosphatase inhibitor Calyculin A (100 nM, 15 min) where indicated. Immunoprecipitation using a GFP resin followed, after which Lambda Protein Phosphatase (λPP) (800 U, 1 h) was added to the 102mmunoprecipitated of the indicated samples. Cyclin F's binding to its substrates EXO1 and RRM2 (and E3 complex subunits SKP1 and Cullin 1) was visualised via immunoblotting.
D. Left: summarised results from an LC/MS study conducted using short RRM2 peptides, both unphosphorylated 'RRM2 peptide' and with constitutive priming phosphorylation at T33 'pRRM2 peptide', alongside an EV negative control. Unique peptide number, Intensity Based Absolute Quantification (iBAQ) and iBAC fold change ratios are shown. Right: Western blot validation of the resuls of the LC/MS study shown on the left.
Subfigure C is generated by Hongbin Yang and subfigure D is generated by Luke Humphreys.

One argument against this hypothesis is that the EXO1 C-terminus (including the phosphorylation and degron regions) appears quite linear in AlphaFold, the online tool capable of predicting 3D models of protein structures. It is worth noting that the model's confidence for its own prediction is "very low" for this region in particular. However, if the prediction is correct, then this points to the possibility of co-factor requirement preceding Cyclin F binding to EXO1 – which is abrogated by the T824A mutation of the short peptide. One way this could be the case is that the degron is initially inaccessible to Cyclin F due to a different protein, potentially MLH1 or MSH2 (see figure 3iii.A), binding to a site close enough to the Cyclin F degron that this protein's binding physically hinders Cyclin F's accessibility to its degron site (Figure 3vi). In this scenario, a phosphorylation on T824 of EXO1 could inhibit this binding of MLH1/MSH2 and/or displace the already bound MLH1/MSH2 and free up the degron for Cyclin F interaction. If this is in fact the case, then the binding site of MLH1/MSH2 must precede aa 820 on EXO1, which would explain why the synthesised peptides, of

which the longest start at aa 820, are able to bind Cyclin F without the pre-requisite of a phosphorylation (since the other protein that is otherwise blocking the site is no longer able to bind EXO1).

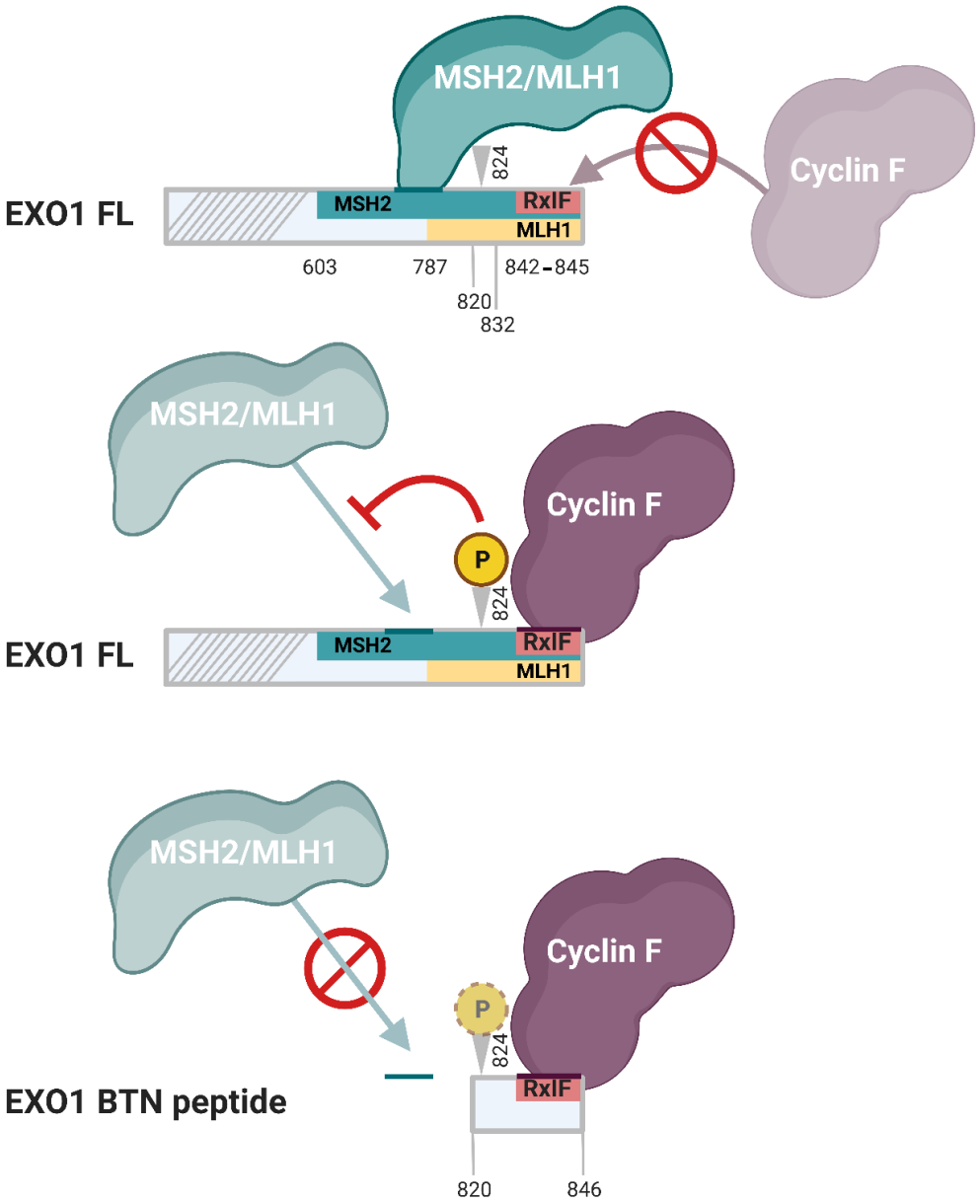


Figure 3vi. Proposed Cyclin F-EXO1 binding mechanism primed by the T824 phosphorylation on EXO1.

Top: in unphosphorylated conditions, MSH2 or MLH1 binds to EXO1 on motifs preceding the Cyclin F RxIF degron site, which hinders Cyclin F binding.
Middle: upon EXO1 T824 phosphorylation, MSH2/MLH1 is displaced, thereby enabling Cyclin F binding to EXO1's C-terminus.
Bottom: when short synthetic biotinylated (BTN) EXO1 peptides are used instead of full-length (FL) EXO1, Cyclin F can bind to EXO1 freely regardless of T824 phosphorylation status since the peptide excludes the MSH2/MLH1 binding site.
Figure generated using BioRender.

The observation that the constitutive phosphorylation on T824 in the short peptide experiment seems to hinder the binding to Cyclin F can perhaps be explained by an increased efficiency of degradation of the pT824 EXO1 peptide by Cyclin F, thereby resulting in a reduced pool of pT824 EXO1 owing to its rapid depletion in the experiment. Since the peptides were normalised based on protein concentration prior to starting the experiment, this experiment requires a repeat where the normalisation is done after the experiment is finished – and this can be accomplished using a biotin antibody that would detect the final peptide levels. Another repeat using MG132 or MLN4924 in the lysate prior to the peptide pull-down is also another means to test this hypothesis – since in this case the degradation will be inhibited and pT824 EXO1 should accumulate.

Another test that could be carried out is a simple over-expression experiment with an SDM-generated phospho-mimetic full length EXO1 (T824D) to see if an IP could recapitulate this short-peptide data. A similar experiment to the BTN-EXO1 peptide one using Cyclin F from whole cell lysates is to be conducted using purified full-length recombinant Cyclin F for further validation.

This data is complemented by a Cyclin F pull-down experiment where the cells were treated with the phosphatase inhibitor Calyculin A to trigger the phosphorylation of residues. In addition, after immunoprecipitation, the material bound to the beads (the immunoprecipitate) was treated with Lambda Protein Phosphatase (λPP) which de-phosphorylates all residues in a non-specific manner. After a short pulse of Calyculin A, the binding of Cyclin F to both its substrates EXO1 and RRM2 increases (Figure 3v.C). EXO1 migrates slower in the SDS page most likely due to its increased negative charge mediated by the phosphorylation of multiple residues, which repels SDS and hence decreases its

binding to the protein, causing a reduced mobility of the phosphorylated protein on the SDS-PAGE gel.

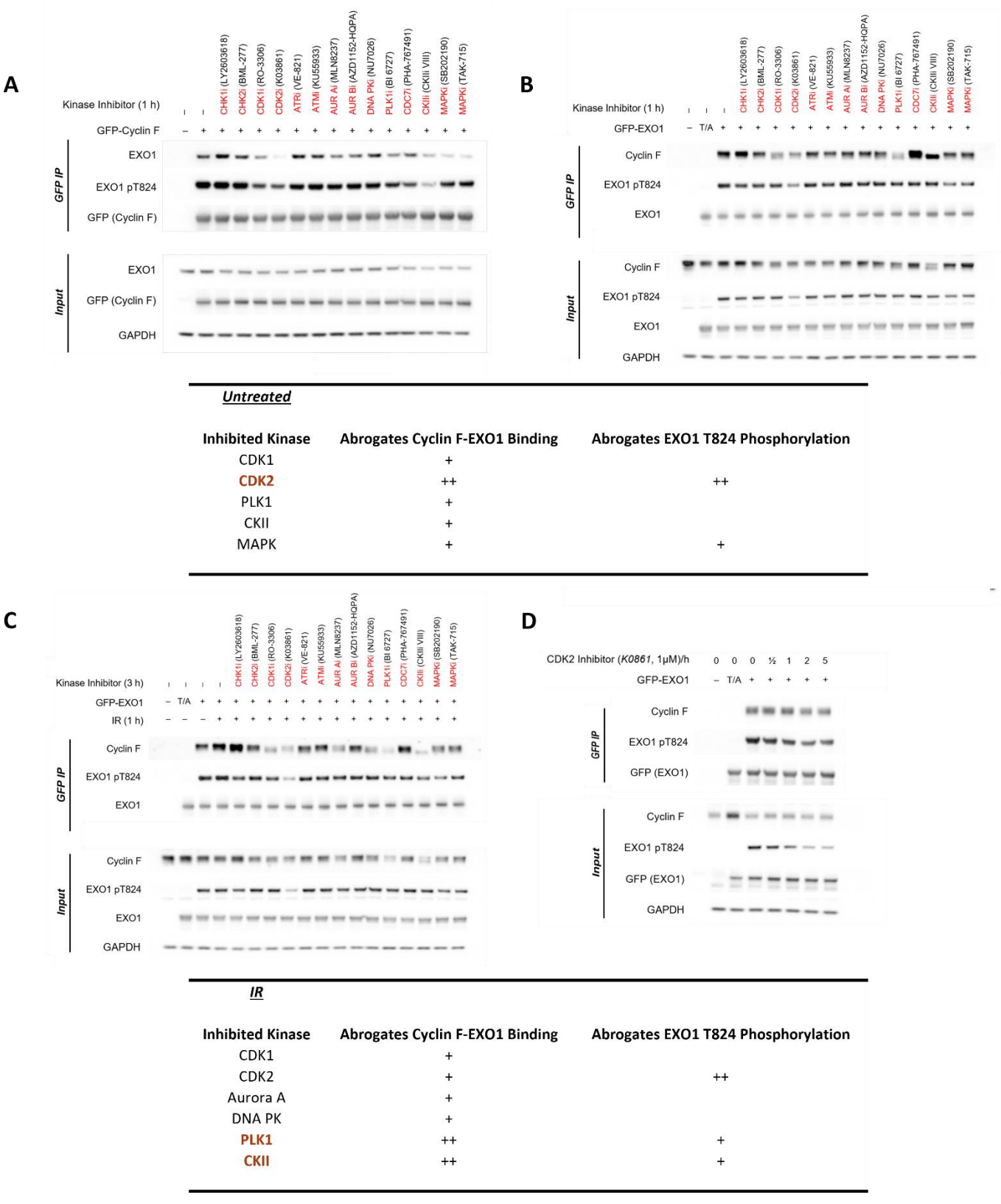
After treatment with λPP, RRM2 dissociates from Cyclin F. On the contrary, while EXO1 migration becomes faster (suggesting de-phosphorylation), it still retains its binding to Cyclin F. This shows that the mechanism of EXO1 engagement by Cyclin F is substantially different than that of RRM2. To further confirm the difference between Cyclin F's binding mechanism to RRM2 compared to EXO1, a parallel experiment was run using short RRM2 peptides as bait for a pull-down assay followed by LC/MS. Quantification of the resultant LC/MS data revealed that the short (~30 aa) RRM2 peptide binds more strongly to Cyclin F following RRM2's priming phosphorylation on T33 (Figure 3v.D). Results from these experiments suggest that EXO1 (like RRM2) requires phosphorylation for Cyclin F interaction, but (unlike RRM2) does not need a sustained phosphorylation to maintain the binding to Cyclin F; after the initial phosphorylation allowing the binding, phosphorylation becomes dispensable in the case of EXO1 and Cyclin F binding. This is in line with the data from the EXO1 short-peptide experiment, and together they strengthen the hypothesis of a phosphorylation even displacing an EXO1 interactor that would otherwise obstruct Cyclin F's access to the EXO1 degron, after which the binding is sustained without a continuous need for EXO1 phosphorylation (Figure 3vi).

One limitation to the experiment using λPP and Calyculin A is that EXO1 is heavily phosphorylated by a multitude of kinases (some inducing inhibitory and some relaying activating phosphorylation events) – evident by how 15 min of Calyculin A treatment resulted in a fully phosphorylated EXO1 (as seen from its complete migration to a higher molecular weight). Therefore, repeating this

experiment with an EXO1 truncation where only the C-terminus is preserved would reveal whether or not the C-terminus acts similarly to RRM2 in these conditions. If it does, then this effect was being diluted by the actions of other kinases acting on EXO1.

After identifying T824 as the priming phosphorylation site on EXO1, I generated a customised antibody for direct detection of EXO1 phosphorylation and the antibody specificity was tested prior to use in experiments (Supplementary Figure 3). To identify the kinase responsible for T824 phosphorylation, a kinase inhibitor screen was carried out. Considering that overexpression of proteins might lead to spurious results, two sets of immunoprecipitation experiments were carried out; one using Cyclin F as bait to look for EXO1 binding following treatment with these kinase inhibitors, and the other doing the reverse by using EXO1 as bait to look for both Cyclin F binding and EXO1 phosphorylation under these conditions. As a control for antibody specificity, EXO1 T824A ("T/A", a mutant lacking the phosphorylation site) was used.

Data shows that some kinase inhibitors such as CHK2i, CDK1i, Aurora Ai, Aurora Bi, PLK1i, CKIIi, and MAPKi partially destabilise EXO1's binding to GFP-tagged Cyclin F while CDK2i almost fully abrogates it (Figure 3vii.A). For the reverse pull-down, CDK1i, CDK2i and PLK1i largely abrogate Cyclin F's binding to GFP-tagged EXO1 while CDK2i is the only kinase that abrogates the binding and simultaneously decreases EXO1 T824 phosphorylation which is evident in both the input and the IP blots (Figure 3vii.B). This denotes that CDK2 is the kinase responsible for the priming phosphorylation on EXO1.



Untreated

Inhibited Kinase	Abrogates Cyclin F-EXO1 Binding	Abrogates EXO1 T824 Phosphorylation
CDK1	+	
CDK2	++	++
PLK1	+	
CKII	+	
MAPK	+	+

IR

Inhibited Kinase	Abrogates Cyclin F-EXO1 Binding	Abrogates EXO1 T824 Phosphorylation
CDK1	+	
CDK2	+	++
Aurora A	+	
DNA PK	+	
PLK1	++	+
CKII	++	+

Figure 3vii. CDK2 is the kinase responsible for the priming phosphorylation on T824 of EXO1 in untreated conditions *in vivo*.

A. HEK293T cells were transfected with GFP-*CCNF* and subjected to a kinase inhibitor screen including 1 h treatment with inhibitors of the indicated set of kinases at 5 μM. Immunoprecipitation using a GFP resin followed, after which

EXO1 T824 phosphorylation and EXO1 binding to Cyclin F were visualised via immunoblotting.

B. HEK293T cells were transfected with GFP-*EXO1* (WT or T824A) and subjected to the same kinase inhibitor screen in A. Immunoprecipitation using a GFP resin followed, after which EXO1 T824 phosphorylation and Cyclin F binding to EXO1 were visualised via immunoblotting.

C. Same as B but with a 3 h treatment instead of 1 h, and an additional treatment with IR (12 Gy) 1 h before harvesting samples.

D. HEK293T cells were transfected with GFP-*EXO1* (WT or T824A) and treated with CDK2i for up to 5 h. Immunoprecipitation using a GFP resin followed, after which EXO1 T824 phosphorylation and Cyclin F binding to EXO1 were visualised via immunoblotting.

The same GFP-*EXO1* pull-down experiment was carried out, but this time while additionally challenging the cells with IR treatment. This was to test whether or not EXO1 has different priming phosphorylation kinases in unperturbed conditions compared to post DNA damage by IR, and if so, to identify the responsible kinase(s) in the latter setting. Results show that CDK1i, CDK2i, Aurora Ai, PLK1i, DNA PKi and CKIIi strongly abrogate the EXO1-Cyclin F binding, with CKIIi and PLK1i being the strongest contenders at this destabilisation (Figure 3vii.C). However, only CDK2i is able to both abrogate the binding and hinder the phosphorylation on T824 EXO1. This could either be due to CDK2 being the priming kinase in both unperturbed and IR-treated conditions, or EXO1 having a different or additional priming kinase – likely CKII or PLK1 – that acts on a different phosphorylation site of EXO1.

To further study CDK2 as the kinase responsible for EXO1 priming phosphorylation, a time-series analysis following CDK2i treatment (for up to 5 h) of cells expressing GFP-*EXO1* was carried out to monitor the progression of the abrogation of both binding to Cyclin F and phosphorylation at EXO1 T824. Loss of EXO1 T824 phosphorylation can be clearly seen in the input blot following a

gradual time-dependent pattern starting 1 h post CDK2i treatment (Figure 3vii.D). Although less intense than the input, differences in Cyclin F binding and EXO1 pT824 can be seen to follow the same pattern in the IP blot. It is highly likely that higher concentrations of CDK2i would result in sharper time-dependent differences, similarly to ones seen in previous figures after 1 h of treatment using 5 μM CDK2i rather than the 1 μM I used for this experiment.

The experiments above indicate that CDK2 is the kinase responsible for EXO1 T824 phosphorylation *in vivo*, although indirect effects within the cell could not be fully excluded. For this reason, the capacity of CDK2 to phosphorylate EXO1 directly was tested *in vitro* using purified components.

To this end, full-length His-MBP-TEV-*EXO1* WT and its priming-phosphorylation mutant His-MBP-TEV-*EXO1* T824A were expressed in BL21(DE3) competent cells (Figure 3viii.A), purified using His-column affinity purification on ÄKTA start (Figure 3viii.B-C), and used for an *in vitro* phosphorylation assay. The assay included reacting the purified EXO1 WT and T824A proteins with either Cyclin A-CDK2 or Cyclin E-CDK2, along with ATP, then checking the phosphorylation levels on EXO1 T824 while the T824A protein served as a negative control.

Data shows that both Cyclin A-CDK2 and Cyclin E-CDK2 are capable of phosphorylating EXO1 at T824 *in vitro* (Figure 3viii.D). Cyclin F substrates are usually primed for Cyclin F binding, and hence UPS-mediated degradation, by CDK-relayed phosphorylation (Burdova et al., 2019c, D'Angiolella et al., 2012). It has been proposed that this phosphorylation might expose a previously obscured

Cyclin F degron, thereby allowing Cyclin F to recognise its substrate (D'Angiolella et al., 2012).

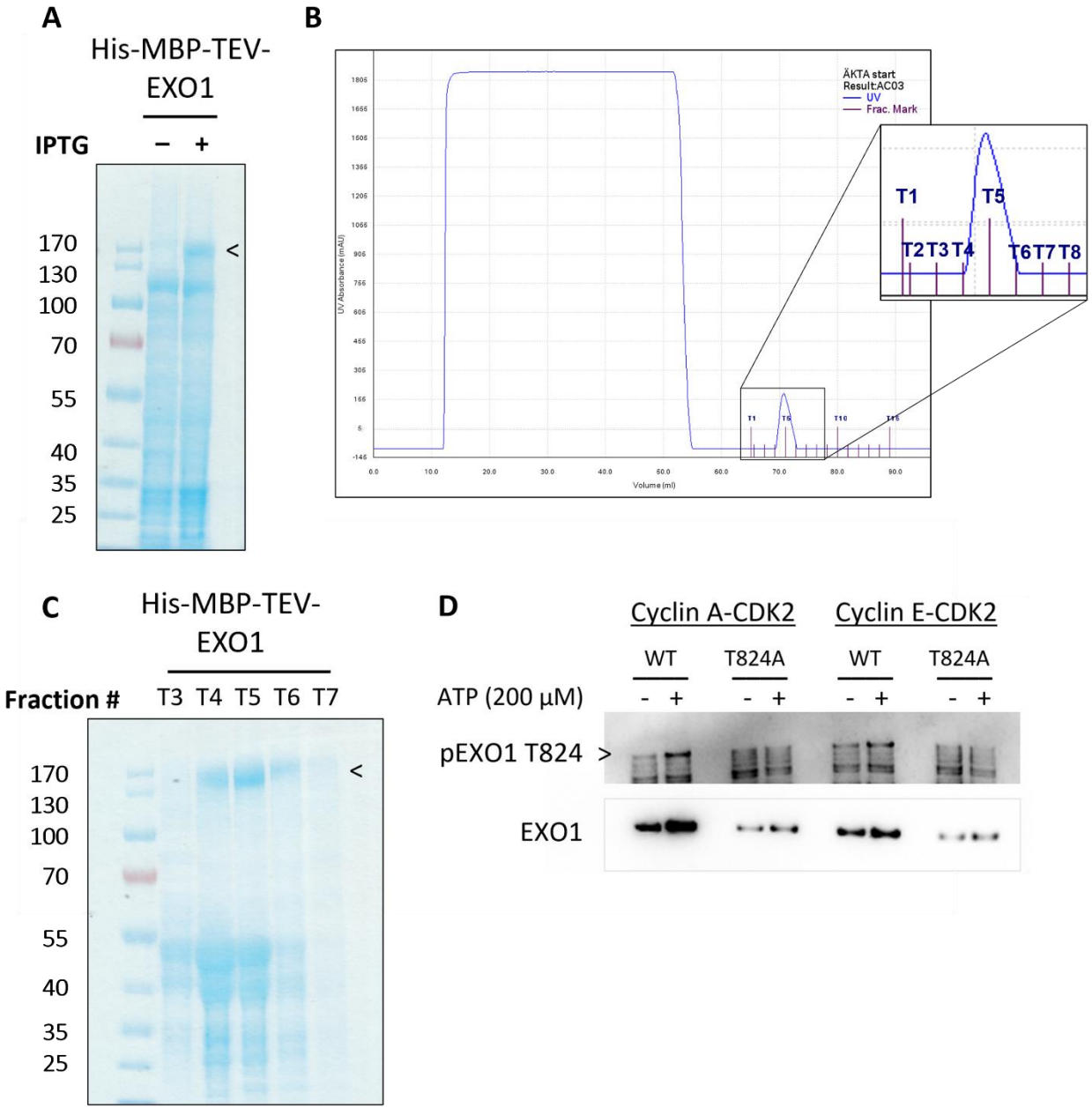


Figure 3viii. Cyclin A/E-CDK2 is the kinase responsible for the priming phosphorylation on T824 of EXO1 *in vitro*.

A. Coomassie blue-stained SDS-PAGE ran using lysates from BL21(DE3) competent cells expressing His-MBP-TEV-EXO1 ± IPTG (0.4 mM, 16˚C, O/N) to induce protein expression.

B. UV absorbance in milli absorbance units (mAU) plotted against volume fractionated by the His-column affinity purification carried out using ÄKTA start (GE Healthcare).

C. Coomassie blue-stained SDS-PAGE ran using fractions produced by the ÄKTA start which the UV absorbance curve indicated should have the desired protein. Fractions 4-6 were collected, dialysed (O/N in 1xPBS at 4˚C), concentrated (using Amicron Ultra-15 30K centrifugal filter, Merck) and used for further experiments.

D. *In vitro* phosphorylation of EXO1 was tested by mixing 2 µg purified His-MBP-TEV-EXO1 (WT or T824A, from C), 400 ng kinase (Cyclin A-CDK2 or Cyclin E-CDK2) and 200 µM ATP for 30 min at 30˚C after which the reaction was stopped and the solution was boiled in Laemmli buffer then immunoblotted.

EXO1 binding to Cyclin F is different than RRM2 and phosphorylation seems to exert a different effect. Two hypotheses can be derived regarding the role of phosphorylation in Cyclin F-EXO1 binding: either that the phosphorylation of EXO1 serves as a secondary direct binding site for Cyclin F and/or that the phosphorylation of EXO1 induces a conformational change that exposes the RxI degron for Cyclin F recognition.

There have speculations as to whether or not there is an intermediary step between this CDK phosphorylation and degron uncovering whereby a co-factor binds the phosphorylated Cyclin F substrate and contributes to this conformational change in protein structure enabling Cyclin F's eventual binding to it (Figure 3ix.A).

It was recently discovered that the isomerase PIN1 (Peptidylprolyl Cis/Trans Isomerase, NIMA-Interacting 1) mediates a conformational change in the BRCA1-BARD1 complex that is required for protecting stalled replication forks from the action of nucleases (Lu et al., 2007, Lu and Zhou, 2007, Daza-Martin et al., 2019). I was curious to investigate whether PIN1, the proline isomerase which

targets the minimal consensus motif pSer/Thr-Pro, has any effect on the TP 824-825 site of EXO1 in terms of a conformational change affecting Cyclin F binding.

While proline has the distinct ability to exist in both the *cis* and the *trans* forms, the other amino acids favour the *trans* form specifically. Hence, mutating proline to other amino acids (ex. alanine or cysteine) should mimic the conformational changes of the peptide bond brought about by PIN1's isomerisation activity (Daza-Martin et al., 2019) .

If PIN1 is indeed the co-factor, then P825A/C mutations should promote Cyclin F-EXO1 binding even with a T824A mutation. To test this, the following GFP-*EXO1* mutants were generated: P825A, P825C, TP/AA and TP/AC (Figure 3ix.B). The immunoprecipitation results showed complete abrogation of EXO1-Cyclin F binding with all of these mutations, indicating that isomerisation of proline 825 is not involved in this isomerisation process and, instead, is essential for *CCNF* binding (Figure 3ix.C). In parallel to the SDM experiment, a PIN1 knock-down experiment in the presence of overexpressed Cyclin F was carried out, and Cyclin F's binding to its substrates was assessed. Substrate binding to Cyclin F showed negligible abrogation in PIN1-depleted settings (Figure 3ix.D).

Since PIN1 does not mediate the Cyclin F-EXO1 interaction, I hypothesised that Cyclin F might have other co-factors. To answer this, a mass spectrometry experiment was carried out where GFP-tagged EXO1 and FLAG-tagged RRM2 were separately co-expressed in HEK293T cells and pulled-down with their respective resin. For each of these cDNA constructs, the following 3 variants were used: EV (EGFP for EXO1, pcDNA 3.1 for RRM2), WT, and priming phosphorylation mutants (EXO1 T824A and RRM2 T33A) (D'Angiolella et al.,

2012). Although there were many interactors identified, I could not obtain conclusive evidence for the presence of a mutual co-factor facilitating Cyclin F-EXO1/RRM2 binding.

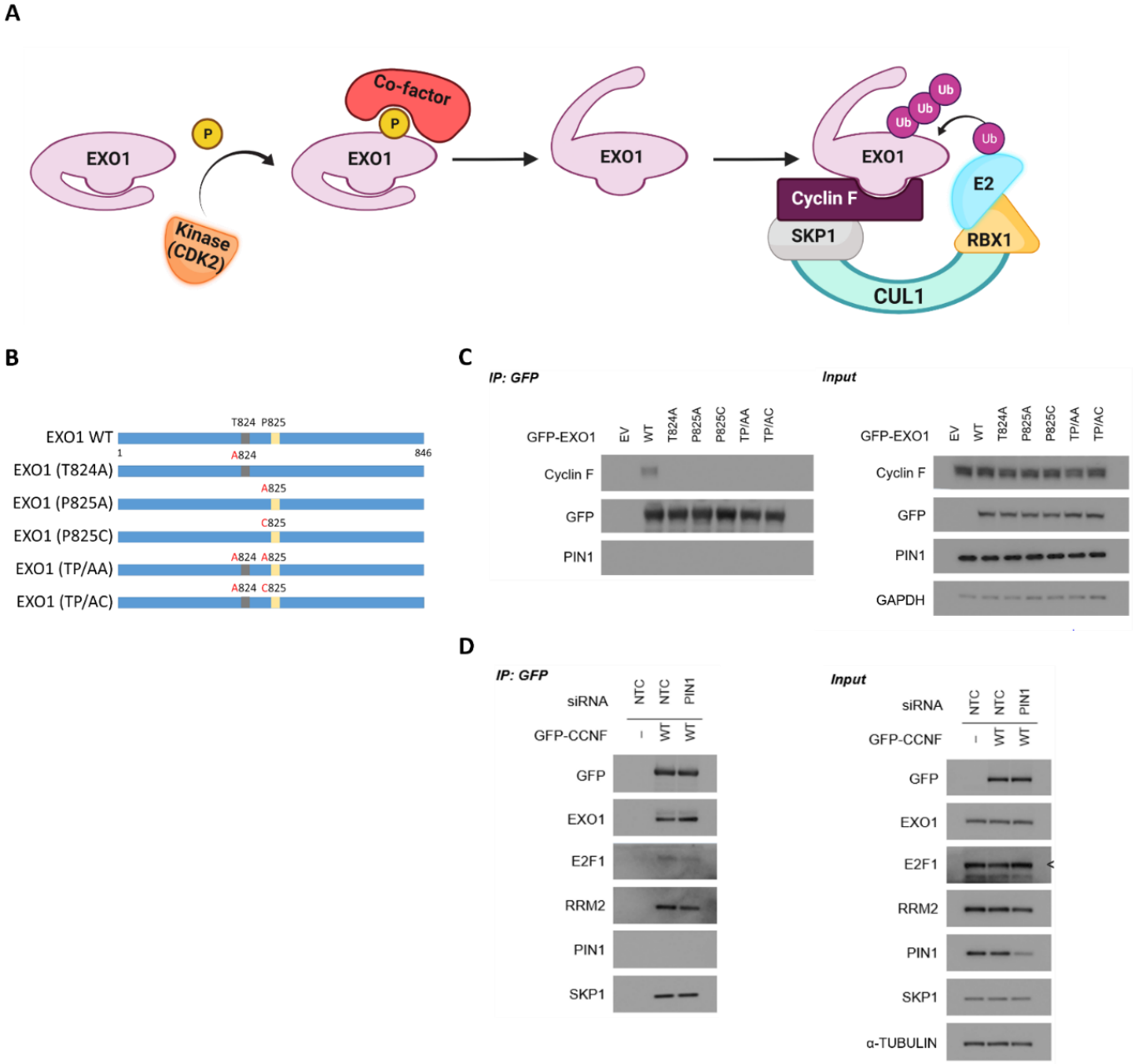


Figure 3ix. PIN1 is not a co-factor of Cyclin F for EXO1 binding.

A. Schematic of EXO1's potential recognition mechanism by Cyclin F. EXO1 potentially has an obscured Cyclin F degron. Degron exposure could occur after EXO1's priming phosphorylation which is potentially followed by a co-factor acting on the phosphorylated EXO1 to alter the protein's structure, thereby revealing the degron. Degron exposure would then allow Cyclin F to recognise

EXO1 and bind it, by which it would mark it for proteasomal degradation. *Figure generated using BioRender.*

B. Schematic of EXO1's potential co-factor binding sites tested through amino acid residue mutations to alanines using SDM.

C. HEK293T cells were transfected with GFP-*EXO1* mutants (shown in B) alongside the GFP-*EXO1* WT or EGFP-EV negative controls. Immunoprecipitation using a GFP resin followed, after which Cyclin F binding to each of the mutants was visualised via immunoblotting.

D. PIN1 was knocked-down by siRNA using HiPerFect (48 h) in HEK293T cells transfected with GFP-*CCNF* using PEI (24 h). Immunoprecipitation with a GFP resin followed, and Cyclin F substrate (EXO1, E2F1 and RRM2) binding was assessed via immunoblots.

Guided by these results, the next step would be to test whether Cyclin F can directly interact with the phosphorylated residues of EXO1. For such experiments, a number of very refined bio-physical techniques like Surface Plasmon Resonance would be quite helpful but they were outside the scope of the current work presented in this thesis.

c. Refinement of Cyclin F Degron

I aligned the degrons of known substrates of Cyclin F and observed a striking similarity between RRM2 and EXO1. In particular, the 842-844 RxI amino acids of EXO1 are followed by the residues 845-846 FQ, similarly to aa 49-53 RxIFQ seen in RRM2. Therefore, I speculated that these 2 amino acids could be part of Cyclin F's degron sites (RxI or RxL). To test this, I mutated the R, I, F and Q individually to alanine in both GFP-*EXO1* and FLAG-*RRM2*. Pull-down experiments showed that mutating the R, I, or F on its own completely hinders EXO1 and RRM2's binding to Cyclin F, while the Q/A mutation did not have a significant effect (Figure 3ix). This experiment helped us refine a new subset of the RxI Cyclin F degron: RxIF.

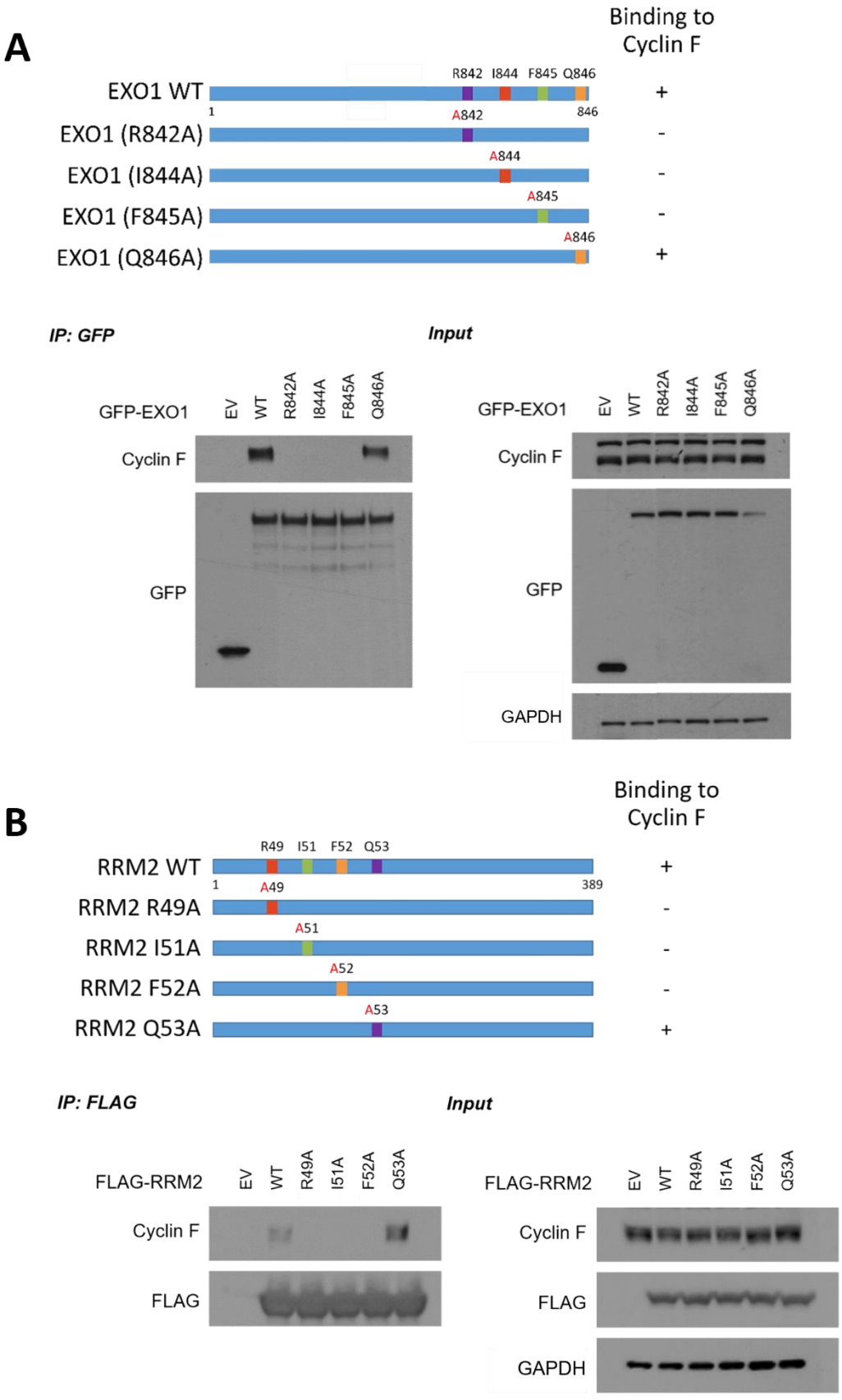


Figure 3ix. Degron refinement of Cyclin F substrates EXO1 and RRM2 to be RxlF and not Rxl only.

A. HEK293T cells were transfected with GFP-*EXO1* mutants (shown above) alongside the GFP-*EXO1* WT or EGFP-EV negative controls. Immunoprecipitation using a GFP resin followed, after which Cyclin F binding to each of the mutants was visualised via immunoblotting.

B. HEK293T cells were transfected with FLAG-*CCNF* mutants (shown above) alongside the FLAG-*CCNF* WT or pcDNA 3.1-EV negative controls. Immunoprecipitation using a GFP resin followed, after which Cyclin F binding to each of the mutants was visualised via immunoblotting.

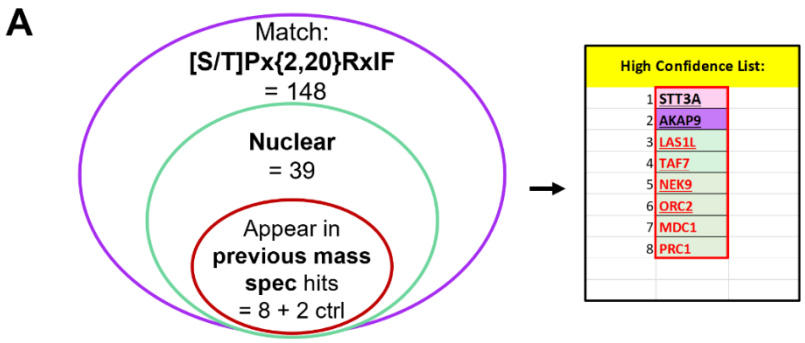
Using this information, I searched the human genome on the sequence matching website *Scansite 4.0* using the new refined Cyclin F degron [S/T]Px(2,20)RxIF where a Ser/Thr-Pro phosphorylation site exists within 2-20 aa from the RxIF degron site. The search returned 148 proteins with the desired sequence (Figure 3x.A).

Since Cyclin F is nuclear and so are most of its substrates, I also filtered for nuclear proteins from the initial 148 hits, which left me with 39 proteins. To narrow down my search even more, I matched those 39 proteins to any hits identified in the D'Angiolella lab's previous experiments using Cyclin F as bait in the absence or presence of the CRL inhibitor MLN4924: the first was a classic LC/MS experiment, and the second was a proximity labelling TurboID experiment for mapping protein–protein interactions (Figure 3x.B).

The final list post-filtration included 8 potential new substrates of Cyclin F: STT3 Oligosaccharyltransferase Complex Catalytic Subunit A/ Integral Transmembrane Protein 1 (STT3A/ITM1), A-Kinase Anchoring Protein 9 (AKAP9), LAS1 Like Ribosome Biogenesis Factor (LAS1L), TATA-Box Binding Protein Associated Factor 7/ Transcription Initiation Factor TFIID 55 KDa Subunit (TAF7/TAFII55), NIMA Related Kinase 9 (NEK9), Origin Recognition Complex Subunit 2 (ORC2), Mediator of DNA Damage Checkpoint 1 (MDC1) and Protein

Regulator of Cytokinesis 1 (PRC1) – along with 2 positive controls (EXO1 and RRM2). I reasoned that I could possibly identify substrates of Cyclin F based on the degron alone, thus, I carried out immunoprecipitation experiments in HEK293T cells where either Cyclin F WT or ΔF was overexpressed, after which the bait's interaction with these potential substrates was assessed (Figure 3x.C).

I could detect an interaction between Cyclin F and EXO1 or RRM2, as expected, and additionally with NEK9, ORC2, LAS1L and AKAP9. Whereas substrates like EXO1 and RRM2 bind Cyclin F ΔF more strongly than Cyclin F WT, NEK9, ORC2, LAS1L and AKAP9 did not. The other four proteins containing the degron (STT3A/ITM1, MDC1, TAF7/TAFII55 and PRC1) that were tested did not bind Cyclin F, neither the WT nor the ΔF mutant. Levels of the same 8 proteins plus 2 controls were assessed in whole cell lysates of HeLa and HeLa *CCNF* K/O and of LIM1215 CRC cells isogenic for KRAS with a Cyclin F knock-out (*KRAS* WT 'Ctrl', *KRAS* WT *CCNF* K/O '*CCNF* K/O', *KRAS* G12V$^{+/-}$ 'Mut' and *KRAS* G12V$^{+/-}$ *CCNF* K/O 'Mut *CCNF* K/O'– these cell lines are described extensively in data chapter 2). Cyclin F substrates, similarly to EXO1 and RRM2, were expected to have a higher level of expression in cells that no longer have Cyclin F (*CCNF* K/O and/or Mut *CCNF* K/O). Only STT3A/ITM1 protein levels were higher in the *CCNF* K/O cell line compared to Ctrl, and MDC1 levels were higher in Mut *CCNF* K/O cells compared to Mut.



B

Lab's Previous Turbo ID

Protein IDs	Protein names	Gene names	-Log Student's T-test p-value MLN_Ctrl (cutoff<1.3) *Significance	Student's T-test q-value MLN_Ctrl	Student's T-test Difference MLN_Ctrl (cutoff<1)
P41002	Cyclin-F	CCNF	0.729	0.632	0.326
Q13616	Cullin-1	CUL1	0.379	0.797	0.210
P63208	S-phase kinase-associated protein 1	SKP1	1.397	0.352	0.718
Q9UK81	F-box/WD repeat-containing protein 11	FBXW11	0.897	0.528	1.798
Q12834	Cell division cycle protein 20 homolog	CDC20	0.685	0.657	1.130
Q9Y297	F-box/WD repeat-containing protein 1A	BTRC	0.930	0.512	1.780
P31350	Ribonucleoside-diphosphate reductase subunit M2	RRM2	3.350	0.136	2.911
Q9UQB4	Exonuclease 1	EXO1	3.650	0.108	6.626
P46977	Dolichyl-diphosphooligosaccharide--protein glycosyltransferase subunit STT3A	STT3A(ITM1)	1.419	0.350	-1.291
Q14571	Inositol 1,4,5-trisphosphate receptor type 2	ITPR2	1.164	0.459	0.324
Q8IZH2	5-3 exoribonuclease 1	XRN1	0.974	0.185	0.123
Q99996	A-kinase anchor protein 9	AKAP9	0.825	0.573	4.499
Q09161	Nuclear cap-binding protein subunit 1	NCBP1	0.683	0.656	-0.609
Q9Y4W2	Ribosomal biogenesis protein LAS1L	LAS1L	0.660	0.663	1.061
Q15545	Transcription initiation factor TFIID subunit 7	TAF7(TAFII55)	0.657	0.658	1.430
P53618	Coatomer subunit beta	COPB1	0.484	0.738	0.313
Q8TD19	Serine/threonine-protein kinase Nek9	NEK9	0.291	0.855	0.454
Q9UBF2	Coatomer subunit gamma-2	COPG2	0.121	0.933	0.241
Q13416	Origin recognition complex subunit 2	ORC2	0.038	0.977	0.099

KEY:
Cytoplasmic
Nuclear
Neither
TurboID+ Mass Spec

Lab's Previous Mass Spec

Accession	Protein names	Gene names	1_Empty YFP			2_CCNF_Untr			3_CCNF+MLN		
			Prot score	N.sign peptides	empai	Prot score	N.sign peptides	empai	Prot score	N.sign peptides	empai
Q15545	Transcription initiation factor TFIID subunit 7 (RNA polymerase II TBP-associated factor sut	TAF7(TAFII55)	1	0	0	1	0	0	1	0	0
P62701	40S ribosomal protein S4, X isoform (SCR10) (Single copy abundant mRNA protein) (Small ri	RS4X	115	3	0.6	64	3	0.6	79	2	0.37
P18124	60S ribosomal protein L7 (Large ribosomal subunit protein uL30)	RL7	90	5	1.23	1	0	0	135	1	0.18
O43663	Protein regulator of cytokinesis 1	PRC1	43	2	0.14	1	0	0	23	1	0.07
Q13416	Origin recognition complex subunit 2	ORC2	1	0	0	1	0	0	1	0	0
Q8TD19	Serine/threonine-protein kinase Nek9 (EC 2.7.11.1) (Nercc1 kinase) (Never in mitosis A-rela	NEK9	58	1	0.04	1	0	0	1	0	0
Q14676	Mediator of DNA damage checkpoint protein 1 (Nuclear factor with BRCT domains 1)	MDC1	1	0	0	1	0	0	1	0	0
Q9Y4W2	Ribosomal biogenesis protein LAS1L (Protein LAS1 homolog)	LAS1L	71	2	0.12	1	0	0	1	0	0
Q14204	Cytoplasmic dynein 1 heavy chain 1 (Cytoplasmic dynein heavy chain 1) (Dynein heavy chai	DYHC1	186	8	0.07	1	0	0	1	0	0
Q5VZX9	F-actin-uncapping protein LRRC16A (CARMIL homolog) (Capping protein regulator and myo	CARL1	1	0	0	1	0	0	1	0	0

C

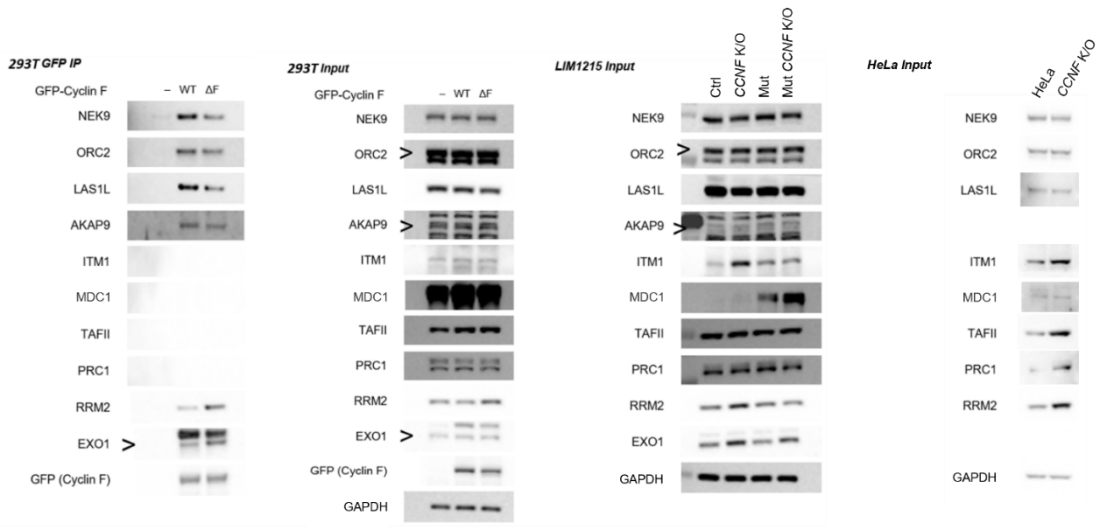


Figure 3x. Cyclin F degron refinement search by cross-checking previous mass spectrometry experiments with *Scansite 4.0* sequence match results.

A. [S/T]Px(2,20)RxIF motif search on *Scansite 4.0* followed by nuclear filtration and hit match with previous lab experiments (shown in B).

B. Top hits in results from previous D'Angiolella lab experiments using Cyclin F as bait ± the CRL inhibitor MLN4924: a mass spectrometry experiment and a proximity labelling TurboID experiment.

C. Left: HEK293T cells were transfected with GFP-*CCNF* WT or ΔF which was followed by immunoprecipition using a GFP resin after which Cyclin F binding to potential substrates was visualised via immunoblotting. Right: immunoblots of whole cell lysates of LIM1215 cells CRC cells isogenic for KRAS with a Cyclin F knock-out (*KRAS* WT 'Ctrl', *KRAS* WT *CCNF* K/O '*CCNF* K/O', *KRAS* G12V$^{+/-}$ 'Mut' and *KRAS* G12V$^{+/-}$ *CCNF* K/O 'Mut *CCNF* K/O').

Both STT3A/ITM1 and MDC1 are therefore potential (yet not confirmed) Cyclin F substrates based on the increase in their expression levels upon Cyclin F loss, and one could speculate that the reason they did not bind Cyclin F in the pull-down experiments in HEK293T cells is that their Cyclin F binding (and consequent ubiquitylation) specifically occurs in certain short-lived cell cycle phases – and thereby requires cell synchronisation prior to pull-down – or upon the introduction of external factors such as DNA damage (Figure 3x.C). It is perhaps the case that the cut-off for this neo-substrate search was too high and that the narrowed down list of 39 proteins should be tested for substrate potential rather than those that only previously came up in older LC/MS and TurboID results. A more efficient cut-off approach could be investigating the degron accessibility of these 39 proteins using AlphaFold, then checking if the nearby phosphorylation sites that could potentially prime Cyclin F binding are in fact commonly phosphorylated in the cell using the website PhosphoSitePlus®.

This chapter details the characterisation of EXO1 as a Cyclin F substrate whose accumulation sensitises cancer cells to ionising radiation. This finding started with the identification of the E3 ligase Cyclin F as a mediator of IR

resistance in glioblastoma, and was followed up by a validation experiment in the form of a cell survival assay. An LC/MS experiment implicated the Cyclin F substrate EXO1 as the underlying regulator of this observed IR-dependent phenotype, and its substrate recruitment mechanism by Cyclin F was investigated. The Cyclin F degron (RxIF 842-845) and priming phosphorylation (T824) sites on EXO1 were confirmed, a model for its priming phosphorylation was proposed, and the kinase behind this phosphorylation was identified (CDK2). RxIF – a new subset of the RxI Cyclin F degron – was highlighted based on an alignment of the degrons of 2 Cyclin F substrates (RRM2 and EXO1), and a degron-matching approach based on a proteome-wide sequence search revealed 148 other potential Cyclin F substrates. Filtration of these results based on cellular localisation and previous identification in LC/MS and proximity labelling experiments conducted by fellow lab members narrowed down the list to 8 members, of which the oligosaccharyltransferase STT3A/ITM1 behaved as a potential substrate.

4. Results Chapter II: The KRAS-Cyclin F Regulatory Network

a. Investigating Cyclin F Regulation by KRAS

i. KRAS Promotes the Degradation of Cyclin F Substrates RRM2 and E2F1

RAS is a hallmark cancer gene owing to its activating mutation in around 1 in 5 cancers. Out of patients harbouring RAS mutations, *KRAS* accounts for ~75% of these mutations (Prior et al., 2020). Based on this, there have been increasing efforts to target the KRAS oncoprotein, or its downstream cascade, in order to improve patient outcomes. For these reasons, I decided to pursue my initial serendipitous observation of a potential feedback mechanism between Cyclin F and KRAS. The aim of this pursuit was to find any clinically exploitable weaknesses along this axis in order to add value to the therapeutic toolkit against *RAS*-mutated cancers, especially ones that quickly develop resistance to the current treatment options.

In collaboration with AstraZeneca researchers, I investigated the protein levels of RRM2 in a panel of NSCLC cell lines. Within this panel, some cell lines had *KRAS* activating mutations (and were sensitive to the WEE1 inhibitor, hence CDK activator, Adavosertib) and some were *KRAS* WT (and WEE1-resistant). I observed that RRM2 appears to be degraded more efficiently in *KRAS* mutant cell lines, especially after treating the cells with Adavosertib as this promotes RRM2's priming phosphorylation by CDKs, and I excluded that this effect was due to an increase in the level of RRM2's priming phosphorylation (Figure 4i.A). Since the priming phosphorylation by CDKs serves as an indicator of the cell cycle phase, it could also be ruled out that *KRAS* has any considerable impact on cell cycle progression – an observation that was also made from a cell cycle

profile experiment using FACS (Supplementary Figure 4). Thus, I considered the possibility that Cyclin F's E3 activity is increased in *KRAS* mutant settings. Interestingly, one previous publication reached similar conclusions with regards to the Cyclin F substrate CCP110, and another study demonstrated that Cyclin F can be activated through phosphorylation by AKT, a kinase downstream of RAS in its signalling cascade (Hu et al., 2015, Choudhury et al., 2017).

Since the previous experiment was done in multiple cell lines with diverse genetic backgrounds needing to be controlled for, I decided to perform follow-up experiments in the isogenic CRC cell lines LIM1215 *KRAS* WT and *KRAS* G12V$^{+/-}$ to test this one parameter (*KRAS* activating mutation).

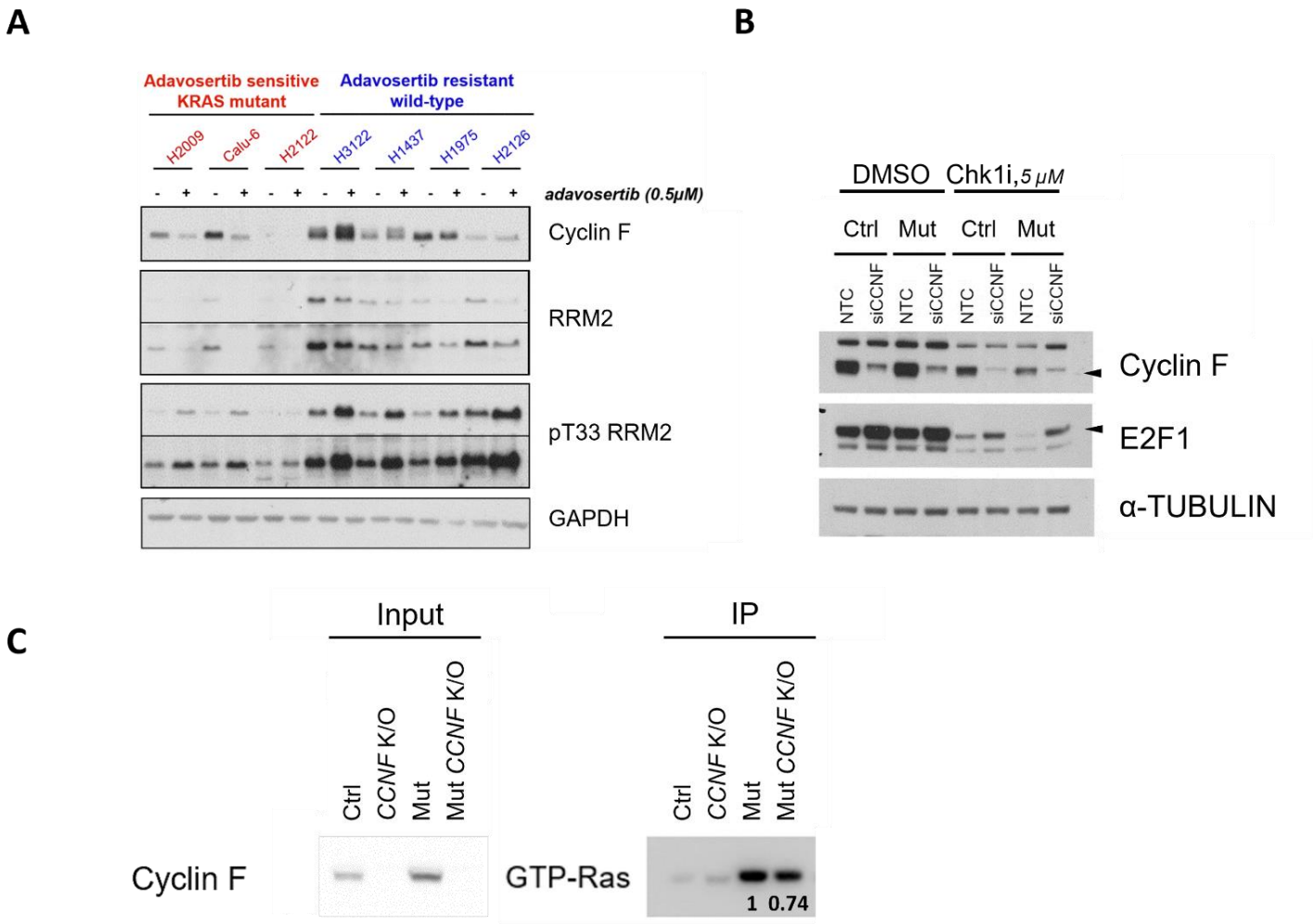


Figure 4i. KRAS and Cyclin F are in a reciprocal regulation loop.

A. Panel of NSCLC cell lines divided into Adavosertib-sensitive *KRAS* mutant cell lines and Adavosertib-resistant *KRAS* WT ones. Cells were treated with Adavosertib (0.5 μM) and post lysis were provided to the VDA lab by AstraZeneca collaborators.

B. LIM1215 *KRAS* WT ('Ctrl') and *KRAS* G12V$^{+/-}$ ('Mut') cells were transfected with si*CCNF* and its non-targeting control (15 nM, 24 h LipoRNAimax) and treated with the CHK1 inhibitor LY2603618 (5 μM, 24 h).

C. RAS activation assay was conducted following the manufacturer's instructions (Millipore, Cat #17-218) in LIM1215 cells (*KRAS* WT 'Ctrl', *KRAS* WT *CCNF* K/O '*CCNF* K/O', *KRAS* G12V$^{+/-}$ 'Mut' and *KRAS* G12V$^{+/-}$ *CCNF* K/O 'Mut *CCNF* K/O'). For each sample, 780 μg lysate and 10 μL RBD-conjugated beads were used for the pull-down (50 min, 4˚C).

I tested the levels of the most recently published Cyclin F substrate, E2F1, in these cells (Burdova et al., 2019a, Clijsters et al., 2019). In untreated conditions, Cyclin F depletion stabilised E2F1 (Figure 4i.B). When cells were treated with the CHK1 inhibitor LY2603618, this induced the Cyclin F-mediated degradation of E2F1. This is because CHK1 normally phosphorylates and thus primes the phosphatase CDC25A for ubiquitin-mediated degradation, and this phosphatase is tasked with removing the inhibitory phosphorylation (relayed by WEE1) on CDKs (Parker and Piwnica-Worms, 1992, Sørensen et al., 2003, Watanabe et al., 1995). Hence, inhibiting CHK1 results in higher CDK activity, higher E2F1 priming phosphorylation, and eventually an enhanced rate of E2F1 degradation by Cyclin F (Burdova et al., 2019c). Upon CHK1 inhibition, the difference in degradation level between the isogenic cell lines was strongly evident. E2F1 appeared to be degraded more efficiently in *KRAS* mutant settings compared to *KRAS* WT settings in CHK1 inhibitor-treated cells, and this was rescued by Cyclin F depletion (Figure 4i.B). Results from this experiment also suggest that Cyclin F activity is increased in cells with *KRAS* activating mutations. However, testing the ubiquitylation activity of Cyclin F in these contexts through

more direct approaches, for example through visualising the ubiquitin ladder on its substrates in an *in vivo* ubiquitylation assay, is required for confirmation.

b. Investigating KRAS regulation by Cyclin F

i. Cyclin F Loss Decreases RAS Activity in KRAS Mutant Cells

Given the results presented above and the published findings (Hu et al., 2015) regarding Cyclin F's altered activity in *KRAS* mutant settings, I decided to investigate the relationship between KRAS and Cyclin F further by generating *CCNF* knock-out stable cell lines using CRISPR-Cas9 from the parental isogenic LIM1215 cell lines. This way I had a total of 4 LIM1215 cell lines: *KRAS* WT ('Ctrl'), *KRAS* G12V$^{+/-}$ ('Mut'), *KRAS* WT *CCNF* K/O ('*CCNF* K/O') and *KRAS* G12V$^{+/-}$ *CCNF* K/O ('Mut *CCNF* K/O'). After isolating single cell clones, I assessed Cyclin F levels and selected cell lines where the Cyclin F protein was undetectable and whose proliferation rates did not vary much (Figure 4i.C, left).

After validating Cyclin F loss, I tested the activity of the RAS oncoprotein using a commercially available kit. This assay utilises the RAS-binding domain of a major RAS interactor called RAF which lies downstream of active RAS in its pro-survival signalling cascade. Active RAS is GTP-bound, while inactive RAS is GDP-bound, and only GTP-RAS binds its downstream effectors and can be pulled-down via immunoprecipitation using this kit. This assay's readout for RAS activity is the GTP-RAS levels within a sample. As expected, the difference in RAS activity between Ctrl and Mut cells is stark, confirming the KRAS G12V$^{+/-}$ activating mutation in the original mutant cell line compared to the control WT (Figure 4i.C, right). What I did not expect to observe was that Cyclin F depletion appeared to induce a reduction of RAS activity in the *KRAS* mutant cell line (Mut *CCNF* K/O) when compared to its *CCNF* WT counterpart (Mut). This pattern was

not observed in the *KRAS* WT cell lines when Cyclin F was lost, in fact the opposite seemed true as GTP-RAS levels appeared higher in the *CCNF* K/O cell line compared to the Ctrl one.

This result pointed out that KRAS activity can be modulated despite the presence of an activating mutation. It also suggested that the presence of Cyclin F helps to sustain KRAS activity. Since increased activity of Cyclin F in *KRAS* mutant settings was previously observed (Figure 4i.A-B and (Hu et al., 2015)), it can be hypothesised that a regulatory loop exists between Cyclin F and KRAS.

ii. Decreased RAS Activity is Reflected in Decreased Resistance of KRAS Mutant Cells to EGFRi

The protein RAS is a central downstream effector of Receptor tyrosine Kinases (RTKs), and it conveys the proliferation signals to initiate gene transcription and cell cycle progression. Cell death resulting from the inhibition of RTKs is largely attributable to inhibiting the activity of the RAS signalling cascade. Indeed, it has long been known that activating mutations in RAS are prognostic indicators for resistance against RTK inhibitor therapy. The most well-established example of this is the Epidermal Growth Factor Receptor (EGFR) whose inhibition constitutes the foundation of important anti-cancer therapies, and the resistance to which constitutes a persistent and pressing medical challenge (Benvenuti et al., 2007, Eberhard et al., 2005, Pao et al., 2005, Siddiqui and Piperdi, 2010). There are two main classes of EGFR inhibitors; ones that bind the extracellular ligand-binding domain of EGFR, thereby preventing its ligand-mediated activation, and those that bind the intracellular tyrosine kinase domain's ATP pocket by reversibly competing with ATP. The former class of drugs includes

the monoclonal antibodies Cetuximab and Panitumumab while the latter includes the small-molecule inhibitors Erlotinib, Gefitinib and Lapatinib.

To exclude drug specific effects I used both classes of EGFR inhibitors and tested whether the LIM1215 cell lines Ctrl, *CCNF* K/O, Mut and Mut *CCNF* K/O had different responses to these inhibitors, which in turn reflects the activity of the RAS protein in these cells. I used a Resazurin-based cell viability assay to test Erlotinib, Gefitinib and Cetuximab sensitivity in the 4 LIM1215 cell lines. If the results were to agree with the GTP-RAS data (Figure 4i.C) (which had the following pattern for KRAS activity levels in order of highest-to-lowest: Mut > Mut *CCNF* K/O > *CCNF* K/O > Ctrl), then we'd expect to see the same pattern of KRAS resistance since KRAS mutational status – and hence activity levels – are a biomarker for EGFR inhibitor resistance.

In accordance with this, Mut was the most EGFR inhibitor-resistant cell line and was followed by Mut *CCNF* K/O, *CCNF* K/O then Ctrl for the 3 drugs tested (Figure 4ii). This data was quantified by calculating the IC50 (Figure 4ii.A-C) and viability (Figure 4ii.D-F) of the different cell lines following EGFR inhibitor treatment. These results confirm the previous speculation that Cyclin F regulates KRAS activity. The data also spotlights Cyclin F as a significant clinically-exploitable target for cancer treatment in combination with EGFR inhibitors. However, the mechanisms at the basis of the different EGFR sensitivity and RAS activity of the tested cell lines were unclear at the time. To start gathering insights into this, I decided to conduct a large-scale proteomic study examining the protein level changes in the 4 LIM1215 cell lines.

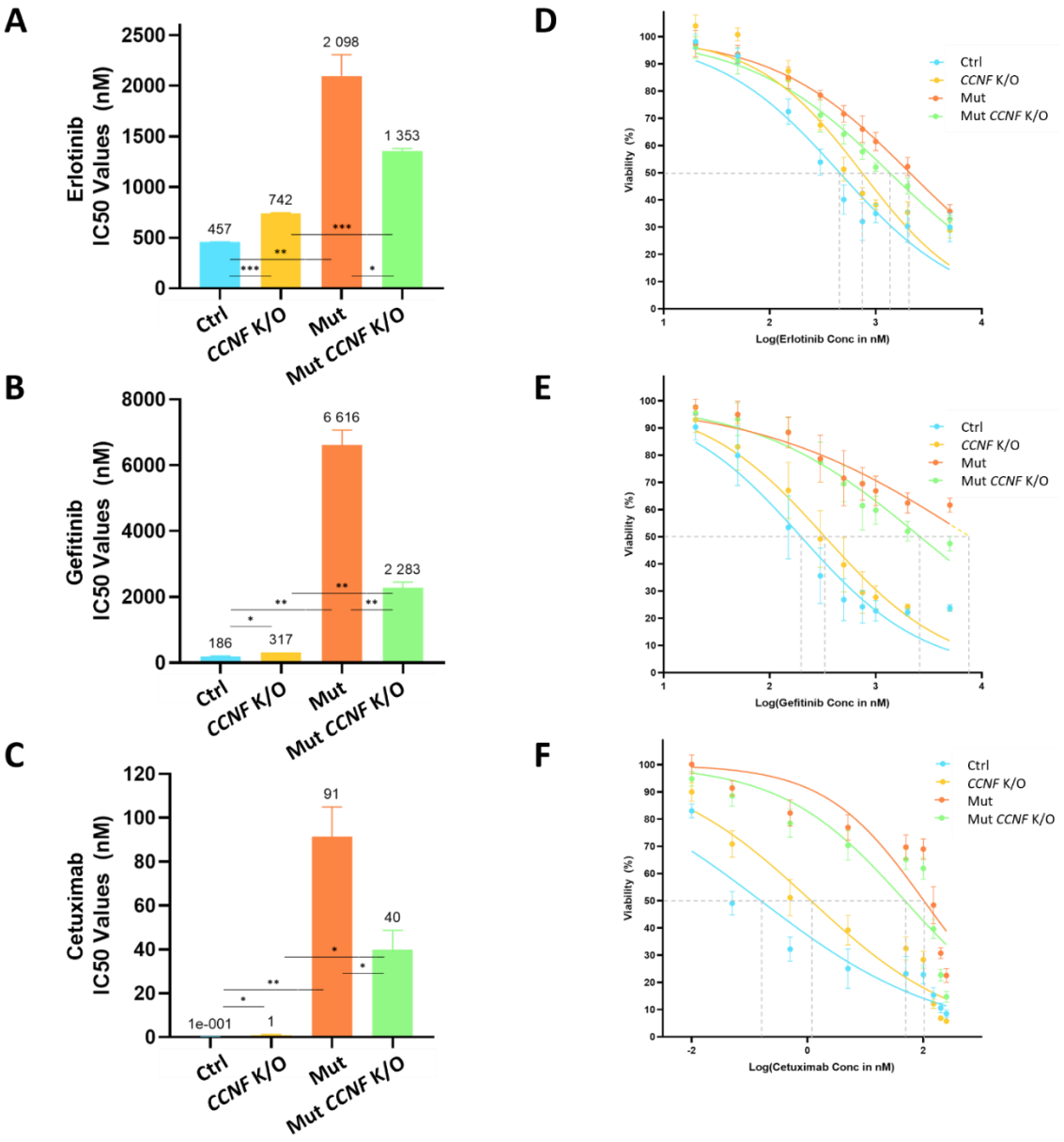


Figure 4ii. Cyclin F loss reduces the resistance of *KRAS* mutant cells to EGFRi treatment.

LIM1215 cells were treated with the EGFR inhibitors for 72 h at a gradient of concentrations, after which their survival was quantified using a Resazurin viability assay.

A-C. IC50 values (in nM) in the 4 LIM1215 cell lines (± *CCNF* ± *KRAS* activating mutations): Ctrl, *CCNF* K/O, Mut and Mut *CCNF* K/O treated with Erlotinib, Gefitinib or Cetuximab, respectively (72 h). N = 3.

D-F. Viability curve of the 4 LIM1215 cell lines (± *CCNF* ± *KRAS* activating mutations) treated with Erlotinib, Gefitinib or Cetuximab (72 h), respectively, at various concentrations of each drug (in Log_{10}(concentration in nM)). N = 3.

Figure generated using GraphPad Prism version 8.0.2.

a. Optimising Mass Spectrometry Data Acquisition Method for Deep Proteomic Study in LIM1215 Cells: DDA, DIA and TMT

Due to the series of results highlighting a potential regulatory loop between Cyclin F and KRAS, I decided to investigate this further by studying the changes in total proteome that occur under the following conditions: ± *CCNF* and/or ± *KRAS* constitutive activation. A proteome analysis in the 4 LIM1215 cell lines was bound to provide multiple important pieces of information depending on which 2 cell lines would be compared at a time (Figure 4iii).

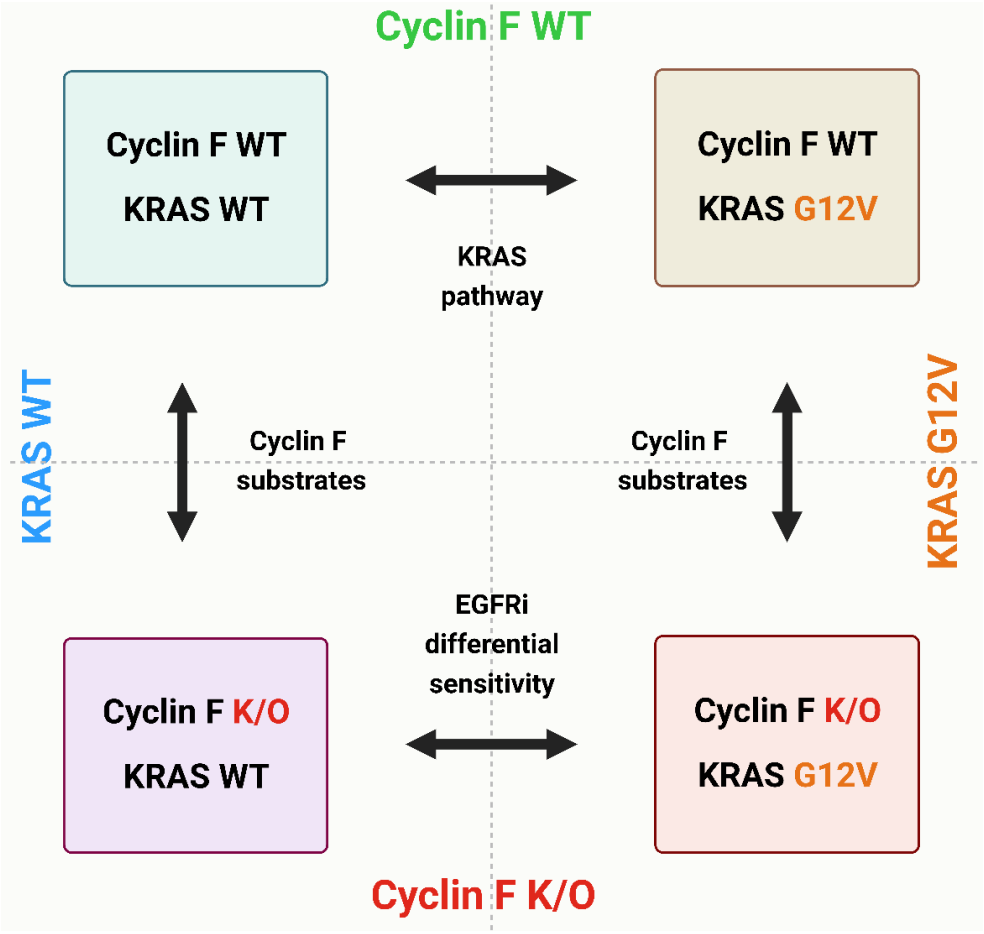


Figure 4iii. Planned proteome analysis of the 4 LIM1215 cell lines.

Results from the proteomic profiling of the LIM1215 cells lines were predicted to provide data on new potential Cyclin F substrates (by comparing the *CCNF* WT vs K/O samples), the reasoning behind the observed differential *CCNF*-dependent EGFRi sensitivity in *KRAS* mutant cell lines (by comparing *KRAS* WT and G12V samples, both in the context of *CCNF* loss) and lastly the signature *KRAS* pathway alterations (by comparing *KRAS* WT and G12V samples, both in *CCNF* WT settings).

Comparing Ctrl vs Mut would provide insight into the proteome changes mediated by KRAS mutation, Mut vs Mut *CCNF* K/O would highlight proteome changes controlled by Cyclin F in *KRAS* mutant settings, *CCNF* K/O vs Mut *CCNF* K/O would perhaps give clues as to why these 2 cell lines behave in an opposite manner to one another when treated with EGFR inhibitors, and Ctrl vs *CCNF* K/O would potentially point out novel Cyclin F substrates (Figure 4iii).

Constitutively active KRAS is known to induce DNA replication stress through various mechanisms, including aberrant replication origin firing and rate of fork progression. This results in the build-up of DNA damage and culminates in genomic instability (Al Zubaidi et al., 2021, Grabocka et al., 2015). Cyclin F has a crucial role in regulating DNA replication and preventing erroneous replication events, but the substrates mediating this phenotype are not yet fully elucidated. Thus, further identification of Cyclin F substrates is a crucial step towards a more refined understanding of the regulation of such significant cellular processes. To observe whether abnormal Cyclin F levels result in a similar phenotype to abnormal RAS activity, I examined DNA fibers in the presence or absence of Cyclin F.

Cyclin F loss gave rise to multiple forms of DNA replication stress, which is likely due to the accumulation of yet unidentified substrates. Examples of such DNA replication stress phenotypes, as revealed by a DNA fiber combing experiment (Figure 4iv.A), include higher rate of replication origin firing (Figure 4iv.B), higher replication fork asymmetry (Figure 4iv.C) and slower DNA replication forks (Figure 4iv.D). These phenotypes could possibly be accentuated by *KRAS* mutations impacting cell survival, but this warrants further investigation.

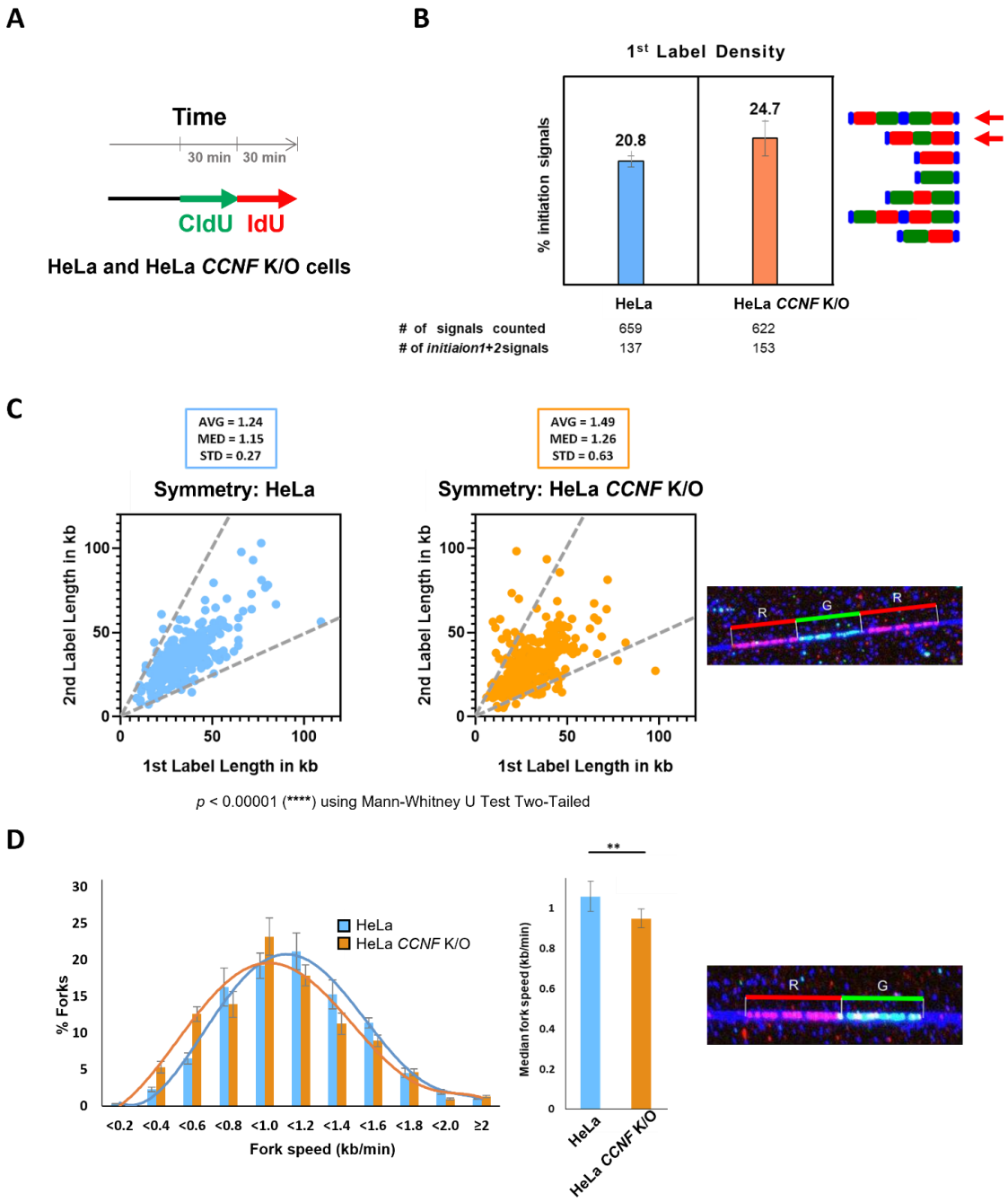


Figure 4iv. Cyclin F loss results in multiple forms of DNA replication stress.

A. Schematic of sample treatment for DNA fiber combing. HeLa and HeLa *CCNF* K/O cells were pulsed with the thymidine nucleoside analogue 5-chloro-2′-deoxyuridine (CldU) for 30 mins, followed by 5-iodo-2′-deoxyuridine (IdU), a different thymidine nucleoside analogue, for a further 30 mins.

B. First label density calculations from at least 600 software-detected and manually-validated signals/sample. Percentages were calculated to represent the frequency of each type of signal, and the sum of frequencies of the 2 types of initiation signals identified (see diagram on right) was used to quantify 1st label

density which is an indicator of the frequency of origin firing (Petermann et al., 2010, Rodriguez-Acebes et al., 2018).

C. XY scatter graphs for HeLa and HeLa *CCNF* K/O samples where 1st red label length in kb (X-axis) is plotted against 2nd red label length in kb (Y-axis) using initiation signals (see image on right). At least 300 events were counted/sample.

D. Nested scatter graphs for HeLa and HeLa *CCNF* K/O samples where 2nd label (red) speed in kb/min is plotted – which is calculated from 2nd label length in kb divided by 2nd pulse duration (30 min) using unidirectional signals (see image on right). At least 300 events were counted/sample.

To have a comprehensive picture of the proteins ubiquitylated in the different conditions highlighted above, I planned to carry out a pull-down experiment where peptides with diGly-modifications are isolated, as such leftover modifications are indicative of previous ubiquitylation events on the protein from which these peptides derive. However, due to technical difficulties relating to the IP samples (discussed later in this chapter), I decided to focus on analysing the total proteome alone.

Proteome analysis using LC/MS is a technique that has only emerged recently and hence requires further refinement. Thus, I decided to compare different available approaches. I started out with a pilot run with the aim of testing multiple data acquisition methods in order to pick out the optimal one to adapt for the large-scale experiment. The 2 methods tested were data-independent acquisition (DIA) and data-dependent acquisition (DDA) where DDA was divided into 2 labelling methods: tandem mass tag (TMT)-labelled and label-free quantification (LFQ) (Figure 4v).

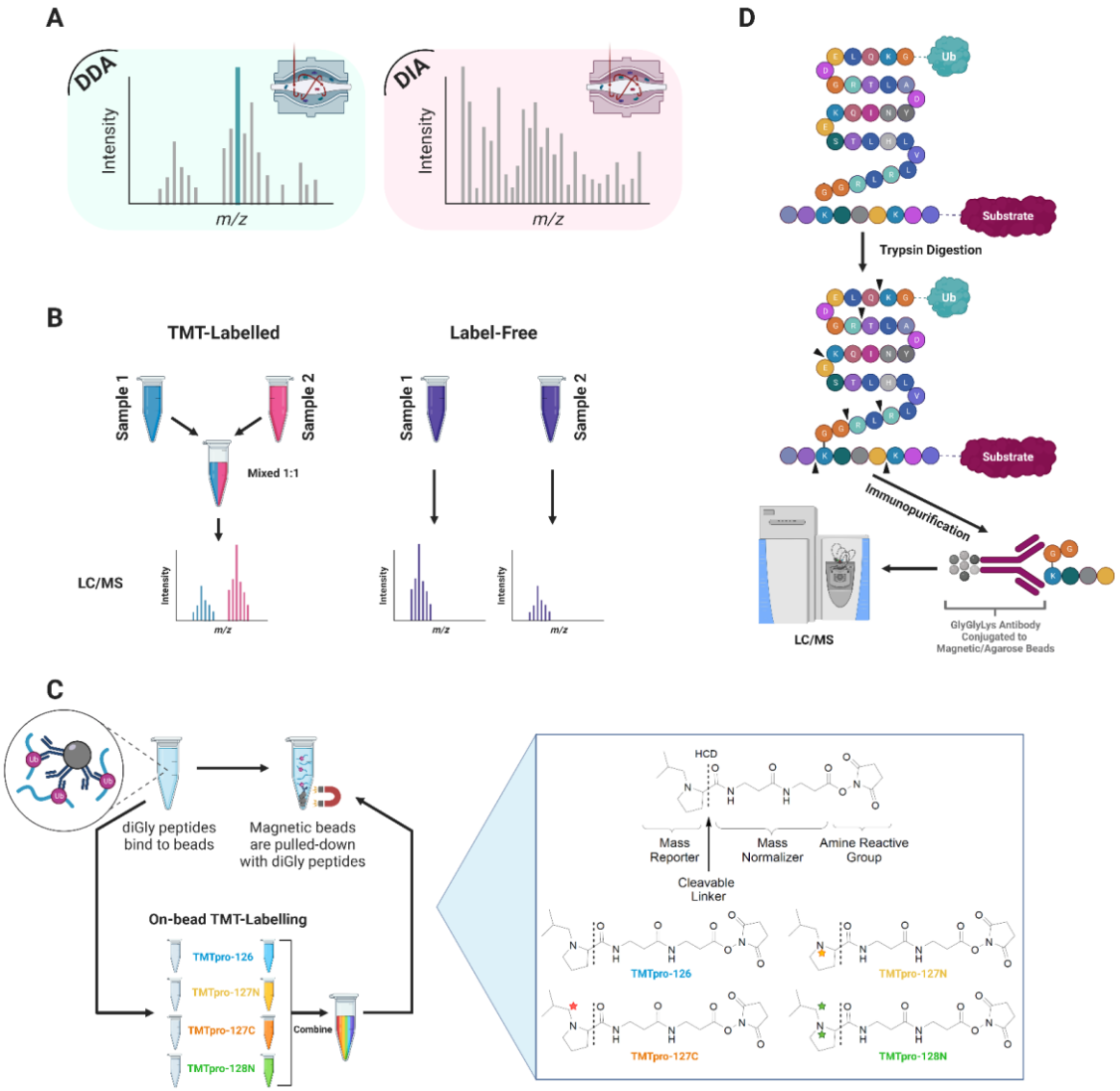


Figure 4v. Data acquisition methods tested: DDA LFQ, TMT and DIA.

A. Schematic of DDA vs DIA mass spectra comparison. *Adapted from (Hansen et al., 2021)*.

B. Schematic of TMT-labelled vs label-free DDA approaches and their mass spectra comparison.

C. Left: schematic of on-bead TMT labelling for the TMT DDA protocol. Right: chemical structure of TMT labels used for the pilot experiment. HCD = higher-energy collision dissociation site (cleavage site). * = ^{13}C and ^{15}N stable isotope positions. *Sub0figure on the right is adapted from Thermo Fisher Scientific's 'TMTpro Mass Tag Labeling Reagents and Kits' user guide*.

D. Schematic of diGly pull-down of ubiquitylated proteins post tryptic digestion.

Figure generated using BioRender.

The main difference between DDA and DIA modes of data collection is that DDA involves the instrument picking the strongest peptide ions in the first cycle of mass spectrometry (MS1 'scan' cycle), then fragmenting these selected ions only in the second cycle (MS2). DIA on the other hand is non-selective; instead of focusing on the most intense ion peaks the spectrometer focuses on a specific and pre-defined mass-to-charge (*m/z*) window for each cycle and fragments all precursors in that window (MS2 directly), then moves on to the next *m/z* window until the entire *m/z* range of all detected precursors is covered (Figure 4v.A) (Venable et al., 2004). As a result, DIA usually has fewer missing values and identifies more hits than DDA.

DDA can be combined with label-free or isotope-based quantification methods. TMT-labelling is a popular example of the latter, and allows the running of all combined samples on the mass spectrometer at once as opposed to loading each sample in a different mass spectrometer run (Figure 4v.B). This method enables more accurate quantification through measuring the relative protein expression levels directly between samples and reduces technical errors that are otherwise produced from run-to-run variations on the mass spectrometer. The labelling step itself involves adding a tandem-mass-tag to each sample, and this tag is composed of one of many possible combinations of additional ^{13}C and ^{15}N isotopes which results in a unique mass shift (known as reporter mass) for each sample (Figure 4v.C). For example, for the pilot experiment the TMT label 126 was used for the Ctrl sample, 127N for the *CCNF* K/O sample, 127C for the Mut sample and 128N for the Mut *CCNF* K/O one. The 'N' or 'C' in the TMT label's name refers to the type of stable isotope present in the mass reporter region of the label, which is cleaved at the higher-energy collision dissociation 'HCD' site

of the TMT label during the LC/MS fragmentation step, and thereby allows the quantification of reporter ion relative abundances (Figure 4v.C, right).

For my initial purpose of studying the ubiquitome, I utilised the highly-sensitive recently-developed method: UbiFast (Udeshi et al., 2020). This technique has been reported to successfully quantify around 10,000 ubiquitylation sites using as little as 0.5 mg protein concentration per sample. The protocol involves trypsin-digestion of the proteins within samples, which enzymatically cleaves the proteins after lysine and arginine resides. Ubiquitin, whose last 3 amino acids are Arg-Gly-Gly, is mostly deposited on lysine residues on substrates. This means that a Gly-Gly (GG or diGly) motif is left-over on lysine residues of the ubiquitylated substrate, and antibodies have been developed to recognise this Lys-ε-Gly-Gly with high specificity (Figure 4v.D). Such antibodies can be conjugated to magnetic or agarose beads and used to enrich the ubiquitylated fragments of proteins within a sample, which can then allow ubiquitylated protein identification and quantification using LC/MS.

The UbiFast protocol has an extra step that separates it from previously conducted diGly enrichment, which is that it employs on-bead TMT labelling (Figure 4v.C). The reason on-bead labelling was carried out was that the binding of Lys-ε-GG on ubiquitylated peptides to the antibody-bead complex protects this GG left-over motif from any TMT labelling, thereby protecting the primary amine of the leftover GG from the amine-reactive NHS-ester group of TMT, which therefore only reacts with the peptide N-terminal amine group and the ε-amine groups of lysine residues in peptide fragments (Udeshi et al., 2020).

I followed this UbiFast TMT-labelling technique, and ran label-free DDA as well as DIA in parallel in order to test the quality of each of these methods in the pilot experiment, and choose the most accurate one for the large-scale follow-up one. For these purposes, only N = 1 was used for this initial experiment using the 4 LIM1215 cell lines: Ctrl, *CCNF* K/O, Mut and Mut *CCNF* K/O.

From the density scatter plots of the total proteome, it appeared that the precursor peptides (plotted using their Log_2(intensity)) for DIA and DDA overlap fairly well when individual samples were compared in both data acquisition methods (Figure 4vi.A). When comparative samples were plotted (by subtracting the second sample's Log_2(intensity) from the first's, giving $Log_2(\frac{\text{intensity sample 1}}{\text{intensity sample 2}})$, the identified peptides' comparative intensities overlapped even more for DIA and DDA (Figure 4vi.B).

Compared to the DIA vs DDA samples, DIA vs TMT individual samples overlapped more accurately in terms of peptide identification and peptide intensity (Figure 4vi.C). Regarding comparative samples, both DIA vs DDA and DIA vs TMT had very high overlap in terms of peptide identification and intensity, but DIA vs DDA's overlap was slightly higher (Figure 4vi.D). Taken together, this showed that while DIA and DDA have an adequately high level of overlap in terms of identified peptides and peptide intensity for individual samples, the DIA and TMT had significantly higher overlap.

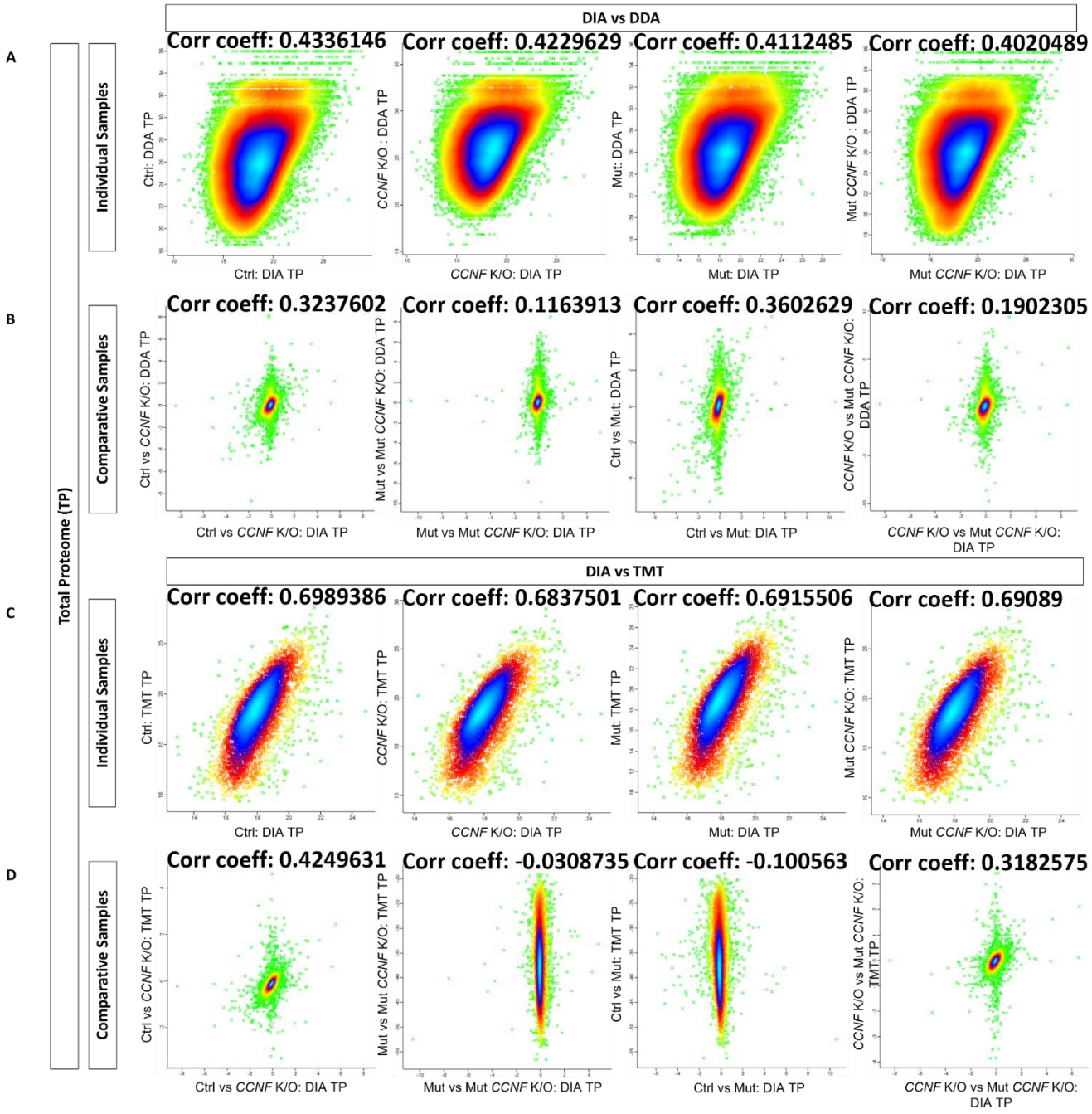


Figure 4vi. Density scatter plots representing total proteome data quality check: DDA vs DIA vs TMT. Correlation coefficient was calculated using Pearson correlation.

Each dot on the scatter plot represents a precursor peptide and its peak intensity shown after Log_2(intensity) transformation. *Figures generated using Perseus software version 1.6.2.2.*

A. Each individual sample's data showing the overlap between the DIA (X-axis) and DDA (Y-axis) results.

B. Comparative data between 2 samples at a time showing the overlap between the DIA (X-axis) and DDA (Y-axis) results. Compared samples have the

Log_2(intensity) values of the 2nd sample subtracted from the Log_2(intensity) value of the 1st giving $Log_2(\frac{\text{intensity sample 1}}{\text{intensity sample 2}})$.

C. Each individual sample's data showing the overlap between the DIA (X-axis) and TMT (Y-axis) results.

D. Comparative data between 2 samples at a time showing the overlap between the DIA (X-axis) and TMT (Y-axis) results. Compared samples have the Log_2(intensity) values of the 2nd sample subtracted from the Log_2(intensity) value of the 1st giving $Log_2(\frac{\text{intensity sample 1}}{\text{intensity sample 2}})$.

Concerning the GG pull-down LC/MS results, despite following the protocol stringently there was still an unidentified technical issue resulting in the failure of TMT labelling on beads. This meant that only the total proteome was correctly TMT-labelled and therefore its data could be analysed whereas the GG data could not. After excluding TMT's GG data, the only GG data left was from DIA and DDA (Figure 4vii). Analysis of the DIA vs DDA data showed strong overlap in ubiquitylated peptide identity and intensity between both data acquisition methods for individual samples (Figure 4vii.A) and an even stronger overlap for comparative samples (Figure 4vii.B).

Post assessing the density scatter plots, I turned to histograms to analyse which samples have the lowest number of missing values and hence needed the fewest imputations in order to replace them. Such imputations involve the replacement of missing values from the normal distribution of overall values within a sample. Data showed that DDA had the highest number of missing values and hence the highest rate of imputations needed to replace them, this was much lower for TMT, and lowest for DIA which had very few missing values (Figure 4viii). Number of missing values is a great reflection of data quality in an inversely related manner, meaning that DIA had the highest data quality with regards to missing values and DDA had the lowest.

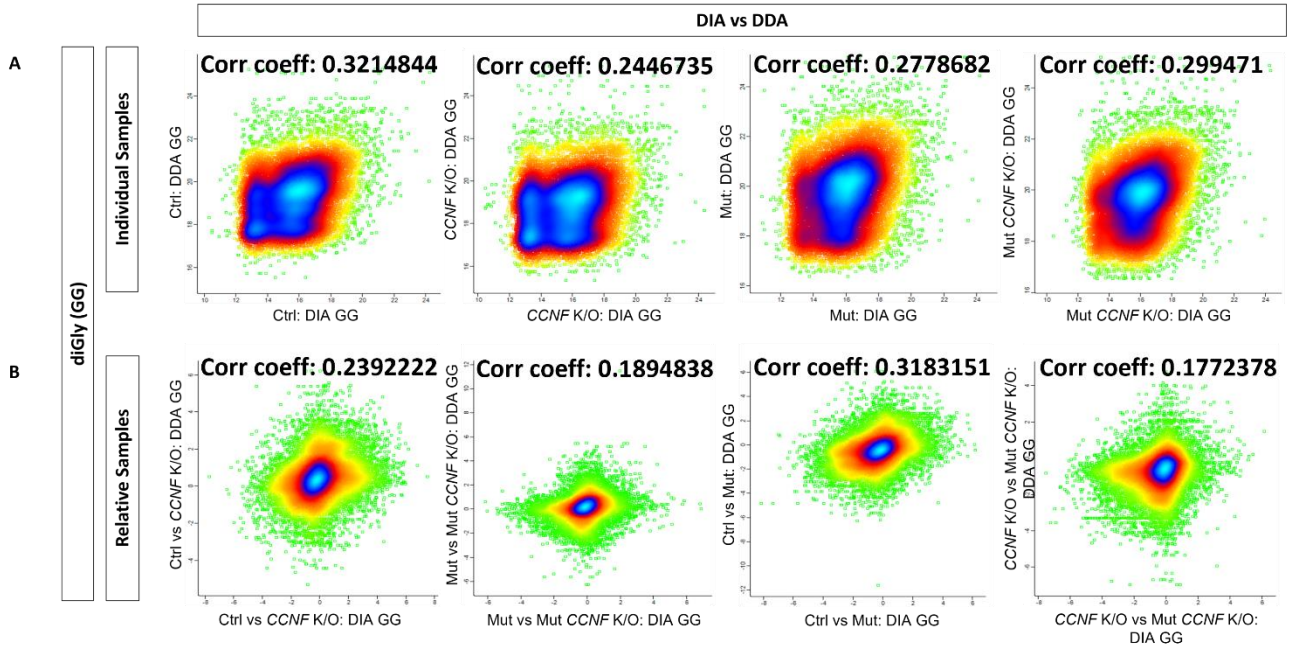


Figure 4vii. Density scatter plots representing diGly data quality check: DDA vs DIA. Correlation coefficient was calculated using Pearson correlation.

Each dot on the scatter plot represents a ubiquitylated precursor peptide and its peak intensity shown after Log_2(intensity) transformation. *Figures generated using Perseus software version 1.6.2.2.*

A. Each individual sample's data showing the overlap between the DIA (X-axis) and DDA (Y-axis) results.

B. Comparative data between 2 samples at a time showing the overlap between the DIA (X-axis) and DDA (Y-axis) results. Compared samples have the Log_2(intensity) values of the 2nd sample subtracted from the Log_2(intensity) value of the 1st giving $Log_2(\frac{\text{intensity sample 1}}{\text{intensity sample 2}})$.

To judge overall data quality between the 3 methods tested, I have conducted several analyses. One was precursor peptide identity and intensity overlap, another was missing values, and the remaining 2 described below were overall number of proteins identified and cost breakdown between the 3 methods. With a total of 8,430 identified proteins (from 93,940 peptides) in its total proteome samples, DIA came up on top for the highest number of proteins

identified and was followed by TMT (5,669 proteins from 47,911 peptides) and finally DDA (4,624 proteins from 38,812 peptides). DIA overlapped DDA in almost all of DDA's identified proteins in the total proteome samples (4,227 out of 4,624 – 91.4%) and also had the majority of TMT's proteins in common with it (5,467 out of 5,669 – 96.4%) (Figure 4ix.A). The 3 methods had 3,993 identified proteins in common for total proteome analysis, which represented 86.4% of DDA's total identified proteins, 70.4% of TMT's and 47.4% of DIA's.

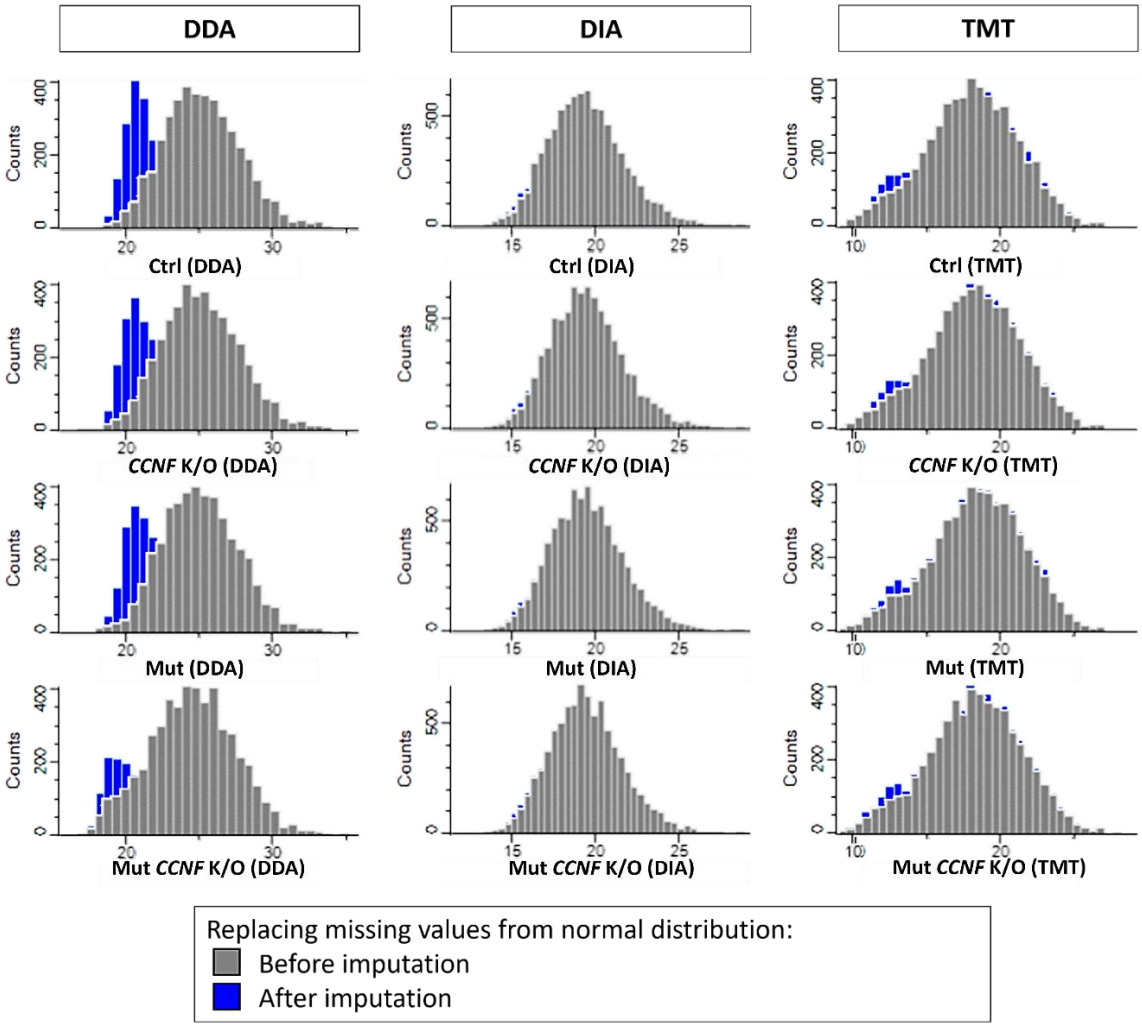


Figure 4viii. Missing values comparison: DDA vs DIA vs TMT.

Histograms representing the number of missing values ('Counts', Y-axis) plotted against Log_2(intensity) (X-axis) of peptide precursors within the 4 LIM1215 samples used (Ctrl, *CCNF* K/O, Mut and Mut *CCNF* K/O) for the 3 data acquisition methods tested (label-free DDA, DIA and TMT). Histograms before (grey) and

after (blue) replacing the missing values by imputation from normal distribution are overlapped for each plot. *Figures generated using Perseus software version 1.6.2.2.*

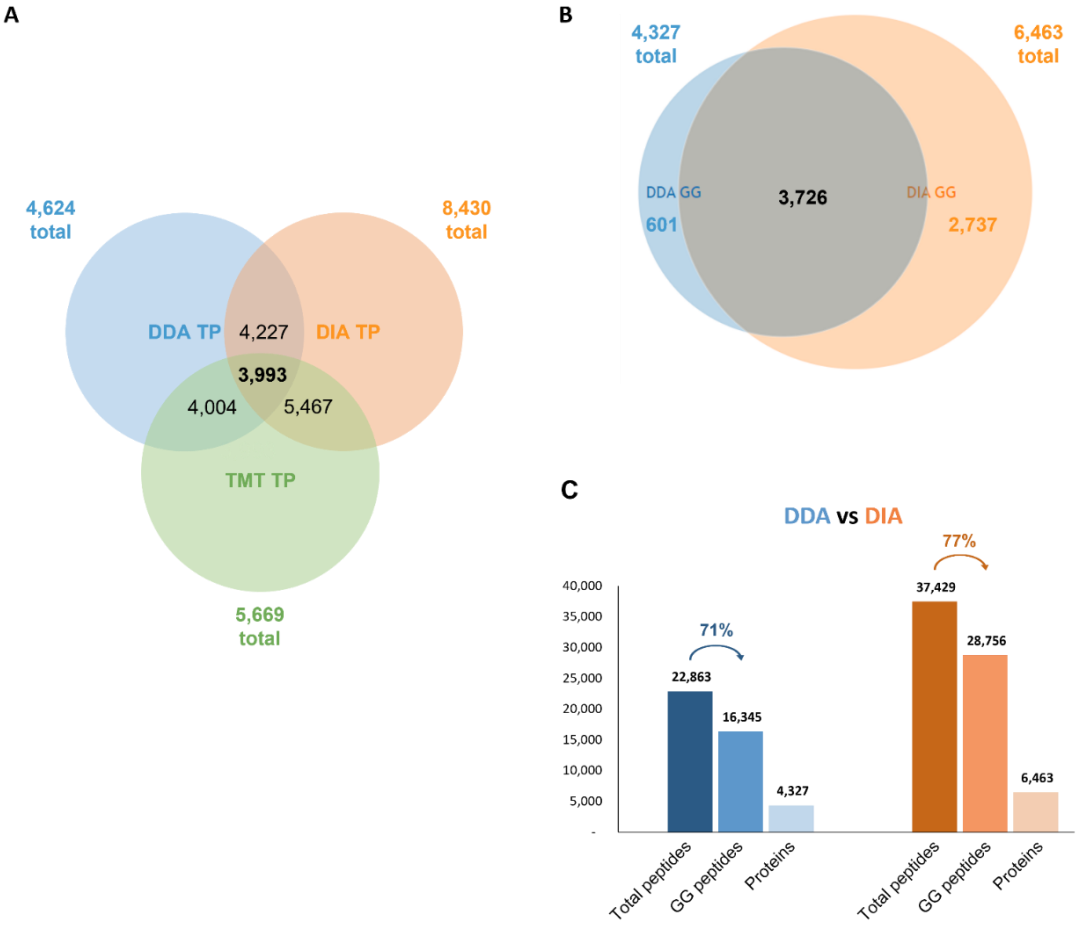
While 91.4% of DDA's proteins in its total proteome samples also appeared in DIA, 86.1% of proteins in its GG-enriched samples were also picked up by DIA (Figure 4ix.B). In both cases DIA had significantly more proteins identified than DDA: 1.8x more for total proteome and 1.5x more for GG. Additionally, DIA identified more GG-enriched peptides relative to overall peptides from the GG samples (77%) compared to DDA (71%), reflecting higher accuracy in retrieving ubiquitylated peptides. (Figure 4ix.C).

When it came to cost breakdown, multiple factors had to be considered for each data acquisition and/or sample labelling method. For all 3 methods the cost included the GG magnetic beads, S-traps (short for suspension trapping and has a hydrophobic compartment to trap proteins and wash off all other contaminants) and number of mass spectrometer runs (see cost breakdown in Figure 4ix.D).

While the GG beads and S-traps costs were the same per sample for all methods, the number of LC/MS runs (= mass spectrometer run time) varied since fractionation was needed for the TMT combined samples due to their complexity. Finalised calculations showed that the costs of running the 4 samples (Ctrl, *CCNF* K/O, Mut and Mut *CCNF* K/O) in N = 1 format was £2,101.56 for DDA or DIA alike, and 2.7x more expensive at £5,740.88 for TMT.

The data quality tests from the pilot experiment show DIA to be the most accurate and comprehensive data acquisition method, followed by TMT then DDA. The cost analysis shows DIA to be also the most affordable. Thus, overall,

I have concluded that DIA is the optimal data acquisition method to use for the large-scale experiment to follow and have indeed employed it for that purpose.



D

Line Item	Details	Cost/Item	Cost for Pilot Experiment
1	1x **16-plex TMT** kit	1,225.42	76.59/sample = £306.36/4 samples (**TMT**)
2	1x **GG enrichment** kit (for 10 samples)	2,510.41	£1,004.16/4 samples (**TMT/DIA/DDA**)
3	12x **S-TRAP** midi spin columns (4xTMT, 4xDIA, 4xDDA)	24.2	£8.07/4 samples (**TMT/DIA/DDA**)
4	2x **high pH fractionation**(1 TP + 1 GG), concatenated into 10 each (20 total fractions, all TMT)	1,701.97	£1,701.97 (**TMT**)
5	**MS run** - TMT deep proteome (10 TP fractions, 10 GG fractions)	2,723.32	£2,723.32 (**TMT**)
6	**MS run** – DIA or DDA (4x TP, 4x GG)	1,089.33	£1,089.33 (**DIA/DDA**)
			TOTAL / 4 samples
			TMT = £303.36 + £1,004.16 + £42.56 + £1,701.97 + £2,723.32 = **£5,740.88** (of which TP = £2,527.08)
			DIA = £1,004.16 + £21.28 + £1,089.33 = **£2,101.56** (of which TP = £552.74)
			DDA = £1,004.16 + £21.28 + £1,089.33 = **£2,101.56** (of which TP = £552.74)

Figure 4ix. Hit overlap and cost breakdown for DDA, DIA and TMT.

A. Venn diagram representing the overlap of overall proteins identified in the total proteome of all samples combined using DDA LFQ, DIA or (DDA-) TMT data acquisition methods.

B. Venn diagram representing the overlap of overall proteins identified in the diGly pull-down of all samples combined using DDA or DIA data acquisition methods. Figures A-B were generated using the online Venn diagram generator tool Venny.

C. Bar chart showing the number of total peptides, GG peptides and proteins identified in the GG-enriched samples using DDA and DIA approaches, and the percentage of the total peptides that is GG-modified for each data acquisition method.

D. Table demonstrating the cost breakdown for using DDA, DIA or TMT methods for data acquisition (± sample labelling) of the 4 LIM1215 samples. Costs are calculated for 4 samples (for both TP and GG fractions all together), and the portion specific to the total proteome (which turned out to be the usable portion of the generated data) only is highlighted for each data acquisition method.

Before proceeding with the large-scale experiment, I conducted an initial quality analysis of the total proteome data provided by the 2 most accurate methods for data acquisition according to my previous evaluation (Figure 4vi-ix): DIA and TMT-labelled DDA.

I looked for potential Cyclin F substrates identified by the two methods, and included in my analysis the potential novel substrates identified based on the degron refinement work presented earlier (in data chapter 1). To this end, I prioritised proteins that are enriched in the *CCNF* K/O sample compared to the Ctrl one, and considered its enrichment in Mut *CCNF* K/O vs Mut samples as an additional means of providing higher confidence in a protein's potential substrate status through acting as a "pseudo-repeat" of Cyclin F loss settings (Figure 4x). Hits enriched in the *CCNF* K/O sample were then filtered for ones that have one of the published or newly identified (in this thesis) Cyclin F degrons.

A

	TMT Total Proteome						Lab's Previous Turbo ID CCNF ΔF > CCNF WT	Lab's Previous Mass Spec MLN+CCNF > NTC+CCNF	Nuclear?
	CCNF Degrons			Ratios (intensity)		Protein name	Student's T-test Log_2(MLN-NTC)	Protein Score Difference MLN / NTC	
	[TS]P.{2,20}R.L	[TS]P.{2,20}R.I	R.IF	*CCNF* K/O / Ctrl	Mut *CCNF* K/O / Mut				
1	DDX3Y			2.25	1.22	ATP-dependent RNA helicase DDX3Y	0.370		✓
2	OAS2			2.24	0.69	2'-5'-oligoadenylate synthase 2			
3	HELLS (LSH)	HELLS (LSH)		2.21	0.78	Lymphoid-specific helicase	0.957		✓
4	LGR5			2.04	0.93	Leucine-rich repeat-containing G-protein coupled receptor 5			
5	CDC20	CDC20		1.80	1.12	Cell division cycle protein 20 homolog	1.13	37.00	
6	BRAT1			1.77	0.93	BRCA1-associated ATM activator 1			✓
7	RRM2	RRM2	RRM2	1.68	1.12	Ribonucleoside-diphosphate reductase subunit M2	2.91	61.00	
8	OAS3			1.64	0.84	2'-5'-oligoadenylate synthase 3			✓
9	OAS1			1.49	0.86	2'-5'-oligoadenylate synthase 1			✓

	DIA Total Proteome						Lab's Previous Turbo ID CCNF ΔF > CCNF WT	Lab's Previous Mass Spec MLN+CCNF > NTC+CCNF	Nuclear?
	CCNF Degrons			Ratios (intensity)		Protein name	Student's T-test Log_2(MLN-NTC)	Protein Score Difference MLN / NTC	
	[TS]P.{2,20}R.L	[TS]P.{2,20}R.I	R.IF	*CCNF* K/O / Ctrl	Mut *CCNF* K/O / Mut				
1	DDX3Y			9.92	1.10	ATP-dependent RNA helicase DDX3Y			✓
2	OAS2			7.68	0.81	2'-5'-oligoadenylate synthase 2			
3		EXO1	EXO1	4.34	1.33	Exonuclease 1	6.63	2.26	
4	PTOV1			3.85	1.03	Prostate tumor-overexpressed gene 1 protein			✓
5	HELLS (LSH)	HELLS (LSH)		4.13	1.01	Lymphoid-specific helicase			✓
6	NEK2			3.12	1.77	Serine/threonine-protein kinase Nek2			✓
7			CDT1	2.71	1.19	DNA replication factor Cdt1	4.91	1.97	✓
8	BORA			2.76	5.15	Protein aurora borealis	2.01	38.00	✓
9		RUNX2		2.72	0.97	Runt-related transcription factor 2			✓

B



Figure 4x. Initial short-listing of Cyclin F neo-substrates from DIA and TMT total proteome data.

A. Table showing a refined list of high confidence potential Cyclin F substrates. Hits were filtered by: enrichment in *CCNF* K/O and Mut *CCNF* K/O cells compared to their respective controls, possessing a Cyclin F degron, nuclear localisation and cross-over with the lab's previous Cyclin F interactome search (LC/MS and TurboID).

B. Top hits from (A) tested via immunoblots. Left and middle: HEK293T cells were transfected with GFP-*CCNF* mutants (WT and ΔF) and immunoprecipitated using a GFP resin after which Cyclin F binding to each of the potential substrates was visualised via immunoblots. Right: immunoblots of whole cell lysates of HeLa *CCNF* WT and *CCNF* K/O samples.

Whether the proteins were nuclear or not was also taken into consideration, given that Cyclin F itself is a nuclear protein and so are the majority

of its substrates. The refined list was then compared to the previous results from the D'Angiolella lab's mass spectrometry experiment (± MLN4924) and proximity labelling TurboID experiment, both using Cyclin F as bait. A final list of potential Cyclin F substrates was drawn up based on cellular location, protein levels and cross-over with the lab's previous Cyclin F interactome search. A few positive controls came up as top-ranking hits such as the Cyclin F substrates RRM2 and EXO1 (D'Angiolella et al., 2012, Elia et al., 2015) and the Cyclin F interactor CDC20 (Choudhury et al., 2016). Some selected hits from the final list (highlighted in red, Figure 4x.A) were tested via Western blot (Figure 4x.B).

Judging by the input levels in HeLa cells with or without Cyclin F, BRCA1 Associated ATM Activator 1 (BRAT1), Lymphoid-Specific Helicase (HELLS/LSH) and Protein Aurora Borealis (BORA) behave as typical Cyclin F substrates since they are enriched in cells depleted of this E3 ligase. It is important to note that HELLS is also enriched in the TurboID experiment using Cyclin F as bait in samples treated with the NEDDylation (thus CRL-activation) inhibitor MLN4924 compared to the untreated controls.

HELLS/LSH was not detected in Cyclin F immunoprecipitates and was only detected after TurboID, suggesting that the interaction between Cyclin F and HELLS might be disrupted following cellular lysis. This presumption is based on the fact that proximity labelling in the TurboID experiment is conducted in undisturbed live cells and the pull-down of these already-labelled Cyclin F interactors occurs post lysis, meaning that the substrates are already marked *in vivo* before the *in vitro* pull-down. On the other hand, in conventional IP approaches the binding between unlabelled substrates and tagged Cyclin F occurs *in vivo* and the substrates are co-immunoprecipitated with Cyclin F *in vitro*,

which means if there is any disruption to substrate binding during the lysis procedure then there would be no way to identify these substrates that were bound to Cyclin F in the live cells but lost this binding *in vitro*. Hence, the fact that HELLS is pulled-down with Cyclin F in a substrate dependent manner in the TurboID experiment gives more credibility to the substrate potential of HELLS despite its failure to co-immunoprecipitate with Cyclin F using conventional pull-down methods.

BRAT1 and BORA proteins were not increased in association to the Cyclin F ΔF mutant compared to Cyclin F WT. This does not fully exclude that they are Cyclin F substrates and could alternatively suggest different mechanisms of recognition and ubiquitylation – one speculation could be that BRAT1 might behave as a Cyclin F substrate exclusively post DNA damage since it is an ATM-activating protein that is reportedly involved in the DDR (Ouchi and Ouchi, 2010, So and Ouchi, 2011).

Meanwhile, the chromatin licensing protein CDT1 is pulled-down more strongly with Cyclin F ΔF compared to the WT control and appears to be enriched in the input of the samples with Cyclin F ΔF overexpression, this is in line with the behaviour of Cyclin F substrates (see RRM2). However, CDT1 does not seem to be enriched in HeLa cells that have a Cyclin F knock-out. This could be due to this being a cell line specific event (in HEK293T vs HeLa). Based on this pilot LC/MS experiment and subsequent data analysis, it can be concluded that BRAT1, HELLS/LSH, BORA and CDT1 are likely substrates of Cyclin F but further validation is required.

This chapter explains how an initial observation that the RAS oncoprotein regulates Cyclin F through the apparent accelerated turnover of its substrates RRM2 and E2F1 led to the investigation of the opposite end of this regulatory pathway; RAS regulation by Cyclin F. This regulation of the hallmark oncoprotein was validated through an EGFR inhibitor sensitivity experiment, where the survival of 4 cell lines in all possible combinations of ± *CCNF* ± *KRAS*-mutations was assessed. The decreased resistance of *KRAS*-mutant cells to EGFR inhibition in settings of Cyclin F loss confirmed this regulation. One limitation to this study is that the *KRAS* G12V mutant cell line is a commercial one that was purchased by our lab. In that case, it might exhibit clonal effects. One control for this could be transiently overexpressing *KRAS* G12V in the parental *KRAS* WT cell line that is also provided by the company, and testing whether or not this recapitulates the phenotype of the *KRAS* G12V stable cell line.

Since the regulation of *KRAS* by Cyclin F that is observed in this chapter was considered to be most likely indirect owing to RAS being cytosolic/membrane-bound and Cyclin F being nuclear, an investigation of the pathways underlying this phenotype was necessary. Proteomic profiling was the method of choice to acquire these answers, but before such large-scale study was undertaken, an optimisation experiment was carried out comparing different mass spectrometry techniques; data-dependent and data-independent acquisition methods, as well as label-free and TMT-labelled methods. Data quality and cost analyses led to the conclusion that the DIA label-free method is the optimal one for the purpose of this study, and was therefore adopted for the large-scale experiment in the following chapter.

5. Results Chapter III: Exploring Proteome Changes Induced by Cyclin F's E3 Ligase Activity and the KRAS-Cyclin F Regulatory Network

The large-scale experiment was conducted using the same 4 LIM1215 cell lines (Ctrl, *CCNF* K/O, Mut and Mut *CCNF* K/O), but this time in biological triplicates. After coming out as the optimal data acquisition method based on the conclusion from the analysis of the pilot study, DIA was used for this LC/MS experiment.

Principal component analysis (PCA) plots were drawn out for both the total proteome samples as well as the diGly to understand the reliability of the biological triplicates (Figure 5i). The total proteome PCA plot shows triplicates to be clustered very closely together for each sample, indicating high similarity. However, the PCA of the diGly-enriched samples did not show the same accuracy with replicate clustering; biological repeats from the same sample were scattered far enough apart to indicate high variation across replicates. This is highly likely due to the need for further optimisation of the complex pull-down technique to minimise human and technical errors contributing to this vast difference between replicates. Additionally, one of the diGly replicates for the Mut sample did not return any data when run on the mass spectrometer, indicating an unidentified error with sample preparation rendering it unusable. For these reasons, the data analysis was conducted using only the total proteome results after the GG results failed this critical quality control checkpoint. Proteomic profiling generates a plethora of data that is often complemented by the diGLY

results, but in this case, the complementation would have to arise from follow-up validation experiments instead.

Total proteome data was then plotted as a hierarchal heat-map clustergram where *KRAS* mutational status (WT vs mutant) served as the highest level of the hierarchy, followed by Cyclin F levels (WT vs K/O). This allowed a wider view of the changes in gene clusters based on *KRAS* mutational status, followed by an overview of the effects of Cyclin F loss in these cell lines (Figure 5ii.A).

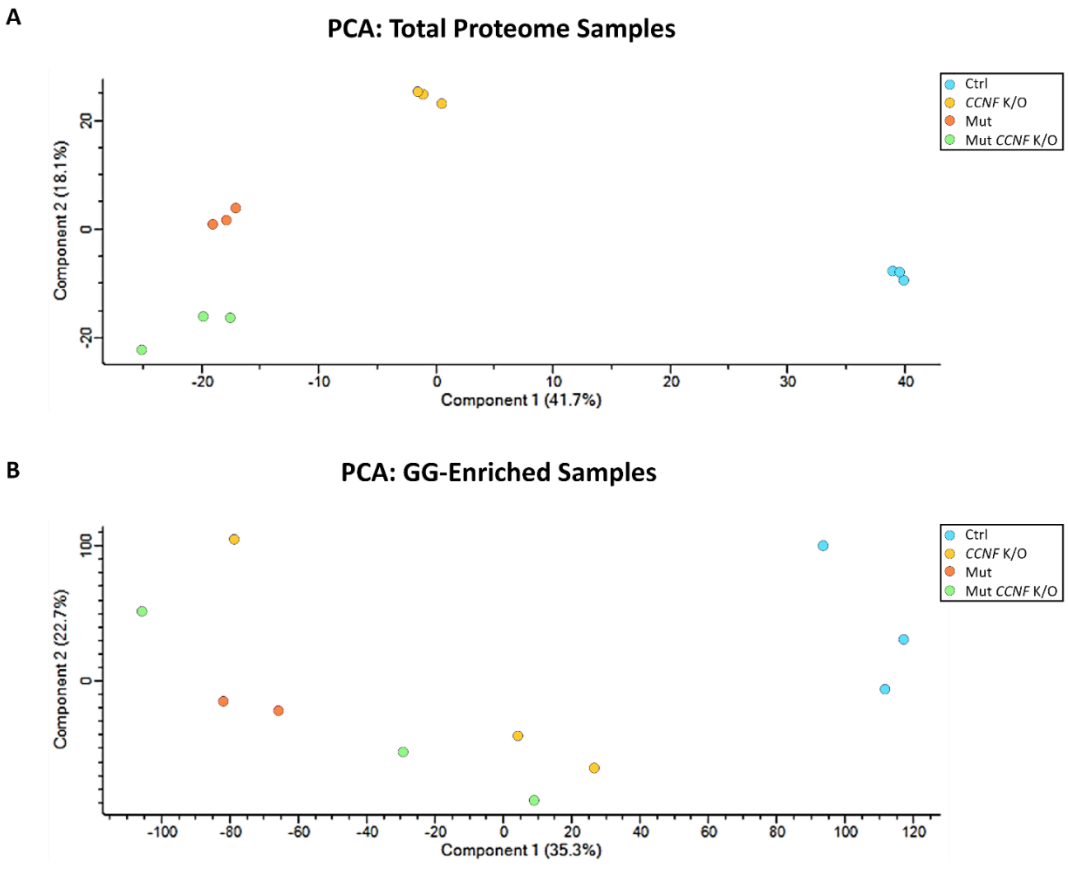


Figure 5i. Principal component analysis (PCA) plot for the 4 LIM1215 samples ran in triplicates.

A. PCA of the total proteome samples for the LIM1215 samples (± *CCNF* and/or ± *KRAS* activating mutations).

B. PCA of the GG-enriched samples for the LIM1215 samples (± *CCNF* and/or ± *KRAS* activating mutations).

Figures generated using Perseus software version 1.6.2.2.

Six main clusters were chosen as representative for the data quality by highlighting differences between the 4 samples. For example, the profile graph of cluster #7263 shows that proteins in this cluster are downregulated only in the sample with the combination of Cyclin F loss and an activating mutation in *KRAS*, and upregulated in the 3 other cell lines (Figure 5ii.B). Cluster #7285 is similar in that 3 out of 4 cell lines have an upregulation of the proteins in this cluster, whereas the control sample which is WT for both *CCNF* and *KRAS* has a downregulation in these genes. Cluster #7162 highlights differences based on *KRAS* mutational status where the *KRAS* WT samples have an upregulation of the proteins in this cluster, contrastingly to the *KRAS* mutant samples where a downregulation is observed instead. Equally as important is cluster #7293 which represents a number of proteins that are upregulated in cells where Cyclin F is lost, thereby comprising a list of potential Cyclin F substrates. Due to the heavily condensed and simplified nature of the data from the clustergrams and profile diagrams, they served a purely qualitative purpose whereas the quantitative data was extracted from volcano plots instead (discussed later in this chapter).

After assessing the clustergram, I turned to histograms for the last quality control check, which is number of missing values. As expected from the earlier pilot experiment testing multiple sample labelling and data acquisition methods (Figure 4viii), this label free DIA approach has a very small number of missing

values, which means that very few imputations are needed to replace these values from the normal distribution, thereby reflecting rich data quality (Supplementary Figure 5).

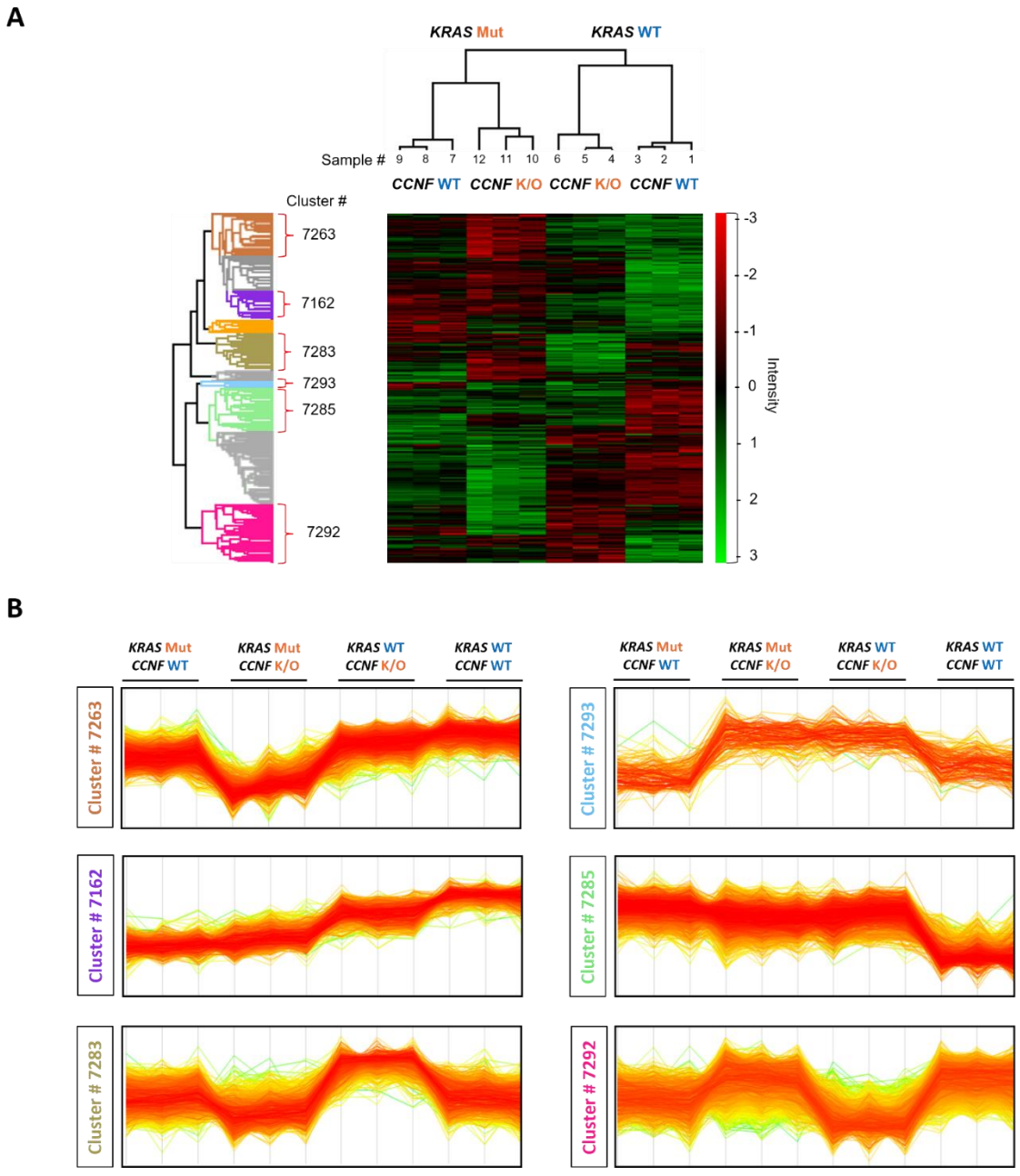


Figure 5ii. Hierarchical clustering of total proteome data filtered by Anova q-value (5% false-discovery rate 'FDR') with Z-score presented as intensity.

A. Clustergram of LIM1215 samples (± *CCNF* and/or ± *KRAS* activating mutations) based on intensity (Z-score).

B. Profile graphs of proteins changing in each cluster outlined in A.

Figures generated using Perseus software version 1.6.2.2.

Volcano plots were drawn out for the 4 samples and, through a preliminary review of the data, 2 proteins stood out as ones that consistently shift drastically across samples; the interferon protein ISG15 and Mitogen-Activated Protein Kinase Kinase 6 (MAP2K6) (Figure 5iii.A-D). Before any in-depth analysis of the data, including the rationale behind the shifts in these 2 proteins in the observed directions, an initial means of validation that the experiment worked and is indeed reflective of basal protein levels in the respective samples was conducted. This quality control check involved using a freshly defrosted batch of spared cell lysates of the 4 samples, identical to the batch used for this large-scale LC/MS experiment, to assess protein levels of the 2 selected representative proteins – ISG15 and MAP2K6 – through immunoblotting. The Western blot confirmed the volcano plots' results; ISG15 and MAP2K6 are both enriched in the *CCNF* K/O and Mut cell lines compared to the Ctrl one, and they are depleted in the Mut *CCNF* K/O sample compared to the Mut one (Figure 5iii.E). Once this clear validation was obtained, the in-depth data analysis was initiated.

a. Cyclin F Potential Neo-substrates Identification (Mut and Ctrl ±*CCNF*)

The total proteome datasets obtained from the different cell lines were rich in data, thus, to simplify the data analysis I broke down the comparisons into subsets. In this section I will discuss the comparison between cells expressing Cyclin F and cells lacking it in both *KRAS* WT and KRAS *G12V*$^{+/-}$ settings.

Proteins accumulating in cells where Cyclin F has been knocked-out are potential Cyclin F substrates, whereas reduced proteins in these settings represent indirect effects due to Cyclin F depletion.

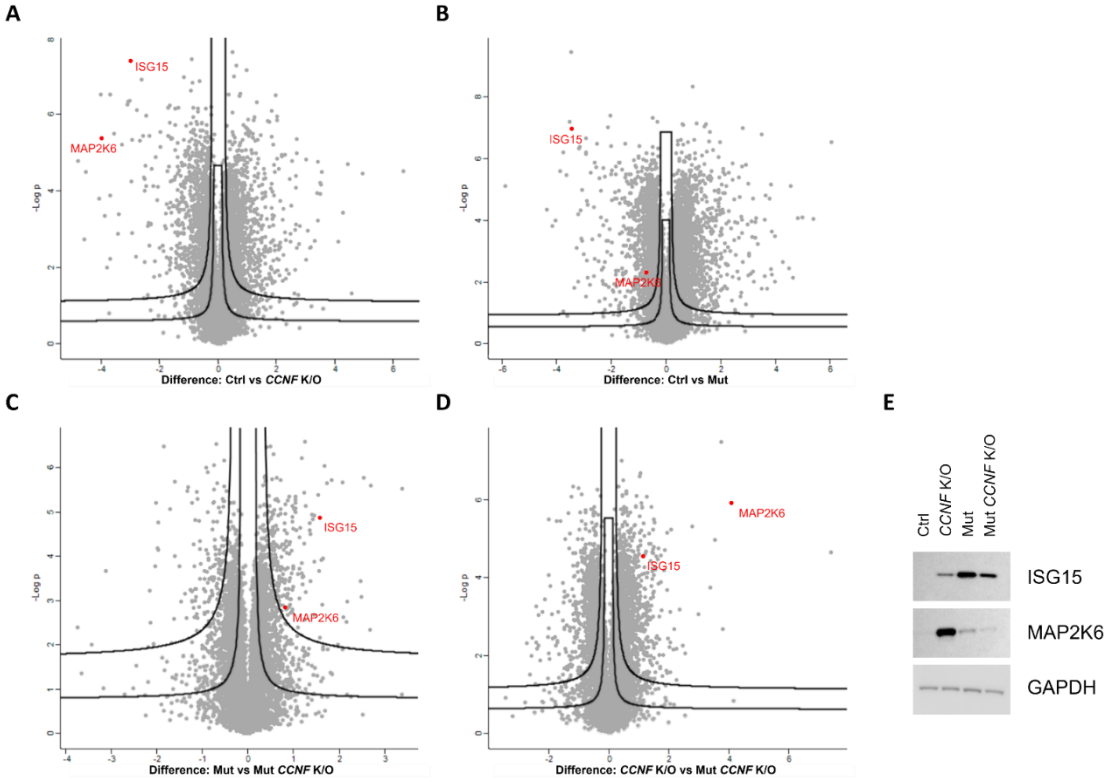


Figure 5iii. Volcano plots of comparative samples and western blot validation.

A-D: Volcano plots representing protein fold changes (X-axis: $Log_2(\frac{\text{intensity sample 1}}{\text{intensity sample 2}})$) against -Log(p-value) (Y-axis) across samples. S0 (parameter for displaying fold change) = 0.1, FDR = 1% (narrower curves) or 5% (wider curves). *Figure generated using Perseus software version 1.6.2.2.*

E. Immunoblot of whole cell lysates of the 4 LIM1215 samples used for this study.

From an initial comparison, an interesting observation was made: Cyclin F loss strongly triggers the interferon response (data presented in Figure 5iv.A and model illustrated in Figure 5v). Another interesting observation was that a similar

interferon response is activated in a *KRAS*-activating-mutation dependent manner in the isogenic cell lines (Figure 5iv.B & Figure 5v). The similarity is high enough that when the 2 samples *CCNF* K/O and Mut are compared, the is no significant shift in interferon pathway proteins (Figure 5iv.C). This meant that proteins heavily enriched in the *CCNF* K/O sample (in the same direction where Cyclin F substrates are expected to show up) will be inevitably masked by shifts of massive fold change in interferon pathway proteins instead.

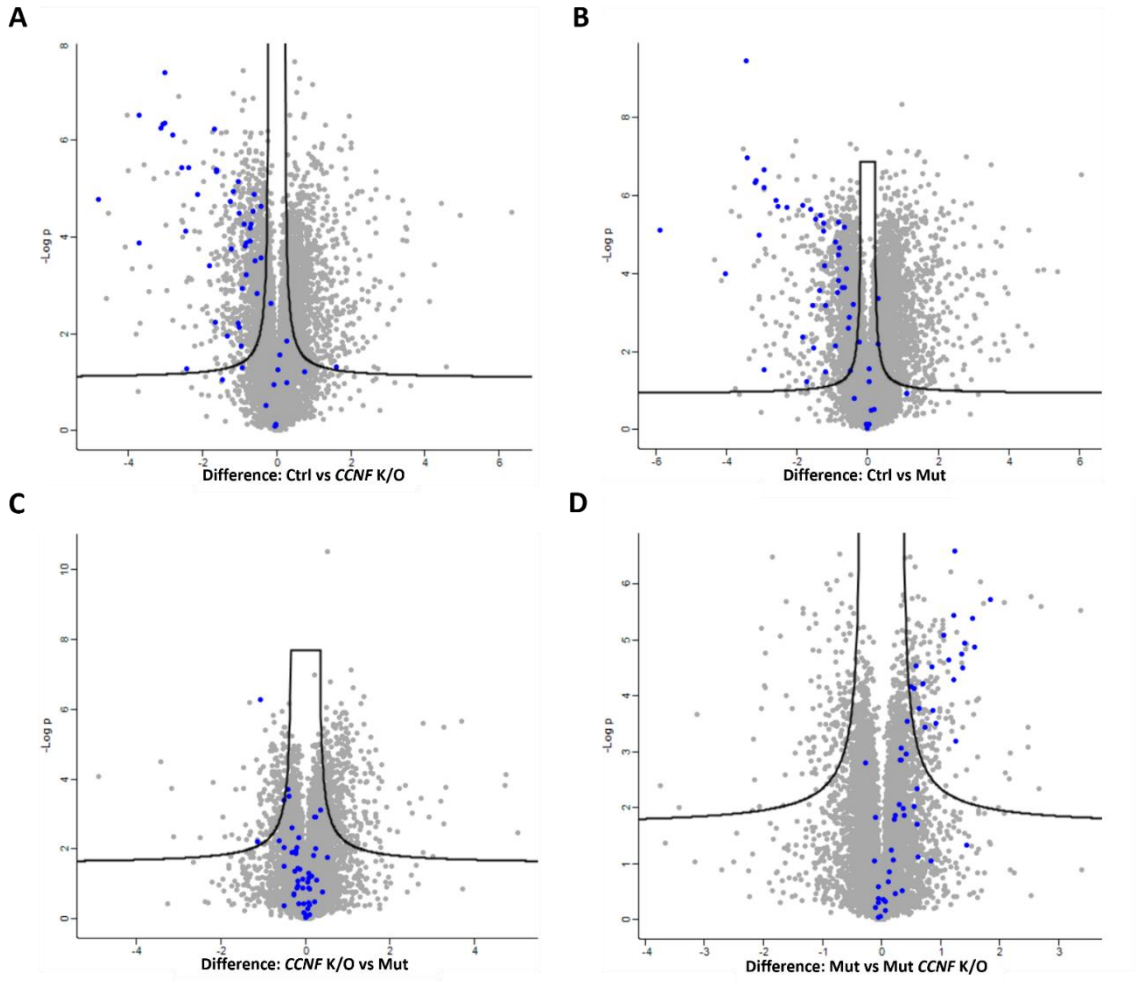


Figure 5iv. Volcano plots highlighting interferon response proteins (blue) in comparative samples.

A-D: Volcano plots representing protein fold changes (X-axis: $\text{Log}_2(\frac{\text{intensity sample 1}}{\text{intensity sample 2}})$) against -Log(p-value) (Y-axis) across samples, highlighting

shifts in ~ 55 interferon response proteins (blue). S0 (parameter for displaying fold change) = 0.1, FDR = 1%. *Figures generated using Perseus software version 1.6.2.2.*

While this is the case for Cyclin F loss in the *KRAS* WT samples, the opposite holds true for the *KRAS* mutant ones (Figure 5iv-v). The volcano plot comparing protein level differences in the Mut and Mut *CCNF* K/O samples show the interferon pathway to be more active in the Mut sample, thereby none of these heavily shifted proteins have moved in the same direction that Cyclin F substrates are expected to, so no substrate masking is expected (Figure 5iv.D). For these reasons, potential Cyclin F substrates identified from the *KRAS* mutant samples (±*CCNF*) have been given priority in this data analysis over ones identified from the *KRAS* WT ones.

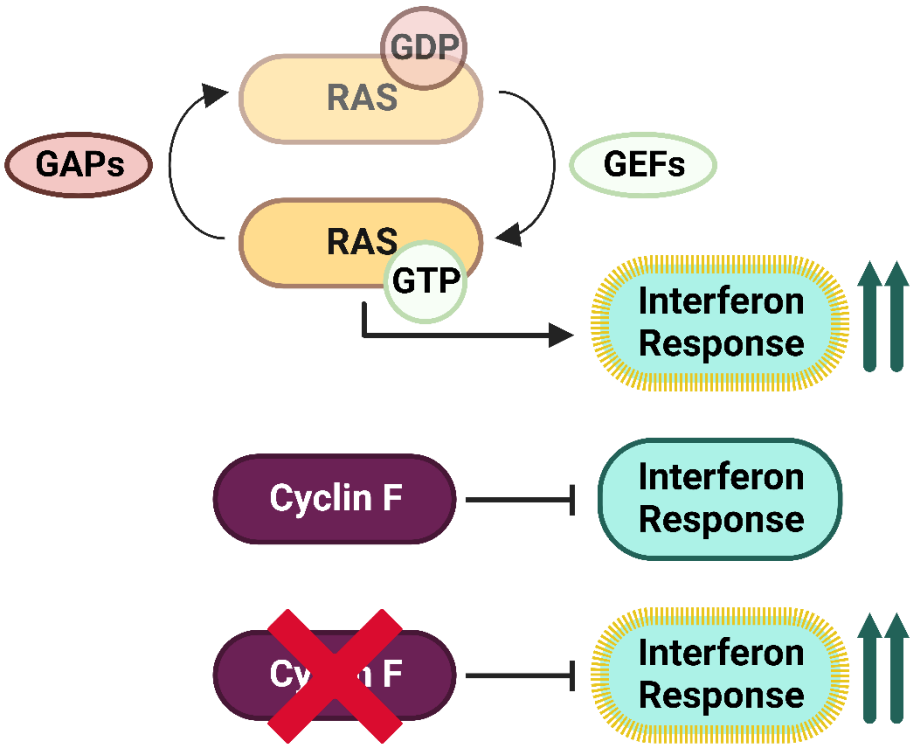


Figure 5v. Illustration of the observed activation of the interferon response pathway.

Cells with activating mutations in *KRAS* showed an intense enrichment of interferon proteins compared to their *KRAS* WT counterparts. Cells depleted of

Cyclin F showed quite a similar intensity of enrichment for the same pathway. *Figure generated using BioRender.*

Significant hits (filtered using a stringent 1% FDR) were extracted from the volcano blots of both Mut vs Mut *CCNF* K/O & Ctrl vs *CCNF* K/O samples, and drawn up in 2 respective tables in order of decreasing fold change (Figure 5vi.A-B). Proteins enriched in samples with a knock-out in Cyclin F were then filtered based on whether or not they have any of the known – or newly identified in this thesis – Cyclin F degrons: [T/S]Px[2,20]RxL, [T/S]Px[2,20]RxI, [T/S]Px[2,20]RxIF and [R]x[I][F] (without the priming phosphorylation site). Nuclear localisation was also taken into account.

RRM2 served as a positive control in this list. With the aim of selecting a few high-confidence proteins to test for Cyclin F substrate potential (Figure 5vi.C), priority was given to nuclear ones that are most heavily enriched in the Mut *CCNF* K/O samples compared to its Mut control. In line with this, Zinc Finger Matrin-Type 3 (ZMAT3), Helicase Like Transcription Factor (HLTF), DNA Topoisomerase II Alpha (TOP2A) and RecQ Mediated Genome Instability 1 (RMI1) were selected for testing. PRC1 was also selected but it had already been tested for substrate potential in an earlier chapter and appeared to be marginally more enriched in HeLa *CCNF* K/O cells compared to their *CCNF* WT counterpart (Figure 3x.C).

I performed a pull-down experiment using Cyclin F (and its non-degrading/non-ubiquitylating mutant ΔF) as bait, and examined whole cell lysates of the 4 LIM1215 cell lines (± *CCNF* K/O ± *KRAS* mutation) and the 2 HeLa ones (± *CCNF* K/O) in parallel in order to test the substrate status of these 3 proteins (Figure 5vi.D).

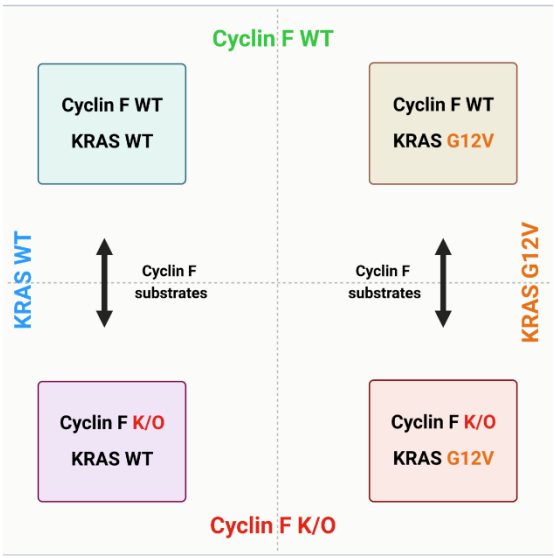
A

	Total Proteome: *CCNF* K/O / Ctrl						
	CCNF Degrons				p-value	Intensity *CCNF* K/O / Ctrl	Nuclear?
	[TS]P.{2,20}R.L	[TS]P.{2,20}R.I	R.IF	[TS]P.{2,20}R.IF			
1	RSAD2				1.72E-05	28.04	
2	FANCG				1.00E-02	13.96	✓
3	DDX3Y				3.27E-06	11.98	✓
4	AFF2				4.22E-04	10.65	✓
5	OAS2				4.37E-07	8.15	✓
6	FARP1				1.30E-03	7.75	
7			ACSL1		1.24E-07	6.24	
8	ATF3				4.48E-05	5.90	✓
9		SAMD9			9.86E-05	5.78	
10	CMPK2	CMPK2	CMPK2	CMPK2	1.11E-06	5.58	
11	PADI1				7.23E-04	4.98	

B

	Total Proteome: Mut *CCNF* K/O / Mut						
	CCNF Degrons				p-value	Intensity Mut *CCNF* K/O / Mut	Nuclear?
	[TS]P.{2,20}R.L	[TS]P.{2,20}R.I	R.IF	[TS]P.{2,20}R.IF			
1	RRM2	RRM2	RRM2	RRM2	9.74E-03	10.73	✓
2	RMI1		RMI1		2.18E-04	8.70	✓
3	PRC1	PRC1	PRC1	PRC1	9.45E-03	4.17	✓
4		AOC1			7.24E-05	3.93	
5			HKDC1		3.53E-06	2.18	
6			HGF		4.71E-03	2.17	
7	PALLD				1.39E-03	2.09	
8		ZMAT3			1.86E-03	1.92	✓
9	MYADM				3.28E-04	1.92	
10	HLTF	HLTF			2.24E-04	1.85	✓
11	TOP2A	TOP2A	TOP2A		1.04E-05	1.85	✓

C



D

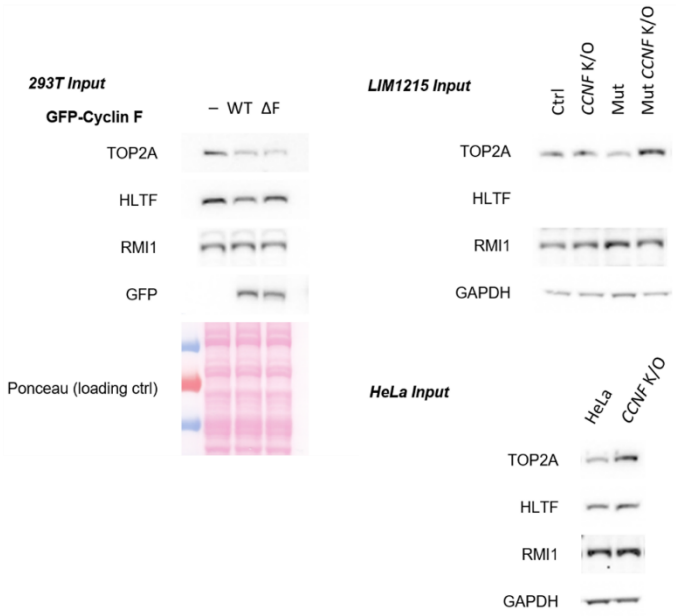


Figure 5vi. Refined list of likely Cyclin F substrates from total proteome data.

A-B. Table showing a refined list of high confidence potential Cyclin F substrates. Hits were filtered by: enrichment in *CCNF* K/O (A) and Mut *CCNF* K/O (B) cells compared to their respective controls, possessing a Cyclin F degron and nuclear localisation.
C. Schematic of the samples compared for this analysis.
D. Top hits from (A-B) tested via immunoblots. Left: HEK293T cells were transfected with GFP-*CCNF* mutants (WT and ΔF) and immunoprecipitated using a GFP resin after which Cyclin F binding to each of the potential substrates was visualised via immunoblots (only input data shown). Middle and right: immunoblots of whole cell lysates of LIM1215 (± *CCNF* K/O ± *KRAS* mutation) and HeLa (± *CCNF* K/O) cells, respectively.

All 3 of the DNA associated proteins TOP2A, HLTF and RMI1 were not pulled-down by Cyclin F (IP data not shown, only inputs are), which could be due

to these 3 proteins – a topoisomerase, a helicase and an HR DNA repair protein, respectively – being strongly chromatin-bound and hence requiring DNA shearing using a different type of lysis buffer (as opposed to the classic NP-40 one used for the majority IP experiments in this thesis) prior to co-immunoprecipitation (Figure 5vi.D). TOP2A, HTLF and RMI1 are all enriched in the *CCNF* K/O HeLa cells compared to the *CCNF* WT control. TOP2A is also enriched in the *CCNF* K/O LIM1215 cells in *KRAS* mutant settings. In the HEK293T input for the attempted IP experiment, HLTF behaves in an identical manner to Cyclin F substrates: it is degraded when Cyclin F WT is overexpressed and remains unchanged when Cyclin F ΔF (or the empty vector) is overexpressed.

ZMAT3 failed to be detected by the antibody used across the 3 cell lines whose whole cell lysates have been used for this immunoblot, most likely due to poor antibody quality. In conclusion, TOP2A, HLTF and RMI1 are likely novel substrates of Cyclin F that require further investigation. This adds to the list of potential Cyclin F substrates identified in previous chapters, which currently includes: BRAT1, HELLS/LSH, BORA, CDT1, STT3A/ITM1, MDC1 and now TOP2A, HLTF and RMI1.

Top hits from the comparative lists of samples ±*CCNF*, outlined in Figure 5vi, were uploaded to Enrichr – a comprehensive gene set enrichment analysis web server, to look for the most impacted pathways upon Cyclin F loss

As expected, the most heavily altered pathways in the list of proteins enriched in the *CCNF* K/O compared to the Ctrl sample were interferon ones, followed by inflammatory and immune response ones (Supplementary Figure 6). On the other hand, and more in line with what is expected out of Cyclin F

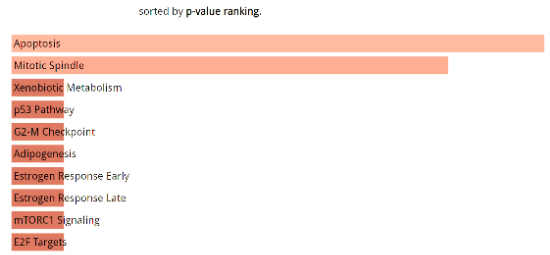
substrates, some of the most impacted pathways in the list of proteins enriched in the Mut *CCNF* K/O compared to the Mut sample included G_2/M checkpoint proteins (TOP2A and PRC1) and E2F target ones (TOP2A and RRM2) (Figure 5vii).

A

MSigDB Hallmark 2020

Mut *CCNF* K/O / *CCNF* K/O						
Term	Overlap	p-value	q-value (p-value adjusted for FDR)	Odds Ratio	Combined Score	Genes
Apoptosis	3/161	0.001772	0.032321	13.93249	88.27109	TOP2A;HGF;HMOX1
Mitotic Spindle	3/199	0.003232	0.032321	11.20975	64.28377	TOP2A;PRC1;PALLD
Xenobiotic Metabolism	2/200	0.036031	0.072062	7.132756	23.70483	ALDH2;HMOX1
p53 Pathway	2/200	0.036031	0.072062	7.132756	23.70483	ZMAT3;HMOX1
G2-M Checkpoint	2/200	0.036031	0.072062	7.132756	23.70483	**TOP2A;PRC1**
Adipogenesis	2/200	0.036031	0.072062	7.132756	23.70483	ALDH2;SQOR
Estrogen Response Early	2/200	0.036031	0.072062	7.132756	23.70483	SVIL;MYOF
Estrogen Response Late	2/200	0.036031	0.072062	7.132756	23.70483	TOP2A;MYOF
mTORC1 Signaling	2/200	0.036031	0.072062	7.132756	23.70483	RRM2;LGMN
E2F Targets	2/200	0.036031	0.072062	7.132756	23.70483	**TOP2A;RRM2**
Cholesterol Homeostasis	1/74	0.105317	0.191486	9.398677	21.15432	LGMN
IL-6/JAK/STAT3 Signaling	1/87	0.122676	0.204461	7.972735	16.72843	HMOX1
Protein Secretion	1/96	0.134503	0.206928	7.214156	14.47282	GALC
Pperoxisome	1/104	0.144886	0.20698	6.651155	12.84876	TOP2A
Coagulation	1/138	0.187686	0.250248	4.991946	8.351452	LGMN
UV Response Up	1/158	0.211887	0.260462	4.351636	6.752441	HMOX1
Hypoxia	1/200	0.260462	0.260462	3.425923	4.608891	HMOX1
Myogenesis	1/200	0.260462	0.260462	3.425923	4.608891	SVIL
KRAS Signaling Up	1/200	0.260462	0.260462	3.425923	4.608891	HKDC1
Complement	1/200	0.260462	0.260462	3.425923	4.608891	LGMN

B



C

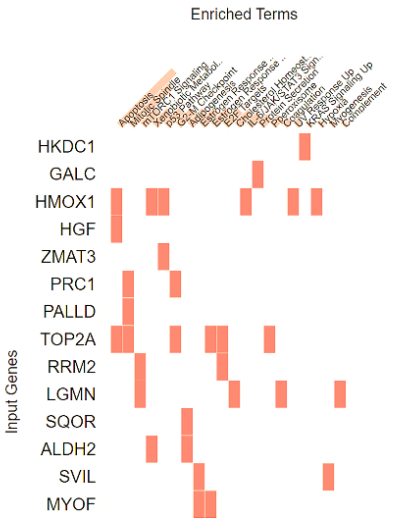


Figure 5vii. Enrichr-identified significant pathway alterations of proteins enriched in Mut *CCNF* K/O vs Mut.

Altered pathways and the genes involved are presented in table format showing the p- and q- (adjusted p-) values (A), in a bar graph sorted by p-value (B) and in a clustergram showing clusters of altered genes in these pathways (C). *Figures generated using Enrichr (https://maayanlab.cloud/Enrichr/)*

b. KRAS-Dependent Proteome Alterations (Mut vs Ctrl)

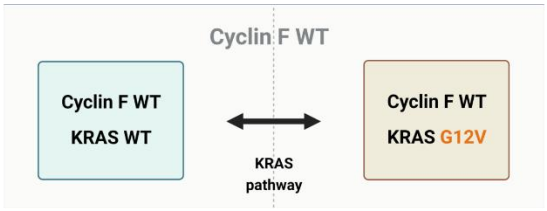
Upon completion of the search for novel Cyclin F substrates, the next task was to assess proteome-wide differences dependent on the mutational status of

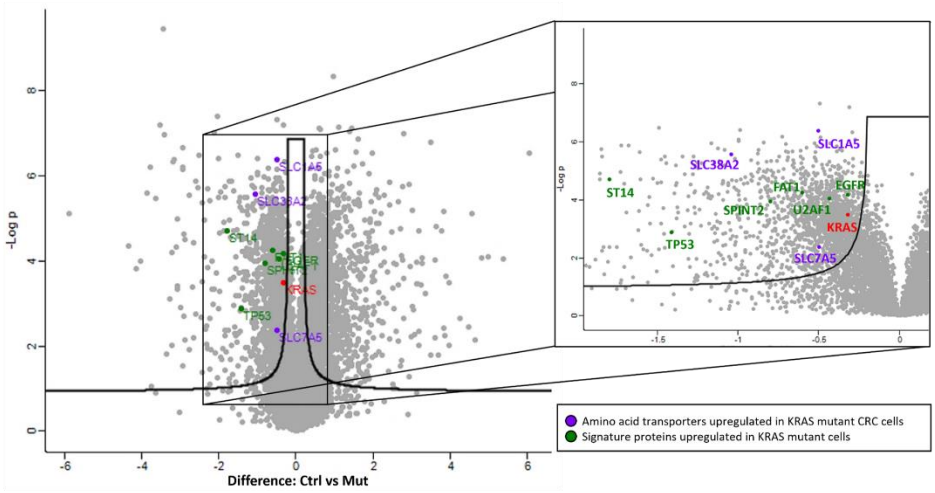
RAS. For this purpose, volcano plots comparing the 2 samples Ctrl and Mut were drawn up and heavily altered proteins were identified (Figure 5viii). A number of hits enriched in the Mut sample served as positive controls. These hits included the amino acid transporters (AATs) Solute Carrier Family 7 Member 5 (SLC7A5/LAT1), Family 38 Member 2 (SLC38A2/SNAT2) and Family 1 Member 5 (SLC1A5/ASCT2). These three AATs (highlighted in purple, Figure 5viii.A) are reportedly upregulated in *KRAS* mutant cells, more specifically in *KRAS* G12D CRC, and correlate with increased amino acid uptake resulting in glutamine accumulation and its exchange for leucine – a known activator of the essential regulator of cell growth and metabolism mTORC1 – to sustain cancer cell proliferation (Kandasamy et al., 2021).

Another set of proteins upregulated in the Mut sample served as positive controls, these include the signature *KRAS* mutant proteins (highlighted in green, Figure 5viii.A): Suppressor of Tumorigenicity 14 (ST14), Tumour Protein P53 (TP53), serine Peptidase Inhibitor, Kunitz Type 2 (SPINT2), FAT Tumour Suppressor Atypical Cadherin 1 (FAT1), U2 Small Nuclear RNA Auxiliary Factor 1 (U2AF1) and, of course, EGFR (Liu et al., 2021).

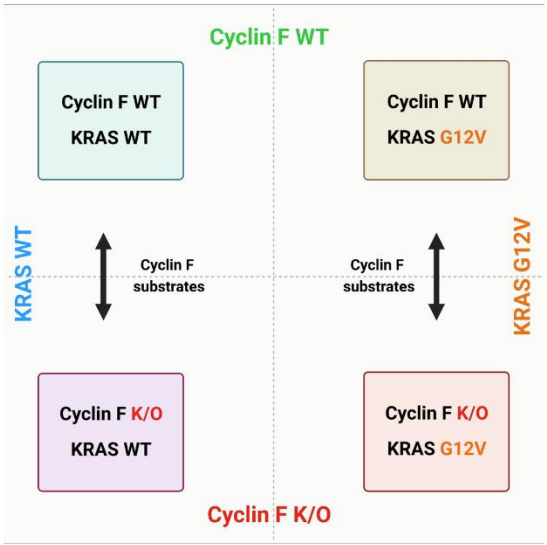
Following the validation that the generated LC/MS data is consistent with *KRAS*-dependent proteome changes reported in the literature, I noticed a specific trend in the data. Published Cyclin F substrates RRM2, NUSAP1 and Stem-Loop Binding Protein (SLBP) (D'Angiolella et al., 2012, Dankert et al., 2016, Emanuele et al., 2011) were collectively more enriched in the Ctrl sample compared to the *KRAS* mutant one (highlighted in blue, Figure 5viii.B).

A


Cyclin F WT
Cyclin F WT
KRAS WT
Cyclin F WT
KRAS G12V
KRAS
pathway


-Log p
Difference: Ctrl vs Mut
SLC1A5
SLC38A2
ST14
FAT1
EGFR
SPINT2
U2AF1
KRAS
TP53
SLC7A5
Amino acid transporters upregulated in KRAS mutant CRC cells
Signature proteins upregulated in KRAS mutant cells

B


Cyclin F WT
Cyclin F WT
KRAS WT
Cyclin F WT
KRAS G12V
KRAS WT
Cyclin F
substrates
Cyclin F
substrates
KRAS G12V
Cyclin F K/O
KRAS WT
Cyclin F K/O
KRAS G12V
Cyclin F K/O

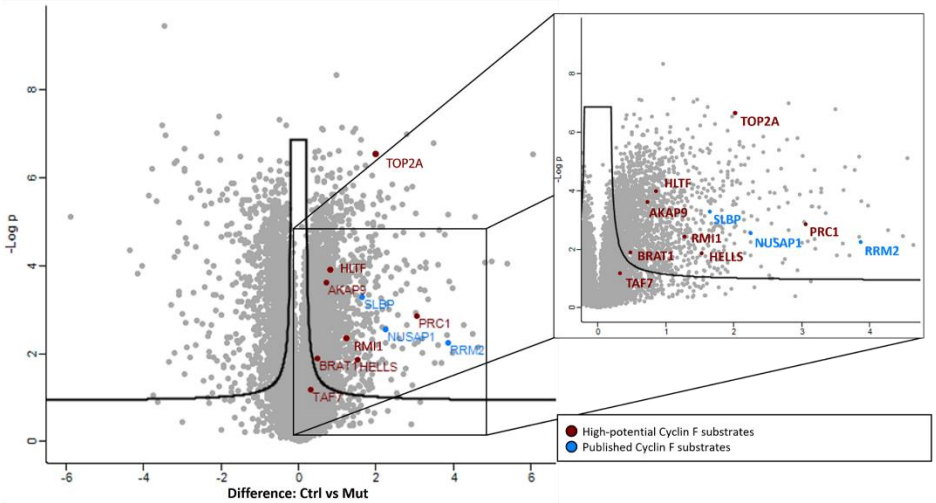

-Log p
Difference: Ctrl vs Mut
TOP2A
HLTF
AKAP9
SLBP
PRC1
NUSAP1
RMI1
RRM2
BRAT1
HELLS
TAF7
High-potential Cyclin F substrates
Published Cyclin F substrates

Figure 5viii. Volcano plots highlighting KRAS-dependent proteome differences in Ctrl vs Mut samples.

A-B: Schematics and volcano plots representing protein fold changes (X-axis: $Log_2(\frac{\text{intensity sample 1}}{\text{intensity sample 2}})$) against -Log(p-value) (Y-axis) across samples, highlighting KRAS signature protein alterations (A) and Cyclin F published as well as newly identified (in this thesis) potential substrates (B). S0 (parameter for displaying fold change) = 0.1, FDR = 1%. *Figures generated using Perseus software version 1.6.2.2.*

Additionally, potential Cyclin F substrates identified in this thesis – such as RMI1, HTLF, TOP2A, BRAT1, HELLS/LSH, PRC1, TAF7/TAFII55 and AKAP9 – follow the same trend since they are enriched in the control sample (*KRAS* WT) compared to the *KRAS* G12V$^{+/-}$ one (highlighted in brown, Figure 5viii.B). This shows that the levels of Cyclin F substrates are reduced when *KRAS* is mutated, which indicates an increased rate of Cyclin F-mediated degradation of said substrates in these settings. This confirms – in an unbiased manner – that Cyclin F is more active in *KRAS* mutant settings, therefore its E3 ligase role is more pronounced and its substrates are depleted at higher rates in the *KRAS* mutant samples. On the other hand, lower Cyclin F activity is observed in cells wild-type for *KRAS* since Cyclin F substrates are enriched in this sample in comparison to the *KRAS* G12V$^{+/-}$ one.

c. Combined KRAS and Cyclin F-Dependent Proteome Alterations (*CCNF* K/O ±*KRAS* mutation)

Looking at the analysed data all together, an intriguing trend stood out: the levels of ISG15 in the 4 LIM1215 cell lines from Figure 5iii very closely matched the level of these cell lines' resistance to the EGFR inhibitors shown in Figure 4ii. ISG15 levels were highest in the Mut sample, followed by Mut *CCNF*

K/O, then *CCNF* K/O and finally Ctrl. The extent of resistance to either Erlotinib, Gefitinib or Cetuximab followed the same trend where Mut was the cell line most resistant to EFGRi therapy followed by Mut *CCNF* K/O then *CCNF* K/O, while the Ctrl sample was the most responsive to the treatment. In both cases, the samples WT for *KRAS* behaved in an opposing manner to those with an activating *KRAS* mutation; when Cyclin F is lost in *KRAS* WT cells they acquire more resistance to EGFR inhibition and upregulate the levels of ISG15 (and interferon response), whereas when Cyclin F is lost in *KRAS* mutant cells they become more responsive to EGFRi treatment and downregulate their ISG15 levels (and interferon response).

Based on these 2 observations – ISG15 levels closely matching resistance levels across the 4 samples, and Cyclin F loss having contrasting effects depending on *KRAS* mutational status – I wondered if ISG15 along with similarly behaving proteins are implicated in this EGFRi resistance. The next step was to search the total proteome data for other proteins whose levels follow the same pattern as ISG15 upon Cyclin F loss, enriched in the *KRAS* WT sample and depleted in the *KRAS* G12V one, in the hopes of finding the pathway or family of proteins behind this phenotype.

I extracted the significant hits from the volcano plot of *CCNF* K/O vs Mut *CCNF* K/O, then filtered those for proteins whose levels are both: higher in *CCNF* K/O than in Ctrl, and higher in Mut than in Mut *CCNF* K/O (Figure 5ix.A). This shortened list comprised 139 proteins, which I uploaded onto Enrichr to have a wider view of the main pathways involved. The top pathways that came up were interferon response ones followed by PI3K/AKT/mTOR signalling (Figure 5ix.B). MAP2K6 was one of the proteins that came up in the PI3K/AKT/mTOR pathway,

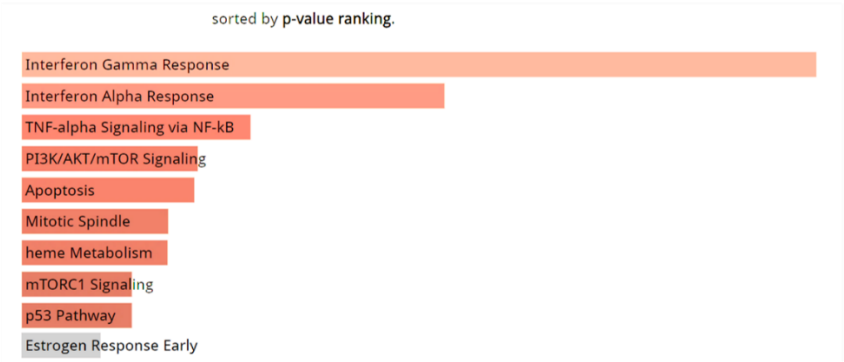
and it was highlighted in the table because it is the most heavily altered protein (after Fascin) between these 2 samples as seen in the volcano plot of *CCNF* K/O vs Mut *CCNF* K/O (Figure 5ix.D).

A

MSigDB Hallmark 2020

CCNF K/O / Mut *CCNF* K/O				
Term	**Overlap**	**P-value**	**Adjusted P-value**	**Genes**
Interferon Gamma Response	18/200	1.16E-14	4.18E-13	IFITM3;CDKN1A;IFITM2;DDX58;MX2;MX1;ISG15;IFIT1;SAMHD1;USP18;IFIT3;IFIT2;OASL;HELZ2;NFKBIA;OAS2;CASP3;OAS3
Interferon Alpha Response	9/97	4.81E-08	8.65E-07	IFITM3;HELZ2;IFITM2;MX1;ISG15;USP18;IFIT3;IFIT2;OASL
TNF-alpha Signaling via NF-kB	8/200	1.36E-04	0.001633	MAP2K3;NFKBIA;CDKN1A;TUBB2A;TNIP1;DDX58;SQSTM1;IFIT2
PI3K/AKT/mTOR Signaling	5/105	0.001174	0.009839	MAP2K3;CDKN1A;DUSP3;SQSTM1;**MAP2K6**
Apoptosis	6/161	0.001367	0.009839	IFITM3;CDKN1A;BIK;CASP3;HMGB2;SQSTM1
Mitotic Spindle	6/199	0.003938	0.020754	BCR;EPB41;MID1IP1;CNTRL;FSCN1;DOCK2
heme Metabolism	6/200	0.004035	0.020754	MAP2K3;SELENBP1;BCAM;EPB41;NCOA4;NUDT4
mTORC1 Signaling	5/200	0.017555	0.07022	MAP2K3;CDKN1A;HSPA4;BCAT1;SQSTM1
p53 Pathway	5/200	0.017555	0.07022	CDKN1A;SESN1;CTSD;ZFP36L1;RAD9A

B



C

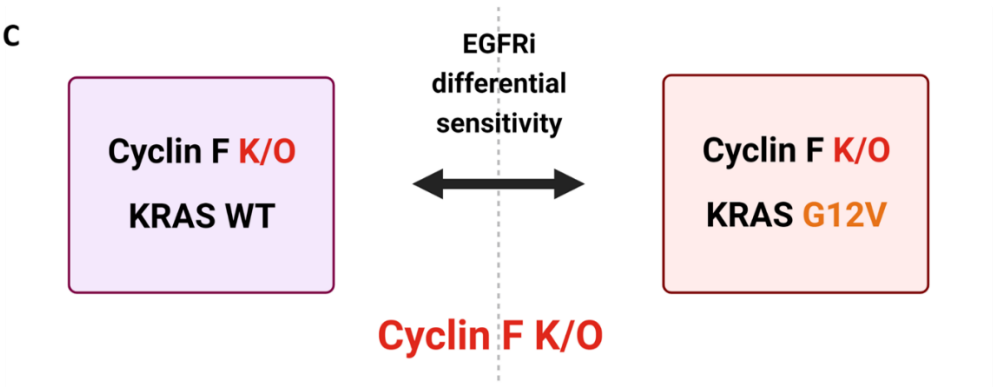


Figure 5ix. Enrichr-identified significant pathway alterations of proteins enriched in both: *CCNF* K/O vs Ctrl, and Mut vs Mut *CCNF* K/O.

Altered pathways and the genes involved are presented in table format showing the p- and q- (adjusted p-) values (A), in a bar graph sorted by p-value (B) and in

a schematic (C). *Figures generated using Enrichr (https://maayanlab.cloud/Enrichr/)*

I plotted the levels of the proteins identified in this comparison across all 4 LIM1215 samples and was able to indeed observe this pattern reminiscent of RTKi resistance across the 4 samples (Figure 5x). For all the proteins plotted, including ones within the interferon gamma response (Figure 5x.A) or the PI3K/AKT/mTOR signalling (Figure 5x.B) pathways, their levels increased when Cyclin F was lost in the *KRAS* WT sample and dropped when it was lost in the *KRAS* mutant one.

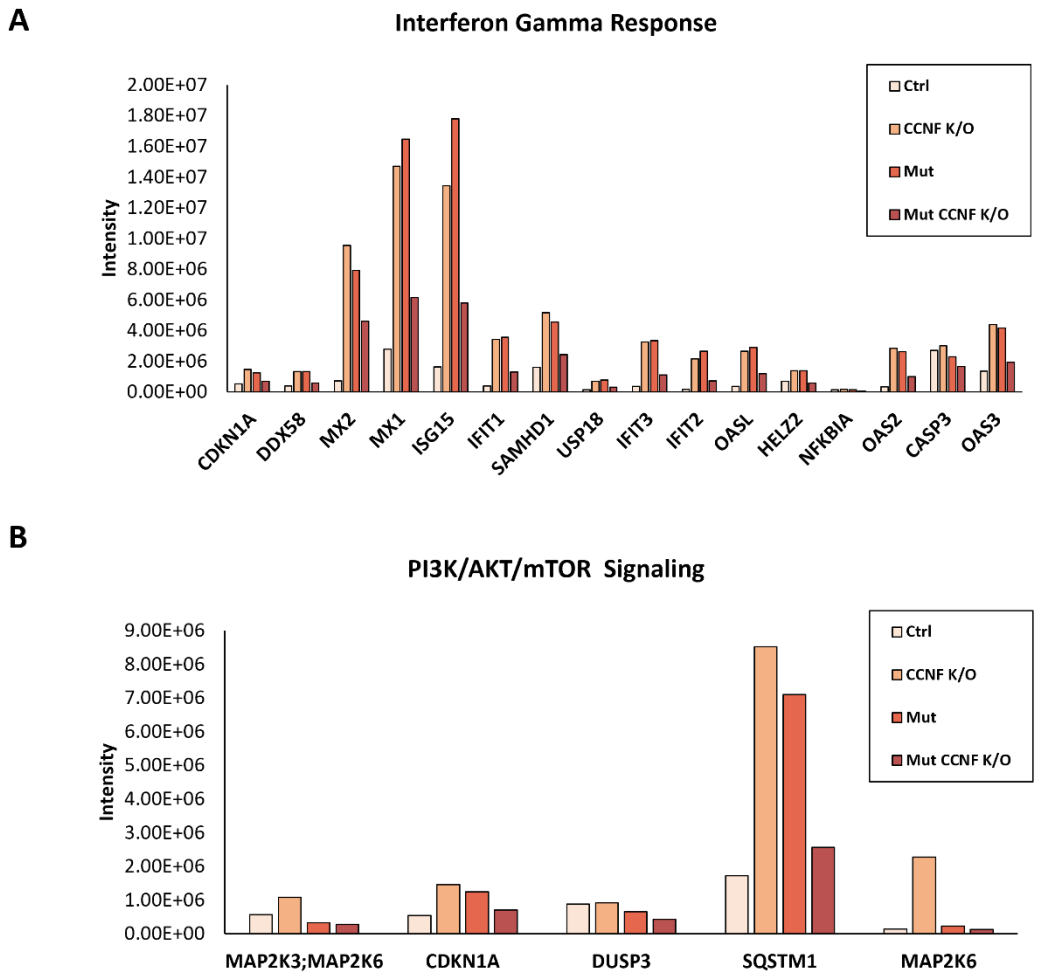


Figure 5x. Protein levels of members of the signalling pathways altered the most between *CCNF* K/O and Mut *CCNF* K/O samples.

A-B. Bar charts showing protein intensities across all LIM1215 cell lines for hits in the interferon gamma response (A) and PI3K/AKT/mTOR signalling (B) pathways.

This chapter covers the analysis of multiple data subsets extracted from the proteomic profiling results of cells that have different Cyclin F (WT or K/O) and/or *KRAS* (WT of G12V$^{+/-}$) statuses. The first main data stream was the Cyclin F substrates one, and for this the *CCNF* K/O samples were compared to their WT counterparts – regardless of *KRAS* status. In these settings, a short list of proteins showing enrichment in the K/O cell lines was extracted and then tested via Western blotting. Three proteins from this list, namely TOP2A, HTLF and RMI1, showed Cyclin F substrate potential, but are subject to further investigations to confirm this.

The second main data stream was the comparison between the *KRAS* WT *CCNF* K/O and the *KRAS* G12V$^{+/-}$ *CCNF* K/O cell lines, since the loss of Cyclin F in each resulted in polar opposite phenotypes when the cells were challenged with EGFR/RTK inhibitors (covered in detail in data chapter II). Comparing these 2 samples resulted in 139 significant hits that are differentially expressed between both conditions. One way to test these individually is through generating a mini CRISPR library with a readout that reflects either EGFRi sensitivity or interferon pathway activation, since the most altered pathway between the 2 cell lines was the interferon response one. Another heavily altered pathway was PI3K/AKT/mTOR signalling, so this warranted further assessment of each of these 2 pathways, which is covered in the next chapter.

6. Results Chapter IV: Role of the Cyclin F-KRAS Regulatory Network in the RTKi Response

Following the analysis of the altered pathways in *CCNF* K/O and Mut *CCNF* K/O cells, the next step was to figure out clinically-exploitable weaknesses along this axis starting with the 2 cell lines that behave in an opposite manner when treated with EGFR inhibitors; when Cyclin F is lost from *KRAS* WT cells they grow more resistant to EGFRi treatment whereas when *KRAS* G12V$^{+/-}$ cells lose Cyclin F they become more sensitive and thereby responsive to EGFR inhibition. The aim was to better understand how the interferon response and PI3K/AKT/mTOR signalling pathways are driving this difference, and more importantly, how they can be of clinical use for cancer therapy.

a. Interferon Pathway and the RTKi Response

With regards to interferon activation, the target was to inhibit this response and observe the effect on sensitivity to EGFRi. For this purpose, I used an inhibitor of Stimulator of Interferon Response CGAMP Interactor (STING) since STING is an activator of type I interferon responses and therefore lies upstream of such pathways. Gefitinib was chosen as a sample EGFRi and used at the concentration where the biggest difference in viabilities between LIM1215 cell lines was observed (2 μM, Figure 4ii.B), and cells were treated with it in combination with the STING inhibitor H151 (Figure 6i.A). When viabilities are normalised to treatment with Gefitinib alone, the Mut cell line seems to be the most sensitive to the combined Gefitinib + STINGi treatment with an impressive 61% drop in viability. Being the cell line that was most resistant to Gefitinib treatment alone, this combined approach could prove useful in overcoming resistance to RTK inhibitor therapy in patients with cancers that have

constitutively active KRAS (~14% of all cancers, ~90% of pancreatic ductal adenocarcinoma, 40% of CRC and 30% of lung adenocarcinoma (Network, 2012, Network, 2014, Network, 2017, Prior et al., 2020)). In terms of sensitivity to the combined approach of Gefitinib + STINGi, Mut *CCNF* K/O cells seem to be close seconds with a 59% drop in viability. The *CCNF* K/O sample only has a 31% drop in viability after treatment with the combined approach compared to Gefitinib alone, and is followed by the Ctrl sample that seems to benefit the least from this combination of inhibitors with only a 17% drop in viability. When data is normalised to the untreated control (as opposed to Gefitinib treatment) (Figure 6i.A), *KRAS* mutant cells' Gefitinib resistance compared to their *KRAS* WT counterparts seems to drop from 3-4 fold to less than 2 fold when STINGi is combined with Gefitinib. The *KRAS* mutant *CCNF* K/O cell line has lower survival than its *CCNF* WT counterpart when treated with both Gefitinib and STINGi together.

The activity of STINGi was confirmed using immunoblots of treated cells where levels of ISG15 and phosphorylated Signal Transducer and Activator of Transcription 1 (STAT1) served as the readout for interferon pathway activity, which was clearly suppressed in a time and concentration dependent manner using STINGi (Figure 6i.C-D).

Taken together, this highlights the clinically relevant exploitable weakness of *KRAS* mutant and EGFRi resistant cells to interferon pathway inhibition when combined with EGFR inhibitor treatment.

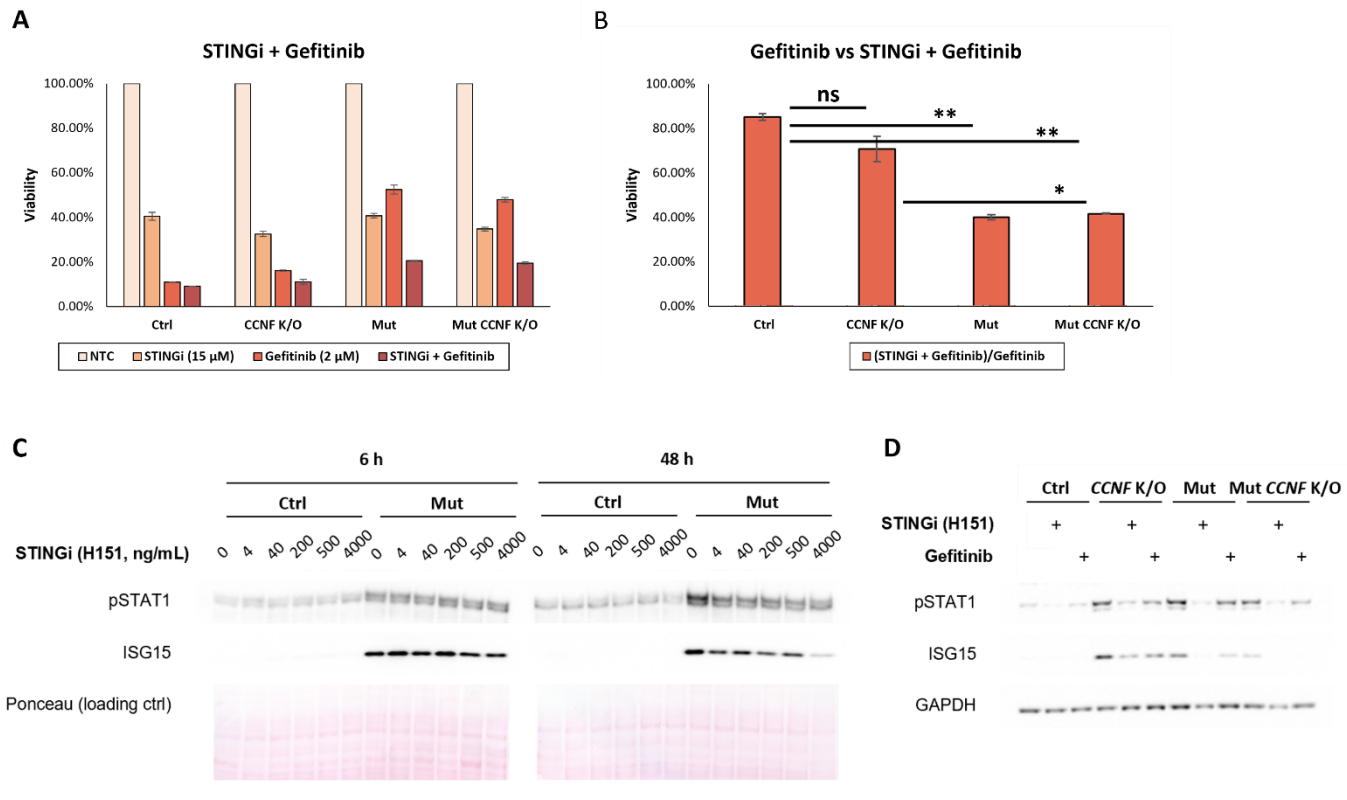


Figure 6i. Effect of STING inhibition on the EGFRi response of LIM1215 cells.

A. LIM1215 cells were treated with STINGi (15 µM), Gefitinib (2 µM), both or neither for 5 days, after which their survival was quantified using a Resazurin viability assay.

B. With data from (A), viability of cells treated with STINGi and Gefitinib together was normalised to viability of cells treated with Gefitinib alone. Statistical significance was calculated using Student's t-test.

C. LIM1215 Ctrl and Mut cells were treated with STINGi at a concentration gradient of 0-4 µM for 6 or 24 h prior to harvest. Cells were then lysed, immunoblotted and probed for interferon response markers.

D. Spare cells from the LIM1215 samples used in (A-B) were lysed and immunoblotted to confirm STING inhibition.

b. MAP2K6, p38 MAPK and the RTKi Response

After exploring the most altered pathway in the *CCNF* K/O vs Mut *CCNF* K/O comparison, the focus shifted to the second pathway: PI3K/AKT/mTOR signalling. Since MAP2K6 (a mitogen-activated kinase that is a member of this PI3K/AKT/mTOR pathway) is the most altered gene when *CCNF* K/O and Mut

CCNF K/O are compared due to its heavy enrichment in *CCNF* K/O samples (Figure 5iii. D-E), I decided to tackle the question from both sides by testing the effect of either overexpressing MAP2K6 or inhibiting its downstream pathways on the cellular resistance to EGFR inhibition. MAP2K6 lies upstream of p38 MAPK and is responsible for its activation (Remy et al., 2010). For this reason, I used 2 highly specific p38 MAPK inhibitors (SB202190 'MAPK1i' for p38α/β and TAK-715 'MAPK2i' for p38α) to observe the effects of suppressing MAP2K6 signalling in cells treated with Gefitinib.

Using either inhibitor to inhibit p38 MAPK did not induce differences in viability when used in combination with Gefitinib compared to the viability of cells treated with Gefitinib alone (Figure 6ii). Even for the slight differences observed, there was no clear pattern observed that could be linked to the Cyclin F or *KRAS* status in the cells.

Since inhibiting the pathways downstream of MAP2K6 was not the answer, I attempted the opposite approach next: overexpressing MAP2K6 then treating the cells with Gefitinib. For this purpose, LIM1215 cells were transfected with pCDNA3.1-MAP2K6 (or empty vector control), treated with Gefitinib, then their viability was assessed relative to the respective controls (Figure 6iii.A). Additionally, spare cells from all samples were collected, lysed and immunoblotted to confirm MAP2K6 overexpression. MAP2K6 levels were in accordance with the levels expected in an overexpression experiment (Figure 6iii.B).

Viability and hence Gefititinib sensitivity of all LIM1215 cells were not affected by the overexpression of MAP2K6. When MAP2K6 overexpression +

Gefitinib samples were normalised to MAP2K6-only samples and compared to EV + Gefitinib samples that were normalised to EV-only samples, there was no significant difference in viability driven by MAP2K6 overexpression. Based on the negative data for both inhibition and overexpression experiments, it can be concluded that MAP2K6 does not contribute to the differential sensitivity to Gefitinib that is observed in LIM1215 *CCNF* K/O vs Mut *CCNF* K/O samples.

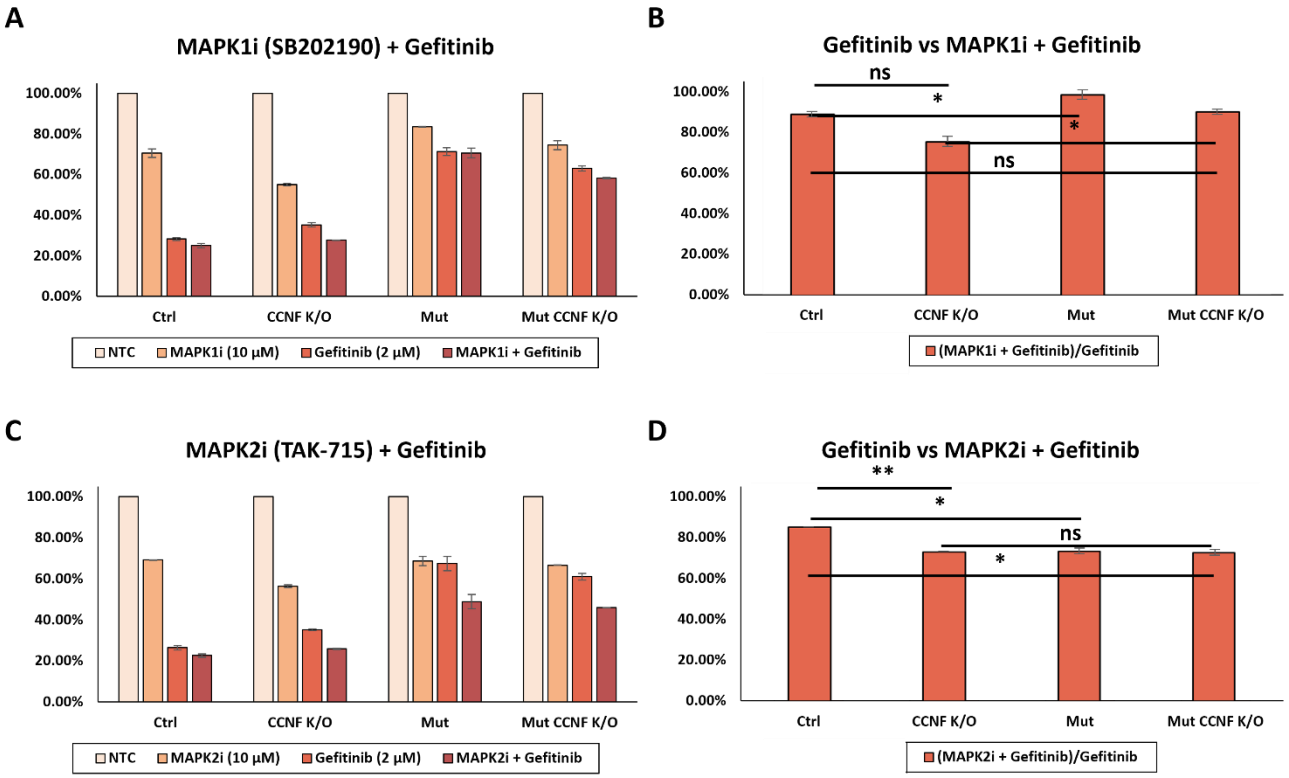


Figure 6ii. Effect of p38 MAPK inhibition on the EGFRi response of LIM1215 cells.

LIM1215 cells were treated with a p38 MAPK inhibitor (SB202190 'MAPK1i' (A-B), TAK-715 'MAPK2i' (C-D)) (10 µM), Gefitinib (2 µM), both or neither for 72 h, after which their survival was quantified using a Resazurin viability assay.

B & D. With data from (A) or (C), respectively, viability of cells treated with MAPKi and Gefitinib together was normalised to viability of cells treated with Gefitinib alone. Statistical significance was calculated using Student's t-test.

This means that the interferon response, possibly through Janus Kinase – Signal Transducer and Activator of Transcription (JAK-STAT) pathway activation,

represents an important contributor to the mechanisms of resistance induced by *KRAS* activation (assuming that the STING inhibitor only targets this pathway). Inhibiting individual members of the interferon pathways that are enriched in the *KRAS*-mutant samples, starting from those higher up in the signalling cascade and then working our way down, then assessing the potential change in EGFRi sensitivity is one way to test this. While the PI3K/AKT/mTOR signalling pathway has been implicated before in the resistance to EGFR inhibitor therapy (Fang et al., 2020), it does not participate in the resistance mechanisms in the CRC models used in this thesis. Further investigation is required to unravel the contribution of Cyclin F-dependent response to EGFR inhibition as in the presented experiments of this chapter I did not observe a significant effect on cell survival mediated by Cyclin F loss at the Gefitinib concentration I used (2 μM), whereas in earlier experiments where Gefitinib was used at higher concentrations (up to 5 μM) the difference was a lot more pronounced (Figure 4ii.B & E).

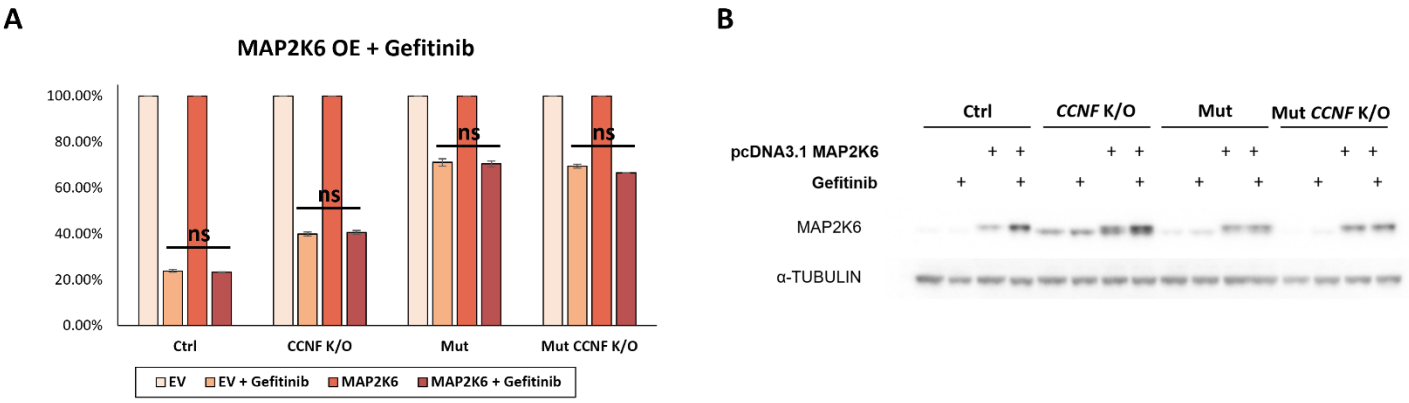


Figure 6iii. Effect of MAP2K6 overexpression on the EGFRi response of LIM1215 cells.

A. LIM1215 cells were transfected with pCDNA 3.1-MAP2K6 or pCDNA 3.1 empty vector control in 10-cm dishes, then re-seeded the next day in 96-wells and treated after with Gefitinib for 72 h following which their survival was quantified using a Resazurin viability assay. Statistical significance was calculated using Student's t-test.

B. Spare cells from the LIM1215 samples used in (A) were lysed and immunoblotted to confirm MAP2K6 overexpression.

7. Discussion and Future Work

I. Overview

Our lab aimed to identify the E3 ligases involved in the response to radiotherapy, a main element of the treatment paradigm of solid tumours, and have approached this task through IR-coupled CRISPR screens conducted in glioblastoma cells. This experiment highlighted an involvement of the F-box protein Cyclin F in generating cellular resistance to ionising radiation.

The results presented in this thesis dissect the mechanism of this Cyclin F involvement in the ionising radiation response. I identify the Cyclin F-EXO1 axis as a major mediator of the defective IR response of cells lacking Cyclin F. Following this, I unravel the dynamics of EXO1 ubiquitylation by Cyclin F – including its degron site, phosphorylation site and phosphorylating kinase. This adds new depths to our understanding of Cyclin F's functions and mode of action.

Additionally, I refine a subset of the Cyclin F degron RxI based on a similarity between EXO1 and another Cyclin F substrate, RRM2, and use this refined RxIF degron for a degron-matching approach in a genome-wide search for Cyclin F substrates. This method, coupled with an analysis of Cyclin F-dependent total proteome changes, led to the identification of potential Cyclin F substrates involved in genome stability. It also helped uncover further specificity in the substrate selection operated by cyclins, with implications in the quantitative model of cell cycle control.

A serendipitous observation regarding Cyclin F regulation by the oncoprotein RAS prompted further investigations of this pathway. I uncovered a feedback loop whereby Cyclin F and RAS communicate to

regulate cell survival and the cell cycle. The implications of these observations are multifaceted: the discovery of a novel link between MAP kinase activation and the G_2-phase of the cell cycle opens the door to questions on how the restriction point in G_1 is influenced by previous cell cycle transitions, and the elucidation of a few parallel pathways (such as the interferon response) which could contribute to reinforcing and/or modulating the response to RTK inhibitors has far reaching potential applications in the clinic.

II. Cyclin F as a novel target in multiple malignancies

Cyclin F has been previously linked to DNA repair. Such published reports implicated 3 Cyclin F substrates/interactors: RRM2, b-MYB and EXO1. The RNR regulatory subunit RRM2 has an essential role in producing dNTPs, the building blocks for DNA repair and replication. RRM2 is a substrate of Cyclin F that is targeted for degradation in G_2/M after fulfilling its DNA synthesis functions in G_1/S, and through this, Cyclin F limits dNTP production to S-phase (D'Angiolella et al., 2012). Cyclin F has also been shown to inhibit the mitotic transcriptional activator b-MYB in response to IR in order to restrict the cells in G_2 until the DNA damage has been adequately repaired (Klein et al., 2015b).

The third substrate is the exonuclease EXO1, which is important for executing end resection during DNA repair. EXO1 levels have been shown to drop after DNA damage by UV, IR, the topoisomerase poison CPT and the RNR inhibitor HU, among others (Tomimatsu et al., 2017, El-Shemerly et al., 2005, El-Shemerly et al., 2008, Elia et al., 2015). This degradation has been confirmed to be SCF-mediated, and in the case of the UV-mimetic drug 4NQO, the SCF

complex was identified to be $SCF^{Cyclin\ F}$. However, it remained unclear whether this Cyclin F regulation of EXO1 was direct, and the SCF complex responsible for EXO1 degradation after treatment with the rest of the DNA-damaging agents mentioned above, including IR, was yet unidentified since mechanistic studies on these fronts were lacking.

My work identifies EXO1 as the Cyclin F substrate that is mediating Cyclin F's IR-shielding roles in the cell through a series of experiments where each validates this discovery at gradually increasing levels of detail. The first was a mass spectrometry experiment where Cyclin F WT or its non-degrading/non-ubiquitylating mutant ΔF were used as bait in an IP assay in IR-treated cells. EXO1 came up as the top interactor, and its role in this Cyclin F-driven phenotype was confirmed by a clonogenics assay where *CCNF*, *EXO1* or both were knocked-out or knocked-down. In the case of both partial (knock-down) or full (knock-out) depletion of *EXO1* in *CCNF* depleted cells, cell viability was fully rescued back to basal levels, demonstrating that Cyclin F's main role after IR is to mediate EXO1 degradation. The substrate status of EXO1 was validated at the protein level using an *in vivo* ubiquitylation assay as well as a CHX chase assay, where witnessing a failure to ubiquitylate EXO1 by Cyclin F ΔF and a stabilisation of EXO1 in *CCNF* K/O cell lines, respectively, led to the conclusion that EXO1 is a Cyclin F substrate. Additionally, MLN4924, the specific CRL inhibitor, rescued EXO1 degradation both in untreated and IR-treated conditions. I proceeded to later discover the specific degron site for Cyclin F binding (RxIF 842-845) and priming phosphorylation (T824) on EXO1, as well the kinase relaying this phosphorylation (CDK2), thereby further elucidating the mechanism of EXO1

recognition by Cyclin F, which echoed the mechanism of recognition used for RRM2.

DSB repair can occur through the error-free HR or the error-prone NHEJ; the former is an intricate process initiated by considerable end processing and involves the presence of a sister chromatid to serve as a template, and the latter is a simpler one where damaged DNA ends are ligated together directly without extensive end processing (Burma et al., 2006, Heyer et al., 2010). S and G_2 CDKs have been shown to control the choice of DNA repair pathway by promoting DNA end resection which commits the cell to HR and suppresses NHEJ, and thereby restricts HR to cell cycle phases where a template is available (Ferretti et al., 2013). After an initial short-range resection step, long-range end resection follows which largely relies on EXO1 and generates single-stranded DNA (ssDNA) as the first step for DNA repair (Nicolette et al., 2010).

UPS-mediated degradation of EXO1 ensures its tightly-controlled repair of damaged DNA, however failure to degrade this exonuclease has been shown to be quite detrimental for the cell – specifically its genome stability and therefore survival in the face of DNA-damaging agents. In line with EXO1's role in end resection, its upregulation was shown to drive DNA hyper-resection and result in excessive ssDNA levels which impeded both NHEJ and HR (Tomimatsu et al., 2017). This was confirmed by expressing either a non-degradable EXO1 mutant or a dominant negative CUL1 (with a truncation preventing RBX/E2 binding yet allowing binding to other CRL1 complex components and therefore titrates them out by locking them into inactive complexes (Jin et al., 2005)). This over-generation of ssDNA coupled with impaired DNA repair mechanisms was proven to be a recipe for chromosomal instability and sensitivity to DNA-damaging

agents, and all was shown to arise from failure to execute DNA damage-induced EXO1 degradation (Tomimatsu et al., 2017).

It can be speculated that this phenotype resulting from the hyper-resection-mediated suppression of NHEJ and HR owing to EXO1 build-up is due to the cell resorting to the highly erroneous TMEJ/Alt-EJ pathway instead to repair the damage, which has been shown to be favoured when essential HR or NHEJ pathway members are defective (Ceccaldi et al., 2015, Schrempf et al., 2021, Wyatt et al., 2016). One example of this is demonstrated by cells lacking the NHEJ resection-antagonising elements KU and 53BP1, thereby resulting in excessive resection similar to that seen in the above mentioned study by Tomimatsu *et al*. (Wyatt et al., 2016, Tomimatsu et al., 2017).

The CRISPR screen finding that Cyclin F is involved in the cellular resistance to IR whereby its loss increases the cell's radiosensitivity, followed by the discovery that failure to target the Cyclin F substrate EXO1 for proteasomal degradation is the reason behind this IR hypersensitivity, both presented in this thesis, are in line with the previously reported EXO1-accumulation-mediated impaired DNA DSB repair and improved response to factors causing DNA-damage. For all these aforementioned reasons, developing Cyclin F inhibitors could prove to be a promising pharmaceutical endeavour – especially in combination with treatments attenuating DNA repair pathways.

EXO1 accumulation would not be the only vulnerability that a novel Cyclin F inhibitor would exploit. RRM2, an essential DNA repair machinery component, would also build-up within cells. Elevated levels of RRM2 directly result in elevated dNTP levels, which in turn negatively affects DNA synthesis fidelity as it increases the rate of base misincorporation, decreases the rate of

proofreading, and eventually results in spontaneous mutations that compromise genome stability (Mathews, 2006). One could speculate that this mechanism might further exacerbate the sensitivity of Cyclin F-inhibited cancer cells to DNA-damaging therapy, to the benefit of patients.

Cyclin F depletion would additionally contribute to genome instability through failure to enforce an effective G_2/M checkpoint in the face of DNA damage by IR as a result of failure to inhibit the Cyclin F interactor b-MYB, and would therefore allow the cells to enter mitosis prematurely with damaged DNA (Klein et al., 2015b). Cyclin F loss has also been shown to be synthetic lethal with checkpoint inhibition following a DNA replication catastrophe orchestrated by the aberrantly increased levels of another of its substrates, the transcriptional activator E2F1 (Burdova et al., 2019a).

The above reasons make Cyclin F an attractive target for cancer therapy, especially where the treatment employs combinatorial approaches such as a Cyclin F inhibitor and a DNA-damaging agent or checkpoint inhibitor.

In addition to the Cyclin F substrates detailed above, 3 potentially new Cyclin F substrates with roles in DNA maintenance have been identified in this thesis: TOP2A, HLTF and RMI1. These substrates were discovered following 2 approaches: the first was a sequence search using Cyclin F's new degron that was refined in this thesis (discussed in more depth in the next section) and the second was using mass spectrometry to examine the total proteome changes that occur following Cyclin F loss.

RMI1 is a protein required for successful HR-mediated DNA repair. After DNA synthesis and strand ligation in this repair pathway, an intermediate known as double Holliday junction (dHJ) is formed which needs to be resolved before

DNA repair is complete. The dissolution of this intermediate involves the concerted efforts of a tetrameric complex where RMI1 is one of its 4 essential members (Bythell-Douglas and Deans, 2021, Wu et al., 2006). TOP2A is a topoisomerase that is essential for unwinding the DNA double helix and resolving any knotting or tangling that arises along its length. Lastly, HLTF is a helicase-like transcription factor with E3 ligase properties by which it targets Proliferating Cell Nuclear Antigen (PCNA) for K63 ubiquitylation – a DNA polymerase co-factor that is critical for DNA replication, whose ubiquitylation serves as a switch between different DNA damage bypass pathways (Unk et al., 2008, Ripley et al., 2020).

Due to the heavy DNA repair involvement of these 3 likely Cyclin F substrates identified in this thesis, and knowing Cyclin F's pronounced impact on the DDR and genome stability through its substrates, further investigations of the substrate status and ubiquitylation mechanism of HLTF, TOP2A and RMI1 represent important follow-up studies.

III. Cyclin F recognises a novel degron not shared with other cyclins

After carrying out a sequence alignment with all known Cyclin F substrates, I have come to the realisation that RRM2 and EXO1 have a unique similarity that distinguishes them from the rest; they both have the published RxI degron followed by the 2 amino acids F and Q. After testing out the importance of each of the degron's aa residues individually in both RRM2 and EXO1 using SDM and IP approaches, I have come to the conclusion that R, I and F are all essential for Cyclin F binding whereby the mutation of each of these residues on its own is enough to fully abrogate both proteins' binding to Cyclin F.

This experiment introduced the newly refined subset of the RxI Cyclin F degron: RxIF. Following these assays where an overexpression system was used, I validated these results with a pull-down experiment using biotinylated short peptides after conjugating them to streptavidin beads. The peptide (BTN-EXO1 820-846) including the degron and the phosphorylation site bound with high specificity to Cyclin F, and no binding could be visualised to the Cyclin most similar to Cyclin F: Cyclin A. Even the shorter peptide (BTN-EXO1 832-846) that only included the degron site without the phosphorylation one still bound Cyclin F with high specificity, but in that case a very weak binding to Cyclin A could also be visualised – likely because the peptide is too short and in no need of any pre-binding/priming modifications which comes at the cost of a slight reduction in binding specificity.

While Cyclin F differs from other cyclins due to the nature of its E3 ligase activity, it still engages its ubiquitylation substrates the same way other cyclins engage their phosphorylation ones: through a hydrophobic patch in the cyclin box that has the conserved sequence MRAIL. Another point of similarity is that cyclins, including Cyclin F, are able to recognise their substrates through the RxL motif on targeted proteins (Schulman et al., 1998). In fact, in a number of cases – such as the EXO1 case presented here – substrates are targeted sequentially: CDKs coupled to cyclins target the protein first in order to phosphorylate it, and this primes it for the Cyclin F binding that occurs after.

While Cyclin F is still able to bind substrates through recognising the RxL degron (ex. E2F1: RRL 90-92), the substrate recognition site common among cyclins, it also binds substrates through the RxIF degron (ex. RRM2, EXO1) which is unique to Cyclin F only.

Redundancy in cyclin roles is common. In yeast, it was proposed that the cell cycle progresses based on the quantitative model developed as part of Paul Nurse's pioneering cell cycle research (Stern and Nurse, 1996). According to this model, the ordered cell cycle progression is achieved based on the levels of a single CDK (CDK1/Cdc2), in complex with one cyclin (Cdc13). The model proposed that this occurs in a manner dependent on the level of both proteins where an increase in CDK1 levels from very low to moderate signals for S-phase entry, an additional increase to high levels signals for mitotic entry, and the degradation of Cdc13 signals for mitotic exit (Stern and Nurse, 1996). Three other cyclins mentioned in the review are Puc1 (G_1 cyclin), Cig 1 and Cig 2 (S-phase cyclins), but their roles are deemed non-essential as they can all be replaced by Cdc13 which was previously thought to be exclusively a mitotic cyclin.

This yeast-based model served as a basic framework for understanding cell cycle progression, and a quite recent study mirrored this in humans (Lau et al., 2021). The work in mammalian cells has shown CDK1 is essential while CDK2 is not, and has demonstrated how CDK1 assumes the function of a G_1/S CDK when CDK2 is lacking (Lau et al., 2021). In contrast to this, the researchers demonstrated that Cyclin B-CDK2 can only partially assume CDK1's role in its absence, but when its levels are increased to match usual levels of CDK1, CDK2 can overcome cell cycle defects driven by CDK1 loss (Lau et al., 2021). Taken together, these results show that similarly to events in yeast, the difference between G_2/M and G_1/S CDKs in humans can also be described as quantitative (Lau et al., 2021).

This redundancy that appears to be conserved from simpler to more complex organisms highlights the importance of rare occurrences where similar

cyclins or CDKs stray away from assuming one another's functions. In this thesis I present one of such cases, the RxIF degron of Cyclin F that fails to bind its most similar cyclin: Cyclin A.

RxL is recognised by multiple human cyclins (ex. Cyclins A, E and F) as docking sites for the CDK-cyclin (or SCF in the case of Cyclin F) complexes (D'Angiolella et al., 2012, Schulman et al., 1998, Takeda et al., 2001). Breakthrough work – largely by Mart Loog's research group – has introduced a number of highly cell cycle-specific cyclin docking sites in yeast. This set includes: LP in G_1-, NLxxxL and RxL in S-, PxF in G_2-, and LxF in M-phases of the cell cycle (Bhaduri and Pryciak, 2011, Kõivomägi et al., 2011, Örd et al., 2020, Örd et al., 2019, Faustova et al., 2021).

My recent findings from *in vitro* phosphorylation experiments using full-length purified EXO1 have shown that both Cyclin A and Cyclin E in complex with CDK2 are able to phosphorylate EXO1 on its identified priming phosphorylation site. While the investigation of the cyclin docking site on EXO1 was out of scope for this project, EXO1 does have 2 RxL motifs: RQL 204-206 and RKL 293-295. One could speculate that the RxL docking of Cyclin A and Cyclin E in complex with CDK2 in S-phase, followed by the docking of Cyclin F in its SCF complex to the RxIF motif in G_2/M-phase, introduces an additional cell cycle-specific cyclin docking site process like those uncovered in yeast. In this case, the RxIF motif could perhaps serve as an additional docking site to the G_2-specific PxF or M-specific LxF motifs if these docking sites discovered in yeast were to be confirmed in humans, or it could otherwise serve as their human equivalent.

Although both EXO1 and RRM2 share the same RxIF degron, work presented here highlights a different phosphorylation mechanism. From the

results of the biotinylated-peptide pull-down experiment, it was observed that when shorter forms of EXO1 are used as bait in immunoprecipitation experiments, priming phosphorylation is no longer needed for Cyclin F binding. It was speculated that the phosphorylation and binding model behind this is that full-length EXO1 binds to MLH1 or MSH2 within close proximity to its RxIF motif which hinders degron accessibility for Cyclin F, and the phosphorylation of T824 on EXO1 abrogates this MLH1/MSH2 binding thereby allowing Cyclin F binding instead. In the short peptides, the binding site for MLH1/MSH2 is lost and therefore no phosphorylation is required to inhibit its binding to EXO1, so Cyclin F binds readily with or without this phosphorylation event.

It was also shown that the EXO1-Cyclin F binding (in full-length settings) requires this priming phosphorylation for binding initiation but not binding maintenance. In contrast to this, RRM2 phosphorylation is required for RRM2-Cyclin F binding initiation as well as maintenance. I have shown that de-phosphorylation abolishes the RRM2-Cyclin F binding, but fails to do so for EXO1-Cyclin F whose binding remains in effect even after the phosphate group has been removed. This continued reliance on phosphorylation to sustain the binding for RRM2 compared to only requiring phosphorylation prior to binding for EXO1 highlights a different mechanism of substrate engagement between these 2 proteins and Cyclin F.

The above EXO1 peptide experiments are awaiting further validation, this time using full-length Cyclin F and EXO1 purified proteins to eliminate any possible indirect effects arising from using whole cell lysates and short peptides. In terms of further future work for this project, I plan to use these described full-length isolated proteins to repeat the *in vitro* phosphorylation step of full-length

EXO1, but this time follow it by incubation with full-length purified Cyclin F, CUL1, SKP1 (the 3 together forming the $SCF^{Cyclin\ F}$ E3 ligase complex), RBX1 (the E3-E2 adaptor), E1, ATP, UBCH3/UBCH5C (the E2s), NEDD8 (the CRL1 activator) and ubiquitin.

DNA fiber combing, similar to the one presented in this thesis to assess DNA replication stress resulting from Cyclin F loss, will be carried out in the same 2 cell lines in addition to ones with *EXO1* K/O and a double knock-out of both *EXO1* and Cyclin F. This is needed to visualise the nature of the damage/stress to the DNA that builds up following EXO1 accumulation in the *CCNF* K/O sample, in comparison to the combined *EXO1-CCNF* K/O sample. It will be interesting to test if this double knock-out rescues the phenotype of Cyclin F loss (like it did in the clonogenics assays).

The same fiber combing experiment will be conducted in LN229 cells (where the initial IR-coupled CRISPR screen was conducted) stably expressing *EXO1* WT or the degron-mutant *EXO1* R842A, in parallel to the EV negative control. 'SMART' DNA resection assay will also be conducted in the LN229 stable cell lines to understand the effect of EXO1's accumulation on the length of the DNA resection tracks.

Lastly, investigating other Cyclin F proposed substrates that are involved in DNA replication/repair fidelity is important to establish the role of Cyclin F in DNA repair outside of IR-induced settings. Interestingly, HLTF, TOP2A and RMI1 are all important for mediating fork remodelling, so Cyclin F could potentially contribute in multiple ways to this process.

IV. KRAS-Cyclin F regulatory loop

While studying Cyclin F and its E3 ligase potential in different contexts, I observed that RRM2 levels are more depleted in cell lines with activating *KRAS* mutations compared to their *KRAS* WT counterpart. After excluding that this is due to an increase in the priming phosphorylation of RRM2, I hypothesised that Cyclin F is more active in these settings. This was further proved soon after through examining the levels of another Cyclin F substrate, E2F1, after Cyclin F knock-down in cells isogenic for *KRAS*. A similar observation was previously made for the Cyclin F substrate CCP110, and it has been demonstrated that Cyclin F can be activated through phosphorylation by a kinase downstream of RAS: AKT (Hu et al., 2015, Choudhury et al., 2017).

Almost a fifth of cancers harbour a *RAS* mutation (Prior et al., 2020). Such mutations constitutively activate the potent oncoprotein, and this overstimulates its downstream signalling cascades that control essential cellular functions such as proliferation, growth and differentiation (Murugan et al., 2019). This aberrant activation is frequently implicated in tumorigenesis due to the ability of cancer cells to hijack these essential cellular functions for their own survival.

Together, the above reasons prompted me to understand this hypothesised *RAS* regulation of Cyclin F in further detail. For this purpose, I generated *CCNF* K/O stable cells from the commercially available LIM1215 cell lines that are isogenic for *KRAS* (WT and G12V). While validating the *RAS* activity levels of the whole LIM1215 panel, including the original *KRAS* WT/G12V cell lines and the newly derived *CCNF*-depleted ones, I made a striking observation that Cyclin F's apparent regulation by *KRAS* is reciprocal: Cyclin F also regulates *RAS* activity. I validated this through a cell viability assay where these 4 cell lines

were treated with various EGFR inhibitors, since *KRAS* mutant cells are known to be resistant to this type of treatment due to their aberrantly increased *RAS* activity. My presented findings prove that when Cyclin F is lost in *KRAS* mutant settings, this partially re-sensitises the cells to EGFR inhibition, which is in line with the observed decrease in *RAS* activity as a result of Cyclin F depletion.

I have also examined the cell cycle profile of these cells to try and understand how Cyclin F activity is regulated by *KRAS*. While I did observe more G_2/M cells in the *KRAS* mutant cells compared to the WT control, this increase was marginal and not high enough to justify the observed change in this G_2/M cyclin's activity (Supplementary Figure 4). This, combined with the previous data on a stable level of CDK-mediated phosphorylation (which is an indicator of cell cycle phase) of RRM2 independently of *KRAS* status, drove the conclusion that *KRAS* did not significantly alter the cell cycle progression in this study.

To understand the nature of this KRAS-Cyclin F reciprocal regulation, more specifically through unravelling the participating members of this KRAS-Cyclin F axis, I adapted an LC/MS-based total proteome approach. Prior to implementing this, I carried out a pilot experiment in which I aimed to compare all available data acquisition and sample labelling methods – since this technique is relatively recently developed and there are ongoing debates on the best settings to use.

After comparing DDA, DIA and TMT-labelling techniques, I concluded that DIA was the ideal method to use since it outperformed the other 2 in every one of the following areas: number of hits identified, quality of hits identified, number of missing values (and hence the need to imputate them from the sample's normal distribution) and cost efficiency. Implementation of the DIA data

acquisition method allowed us to make important observations not only relating to Cyclin F itself but also involving the role of *KRAS* in cancer. This is described in depth in the following section.

V. Mechanisms of proteome variation dependent on the KRAS-Cyclin F axis

Using the chosen DIA approach for the large-scale LC/MS experiment, data-rich results were generated so I separated them into different data streams for analysis. The first was a comparison between *KRAS* WT and *KRAS* G12V cells, which complements the recently published study detailing the proteomic and phospho-proteomic landscape of *KRAS* mutant tumours in 43 cell lines – including 4 CRC cell lines of which LIM1215 is not one – with half of those having G12V mutations similarly to the LIM1215 in this thesis (Liu et al., 2021).

The first step I took when this study was published was to use the proteomic changes common to both this study and mine as positive controls for this *KRAS* WT vs *KRAS* G12V subset of my data. These hits were established in the study as signature *KRAS* mutant proteins, and many of them overlapped with my hits enriched in *KRAS* mutant cells compared to the WT control. Such hits included the tumour suppressors TP53, ST14 and FAT1, along with EGFR, SPINT2, and U2AF1 (Liu et al., 2021).

Another recent study reported an upregulation of the three amino acid transporters SLC7A5, SLC38A2 and SLC1A5 in *KRAS* mutant CRC cells (Kandasamy et al., 2021). The justification for such increased levels is that tumour growth requires high glutamine and leucine concentrations to sustain its proliferative signalling through the activation of mTORC1 – an essential regulator of cell growth and metabolism. I have also used these hits as positive controls,

and all three proved to be indeed enriched in my *KRAS* mutant cells. The cells used in the published study have G12D mutations, while mine have G12V mutations. Since both mutations aberrantly activate RAS, it is possible to conclude that the alterations detected are common to both G12V and G12D mutations

After this validation of common enrichment events in *KRAS* mutant tumours, I analysed the data further in search of new insights. The first was that the published Cyclin F substrates RRM2, NUSAP1 and SLBP (D'Angiolella et al., 2012, Dankert et al., 2016, Emanuele et al., 2011) are depleted in the *KRAS* G12V cells compared to their WT counterpart. Similarly, potential Cyclin F substrates identified in this thesis (RMI1, HTLF, TOP2A, BRAT1, HELLS/LSH, PRC1, TAF7/TAFII55 and AKAP9) follow the same pattern whereby they are also depleted in the *KRAS* G12V sample compared to the *KRAS* WT one.

This reinforces my hypothesis of increased Cyclin F activity, and hence promoted degradation of its substrates, in *KRAS* mutant settings – and establishes, in an unbiased manner, *RAS* as a positive Cyclin F regulator. The effect of *RAS* on Cyclin F is likely indirect as the localisation of Cyclin F is mostly nuclear, thus, the signalling pathways co-ordinating this *RAS* regulation of Cyclin F remain to be identified. A possible explanation of this mechanism is through AKT; Cyclin F has been reported to be stabilised and activated by AKT-mediated phosphorylation (Choudhury et al., 2017).

It has also come to my attention that samples with either Cyclin F loss or *RAS* oncogenic activation strongly trigger the interferon response in this study. This was quite an interesting and unexpected finding, since *RAS* has been repeatedly shown to suppress the immune response in earlier studies – more

specifically interferon gamma (IFN-γ) and interferon alpha (IFN-α) responses (Battcock et al., 2006, Chen et al., 2017, Liao et al., 2019).

Data presented from this D.Phil project therefore introduces a rare account of *RAS* G12V activating the immune response, which might initially seem counter-intuitive since the immune response is expected to antagonise tumorigenic *RAS*-mediated signalling, however, recent evidence suggests that this process is multi-layered and more complex than originally thought. While the interferon gene *STING* is widely considered as a tumour suppressor, hence loss-of-function mutations are expected to arise in tumour cells to evade this pathway, it is interestingly rarely inactivated through mutations or copy number alterations in cancers (Bakhoum and Cantley, 2018). An elegant study published in the last few months found a justification for this curious phenomenon. Data shows that the cGAS-STING pathway can also have pro-tumorigenic roles through pro-survival signalling in genetically unstable cancers by activating Interleukin-6 (Hong et al., 2022).

One could also speculate that in *RAS* mutant cells where the interferon response is subdued, depleting Cyclin F could help re-activate the pathway to facilitate immune recognition. This, coupled with the justifications presented earlier (in the discussion section '*Cyclin F as a novel target in multiple malignancies*'), provides further evidence of the clinical potential of Cyclin F inhibition.

Another interesting observation from my results is that a striking difference is seen between the effect of Cyclin F loss on *KRAS* WT cells compared to *KRAS* mutant ones under treatment with EGFR inhibitors. *KRAS* mutant cells treated with any of the three EGFR inhibitors (Gefitinib, Erlotinib or Cetuximab) used for

the study show a significant drop in the signature *KRAS*-induced resistance to this drug class, whereas the EGFR-responsive *KRAS* WT cells show a slight increase in resistance to the treatment when Cyclin F is absent. To understand the basis of this response, I have analysed the proteomic differences between the *KRAS* WT *CCNF* K/O cells and the *KRAS* G12V *CCNF* K/O ones.

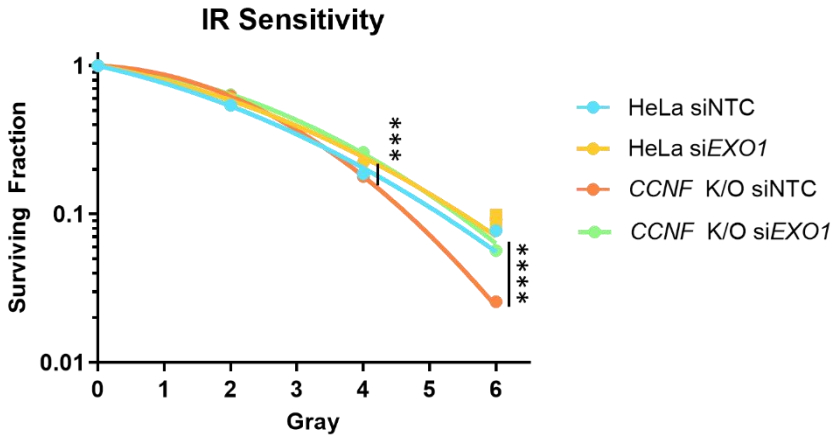
Once again, interferon alterations seem to be at play since protein levels of this pathway members behave in opposite directions to one another in the two samples examined. To test the significance of this in terms of tumour response, I inhibited STING (as a representative of the interferon response) and observed that this inhibition synergises with EGFR inhibitor treatment in *KRAS* mutant cancer cells – an effect that is not recapitulated in *KRAS* WT ones. Cyclin F depletion appeared to have no significant effect in these settings, as the increased drug sensitivity seemed to be fully driven by *KRAS'* mutational status. This, coupled with the recently reported pro-survival roles of STING, is grounds for combining STING inhibitor therapy with RTK inhibition for the treatment of RTKi-resistant and genetically unstable tumours in the clinic.

Understanding the mechanisms giving rise to the effects seen in Cyclin F-depleted cells in *KRAS* mutant settings requires further research. As described in the previous paragraph, the interferon pathway did not play a role in the increased sensitivity to EGFR inhibitors driven by Cyclin F loss. I also tested the potential role of MAP kinases downstream of RAS through either overexpressing a major MAPK-pathway member or inhibiting its downstream signalling, however, also in this case neither of these approaches could be connected to Cyclin F loss. Thus, the mechanism behind how the loss of Cyclin F can re-sensitise tumours with KRAS mutations to EGFR inhibitors requires further research.

I believe it will be important to test the contribution of Aurora kinases to this phenotype. It has been previously shown that Aurora Kinase A drives the evolution of resistance to EGFR inhibitors in lung cancer (Shah et al., 2019). Several members of our research group, myself included, have observed a profound activation of Aurora kinases after Cyclin F depletion (data not presented in this thesis). One possibility could be that this published role of Aurora kinases in generating resistance against EGFR inhibition is at the basis of the observed reduced sensitivity to EGFR inhibitors in *KRAS* WT cells where Cyclin F has been depleted compared to *KRAS* WT cells with normal Cyclin F levels. One could speculate that this axis functions differently in *KRAS* mutant settings where Cyclin F loss could potentially trigger different events that culminate in Aurora kinase-mediated EGFR inhibitor sensitivity instead. This hypothesis could be tested in follow up studies.

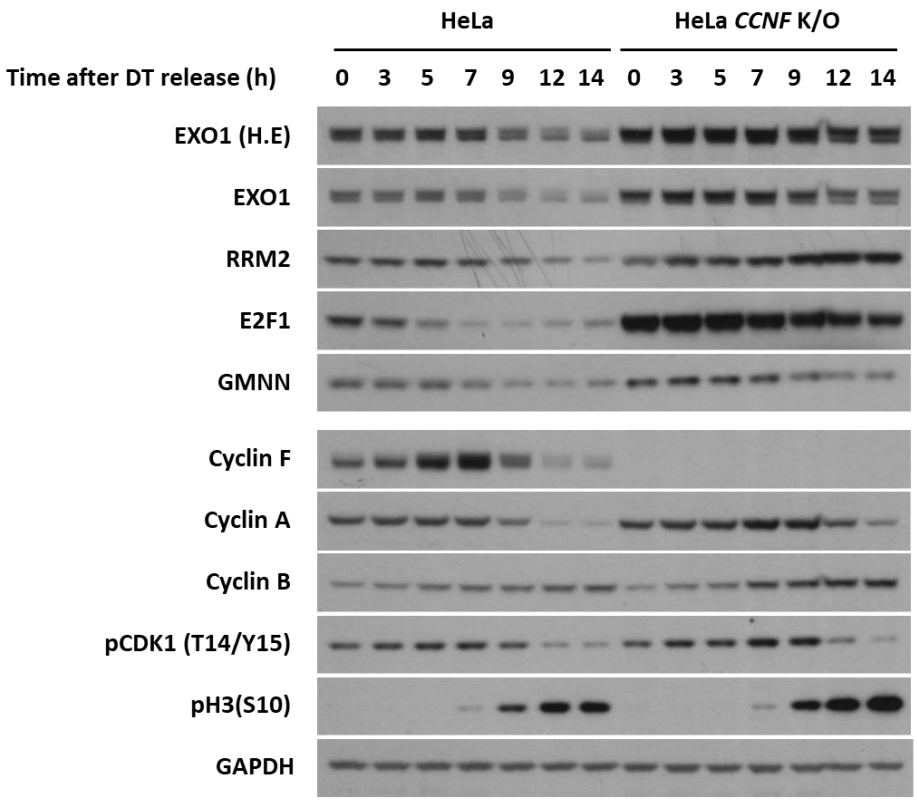
Together, results from both *EXO1-CCNF* and *KRAS-CCNF* projects reveal novel roles for Cyclin F in the DNA damage response and DNA repair in addition to interferon signalling, and highlight novel pathways as well as individual proteins that can be clinically exploited to improve the current treatment paradigms and improve patient outcomes.

8. Supplementary Figures



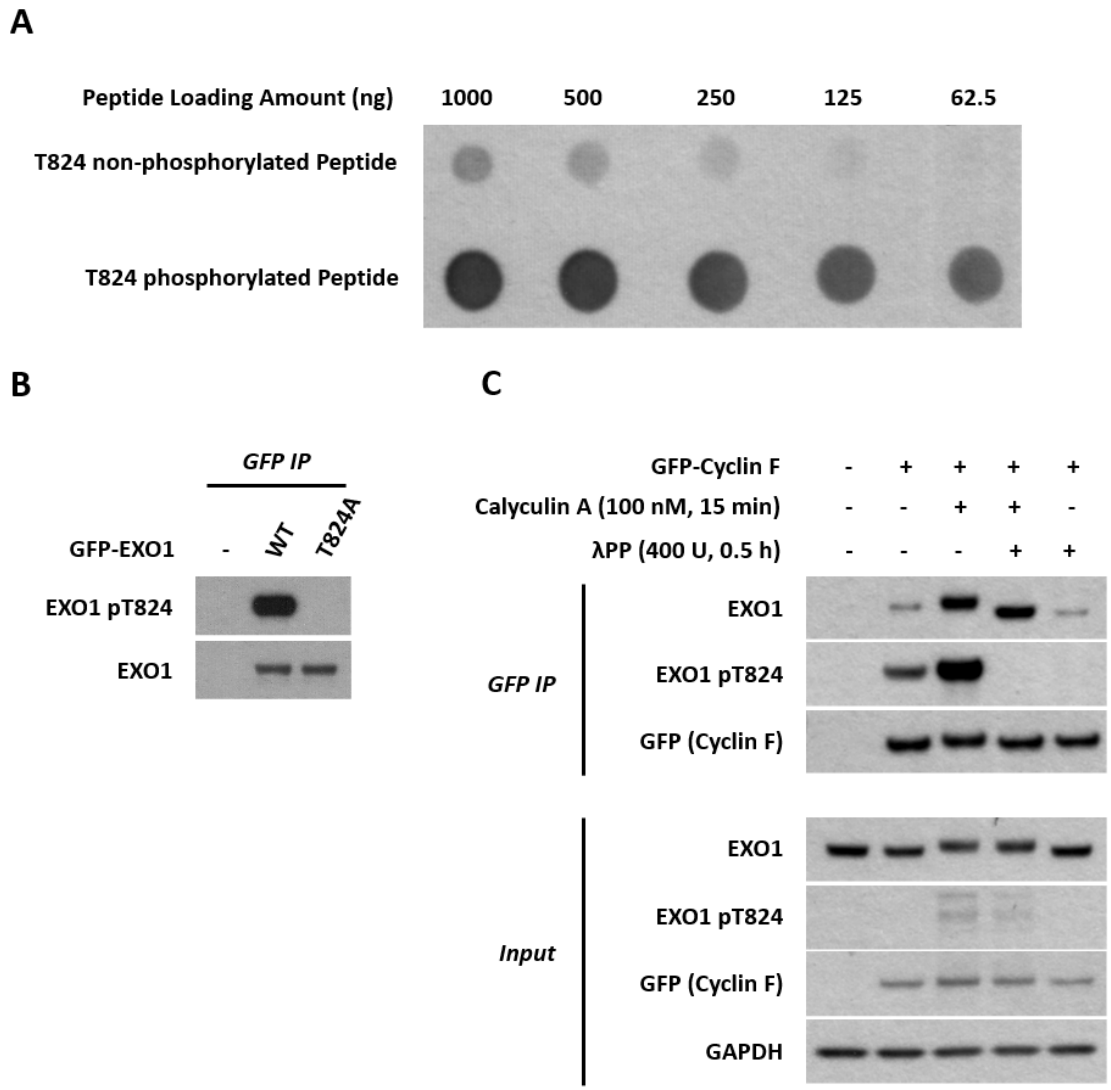
Supplementary Figure 1. *CCNF* loss sensitises cells to IR due to EXO1 accumulation which is rescued by si*EXO1* depletion.

HeLa and HeLa *CCNF* K/O were transfected with siRNA against EXO1 (or NTC) for 48 h before they were treated with IR at the indicated doses (0-6 Gy) and left to recover for 14 days after which surviving colonies were quantified then plotted.



Supplementary Figure 2. Cyclin F targets EXO1 for ubiquitylation in G_2/M.

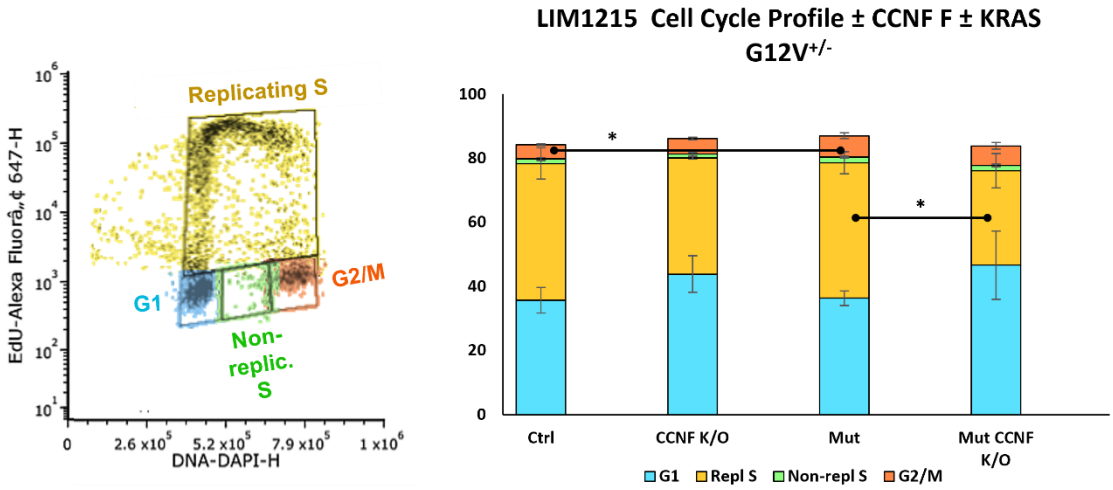
HeLa and HeLa *CCNF* K/O protein levels following release from a double-thymidine (DT) block. HeLa cells were seeded at 30% confluency, and blocked using 2 mM thymidine for 16 h. thymidine was washed out after, and the cells were allowed to proceed through the cell cycle for a further 8 h. Cells were then blocked a second time with 2 mM thymidine for 16 h. The thymidine was then washed out, and cells were harvested at the indicated time points post thymidine release and represent different phases of the cell cycle.



Supplementary Figure 3. Specificity testing of EXO1 pT824 primary antibody.

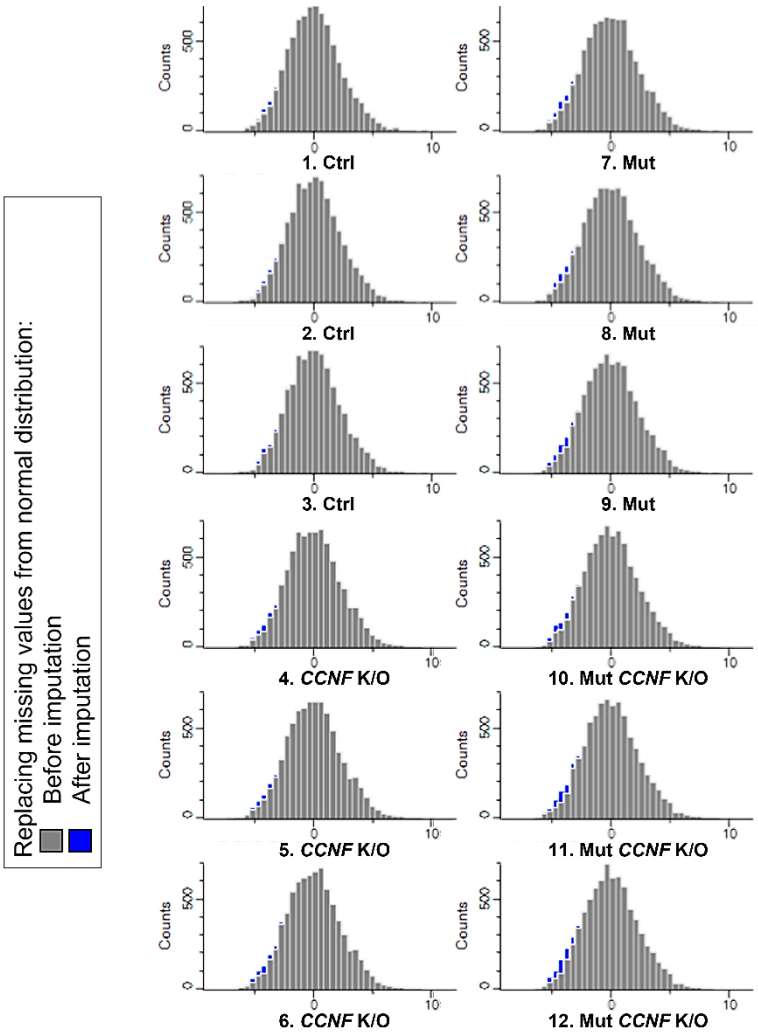
Custom generated EXO1 pT824 antibody was tested for direct detection of phosphorylated EXO1 at the T824 residue by:

1. An antibody dot blot assay using an EXO1 T824 phosphorylated peptide and its non-phosphorylated control,
2. A pull-down assay of *EXO1* WT and its phosphorylation mutant T824A in HEK293T cells,
3. A pull-down assay of Cyclin F in HEK293T cells treated with the phosphatase inhibitor Calyculin A (100 nM, 15 min), after which Lambda Protein Phosphatase (λPP) (400 U, 30 min) was added to the immunoprecipitate.



Supplementary Figure 4. Cell cycle profile of LIM1215 cells.

Cell cycle profile of the 4 LIM1215 cell lines: Ctrl, *CCNF* K/O, Mut and Mut *CCNF* K/O outlining the portion of cells in G_1, S (replicating and non-replicating) and G_2/M. Using FACS, cells were sorted according to their DNA content (measured by DAPI, X-axis) and incorporation of EdU (marker of replicating cells, Y-axis). Statistical significance was calculated using Student's t-test.



Supplementary Figure 5. Missing values across samples, N = 3.

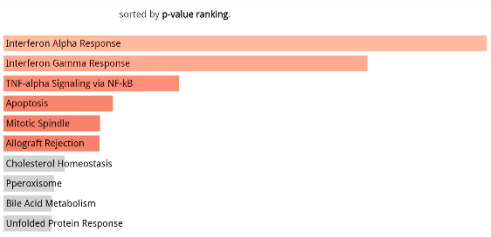
Histograms representing the number of missing values ('Counts', Y-axis) plotted against Log_2(intensity) (X-axis) of peptide precursors within the 4 LIM1215 samples used (Ctrl, *CCNF* K/O, Mut and Mut *CCNF* K/O). Histograms before (grey) and after (blue) replacing the missing values by imputation from normal distribution are overlapped for each plot. *Figures generated using Perseus software version 1.6.2.2.*

A

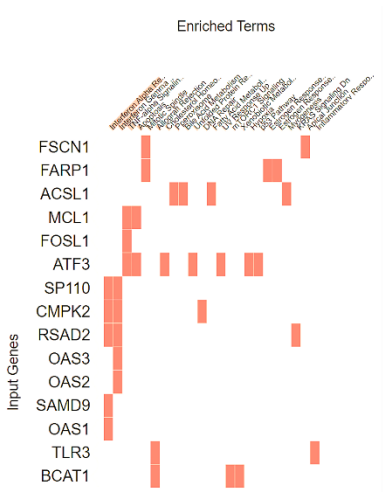
MSigDB Hallmark 2020

CCNF K/O / Ctrl						
Term	Overlap	p-value	q-value (p-value adjusted for FDR)	Odds Ratio	Combined Score	Genes
Interferon Alpha Response	5/97	3.72E-07	8.55E-06	41.54891	615.1309	SAMD9;RSAD2;OAS1;SP110;CMPK2
Interferon Gamma Response	5/200	1.31E-05	1.50E-04	19.50099	219.2771	RSAD2;SP110;**OAS2**;OAS3;CMPK2
TNF-alpha Signaling via NF-kB	3/200	0.003603	0.027621	10.75344	60.49955	**FOSL1**;ATF3;MCL1
Apoptosis	2/161	0.025705	0.146692	8.592496	31.45769	ATF3;MCL1
Mitotic Spindle	2/199	0.037921	0.146692	6.921757	22.64976	FARP1;FSCN1
Allograft Rejection	2/200	0.038267	0.146692	6.886451	22.47156	BCAT1;TLR3
Cholesterol Homeostasis	1/74	0.108633	0.267868	9.084932	20.16657	ATF3
Peroxisome	1/104	0.149339	0.267868	6.429126	12.22521	ACSL1
Bile Acid Metabolism	1/112	0.159887	0.267868	5.963363	10.93257	ACSL1
Unfolded Protein Response	1/113	0.161196	0.267868	5.909821	10.78621	ATF3
DNA Repair	1/150	0.208283	0.267868	4.434004	6.956316	CMPK2
Fatty Acid Metabolism	1/158	0.218123	0.267868	4.206369	6.405032	ACSL1
UV Response Up	1/158	0.218123	0.267868	4.206369	6.405032	ATF3
Xenobiotic Metabolism	1/200	0.267868	0.267868	3.311558	4.362182	BCAT1
Hypoxia	1/200	0.267868	0.267868	3.311558	4.362182	ATF3
p53 Pathway	1/200	0.267868	0.267868	3.311558	4.362182	ATF3
Estrogen Response Early	1/200	0.267868	0.267868	3.311558	4.362182	FARP1
Estrogen Response Late	1/200	0.267868	0.267868	3.311558	4.362182	FARP1
Myogenesis	1/200	0.267868	0.267868	3.311558	4.362182	ACSL1
KRAS Signaling Dn	1/200	0.267868	0.267868	3.311558	4.362182	RSAD2
Apical Junction	1/200	0.267868	0.267868	3.311558	4.362182	FSCN1
mTORC1 Signaling	1/200	0.267868	0.267868	3.311558	4.362182	BCAT1
Inflammatory Response	1/200	0.267868	0.267868	3.311558	4.362182	TLR3

B



C



Supplementary Figure 6. Enrichr-identified significant pathway alterations of proteins enriched in *CCNF* K/O vs Ctrl.

Altered pathways and the genes involved are presented in table format showing the p- and q- (adjusted p-) values (A), in a bar graph sorted by p-value (B) and in a clustergram showing clusters of altered genes in these pathways (C). *Figures generated using Enrichr (https://maayanlab.cloud/Enrichr/)*

9. References

AALTO, A., MARTÍNEZ-CHACÓN, G., KIETZ, C., TSYGANOVA, N., KREUTZER, J., KALLIO, P., BROEMER, M. & MEINANDER, A. 2022. M1-linked ubiquitination facilitates NF-κB activation and survival during sterile inflammation. *Febs j,* 289**,** 5180-5197.

AALTO, A. L., MOHAN, A. K., SCHWINTZER, L., KUPKA, S., KIETZ, C., WALCZAK, H., BROEMER, M. & MEINANDER, A. 2019. M1-linked ubiquitination by LUBEL is required for inflammatory responses to oral infection in Drosophila. *Cell Death Differ,* 26**,** 860-876.

AHRABI, S., SARKAR, S., PFISTER, S. X., PIROVANO, G., HIGGINS, G. S., PORTER, A. C. & HUMPHREY, T. C. 2016. A role for human homologous recombination factors in suppressing microhomology-mediated end joining. *Nucleic Acids Res,* 44**,** 5743-57.

AL ZUBAIDI, T., GEHRISCH, O. H. F., GENOIS, M. M., LIU, Q., LU, S., KUNG, J., XIE, Y., SCHUEMANN, J., LU, H. M., HATA, A. N., ZOU, L., BORGMANN, K. & WILLERS, H. 2021. Targeting the DNA replication stress phenotype of KRAS mutant cancer cells. *Sci Rep,* 11**,** 3656.

ALESSI, D. R., JAMES, S. R., DOWNES, C. P., HOLMES, A. B., GAFFNEY, P. R., REESE, C. B. & COHEN, P. 1997. Characterization of a 3-phosphoinositide-dependent protein kinase which phosphorylates and activates protein kinase Balpha. *Curr Biol,* 7**,** 261-9.

AMERIK, A. Y. & HOCHSTRASSER, M. 2004. Mechanism and function of deubiquitinating enzymes. *Biochim Biophys Acta,* 1695**,** 189-207.

AMGEN. 2019. *Amgen Announces New Clinical Data Evaluating Novel Investigational KRAS(G12C) Inhibitor In Larger Patient Group At WCLC 2019* [Online]. Available: https://www.amgen.com/newsroom/press-releases/2019/09/amgen-announces-new-clinical-data-evaluating-novel-investigational-krasg12c-inhibitor-in-larger-patient-group-at-wclc-2019 [Accessed].

ARAVIND, L. & KOONIN, E. V. 2000. The U box is a modified RING finger - a common domain in ubiquitination. *Curr Biol,* 10**,** R132-4.

BAEK, K., KRIST, D. T., PRABU, J. R., HILL, S., KLÜGEL, M., NEUMAIER, L. M., VON GRONAU, S., KLEIGER, G. & SCHULMAN, B. A. 2020. NEDD8 nucleates a multivalent cullin-RING-UBE2D ubiquitin ligation assembly. *Nature,* 578**,** 461-466.

BAI, C., SEN, P., HOFMANN, K., MA, L., GOEBL, M., HARPER, J. W. & ELLEDGE, S. J. 1996. SKP1 connects cell cycle regulators to the ubiquitin proteolysis machinery through a novel motif, the F-box. *Cell,* 86**,** 263-74.

BAKHOUM, S. F. & CANTLEY, L. C. 2018. The Multifaceted Role of Chromosomal Instability in Cancer and Its Microenvironment. *Cell,* 174**,** 1347-1360.

BATTCOCK, S. M., COLLIER, T. W., ZU, D. & HIRASAWA, K. 2006. Negative regulation of the alpha interferon-induced antiviral response by the Ras/Raf/MEK pathway. *J Virol,* 80**,** 4422-30.

BÉKÉS, M., LANGLEY, D. R. & CREWS, C. M. 2022. PROTAC targeted protein degraders: the past is prologue. *Nat Rev Drug Discov,* 21**,** 181-200.

BENVENUTI, S., SARTORE-BIANCHI, A., DI NICOLANTONIO, F., ZANON, C., MORONI, M., VERONESE, S., SIENA, S. & BARDELLI, A. 2007. Oncogenic activation of the RAS/RAF signaling pathway impairs the response of metastatic colorectal cancers to anti-epidermal growth factor receptor antibody therapies. *Cancer Res,* 67**,** 2643-8.

BHADURI, S. & PRYCIAK, P. M. 2011. Cyclin-specific docking motifs promote phosphorylation of yeast signaling proteins by G1/S Cdk complexes. *Curr Biol,* 21**,** 1615-23.

BHATTACHARYA, S., GARRIGA, J., CALBÓ, J., YONG, T., HAINES, D. S. & GRAÑA, X. 2003. SKP2 associates with p130 and accelerates p130 ubiquitylation and degradation in human cells. *Oncogene,* 22**,** 2443-51.

BIGENZAHN, J. W., COLLU, G. M., KARTNIG, F., PIERAKS, M., VLADIMER, G. I., HEINZ, L. X., SEDLYAROV, V., SCHISCHLIK, F., FAUSTER, A., REBSAMEN, M., PARAPATICS, K., BLOMEN, V. A., MÜLLER, A. C., WINTER, G. E., KRALOVICS, R., BRUMMELKAMP, T. R., MLODZIK, M. & SUPERTI-FURGA, G. 2018. LZTR1 is a regulator of RAS ubiquitination and signaling. *Science,* 362**,** 1171-1177.

BONDESON, D. P., MARES, A., SMITH, I. E., KO, E., CAMPOS, S., MIAH, A. H., MULHOLLAND, K. E., ROUTLY, N., BUCKLEY, D. L., GUSTAFSON, J. L., ZINN, N., GRANDI, P., SHIMAMURA, S., BERGAMINI, G., FAELTH-SAVITSKI, M., BANTSCHEFF, M., COX, C., GORDON, D. A., WILLARD, R. R., FLANAGAN, J. J., CASILLAS, L. N., VOTTA, B. J., DEN BESTEN, W., FAMM, K., KRUIDENIER, L., CARTER, P. S., HARLING, J. D., CHURCHER, I. & CREWS, C. M. 2015. Catalytic in vivo protein knockdown by small-molecule PROTACs. *Nat Chem Biol,* 11**,** 611-7.

BORNSTEIN, G., BLOOM, J., SITRY-SHEVAH, D., NAKAYAMA, K., PAGANO, M. & HERSHKO, A. 2003. Role of the SCFSkp2 ubiquitin ligase in the degradation of p21Cip1 in S phase. *J Biol Chem,* 278**,** 25752-7.

BOS, J. L., REHMANN, H. & WITTINGHOFER, A. 2007. GEFs and GAPs: critical elements in the control of small G proteins. *Cell,* 129**,** 865-77.

BRENNER, D. J. 2008. The linear-quadratic model is an appropriate methodology for determining isoeffective doses at large doses per fraction. *Semin Radiat Oncol,* 18**,** 234-9.

BRUICK, R. K. & MCKNIGHT, S. L. 2001. A Conserved Family of Prolyl-4-Hydroxylases That Modify HIF. *Science,* 294**,** 1337-1340.

BURDOVA, K., YANG, H., FAEDDA, R., HUME, S., CHAUHAN, J., EBNER, D., KESSLER, B. M., VENDRELL, I., DREWRY, D. H., WELLS, C. I., HATCH, S. B., DIANOV, G. L., BUFFA, F. M. & D'ANGIOLELLA, V. 2019a. E2F1 proteolysis via SCF-cyclin F underlies synthetic lethality between cyclin F loss and Chk1 inhibition. *Embo j,* 38**,** e101443.

BURDOVA, K., YANG, H., FAEDDA, R., HUME, S., CHAUHAN, J., EBNER, D., KESSLER, B. M., VENDRELL, I., DREWRY, D. H., WELLS, C. I., HATCH, S. B., DIANOV, G. L., BUFFA, F. M. & D'ANGIOLELLA, V. 2019b. E2F1 proteolysis via SCF-cyclin F underlies synthetic lethality between cyclin F loss and Chk1 inhibition. *Embo j***,** e101443.

BURDOVA, K., YANG, H., FAEDDA, R., HUME, S., EBNER, D., KESSLER, B. M., VENDRELL, I., DREWRY, D. H., WELLS, C. I., HATCH, S. B. & D'ANGIOLELLA, V. 2019c. Cyclin F-Chk1 synthetic lethality mediated by E2F1 degradation. 509810.

BURMA, S., CHEN, B. P. & CHEN, D. J. 2006. Role of non-homologous end joining (NHEJ) in maintaining genomic integrity. *DNA Repair (Amst),* 5**,** 1042-8.

BUSINO, L., BASSERMANN, F., MAIOLICA, A., LEE, C., NOLAN, P. M., GODINHO, S. I., DRAETTA, G. F. & PAGANO, M. 2007. SCFFbxl3 controls the oscillation of the circadian clock by directing the degradation of cryptochrome proteins. *Science,* 316**,** 900-4.

BUSINO, L., DONZELLI, M., CHIESA, M., GUARDAVACCARO, D., GANOTH, D., DORRELLO, N. V., HERSHKO, A., PAGANO, M. & DRAETTA, G. F. 2003. Degradation of Cdc25A by beta-TrCP during S phase and in response to DNA damage. *Nature,* 426**,** 87-91.

BYTHELL-DOUGLAS, R. & DEANS, A. J. 2021. A Structural Guide to the Bloom Syndrome Complex. *Structure,* 29**,** 99-113.

CARRANO, A. C., EYTAN, E., HERSHKO, A. & PAGANO, M. 1999. SKP2 is required for ubiquitin-mediated degradation of the CDK inhibitor p27. *Nat Cell Biol,* 1**,** 193-9.

CASTEL, P., CHENG, A., CUEVAS-NAVARRO, A., EVERMAN, D. B., PAPAGEORGE, A. G., SIMANSHU, D. K., TANKKA, A., GALEAS, J., URISMAN, A. & MCCORMICK, F. 2019. RIT1 oncoproteins escape LZTR1-mediated proteolysis. *Science,* 363**,** 1226-1230.

CAVADINI, S., FISCHER, E. S., BUNKER, R. D., POTENZA, A., LINGARAJU, G. M., GOLDIE, K. N., MOHAMED, W. I., FATY, M., PETZOLD, G., BECKWITH, R. E., TICHKULE, R. B., HASSIEPEN, U., ABDULRAHMAN, W., PANTELIC, R. S., MATSUMOTO, S., SUGASAWA, K.,

STAHLBERG, H. & THOMÄ, N. H. 2016. Cullin-RING ubiquitin E3 ligase regulation by the COP9 signalosome. *Nature,* 531**,** 598-603.
CECCALDI, R., LIU, J. C., AMUNUGAMA, R., HAJDU, I., PRIMACK, B., PETALCORIN, M. I., O'CONNOR, K. W., KONSTANTINOPOULOS, P. A., ELLEDGE, S. J., BOULTON, S. J., YUSUFZAI, T. & D'ANDREA, A. D. 2015. Homologous-recombination-deficient tumours are dependent on Polθ-mediated repair. *Nature,* 518**,** 258-62.
CENCIARELLI, C., CHIAUR, D. S., GUARDAVACCARO, D., PARKS, W., VIDAL, M. & PAGANO, M. 1999. Identification of a family of human F-box proteins. *Curr Biol,* 9**,** 1177-9.
CHAN, N. L. & HILL, C. P. 2001. Defining polyubiquitin chain topology. *Nat Struct Biol,* 8**,** 650-2.
CHANG, L., ZHANG, Z., YANG, J., MCLAUGHLIN, S. H. & BARFORD, D. 2015. Atomic structure of the APC/C and its mechanism of protein ubiquitination. *Nature,* 522**,** 450-454.
CHANG, L. F., ZHANG, Z., YANG, J., MCLAUGHLIN, S. H. & BARFORD, D. 2014. Molecular architecture and mechanism of the anaphase-promoting complex. *Nature,* 513**,** 388-393.
CHANG, Y. F., CHENG, C. M., CHANG, L. K., JONG, Y. J. & YUO, C. Y. 2006. The F-box protein Fbxo7 interacts with human inhibitor of apoptosis protein cIAP1 and promotes cIAP1 ubiquitination. *Biochem Biophys Res Commun,* 342**,** 1022-6.
CHAU, V., TOBIAS, J. W., BACHMAIR, A., MARRIOTT, D., ECKER, D. J., GONDA, D. K. & VARSHAVSKY, A. 1989. A multiubiquitin chain is confined to specific lysine in a targeted short-lived protein. *Science,* 243**,** 1576-83.
CHAUSSEPIED, M. & GINSBERG, D. 2004. Transcriptional regulation of AKT activation by E2F. *Mol Cell,* 16**,** 831-7.
CHEN, B. B., GLASSER, J. R., COON, T. A. & MALLAMPALLI, R. K. 2012a. F-box protein FBXL2 exerts human lung tumor suppressor-like activity by ubiquitin-mediated degradation of cyclin D3 resulting in cell cycle arrest. *Oncogene,* 31**,** 2566-79.
CHEN, B. B., GLASSER, J. R., COON, T. A. & MALLAMPALLI, R. K. 2013. Skp-cullin-F box E3 ligase component FBXL2 ubiquitinates Aurora B to inhibit tumorigenesis. *Cell Death Dis,* 4**,** e759.
CHEN, B. B., GLASSER, J. R., COON, T. A., ZOU, C., MILLER, H. L., FENTON, M., MCDYER, J. F., BOYIADZIS, M. & MALLAMPALLI, R. K. 2012b. F-box protein FBXL2 targets cyclin D2 for ubiquitination and degradation to inhibit leukemic cell proliferation. *Blood,* 119**,** 3132-41.
CHEN, G. A., LIN, Y. R., CHUNG, H. T. & HWANG, L. H. 2017. H-Ras Exerts Opposing Effects on Type I Interferon Responses Depending on Its Activation Status. *Front Immunol,* 8**,** 972.
CHEN, H. Y. & CHEN, R. H. 2016. Cullin 3 Ubiquitin Ligases in Cancer Biology: Functions and Therapeutic Implications. *Front Oncol,* 6**,** 113.
CHEN, H. Z., TSAI, S. Y. & LEONE, G. 2009. Emerging roles of E2Fs in cancer: an exit from cell cycle control. *Nat Rev Cancer,* 9**,** 785-97.
CHEN, Z., IORIS, R. M., RICHARDSON, S., VAN ESS, A. N., VENDRELL, I., KESSLER, B. M., BUFFA, F. M., BUSINO, L., CLIFFORD, S. C., BULLOCK, A. N. & D'ANGIOLELLA, V. 2022. Disease-associated KBTBD4 mutations in medulloblastoma elicit neomorphic ubiquitylation activity to promote CoREST degradation. *Cell Death Differ*.
CHEN, Z. W., LIU, B., TANG, N. W., XU, Y. H., YE, X. Y., LI, Z. M., NIU, X. M., SHEN, S. P., LU, S. & XU, L. 2014. FBXL5-mediated degradation of single-stranded DNA-binding protein hSSB1 controls DNA damage response. *Nucleic Acids Res,* 42**,** 11560-9.
CHIORAZZI, M., RUI, L., YANG, Y., CERIBELLI, M., TISHBI, N., MAURER, C. W., RANUNCOLO, S. M., ZHAO, H., XU, W., CHAN, W. C., JAFFE, E. S., GASCOYNE, R. D., CAMPO, E., ROSENWALD, A., OTT, G., DELABIE, J., RIMSZA, L. M., SHAHAM, S. & STAUDT, L. M. 2013. Related F-box proteins control cell death in Caenorhabditis elegans and human lymphoma. *Proc Natl Acad Sci U S A,* 110**,** 3943-8.

CHIU, Y. H., SUN, Q. & CHEN, Z. J. 2007. E1-L2 activates both ubiquitin and FAT10. *Mol Cell,* 27**,** 1014-23.

CHOU, H. C., BHALLA, K., DEMERDESH, O. E., KLINGBEIL, O., HANINGTON, K., AGANEZOV, S., ANDREWS, P., ALSUDANI, H., CHANG, K., VAKOC, C. R., SCHATZ, M. C., MCCOMBIE, W. R. & STILLMAN, B. 2021. The human origin recognition complex is essential for pre-RC assembly, mitosis, and maintenance of nuclear structure. *Elife,* 10.

CHOUDHURY, R., BONACCI, T., ARCECI, A., LAHIRI, D., MILLS, C. A., KERNAN, J. L., BRANIGAN, T. B., DECAPRIO, J. A., BURKE, D. J. & EMANUELE, M. J. 2016. APC/C and SCF(cyclin F) Constitute a Reciprocal Feedback Circuit Controlling S-Phase Entry. *Cell Rep,* 16**,** 3359-3372.

CHOUDHURY, R., BONACCI, T., WANG, X., TRUONG, A., ARCECI, A., ZHANG, Y., MILLS, C. A., KERNAN, J. L., LIU, P. & EMANUELE, M. J. 2017. The E3 Ubiquitin Ligase SCF(Cyclin F) Transmits AKT Signaling to the Cell-Cycle Machinery. *Cell Rep,* 20**,** 3212-3222.

CLAGUE, M. J., BARSUKOV, I., COULSON, J. M., LIU, H., RIGDEN, D. J. & URBÉ, S. 2013. Deubiquitylases from genes to organism. *Physiol Rev,* 93**,** 1289-315.

CLAGUE, M. J., HERIDE, C. & URBÉ, S. 2015. The demographics of the ubiquitin system. *Trends Cell Biol,* 25**,** 417-26.

CLEMENT, E., INUZUKA, H., NIHIRA, N. T., WEI, W. & TOKER, A. 2018. Skp2-dependent reactivation of AKT drives resistance to PI3K inhibitors. *Sci Signal,* 11.

CLIJSTERS, L., HOENCAMP, C., CALIS, J. J. A., MARZIO, A., HANDGRAAF, S. M., CUITINO, M. C., ROSENBERG, B. R., LEONE, G. & PAGANO, M. 2019. Cyclin F Controls Cell-Cycle Transcriptional Outputs by Directing the Degradation of the Three Activator E2Fs. *Mol Cell,* 74**,** 1264-1277.e7.

CLOSE, V., CLOSE, W., KUGLER, S. J., REICHENZELLER, M., YOSIFOV, D. Y., BLOEHDORN, J., PAN, L., TAUSCH, E., WESTHOFF, M. A., DÖHNER, H., STILGENBAUER, S., OSWALD, F. & MERTENS, D. 2019. FBXW7 mutations reduce binding of NOTCH1, leading to cleaved NOTCH1 accumulation and target gene activation in CLL. *Blood,* 133**,** 830-839.

COON, T. A., GLASSER, J. R., MALLAMPALLI, R. K. & CHEN, B. B. 2012. Novel E3 ligase component FBXL7 ubiquitinates and degrades Aurora A, causing mitotic arrest. *Cell Cycle,* 11**,** 721-9.

CUI, Y. H., KIM, H., LEE, M., YI, J. M., KIM, R. K., UDDIN, N., YOO, K. C., KANG, J. H., CHOI, M. Y., CHA, H. J., KWON, O. S., BAE, I. H., KIM, M. J., KAUSHIK, N. & LEE, S. J. 2018. FBXL14 abolishes breast cancer progression by targeting CDCP1 for proteasomal degradation. *Oncogene,* 37**,** 5794-5809.

CULLINAN, S. B., GORDAN, J. D., JIN, J., HARPER, J. W. & DIEHL, J. A. 2004. The Keap1-BTB protein is an adaptor that bridges Nrf2 to a Cul3-based E3 ligase: oxidative stress sensing by a Cul3-Keap1 ligase. *Mol Cell Biol,* 24**,** 8477-86.

D'ANGIOLELLA, V., DONATO, V., FORRESTER, F. M., JEONG, Y. T., PELLACANI, C., KUDO, Y., SARAF, A., FLORENS, L., WASHBURN, M. P. & PAGANO, M. 2012. Cyclin F-mediated degradation of ribonucleotide reductase M2 controls genome integrity and DNA repair. *Cell,* 149**,** 1023-34.

D'ANGIOLELLA, V., DONATO, V., VIJAYAKUMAR, S., SARAF, A., FLORENS, L., WASHBURN, M. P., DYNLACHT, B. & PAGANO, M. 2010. SCF(Cyclin F) controls centrosome homeostasis and mitotic fidelity through CP110 degradation. *Nature,* 466**,** 138-42.

D'ANGIOLELLA, V., ESENCAY, M. & PAGANO, M. 2013. A cyclin without cyclin-dependent kinases: cyclin F controls genome stability through ubiquitin-mediated proteolysis. *Trends Cell Biol,* 23**,** 135-40.

DANG, L., WHITE, D. W., GROSS, S., BENNETT, B. D., BITTINGER, M. A., DRIGGERS, E. M., FANTIN, V. R., JANG, H. G., JIN, S., KEENAN, M. C., MARKS, K. M., PRINS, R. M., WARD, P. S., YEN, K. E., LIAU, L. M., RABINOWITZ, J. D., CANTLEY, L. C., THOMPSON, C. B.,

VANDER HEIDEN, M. G. & SU, S. M. 2009. Cancer-associated IDH1 mutations produce 2-hydroxyglutarate. *Nature,* 462**,** 739-44.

DANKERT, J. F., RONA, G., CLIJSTERS, L., GETER, P., SKAAR, J. R., BERMUDEZ-HERNANDEZ, K., SASSANI, E., FENYÖ, D., UEBERHEIDE, B., SCHNEIDER, R. & PAGANO, M. 2016. Cyclin F-Mediated Degradation of SLBP Limits H2A.X Accumulation and Apoptosis upon Genotoxic Stress in G2. *Mol Cell,* 64**,** 507-519.

DAZA-MARTIN, M., STAROWICZ, K., JAMSHAD, M., TYE, S., RONSON, G. E., MACKAY, H. L., CHAUHAN, A. S., WALKER, A. K., STONE, H. R., BEESLEY, J. F. J., COLES, J. L., GARVIN, A. J., STEWART, G. S., MCCORVIE, T. J., ZHANG, X., DENSHAM, R. M. & MORRIS, J. R. 2019. Isomerization of BRCA1-BARD1 promotes replication fork protection. *Nature,* 571**,** 521-527.

DEHAN, E., BASSERMANN, F., GUARDAVACCARO, D., VASILIVER-SHAMIS, G., COHEN, M., LOWES, K. N., DUSTIN, M., HUANG, D. C., TAUNTON, J. & PAGANO, M. 2009. betaTrCP- and Rsk1/2-mediated degradation of BimEL inhibits apoptosis. *Mol Cell,* 33**,** 109-16.

DESHAIES, R. J. & JOAZEIRO, C. A. P. 2009. RING Domain E3 Ubiquitin Ligases. *Annual Review of Biochemistry,* 78**,** 399-434.

DIAS, D. C., DOLIOS, G., WANG, R. & PAN, Z. Q. 2002. CUL7: A DOC domain-containing cullin selectively binds Skp1.Fbx29 to form an SCF-like complex. *Proc Natl Acad Sci U S A,* 99**,** 16601-6.

DING, Q., HE, X., HSU, J. M., XIA, W., CHEN, C. T., LI, L. Y., LEE, D. F., LIU, J. C., ZHONG, Q., WANG, X. & HUNG, M. C. 2007. Degradation of Mcl-1 by beta-TrCP mediates glycogen synthase kinase 3-induced tumor suppression and chemosensitization. *Mol Cell Biol,* 27**,** 4006-17.

DOAK, B. C., OVER, B., GIORDANETTO, F. & KIHLBERG, J. 2014. Oral druggable space beyond the rule of 5: insights from drugs and clinical candidates. *Chem Biol,* 21**,** 1115-42.

DONG, S., ZHAO, J., WEI, J., BOWSER, R. K., KHOO, A., LIU, Z., LUKETICH, J. D., PENNATHUR, A., MA, H. & ZHAO, Y. 2014. F-box protein complex FBXL19 regulates TGFβ1-induced E-cadherin down-regulation by mediating Rac3 ubiquitination and degradation. *Mol Cancer,* 13**,** 76.

DONZELLI, M., BUSINO, L., CHIESA, M., GANOTH, D., HERSHKO, A. & DRAETTA, G. F. 2004. Hierarchical order of phosphorylation events commits Cdc25A to betaTrCP-dependent degradation. *Cell Cycle,* 3**,** 469-71.

DORRELLO, N. V., PESCHIAROLI, A., GUARDAVACCARO, D., COLBURN, N. H., SHERMAN, N. E. & PAGANO, M. 2006. S6K1- and betaTRCP-mediated degradation of PDCD4 promotes protein translation and cell growth. *Science,* 314**,** 467-71.

DUAN, S., CERMAK, L., PAGAN, J. K., ROSSI, M., MARTINENGO, C., DI CELLE, P. F., CHAPUY, B., SHIPP, M., CHIARLE, R. & PAGANO, M. 2012. FBXO11 targets BCL6 for degradation and is inactivated in diffuse large B-cell lymphomas. *Nature,* 481**,** 90-3.

DUDA, D. M., BORG, L. A., SCOTT, D. C., HUNT, H. W., HAMMEL, M. & SCHULMAN, B. A. 2008. Structural insights into NEDD8 activation of cullin-RING ligases: conformational control of conjugation. *Cell,* 134**,** 995-1006.

DYE, B. T. & SCHULMAN, B. A. 2007. Structural mechanisms underlying posttranslational modification by ubiquitin-like proteins. *Annu Rev Biophys Biomol Struct,* 36**,** 131-50.

DYSON, N. 1998. The regulation of E2F by pRB-family proteins. *Genes Dev,* 12**,** 2245-62.

EBERHARD, D. A., JOHNSON, B. E., AMLER, L. C., GODDARD, A. D., HELDENS, S. L., HERBST, R. S., INCE, W. L., JÄNNE, P. A., JANUARIO, T., JOHNSON, D. H., KLEIN, P., MILLER, V. A., OSTLAND, M. A., RAMIES, D. A., SEBISANOVIC, D., STINSON, J. A., ZHANG, Y. R., SESHAGIRI, S. & HILLAN, K. J. 2005. Mutations in the epidermal growth factor receptor and in KRAS are predictive and prognostic indicators in patients with non-small-cell lung cancer treated with chemotherapy alone and in combination with erlotinib. *J Clin Oncol,* 23**,** 5900-9.

EL-SHEMERLY, M., HESS, D., PYAKUREL, A. K., MOSELHY, S. & FERRARI, S. 2008. ATR-dependent pathways control hEXO1 stability in response to stalled forks. *Nucleic Acids Res,* 36**,** 511-9.

EL-SHEMERLY, M., JANSCAK, P., HESS, D., JIRICNY, J. & FERRARI, S. 2005. Degradation of human exonuclease 1b upon DNA synthesis inhibition. *Cancer Res,* 65**,** 3604-9.

ELIA, A. E., BOARDMAN, A. P., WANG, D. C., HUTTLIN, E. L., EVERLEY, R. A., DEPHOURE, N., ZHOU, C., KOREN, I., GYGI, S. P. & ELLEDGE, S. J. 2015. Quantitative Proteomic Atlas of Ubiquitination and Acetylation in the DNA Damage Response. *Mol Cell,* 59**,** 867-81.

EMANUELE, M. J., ELIA, A. E., XU, Q., THOMA, C. R., IZHAR, L., LENG, Y., GUO, A., CHEN, Y. N., RUSH, J., HSU, P. W., YEN, H. C. & ELLEDGE, S. J. 2011. Global identification of modular cullin-RING ligase substrates. *Cell,* 147**,** 459-74.

ENKHBAYAR, P., KAMIYA, M., OSAKI, M., MATSUMOTO, T. & MATSUSHIMA, N. 2004. Structural principles of leucine-rich repeat (LRR) proteins. *Proteins,* 54**,** 394-403.

ENRICO, T. P., STALLAERT, W., WICK, E. T., NGOI, P., WANG, X., RUBIN, S. M., BROWN, N. G., PURVIS, J. E. & EMANUELE, M. J. 2021. Cyclin F drives proliferation through SCF-dependent degradation of the retinoblastoma-like tumor suppressor p130/RBL2. *Elife,* 10.

EPSTEIN, A. C. R., GLEADLE, J. M., MCNEILL, L. A., HEWITSON, K. S., O'ROURKE, J., MOLE, D. R., MUKHERJI, M., METZEN, E., WILSON, M. I., DHANDA, A., TIAN, Y.-M., MASSON, N., HAMILTON, D. L., JAAKKOLA, P., BARSTEAD, R., HODGKIN, J., MAXWELL, P. H., PUGH, C. W., SCHOFIELD, C. J. & RATCLIFFE, P. J. 2001. C. elegans EGL-9 and Mammalian Homologs Define a Family of Dioxygenases that Regulate HIF by Prolyl Hydroxylation. *Cell,* 107**,** 43-54.

ESTELLER, M., GARCIA-FONCILLAS, J., ANDION, E., GOODMAN, S. N., HIDALGO, O. F., VANACLOCHA, V., BAYLIN, S. B. & HERMAN, J. G. 2000. Inactivation of the DNA-repair gene MGMT and the clinical response of gliomas to alkylating agents. *N Engl J Med,* 343**,** 1350-4.

FANG, W., HUANG, Y., GU, W., GAN, J., WANG, W., ZHANG, S., WANG, K., ZHAN, J., YANG, Y., HUANG, Y., ZHAO, H. & ZHANG, L. 2020. PI3K-AKT-mTOR pathway alterations in advanced NSCLC patients after progression on EGFR-TKI and clinical response to EGFR-TKI plus everolimus combination therapy. *Transl Lung Cancer Res,* 9**,** 1258-1267.

FANG, X., ZHOU, W., WU, Q., HUANG, Z., SHI, Y., YANG, K., CHEN, C., XIE, Q., MACK, S. C., WANG, X., CARCABOSO, A. M., SLOAN, A. E., OUYANG, G., MCLENDON, R. E., BIAN, X. W., RICH, J. N. & BAO, S. 2017. Deubiquitinase USP13 maintains glioblastoma stem cells by antagonizing FBXL14-mediated Myc ubiquitination. *J Exp Med,* 214**,** 245-267.

FAUSTOVA, I., BULATOVIC, L., MATIYEVSKAYA, F., VALK, E., ÖRD, M. & LOOG, M. 2021. A new linear cyclin docking motif that mediates exclusively S-phase CDK-specific signaling. *Embo j,* 40**,** e105839.

FDA. 2021. *FDA grants accelerated approval to sotorasib for KRAS G12C mutated NSCLC* [Online]. Available: https://www.fda.gov/drugs/resources-information-approved-drugs/fda-grants-accelerated-approval-sotorasib-kras-g12c-mutated-nsclc [Accessed].

FEI, C., LI, Z., LI, C., CHEN, Y., CHEN, Z., HE, X., MAO, L., WANG, X., ZENG, R. & LI, L. 2013. Smurf1-mediated Lys29-linked nonproteolytic polyubiquitination of axin negatively regulates Wnt/β-catenin signaling. *Mol Cell Biol,* 33**,** 4095-105.

FENG, C., YANG, F. & WANG, J. 2017. FBXO4 inhibits lung cancer cell survival by targeting Mcl-1 for degradation. *Cancer Gene Ther,* 24**,** 342-347.

FERRETTI, L. P., LAFRANCHI, L. & SARTORI, A. A. 2013. Controlling DNA-end resection: a new task for CDKs. *Front Genet,* 4**,** 99.

FINLEY, D., OZKAYNAK, E. & VARSHAVSKY, A. 1987. The yeast polyubiquitin gene is essential for resistance to high temperatures, starvation, and other stresses. *Cell,* 48**,** 1035-46.

FOUAD, S., HAUTON, D. & D'ANGIOLELLA, V. 2020. E2F1: Cause and Consequence of DNA Replication Stress. *Front Mol Biosci,* 7**,** 599332.

FOUAD, S., WELLS, O. S., HILL, M. A. & D'ANGIOLELLA, V. 2019. Cullin Ring Ubiquitin Ligases (CRLs) in Cancer: Responses to Ionizing Radiation (IR) Treatment. *Front Physiol,* 10**,** 1144.

FRESCAS, D. & PAGANO, M. 2008. Deregulated proteolysis by the F-box proteins SKP2 and beta-TrCP: tipping the scales of cancer. *Nat Rev Cancer,* 8**,** 438-49.

FUNG, E., RICHTER, C., YANG, H. B., SCHÄFFER, I., FISCHER, R., KESSLER, B. M., BASSERMANN, F. & D'ANGIOLELLA, V. 2018. FBXL13 directs the proteolysis of CEP192 to regulate centrosome homeostasis and cell migration. *EMBO Rep,* 19.

FUNG, T. K., SIU, W. Y., YAM, C. H., LAU, A. & POON, R. Y. 2002. Cyclin F is degraded during G2-M by mechanisms fundamentally different from other cyclins. *J Biol Chem,* 277**,** 35140-9.

GANOTH, D., BORNSTEIN, G., KO, T. K., LARSEN, B., TYERS, M., PAGANO, M. & HERSHKO, A. 2001. The cell-cycle regulatory protein Cks1 is required for SCF(Skp2)-mediated ubiquitinylation of p27. *Nat Cell Biol,* 3**,** 321-4.

GATTI, M., PINATO, S., MAIOLICA, A., ROCCHIO, F., PRATO, M. G., AEBERSOLD, R. & PENENGO, L. 2015. RNF168 promotes noncanonical K27 ubiquitination to signal DNA damage. *Cell Rep,* 10**,** 226-38.

GHEZRAOUI, H., PIGANEAU, M., RENOUF, B., RENAUD, J. B., SALLMYR, A., RUIS, B., OH, S., TOMKINSON, A. E., HENDRICKSON, E. A., GIOVANNANGELI, C., JASIN, M. & BRUNET, E. 2014. Chromosomal translocations in human cells are generated by canonical nonhomologous end-joining. *Mol Cell,* 55**,** 829-842.

GILBERT, M. R., WANG, M., ALDAPE, K. D., STUPP, R., HEGI, M. E., JAECKLE, K. A., ARMSTRONG, T. S., WEFEL, J. S., WON, M., BLUMENTHAL, D. T., MAHAJAN, A., SCHULTZ, C. J., ERRIDGE, S., BAUMERT, B., HOPKINS, K. I., TZUK-SHINA, T., BROWN, P. D., CHAKRAVARTI, A., CURRAN, W. J., JR. & MEHTA, M. P. 2013. Dose-dense temozolomide for newly diagnosed glioblastoma: a randomized phase III clinical trial. *J Clin Oncol,* 31**,** 4085-91.

GLENN, K. A., NELSON, R. F., WEN, H. M., MALLINGER, A. J. & PAULSON, H. L. 2008. Diversity in tissue expression, substrate binding, and SCF complex formation for a lectin family of ubiquitin ligases. *J Biol Chem,* 283**,** 12717-29.

GORSKI, D. H., BECKETT, M. A., JASKOWIAK, N. T., CALVIN, D. P., MAUCERI, H. J., SALLOUM, R. M., SEETHARAM, S., KOONS, A., HARI, D. M., KUFE, D. W. & WEICHSELBAUM, R. R. 1999. Blockade of the Vascular Endothelial Growth Factor Stress Response Increases the Antitumor Effects of Ionizing Radiation. *Cancer Res,* 59**,** 3374-3378.

GRABOCKA, E., COMMISSO, C. & BAR-SAGI, D. 2015. Molecular pathways: targeting the dependence of mutant RAS cancers on the DNA damage response. *Clin Cancer Res,* 21**,** 1243-7.

GUARDAVACCARO, D., FRESCAS, D., DORRELLO, N. V., PESCHIAROLI, A., MULTANI, A. S., CARDOZO, T., LASORELLA, A., IAVARONE, A., CHANG, S., HERNANDO, E. & PAGANO, M. 2008. Control of chromosome stability by the beta-TrCP-REST-Mad2 axis. *Nature,* 452**,** 365-9.

GUNDOGDU, M. & WALDEN, H. 2019. Structural basis of generic versus specific E2-RING E3 interactions in protein ubiquitination. *Protein Sci,* 28**,** 1758-1770.

GUSTAFSSON, N. M. S., FÄRNEGÅRDH, K., BONAGAS, N., NINOU, A. H., GROTH, P., WIITA, E., JÖNSSON, M., HALLBERG, K., LEHTO, J., PENNISI, R., MARTINSSON, J., NORSTRÖM, C., HOLLERS, J., SCHULTZ, J., ANDERSSON, M., MARKOVA, N., MARTTILA, P., KIM, B., NORIN, M., OLIN, T. & HELLEDAY, T. 2018. Targeting PFKFB3 radiosensitizes cancer cells and suppresses homologous recombination. *Nat Commun,* 9**,** 3872.

HAIGIS, K. M. 2017. KRAS Alleles: The Devil Is in the Detail. *Trends Cancer,* 3**,** 686-697.

HALLIN, J., BOWCUT, V., CALINISAN, A., BRIERE, D. M., HARGIS, L., ENGSTROM, L. D., LAGUER, J., MEDWID, J., VANDERPOOL, D., LIFSET, E., TRINH, D., HOFFMAN, N., WANG, X., DAVID LAWSON, J., GUNN, R. J., SMITH, C. R., THOMAS, N. C., MARTINSON, M., BERGSTROM, A., SULLIVAN, F., BOUHANA, K., WINSKI, S., HE, L., FERNANDEZ-BANET, J., PAVLICEK, A., HALING, J. R., RAHBAEK, L., MARX, M. A., OLSON, P. & CHRISTENSEN, J. G. 2022. Anti-tumor efficacy of a potent and selective non-covalent KRAS(G12D) inhibitor. *Nat Med,* 28**,** 2171-2182.

HALLSTROM, T. C. & NEVINS, J. R. 2003. Specificity in the activation and control of transcription factor E2F-dependent apoptosis. *Proc Natl Acad Sci U S A,* 100**,** 10848-53.

HANSEN, F. M., TANZER, M. C., BRÜNING, F., BLUDAU, I., STAFFORD, C., SCHULMAN, B. A., ROBLES, M. S., KARAYEL, O. & MANN, M. 2021. Data-independent acquisition method for ubiquitinome analysis reveals regulation of circadian biology. *Nat Commun,* 12**,** 254.

HART, M., CONCORDET, J. P., LASSOT, I., ALBERT, I., DEL LOS SANTOS, R., DURAND, H., PERRET, C., RUBINFELD, B., MARGOTTIN, F., BENAROUS, R. & POLAKIS, P. 1999. The F-box protein beta-TrCP associates with phosphorylated beta-catenin and regulates its activity in the cell. *Curr Biol,* 9**,** 207-10.

HEGI, M. E., DISERENS, A. C., GORLIA, T., HAMOU, M. F., DE TRIBOLET, N., WELLER, M., KROS, J. M., HAINFELLNER, J. A., MASON, W., MARIANI, L., BROMBERG, J. E., HAU, P., MIRIMANOFF, R. O., CAIRNCROSS, J. G., JANZER, R. C. & STUPP, R. 2005. MGMT gene silencing and benefit from temozolomide in glioblastoma. *N Engl J Med,* 352**,** 997-1003.

HEYER, W. D., EHMSEN, K. T. & LIU, J. 2010. Regulation of homologous recombination in eukaryotes. *Annu Rev Genet,* 44**,** 113-39.

HONG, C., SCHUBERT, M., TIJHUIS, A. E., REQUESENS, M., ROORDA, M., VAN DEN BRINK, A., RUIZ, L. A., BAKKER, P. L., VAN DER SLUIS, T., PIETERS, W., CHEN, M., WARDENAAR, R., VAN DER VEGT, B., SPIERINGS, D. C. J., DE BRUYN, M., VAN VUGT, M. & FOIJER, F. 2022. cGAS-STING drives the IL-6-dependent survival of chromosomally instable cancers. *Nature,* 607**,** 366-373.

HOPF, L. V. M., BAEK, K., KLÜGEL, M., VON GRONAU, S., XIONG, Y. & SCHULMAN, B. A. 2022. Structure of CRL7(FBXW8) reveals coupling with CUL1-RBX1/ROC1 for multi-cullin-RING E3-catalyzed ubiquitin ligation. *Nat Struct Mol Biol,* 29**,** 854-862.

HU, S., LU, Y., ORR, B., GODEK, K., MUSTACHIO, L. M., KAWAKAMI, M., SEKULA, D., COMPTON, D. A., FREEMANTLE, S. & DMITROVSKY, E. 2015. Specific CP110 Phosphorylation Sites Mediate Anaphase Catastrophe after CDK2 Inhibition: Evidence for Cooperation with USP33 Knockdown. *Mol Cancer Ther,* 14**,** 2576-85.

HUANG, H., REGAN, K. M., WANG, F., WANG, D., SMITH, D. I., VAN DEURSEN, J. M. & TINDALL, D. J. 2005. Skp2 inhibits FOXO1 in tumor suppression through ubiquitin-mediated degradation. *Proc Natl Acad Sci U S A,* 102**,** 1649-54.

HUANG, L. E., GU, J., SCHAU, M. & BUNN, H. F. 1998. Regulation of hypoxia-inducible factor 1α is mediated by an O_2-dependent degradation domain via the ubiquitin-proteasome pathway. *Proc Natl Acad Sci U S A,* 95**,** 7987-7992.

HUBER, A. L., PAPP, S. J., CHAN, A. B., HENRIKSSON, E., JORDAN, S. D., KRIEBS, A., NGUYEN, M., WALLACE, M., LI, Z., METALLO, C. M. & LAMIA, K. A. 2016. CRY2 and FBXL3 Cooperatively Degrade c-MYC. *Mol Cell,* 64**,** 774-789.

JEONG, W. J., YOON, J., PARK, J. C., LEE, S. H., LEE, S. H., KADUWAL, S., KIM, H., YOON, J. B. & CHOI, K. Y. 2012. Ras stabilization through aberrant activation of Wnt/beta-catenin signaling promotes intestinal tumorigenesis. *Sci Signal,* 5**,** ra30.

JIN, J., ANG, X. L., SHIROGANE, T. & WADE HARPER, J. 2005. Identification of substrates for F-box proteins. *Methods Enzymol,* 399**,** 287-309.

JIN, J., ARIAS, E. E., CHEN, J., HARPER, J. W. & WALTER, J. C. 2006. A family of diverse Cul4-Ddb1-interacting proteins includes Cdt2, which is required for S phase destruction of the replication factor Cdt1. *Mol Cell,* 23**,** 709-21.

JIN, J., CARDOZO, T., LOVERING, R. C., ELLEDGE, S. J., PAGANO, M. & HARPER, J. W. 2004. Systematic analysis and nomenclature of mammalian F-box proteins. *Genes Dev,* 18**,** 2573-80.

JIN, J., LI, X., GYGI, S. P. & HARPER, J. W. 2007. Dual E1 activation systems for ubiquitin differentially regulate E2 enzyme charging. *Nature,* 447**,** 1135-8.

JIN, L., WILLIAMSON, A., BANERJEE, S., PHILIPP, I. & RAPE, M. 2008. Mechanism of ubiquitin-chain formation by the human anaphase-promoting complex. *Cell,* 133**,** 653-65.

JONES, J., WU, K., YANG, Y., GUERRERO, C., NILLEGODA, N., PAN, Z. Q. & HUANG, L. 2008. A targeted proteomic analysis of the ubiquitin-like modifier nedd8 and associated proteins. *J Proteome Res,* 7**,** 1274-87.

JONES, R. J., BALADANDAYUTHAPANI, V., NEELAPU, S., FAYAD, L. E., ROMAGUERA, J. E., WANG, M., SHARMA, R., YANG, D. & ORLOWSKI, R. Z. 2011. HDM-2 inhibition suppresses expression of ribonucleotide reductase subunit M2, and synergistically enhances gemcitabine-induced cytotoxicity in mantle cell lymphoma. *Blood,* 118**,** 4140-9.

JU, U. I., PARK, J. W., PARK, H. S., KIM, S. J. & CHUN, Y. S. 2015. FBXO11 represses cellular response to hypoxia by destabilizing hypoxia-inducible factor-1α mRNA. *Biochem Biophys Res Commun,* 464**,** 1008-1015.

KAMURA, T., MAENAKA, K., KOTOSHIBA, S., MATSUMOTO, M., KOHDA, D., CONAWAY, R. C., CONAWAY, J. W. & NAKAYAMA, K. I. 2004. VHL-box and SOCS-box domains determine binding specificity for Cul2-Rbx1 and Cul5-Rbx2 modules of ubiquitin ligases. *Genes Dev,* 18**,** 3055-65.

KANDASAMY, P., ZLOBEC, I., NYDEGGER, D. T., PUJOL-GIMÉNEZ, J., BHARDWAJ, R., SHIRASAWA, S., TSUNODA, T. & HEDIGER, M. A. 2021. Oncogenic KRAS mutations enhance amino acid uptake by colorectal cancer cells via the hippo signaling effector YAP1. *Mol Oncol,* 15**,** 2782-2800.

KANE, L. A., LAZAROU, M., FOGEL, A. I., LI, Y., YAMANO, K., SARRAF, S. A., BANERJEE, S. & YOULE, R. J. 2014. PINK1 phosphorylates ubiquitin to activate Parkin E3 ubiquitin ligase activity. *J Cell Biol,* 205**,** 143-53.

KANG, J. H., CHOI, M. Y., CUI, Y. H., KAUSHIK, N., UDDIN, N., YOO, K. C., KIM, M. J. & LEE, S. J. 2017. Regulation of FBXO4-mediated ICAM-1 protein stability in metastatic breast cancer. *Oncotarget,* 8**,** 83100-83113.

KEIJZERS, G., BAKULA, D., PETR, M. A., MADSEN, N. G. K., TEKLU, A., MKRTCHYAN, G., OSBORNE, B. & SCHEIBYE-KNUDSEN, M. 2018. Human Exonuclease 1 (EXO1) Regulatory Functions in DNA Replication with Putative Roles in Cancer. *Int J Mol Sci,* 20.

KENT, L. N. & LEONE, G. 2019. The broken cycle: E2F dysfunction in cancer. *Nat Rev Cancer,* 19**,** 326-338.

KIM, S. E., YOON, J. Y., JEONG, W. J., JEON, S. H., PARK, Y., YOON, J. B., PARK, Y. N., KIM, H. & CHOI, K. Y. 2009. H-Ras is degraded by Wnt/beta-catenin signaling via beta-TrCP-mediated polyubiquitylation. *J Cell Sci,* 122**,** 842-8.

KIPREOS, E. T., LANDER, L. E., WING, J. P., HE, W. W. & HEDGECOCK, E. M. 1996. cul-1 is required for cell cycle exit in C. elegans and identifies a novel gene family. *Cell,* 85**,** 829-39.

KLEIN, D. K., HOFFMANN, S., AHLSKOG, J. K., O'HANLON, K., QUAAS, M., LARSEN, B. D., ROLLAND, B., ROSNER, H. I., WALTER, D., KOUSHOLT, A. N., MENZEL, T., LEES, M., JOHANSEN, J. V., RAPPSILBER, J., ENGELAND, K. & SORENSEN, C. S. 2015a. Cyclin F suppresses B-Myb activity to promote cell cycle checkpoint control. *Nat Commun,* 6**,** 5800.

KLEIN, D. K., HOFFMANN, S., AHLSKOG, J. K., O'HANLON, K., QUAAS, M., LARSEN, B. D., ROLLAND, B., RÖSNER, H. I., WALTER, D., KOUSHOLT, A. N., MENZEL, T., LEES, M., JOHANSEN, J. V., RAPPSILBER, J., ENGELAND, K. & SØRENSEN, C. S. 2015b. Cyclin F suppresses B-Myb activity to promote cell cycle checkpoint control. *Nat Commun,* 6**,** 5800.

KOBAYASHI, A., KANG, M. I., OKAWA, H., OHTSUJI, M., ZENKE, Y., CHIBA, T., IGARASHI, K. & YAMAMOTO, M. 2004. Oxidative stress sensor Keap1 functions as an adaptor for Cul3-based E3 ligase to regulate proteasomal degradation of Nrf2. *Mol Cell Biol,* 24**,** 7130-9.

KOBAYASHI, A., KANG, M. I., WATAI, Y., TONG, K. I., SHIBATA, T., UCHIDA, K. & YAMAMOTO, M. 2006. Oxidative and electrophilic stresses activate Nrf2 through inhibition of ubiquitination activity of Keap1. *Mol Cell Biol,* 26**,** 221-9.

KÕIVOMÄGI, M., VALK, E., VENTA, R., IOFIK, A., LEPIKU, M., MORGAN, D. O. & LOOG, M. 2011. Dynamics of Cdk1 substrate specificity during the cell cycle. *Mol Cell,* 42**,** 610-23.

KOMANDER, D. & RAPE, M. 2012. The ubiquitin code. *Annu Rev Biochem,* 81**,** 203-29.

KONSTANTINOPOULOS, P. A., SPENTZOS, D., FOUNTZILAS, E., FRANCOEUR, N., SANISETTY, S., GRAMMATIKOS, A. P., HECHT, J. L. & CANNISTRA, S. A. 2011. Keap1 mutations and Nrf2 pathway activation in epithelial ovarian cancer. *Cancer Res,* 71**,** 5081-9.

KUCHAY, S., DUAN, S., SCHENKEIN, E., PESCHIAROLI, A., SARAF, A., FLORENS, L., WASHBURN, M. P. & PAGANO, M. 2013. FBXL2- and PTPL1-mediated degradation of p110-free p85β regulatory subunit controls the PI(3)K signalling cascade. *Nat Cell Biol,* 15**,** 472-80.

KULAK, N. A., PICHLER, G., PARON, I., NAGARAJ, N. & MANN, M. 2014. Minimal, encapsulated proteomic-sample processing applied to copy-number estimation in eukaryotic cells. *Nat Methods,* 11**,** 319-24.

KUNZ, B. A., KOHALMI, S. E., KUNKEL, T. A., MATHEWS, C. K., MCINTOSH, E. M. & REIDY, J. A. 1994. International Commission for Protection Against Environmental Mutagens and Carcinogens. Deoxyribonucleoside triphosphate levels: a critical factor in the maintenance of genetic stability. *Mutat Res,* 318**,** 1-64.

LAI, A. C., TOURE, M., HELLERSCHMIED, D., SALAMI, J., JAIME-FIGUEROA, S., KO, E., HINES, J. & CREWS, C. M. 2016. Modular PROTAC Design for the Degradation of Oncogenic BCR-ABL. *Angew Chem Int Ed Engl,* 55**,** 807-10.

LANDER, R., NORDIN, K. & LABONNE, C. 2011. The F-box protein Ppa is a common regulator of core EMT factors Twist, Snail, Slug, and Sip1. *J Cell Biol,* 194**,** 17-25.

LAU, H. W., MA, H. T., YEUNG, T. K., TAM, M. Y., ZHENG, D., CHU, S. K. & POON, R. Y. C. 2021. Quantitative differences between cyclin-dependent kinases underlie the unique functions of CDK1 in human cells. *Cell Rep,* 37**,** 109808.

LAVOIE, J. N., L'ALLEMAIN, G., BRUNET, A., MÜLLER, R. & POUYSSÉGUR, J. 1996. Cyclin D1 expression is regulated positively by the p42/p44MAPK and negatively by the p38/HOGMAPK pathway. *J Biol Chem,* 271**,** 20608-16.

LEE, M. G., WYNDER, C., COOCH, N. & SHIEKHATTAR, R. 2005. An essential role for CoREST in nucleosomal histone 3 lysine 4 demethylation. *Nature,* 437**,** 432-5.

LI, C., DU, L., REN, Y., LIU, X., JIAO, Q., CUI, D., WEN, M., WANG, C., WEI, G., WANG, Y., JI, A. & WANG, Q. 2019. SKP2 promotes breast cancer tumorigenesis and radiation tolerance through PDCD4 ubiquitination. *J Exp Clin Cancer Res,* 38**,** 76.

LI, L. Q., PAN, D., CHEN, H., ZHANG, L. & XIE, W. J. 2016. F-box protein FBXL2 inhibits gastric cancer proliferation by ubiquitin-mediated degradation of forkhead box M1. *FEBS Lett,* 590**,** 445-52.

LIAO, W., OVERMAN, M. J., BOUTIN, A. T., SHANG, X., ZHAO, D., DEY, P., LI, J., WANG, G., LAN, Z., LI, J., TANG, M., JIANG, S., MA, X., CHEN, P., KATKHUDA, R., KORPHAISARN, K., CHAKRAVARTI, D., CHANG, A., SPRING, D. J., CHANG, Q., ZHANG, J., MARU, D. M., MAEDA, D. Y., ZEBALA, J. A., KOPETZ, S., WANG, Y. A. & DEPINHO, R. A. 2019. KRAS-

IRF2 Axis Drives Immune Suppression and Immune Therapy Resistance in Colorectal Cancer. *Cancer Cell,* 35**,** 559-572.e7.

LIN, D. I., BARBASH, O., KUMAR, K. G., WEBER, J. D., HARPER, J. W., KLEIN-SZANTO, A. J., RUSTGI, A., FUCHS, S. Y. & DIEHL, J. A. 2006. Phosphorylation-dependent ubiquitination of cyclin D1 by the SCF(FBX4-alphaB crystallin) complex. *Mol Cell,* 24**,** 355-66.

LIPINSKI, C. A., LOMBARDO, F., DOMINY, B. W. & FEENEY, P. J. 2001. Experimental and computational approaches to estimate solubility and permeability in drug discovery and development settings. *Adv Drug Deliv Rev,* 46**,** 3-26.

LIU, C., LI, Y., SEMENOV, M., HAN, C., BAEG, G. H., TAN, Y., ZHANG, Z., LIN, X. & HE, X. 2002. Control of beta-catenin phosphorylation/degradation by a dual-kinase mechanism. *Cell,* 108**,** 837-47.

LIU, J., HAN, L., LI, B., YANG, J., HUEN, M. S., PAN, X., TSAO, S. W. & CHEUNG, A. L. 2014. F-box only protein 31 (FBXO31) negatively regulates p38 mitogen-activated protein kinase (MAPK) signaling by mediating lysine 48-linked ubiquitination and degradation of mitogen-activated protein kinase kinase 6 (MKK6). *J Biol Chem,* 289**,** 21508-18.

LIU, Y., LEAR, T., ZHAO, Y., ZHAO, J., ZOU, C., CHEN, B. B. & MALLAMPALLI, R. K. 2015. F-box protein Fbxl18 mediates polyubiquitylation and proteasomal degradation of the pro-apoptotic SCF subunit Fbxl7. *Cell Death Dis,* 6**,** e1630.

LIU, Y. C., PAN, J., ZHANG, C., FAN, W., COLLINGE, M., BENDER, J. R. & WEISSMAN, S. M. 1999. A MHC-encoded ubiquitin-like protein (FAT10) binds noncovalently to the spindle assembly checkpoint protein MAD2. *Proc Natl Acad Sci U S A,* 96**,** 4313-8.

LIU, Z., LIU, Y., QIAN, L., JIANG, S., GAI, X., YE, S., CHEN, Y., WANG, X., ZHAI, L., XU, J., PU, C., LI, J., HE, F., HUANG, M. & TAN, M. 2021. A proteomic and phosphoproteomic landscape of KRAS mutant cancers identifies combination therapies. *Mol Cell,* 81**,** 4076-4090.e8.

LU, J., QIAN, Y., ALTIERI, M., DONG, H., WANG, J., RAINA, K., HINES, J., WINKLER, J. D., CREW, A. P., COLEMAN, K. & CREWS, C. M. 2015a. Hijacking the E3 Ubiquitin Ligase Cereblon to Efficiently Target BRD4. *Chem Biol,* 22**,** 755-63.

LU, J., QIAN, Y., ALTIERI, M., DONG, H., WANG, J., RAINA, K., HINES, J., WINKLER, J. D., CREW, A. P., COLEMAN, K. & CREWS, C. M. 2015b. Hijacking the E3 Ubiquitin Ligase Cereblon to Efficiently Target BRD4. *Chem Biol,* 22**,** 755-63.

LU, K. P., FINN, G., LEE, T. H. & NICHOLSON, L. K. 2007. Prolyl cis-trans isomerization as a molecular timer. *Nat Chem Biol,* 3**,** 619-29.

LU, K. P. & ZHOU, X. Z. 2007. The prolyl isomerase PIN1: a pivotal new twist in phosphorylation signalling and disease. *Nat Rev Mol Cell Biol,* 8**,** 904-16.

LUKASIAK, S., SCHILLER, C., OEHLSCHLAEGER, P., SCHMIDTKE, G., KRAUSE, P., LEGLER, D. F., AUTSCHBACH, F., SCHIRMACHER, P., BREUHAHN, K. & GROETTRUP, M. 2008. Proinflammatory cytokines cause FAT10 upregulation in cancers of liver and colon. *Oncogene,* 27**,** 6068-74.

MA, J. L., KIM, E. M., HABER, J. E. & LEE, S. E. 2003. Yeast Mre11 and Rad1 proteins define a Ku-independent mechanism to repair double-strand breaks lacking overlapping end sequences. *Mol Cell Biol,* 23**,** 8820-8.

MAGITS, W. & SABLINA, A. A. 2022. The regulation of the protein interaction network by monoubiquitination. *Curr Opin Struct Biol,* 73**,** 102333.

MALONIA, S. K., DUTTA, P., SANTRA, M. K. & GREEN, M. R. 2015. F-box protein FBXO31 directs degradation of MDM2 to facilitate p53-mediated growth arrest following genotoxic stress. *Proc Natl Acad Sci U S A,* 112**,** 8632-7.

MAO, J. H., KIM, I. J., WU, D., CLIMENT, J., KANG, H. C., DELROSARIO, R. & BALMAIN, A. 2008. FBXW7 targets mTOR for degradation and cooperates with PTEN in tumor suppression. *Science,* 321**,** 1499-502.

MAO, Z., XIAO, H., SHEN, P., YANG, Y., XUE, J., YANG, Y., SHANG, Y., ZHANG, L., LI, X., ZHANG, Y., DU, Y., CHEN, C. C., GUO, R. T. & ZHANG, Y. 2022. KRAS(G12D) can be targeted by potent inhibitors via formation of salt bridge. *Cell Discov,* 8**,** 5.

MARDIS, E. R., DING, L., DOOLING, D. J., LARSON, D. E., MCLELLAN, M. D., CHEN, K., KOBOLDT, D. C., FULTON, R. S., DELEHAUNTY, K. D., MCGRATH, S. D., FULTON, L. A., LOCKE, D. P., MAGRINI, V. J., ABBOTT, R. M., VICKERY, T. L., REED, J. S., ROBINSON, J. S., WYLIE, T., SMITH, S. M., CARMICHAEL, L., ELDRED, J. M., HARRIS, C. C., WALKER, J., PECK, J. B., DU, F., DUKES, A. F., SANDERSON, G. E., BRUMMETT, A. M., CLARK, E., MCMICHAEL, J. F., MEYER, R. J., SCHINDLER, J. K., POHL, C. S., WALLIS, J. W., SHI, X., LIN, L., SCHMIDT, H., TANG, Y., HAIPEK, C., WIECHERT, M. E., IVY, J. V., KALICKI, J., ELLIOTT, G., RIES, R. E., PAYTON, J. E., WESTERVELT, P., TOMASSON, M. H., WATSON, M. A., BATY, J., HEATH, S., SHANNON, W. D., NAGARAJAN, R., LINK, D. C., WALTER, M. J., GRAUBERT, T. A., DIPERSIO, J. F., WILSON, R. K. & LEY, T. J. 2009. Recurring mutations found by sequencing an acute myeloid leukemia genome. *N Engl J Med,* 361**,** 1058-66.

MARGOTTIN-GOGUET, F., HSU, J. Y., LOKTEV, A., HSIEH, H. M., REIMANN, J. D. & JACKSON, P. K. 2003. Prophase destruction of Emi1 by the SCF(betaTrCP/Slimb) ubiquitin ligase activates the anaphase promoting complex to allow progression beyond prometaphase. *Dev Cell,* 4**,** 813-26.

MARÍN, I. 2009. Diversification of the cullin family. *BMC Evol Biol,* 9**,** 267.

MATHEWS, C. K. 2006. DNA precursor metabolism and genomic stability. *Faseb j,* 20**,** 1300-14.

MAVROMMATI, I., FAEDDA, R., GALASSO, G., LI, J., BURDOVA, K., FISCHER, R., KESSLER, B. M., CARRERO, Z. I., GUARDAVACCARO, D., PAGANO, M. & D'ANGIOLELLA, V. 2018. β-TrCP- and Casein Kinase II-Mediated Degradation of Cyclin F Controls Timely Mitotic Progression. *Cell Rep,* 24**,** 3404-3412.

MAXWELL, P. H., WIESENER, M. S., CHANG, G. W., CLIFFORD, S. C., VAUX, E. C., COCKMAN, M. E., WYKOFF, C. C., PUGH, C. W., MAHER, E. R. & RATCLIFFE, P. J. 1999. The tumour suppressor protein VHL targets hypoxia-inducible factors for oxygen-dependent proteolysis. *Nature,* 399**,** 271-5.

MENA, E. L., KJOLBY, R. A. S., SAXTON, R. A., WERNER, A., LEW, B. G., BOYLE, J. M., HARLAND, R. & RAPE, M. 2018. Dimerization quality control ensures neuronal development and survival. *Science,* 362.

MENG, X., LIU, X., GUO, X., JIANG, S., CHEN, T., HU, Z., LIU, H., BAI, Y., XUE, M., HU, R., SUN, S. C., LIU, X., ZHOU, P., HUANG, X., WEI, L., YANG, W. & XU, C. 2018. FBXO38 mediates PD-1 ubiquitination and regulates anti-tumour immunity of T cells. *Nature,* 564**,** 130-135.

MEYER, H. J. & RAPE, M. 2014. Enhanced protein degradation by branched ubiquitin chains. *Cell,* 157**,** 910-21.

MOELLER, B. J., CAO, Y., LI, C. Y. & DEWHIRST, M. W. 2004. Radiation activates HIF-1 to regulate vascular radiosensitivity in tumors: Role of reoxygenation, free radicals, and stress granules. *Cancer Cell,* 5**,** 429-441.

MOHANTY, P., CHATTERJEE, K. S. & DAS, R. 2021. NEDD8 Deamidation Inhibits Cullin RING Ligase Dynamics. *Front Immunol,* 12**,** 695331.

MOORE, A. R., ROSENBERG, S. C., MCCORMICK, F. & MALEK, S. 2020. RAS-targeted therapies: is the undruggable drugged? *Nat Rev Drug Discov,* 19**,** 533-552.

MORI, A., MASUDA, K., OHTSUKA, H., SHIJO, M., ARIAKE, K., FUKASE, K., SAKATA, N., MIZUMA, M., MORIKAWA, T., HAYASHI, H., NAKAGAWA, K., MOTOI, F., NAITOH, T., FUJISHIMA, F. & UNNO, M. 2018. FBXW7 modulates malignant potential and cisplatin-induced apoptosis in cholangiocarcinoma through NOTCH1 and MCL1. *Cancer Sci,* 109**,** 3883-3895.

MORIKAWA, T., HINO, R., UOZAKI, H., MAEDA, D., USHIKU, T., SHINOZAKI, A., SAKATANI, T. & FUKAYAMA, M. 2010. Expression of ribonucleotide reductase M2 subunit in gastric cancer and effects of RRM2 inhibition in vitro. *Hum Pathol,* 41**,** 1742-8.

MULLARD, A. 2021. Targeted protein degraders crowd into the clinic. *Nat Rev Drug Discov,* 20**,** 247-250.

MURUGAN, A. K., GRIECO, M. & TSUCHIDA, N. 2019. RAS mutations in human cancers: Roles in precision medicine. *Semin Cancer Biol*.

NATERI, A. S., RIERA-SANS, L., DA COSTA, C. & BEHRENS, A. 2004. The ubiquitin ligase SCFFbw7 antagonizes apoptotic JNK signaling. *Science,* 303**,** 1374-8.

NETWORK, C. G. A. R. 2012. Comprehensive molecular characterization of human colon and rectal cancer. *Nature,* 487**,** 330-7.

NETWORK, C. G. A. R. 2014. Comprehensive molecular profiling of lung adenocarcinoma. *Nature,* 511**,** 543-50.

NETWORK, C. G. A. R. 2017. Integrated Genomic Characterization of Pancreatic Ductal Adenocarcinoma. *Cancer Cell,* 32**,** 185-203.e13.

NGUYEN, K. M. & BUSINO, L. 2020. The Biology of F-box Proteins: The SCF Family of E3 Ubiquitin Ligases. *Adv Exp Med Biol,* 1217**,** 111-122.

NICASSIO, F., CORRADO, N., VISSERS, J. H., ARECES, L. B., BERGINK, S., MARTEIJN, J. A., GEVERTS, B., HOUTSMULLER, A. B., VERMEULEN, W., DI FIORE, P. P. & CITTERIO, E. 2007. Human USP3 is a chromatin modifier required for S phase progression and genome stability. *Curr Biol,* 17**,** 1972-7.

NICOLETTE, M. L., LEE, K., GUO, Z., RANI, M., CHOW, J. M., LEE, S. E. & PAULL, T. T. 2010. Mre11-Rad50-Xrs2 and Sae2 promote 5' strand resection of DNA double-strand breaks. *Nat Struct Mol Biol,* 17**,** 1478-85.

NORDLUND, P. & REICHARD, P. 2006. Ribonucleotide reductases. *Annu Rev Biochem,* 75**,** 681-706.

NORTHCOTT, P. A., BUCHHALTER, I., MORRISSY, A. S., HOVESTADT, V., WEISCHENFELDT, J., EHRENBERGER, T., GRÖBNER, S., SEGURA-WANG, M., ZICHNER, T., RUDNEVA, V. A., WARNATZ, H. J., SIDIROPOULOS, N., PHILLIPS, A. H., SCHUMACHER, S., KLEINHEINZ, K., WASZAK, S. M., ERKEK, S., JONES, D. T. W., WORST, B. C., KOOL, M., ZAPATKA, M., JÄGER, N., CHAVEZ, L., HUTTER, B., BIEG, M., PARAMASIVAM, N., HEINOLD, M., GU, Z., ISHAQUE, N., JÄGER-SCHMIDT, C., IMBUSCH, C. D., JUGOLD, A., HÜBSCHMANN, D., RISCH, T., AMSTISLAVSKIY, V., GONZALEZ, F. G. R., WEBER, U. D., WOLF, S., ROBINSON, G. W., ZHOU, X., WU, G., FINKELSTEIN, D., LIU, Y., CAVALLI, F. M. G., LUU, B., RAMASWAMY, V., WU, X., KOSTER, J., RYZHOVA, M., CHO, Y. J., POMEROY, S. L., HEROLD-MENDE, C., SCHUHMANN, M., EBINGER, M., LIAU, L. M., MORA, J., MCLENDON, R. E., JABADO, N., KUMABE, T., CHUAH, E., MA, Y., MOORE, R. A., MUNGALL, A. J., MUNGALL, K. L., THIESSEN, N., TSE, K., WONG, T., JONES, S. J. M., WITT, O., MILDE, T., VON DEIMLING, A., CAPPER, D., KORSHUNOV, A., YASPO, M. L., KRIWACKI, R., GAJJAR, A., ZHANG, J., BEROUKHIM, R., FRAENKEL, E., KORBEL, J. O., BRORS, B., SCHLESNER, M., EILS, R., MARRA, M. A., PFISTER, S. M., TAYLOR, M. D. & LICHTER, P. 2017. The whole-genome landscape of medulloblastoma subtypes. *Nature,* 547**,** 311-317.

OHTA, T., IIJIMA, K., MIYAMOTO, M., NAKAHARA, I., TANAKA, H., OHTSUJI, M., SUZUKI, T., KOBAYASHI, A., YOKOTA, J., SAKIYAMA, T., SHIBATA, T., YAMAMOTO, M. & HIROHASHI, S. 2008. Loss of Keap1 function activates Nrf2 and provides advantages for lung cancer cell growth. *Cancer Res,* 68**,** 1303-9.

OHTA, T., MICHEL, J. J., SCHOTTELIUS, A. J. & XIONG, Y. 1999. ROC1, a homolog of APC11, represents a family of cullin partners with an associated ubiquitin ligase activity. *Mol Cell,* 3**,** 535-41.

OHTAKE, F., SAEKI, Y., ISHIDO, S., KANNO, J. & TANAKA, K. 2016. The K48-K63 Branched Ubiquitin Chain Regulates NF-κB Signaling. *Mol Cell,* 64**,** 251-266.

OHTAKE, F., SAEKI, Y., SAKAMOTO, K., OHTAKE, K., NISHIKAWA, H., TSUCHIYA, H., OHTA, T., TANAKA, K. & KANNO, J. 2015. Ubiquitin acetylation inhibits polyubiquitin chain elongation. *EMBO Rep,* 16**,** 192-201.

OLSON, C. M., JIANG, B., ERB, M. A., LIANG, Y., DOCTOR, Z. M., ZHANG, Z., ZHANG, T., KWIATKOWSKI, N., BOUKHALI, M., GREEN, J. L., HAAS, W., NOMANBHOY, T., FISCHER, E. S., YOUNG, R. A., BRADNER, J. E., WINTER, G. E. & GRAY, N. S. 2018. Pharmacological perturbation of CDK9 using selective CDK9 inhibition or degradation. *Nat Chem Biol,* 14**,** 163-170.

ÖRD, M., PUSS, K. K., KIVI, R., MÖLL, K., OJALA, T., BOROVKO, I., FAUSTOVA, I., VENTA, R., VALK, E., KÕIVOMÄGI, M. & LOOG, M. 2020. Proline-Rich Motifs Control G2-CDK Target Phosphorylation and Priming an Anchoring Protein for Polo Kinase Localization. *Cell Rep,* 31**,** 107757.

ÖRD, M., VENTA, R., MÖLL, K., VALK, E. & LOOG, M. 2019. Cyclin-Specific Docking Mechanisms Reveal the Complexity of M-CDK Function in the Cell Cycle. *Mol Cell,* 75**,** 76-89.e3.

OSTREM, J. M., PETERS, U., SOS, M. L., WELLS, J. A. & SHOKAT, K. M. 2013. K-Ras(G12C) inhibitors allosterically control GTP affinity and effector interactions. *Nature,* 503**,** 548-51.

OSTROM, Q. T., CIOFFI, G., GITTLEMAN, H., PATIL, N., WAITE, K., KRUCHKO, C. & BARNHOLTZ-SLOAN, J. S. 2019. CBTRUS Statistical Report: Primary Brain and Other Central Nervous System Tumors Diagnosed in the United States in 2012-2016. *Neuro Oncol,* 21**,** v1-v100.

OSTROM, Q. T., PRICE, M., NEFF, C., CIOFFI, G., WAITE, K. A., KRUCHKO, C. & BARNHOLTZ-SLOAN, J. S. 2022. CBTRUS Statistical Report: Primary Brain and Other Central Nervous System Tumors Diagnosed in the United States in 2015-2019. *Neuro Oncol,* 24**,** v1-v95.

OUCHI, M. & OUCHI, T. 2010. Regulation of ATM/DNA-PKcs Phosphorylation by BRCA1-Associated BAAT1. *Genes Cancer,* 1**,** 1211-4.

PAO, K. C., WOOD, N. T., KNEBEL, A., RAFIE, K., STANLEY, M., MABBITT, P. D., SUNDARAMOORTHY, R., HOFMANN, K., VAN AALTEN, D. M. F. & VIRDEE, S. 2018. Activity-based E3 ligase profiling uncovers an E3 ligase with esterification activity. *Nature,* 556**,** 381-385.

PAO, W., WANG, T. Y., RIELY, G. J., MILLER, V. A., PAN, Q., LADANYI, M., ZAKOWSKI, M. F., HEELAN, R. T., KRIS, M. G. & VARMUS, H. E. 2005. KRAS mutations and primary resistance of lung adenocarcinomas to gefitinib or erlotinib. *PLoS Med,* 2**,** e17.

PARKER, L. L. & PIWNICA-WORMS, H. 1992. Inactivation of the p34cdc2-cyclin B complex by the human WEE1 tyrosine kinase. *Science,* 257**,** 1955-7.

PETERMANN, E., WOODCOCK, M. & HELLEDAY, T. 2010. Chk1 promotes replication fork progression by controlling replication initiation. *Proc Natl Acad Sci U S A,* 107**,** 16090-5.

PIERCE, N. W., LEE, J. E., LIU, X., SWEREDOSKI, M. J., GRAHAM, R. L., LARIMORE, E. A., ROME, M., ZHENG, N., CLURMAN, B. E., HESS, S., SHAN, S. O. & DESHAIES, R. J. 2013. Cand1 promotes assembly of new SCF complexes through dynamic exchange of F box proteins. *Cell,* 153**,** 206-15.

PINTARD, L., WILLEMS, A. & PETER, M. 2004. Cullin-based ubiquitin ligases: Cul3-BTB complexes join the family. *Embo j,* 23**,** 1681-7.

POLAGER, S. & GINSBERG, D. 2008. E2F - at the crossroads of life and death. *Trends Cell Biol,* 18**,** 528-35.

POPOV, N., SCHÜLEIN, C., JAENICKE, L. A. & EILERS, M. 2010. Ubiquitylation of the amino terminus of Myc by SCF(β-TrCP) antagonizes SCF(Fbw7)-mediated turnover. *Nat Cell Biol,* 12**,** 973-81.

PRIOR, I. A., HOOD, F. E. & HARTLEY, J. L. 2020. The Frequency of Ras Mutations in Cancer. *Cancer Res,* 80**,** 2969-2974.

PRUNEDA, J. N., LITTLEFIELD, P. J., SOSS, S. E., NORDQUIST, K. A., CHAZIN, W. J., BRZOVIC, P. S. & KLEVIT, R. E. 2012. Structure of an E3:E2~Ub complex reveals an allosteric mechanism shared among RING/U-box ligases. *Mol Cell,* 47**,** 933-42.

PRUNEDA, J. N., STOLL, K. E., BOLTON, L. J., BRZOVIC, P. S. & KLEVIT, R. E. 2011. Ubiquitin in motion: structural studies of the ubiquitin-conjugating enzyme∼ubiquitin conjugate. *Biochemistry,* 50**,** 1624-33.

RADA, P., ROJO, A. I., CHOWDHRY, S., MCMAHON, M., HAYES, J. D. & CUADRADO, A. 2011. SCF/{beta}-TrCP promotes glycogen synthase kinase 3-dependent degradation of the Nrf2 transcription factor in a Keap1-independent manner. *Mol Cell Biol,* 31**,** 1121-33.

RADUCU, M., FUNG, E., SERRES, S., INFANTE, P., BARBERIS, A., FISCHER, R., BRISTOW, C., THÉZÉNAS, M. L., FINTA, C., CHRISTIANSON, J. C., BUFFA, F. M., KESSLER, B. M., SIBSON, N. R., DI MARCOTULLIO, L., TOFTGÅRD, R. & D'ANGIOLELLA, V. 2016. SCF (Fbxl17) ubiquitylation of Sufu regulates Hedgehog signaling and medulloblastoma development. *Embo j,* 35**,** 1400-16.

RAPE, M. 2018. Ubiquitylation at the crossroads of development and disease. *Nat Rev Mol Cell Biol,* 19**,** 59-70.

REITSMA, J. M., LIU, X., REICHERMEIER, K. M., MORADIAN, A., SWEREDOSKI, M. J., HESS, S. & DESHAIES, R. J. 2017. Composition and Regulation of the Cellular Repertoire of SCF Ubiquitin Ligases. *Cell,* 171**,** 1326-1339.e14.

REMY, G., RISCO, A. M., IÑESTA-VAQUERA, F. A., GONZÁLEZ-TERÁN, B., SABIO, G., DAVIS, R. J. & CUENDA, A. 2010. Differential activation of p38MAPK isoforms by MKK6 and MKK3. *Cell Signal,* 22**,** 660-7.

REYES-TURCU, F. E., VENTII, K. H. & WILKINSON, K. D. 2009. Regulation and cellular roles of ubiquitin-specific deubiquitinating enzymes. *Annu Rev Biochem,* 78**,** 363-97.

RIPLEY, B. M., GILDENBERG, M. S. & WASHINGTON, M. T. 2020. Control of DNA Damage Bypass by Ubiquitylation of PCNA. *Genes (Basel),* 11.

RIVERA, A. L., PELLOSKI, C. E., GILBERT, M. R., COLMAN, H., DE LA CRUZ, C., SULMAN, E. P., BEKELE, B. N. & ALDAPE, K. D. 2010. MGMT promoter methylation is predictive of response to radiotherapy and prognostic in the absence of adjuvant alkylating chemotherapy for glioblastoma. *Neuro Oncol,* 12**,** 116-21.

ROCK, K. L., GRAMM, C., ROTHSTEIN, L., CLARK, K., STEIN, R., DICK, L., HWANG, D. & GOLDBERG, A. L. 1994. Inhibitors of the proteasome block the degradation of most cell proteins and the generation of peptides presented on MHC class I molecules. *Cell,* 78**,** 761-71.

RODRIGUEZ-ACEBES, S., MOURON, S. & MENDEZ, J. 2018. Uncoupling fork speed and origin activity to identify the primary cause of replicative stress phenotypes. *J Biol Chem,* 293**,** 12855-12861.

ROSSI, M., DUAN, S., JEONG, Y. T., HORN, M., SARAF, A., FLORENS, L., WASHBURN, M. P., ANTEBI, A. & PAGANO, M. 2013. Regulation of the CRL4(Cdt2) ubiquitin ligase and cell-cycle exit by the SCF(Fbxo11) ubiquitin ligase. *Mol Cell,* 49**,** 1159-66.

ROTIN, D. & KUMAR, S. 2009. Physiological functions of the HECT family of ubiquitin ligases. *Nature Reviews Molecular Cell Biology,* 10**,** 398.

SAHA, A., LEWIS, S., KLEIGER, G., KUHLMAN, B. & DESHAIES, R. J. 2011. Essential role for ubiquitin-ubiquitin-conjugating enzyme interaction in ubiquitin discharge from Cdc34 to substrate. *Mol Cell,* 42**,** 75-83.

SAKAMOTO, K. M., KIM, K. B., KUMAGAI, A., MERCURIO, F., CREWS, C. M. & DESHAIES, R. J. 2001. Protacs: chimeric molecules that target proteins to the Skp1-Cullin-F box complex for ubiquitination and degradation. *Proc Natl Acad Sci U S A,* 98**,** 8554-9.

SANTRA, M. K., WAJAPEYEE, N. & GREEN, M. R. 2009. F-box protein FBXO31 mediates cyclin D1 degradation to induce G1 arrest after DNA damage. *Nature,* 459**,** 722-5.
SARBASSOV, D. D., GUERTIN, D. A., ALI, S. M. & SABATINI, D. M. 2005. Phosphorylation and regulation of Akt/PKB by the rictor-mTOR complex. *Science,* 307**,** 1098-101.
SARIKAS, A., HARTMANN, T. & PAN, Z. Q. 2011. The cullin protein family. *Genome Biol,* 12**,** 220.
SASSO, J. M., TENCHOV, R., WANG, D., JOHNSON, L. S., WANG, X. & ZHOU, Q. A. 2022. Molecular Glues: The Adhesive Connecting Targeted Protein Degradation to the Clinic. *Biochemistry*.
SCHREMPF, A., SLYSKOVA, J. & LOIZOU, J. I. 2021. Targeting the DNA Repair Enzyme Polymerase θ in Cancer Therapy. *Trends Cancer,* 7**,** 98-111.
SCHULMAN, B. A., LINDSTROM, D. L. & HARLOW, E. 1998. Substrate recruitment to cyclin-dependent kinase 2 by a multipurpose docking site on cyclin A. *Proc Natl Acad Sci U S A,* 95**,** 10453-8.
SELVADURAI, H. J., LUIS, E., DESAI, K., LAN, X., VLADOIU, M. C., WHITLEY, O., GALVIN, C., VANNER, R. J., LEE, L., WHETSTONE, H., KUSHIDA, M., NOWAKOWSKI, T., DIAMANDIS, P., HAWKINS, C., BADER, G., KRIEGSTEIN, A., TAYLOR, M. D. & DIRKS, P. B. 2020. Medulloblastoma Arises from the Persistence of a Rare and Transient Sox2(+) Granule Neuron Precursor. *Cell Rep,* 31**,** 107511.
SEMENZA, G. L. 1999. Regulation of Mammalian O2 Homeostasis by Hypoxia-Inducible Factor 1. *Annu Rev Cell Dev Biol,* 15**,** 551-578.
SEMENZA, G. L. 2003. Targeting HIF-1 for cancer therapy. *Nat Rev Cancer,* 3**,** 721-32.
SHAH, K. N., BHATT, R., ROTOW, J., ROHRBERG, J., OLIVAS, V., WANG, V. E., HEMMATI, G., MARTINS, M. M., MAYNARD, A., KUHN, J., GALEAS, J., DONNELLA, H. J., KAUSHIK, S., KU, A., DUMONT, S., KRINGS, G., HARINGSMA, H. J., ROBILLARD, L., SIMMONS, A. D., HARDING, T. C., MCCORMICK, F., GOGA, A., BLAKELY, C. M., BIVONA, T. G. & BANDYOPADHYAY, S. 2019. Aurora kinase A drives the evolution of resistance to third-generation EGFR inhibitors in lung cancer. *Nat Med,* 25**,** 111-118.
SHI, Y., LAN, F., MATSON, C., MULLIGAN, P., WHETSTINE, J. R., COLE, P. A., CASERO, R. A. & SHI, Y. 2004. Histone demethylation mediated by the nuclear amine oxidase homolog LSD1. *Cell,* 119**,** 941-53.
SHIBATA, T., KOKUBU, A., GOTOH, M., OJIMA, H., OHTA, T., YAMAMOTO, M. & HIROHASHI, S. 2008. Genetic alteration of Keap1 confers constitutive Nrf2 activation and resistance to chemotherapy in gallbladder cancer. *Gastroenterology,* 135**,** 1358-1368, 1368.e1-4.
SHIBATA, T., KOKUBU, A., SAITO, S., NARISAWA-SAITO, M., SASAKI, H., AOYAGI, K., YOSHIMATSU, Y., TACHIMORI, Y., KUSHIMA, R., KIYONO, T. & YAMAMOTO, M. 2011. NRF2 mutation confers malignant potential and resistance to chemoradiation therapy in advanced esophageal squamous cancer. *Neoplasia,* 13**,** 864-73.
SIDDIQUI, A. D. & PIPERDI, B. 2010. KRAS mutation in colon cancer: a marker of resistance to EGFR-I therapy. *Ann Surg Oncol,* 17**,** 1168-76.
SIEPKA, S. M., YOO, S. H., PARK, J., SONG, W., KUMAR, V., HU, Y., LEE, C. & TAKAHASHI, J. S. 2007. Circadian mutant Overtime reveals F-box protein FBXL3 regulation of cryptochrome and period gene expression. *Cell,* 129**,** 1011-23.
SIMANSHU, D. K., NISSLEY, D. V. & MCCORMICK, F. 2017. RAS Proteins and Their Regulators in Human Disease. *Cell,* 170**,** 17-33.
SINGH, A., MISRA, V., THIMMULAPPA, R. K., LEE, H., AMES, S., HOQUE, M. O., HERMAN, J. G., BAYLIN, S. B., SIDRANSKY, D., GABRIELSON, E., BROCK, M. V. & BISWAL, S. 2006. Dysfunctional KEAP1-NRF2 interaction in non-small-cell lung cancer. *PLoS Med,* 3**,** e420.
SKAAR, J. R., PAGAN, J. K. & PAGANO, M. 2013. Mechanisms and function of substrate recruitment by F-box proteins. *Nat Rev Mol Cell Biol,* 14**,** 369-81.

SMITH, T. F., GAITATZES, C., SAXENA, K. & NEER, E. J. 1999. The WD repeat: a common architecture for diverse functions. *Trends Biochem Sci,* 24**,** 181-5.

SO, E. Y. & OUCHI, T. 2011. Functional interaction of BRCA1/ATM-associated BAAT1 with the DNA-PK catalytic subunit. *Exp Ther Med,* 2**,** 443-447.

SONI, A., SIEMANN, M., GRABOS, M., MURMANN, T., PANTELIAS, G. E. & ILIAKIS, G. 2014. Requirement for Parp-1 and DNA ligases 1 or 3 but not of Xrcc1 in chromosomal translocation formation by backup end joining. *Nucleic Acids Res,* 42**,** 6380-92.

SØRENSEN, C. S., SYLJUÅSEN, R. G., FALCK, J., SCHROEDER, T., RÖNNSTRAND, L., KHANNA, K. K., ZHOU, B. B., BARTEK, J. & LUKAS, J. 2003. Chk1 regulates the S phase checkpoint by coupling the physiological turnover and ionizing radiation-induced accelerated proteolysis of Cdc25A. *Cancer Cell,* 3**,** 247-58.

SOUCY, T. A., SMITH, P. G., MILHOLLEN, M. A., BERGER, A. J., GAVIN, J. M., ADHIKARI, S., BROWNELL, J. E., BURKE, K. E., CARDIN, D. P., CRITCHLEY, S., CULLIS, C. A., DOUCETTE, A., GARNSEY, J. J., GAULIN, J. L., GERSHMAN, R. E., LUBLINSKY, A. R., MCDONALD, A., MIZUTANI, H., NARAYANAN, U., OLHAVA, E. J., PELUSO, S., REZAEI, M., SINTCHAK, M. D., TALREJA, T., THOMAS, M. P., TRAORE, T., VYSKOCIL, S., WEATHERHEAD, G. S., YU, J., ZHANG, J., DICK, L. R., CLAIBORNE, C. F., ROLFE, M., BOLEN, J. B. & LANGSTON, S. P. 2009. An inhibitor of NEDD8-activating enzyme as a new approach to treat cancer. *Nature,* 458**,** 732-6.

SPRATT, D. E., WALDEN, H. & SHAW, G. S. 2014. RBR E3 ubiquitin ligases: new structures, new insights, new questions. *The Biochemical journal,* 458**,** 421-437.

SPRATT, D. E., WU, K., KOVACEV, J., PAN, Z. Q. & SHAW, G. S. 2012. Selective recruitment of an E2~ubiquitin complex by an E3 ubiquitin ligase. *J Biol Chem,* 287**,** 17374-17385.

SPRUCK, C., STROHMAIER, H., WATSON, M., SMITH, A. P., RYAN, A., KREK, T. W. & REED, S. I. 2001. A CDK-independent function of mammalian Cks1: targeting of SCF(Skp2) to the CDK inhibitor p27Kip1. *Mol Cell,* 7**,** 639-50.

STEKLOV, M., PANDOLFI, S., BAIETTI, M. F., BATIUK, A., CARAI, P., NAJM, P., ZHANG, M., JANG, H., RENZI, F., CAI, Y., ABBASI ASBAGH, L., PASTOR, T., DE TROYER, M., SIMICEK, M., RADAELLI, E., BREMS, H., LEGIUS, E., TAVERNIER, J., GEVAERT, K., IMPENS, F., MESSIAEN, L., NUSSINOV, R., HEYMANS, S., EYCKERMAN, S. & SABLINA, A. A. 2018. Mutations in LZTR1 drive human disease by dysregulating RAS ubiquitination. *Science,* 362**,** 1177-1182.

STENGEL, K. R., THANGAVEL, C., SOLOMON, D. A., ANGUS, S. P., ZHENG, Y. & KNUDSEN, E. S. 2009. Retinoblastoma/p107/p130 pocket proteins: protein dynamics and interactions with target gene promoters. *J Biol Chem,* 284**,** 19265-71.

STERN, B. & NURSE, P. 1996. A quantitative model for the cdc2 control of S phase and mitosis in fission yeast. *Trends Genet,* 12**,** 345-50.

STEWART, G. S., PANIER, S., TOWNSEND, K., AL-HAKIM, A. K., KOLAS, N. K., MILLER, E. S., NAKADA, S., YLANKO, J., OLIVARIUS, S., MENDEZ, M., OLDREIVE, C., WILDENHAIN, J., TAGLIAFERRO, A., PELLETIER, L., TAUBENHEIM, N., DURANDY, A., BYRD, P. J., STANKOVIC, T., TAYLOR, A. M. & DUROCHER, D. 2009. The RIDDLE syndrome protein mediates a ubiquitin-dependent signaling cascade at sites of DNA damage. *Cell,* 136**,** 420-34.

STEWART, M. D., RITTERHOFF, T., KLEVIT, R. E. & BRZOVIC, P. S. 2016. E2 enzymes: more than just middle men. *Cell Res,* 26**,** 423-40.

STOGIOS, P. J., DOWNS, G. S., JAUHAL, J. J., NANDRA, S. K. & PRIVÉ, G. G. 2005. Sequence and structural analysis of BTB domain proteins. *Genome Biol,* 6**,** R82.

STROHMAIER, H., SPRUCK, C. H., KAISER, P., WON, K. A., SANGFELT, O. & REED, S. I. 2001. Human F-box protein hCdc4 targets cyclin E for proteolysis and is mutated in a breast cancer cell line. *Nature,* 413**,** 316-22.

STUPP, R., MASON, W. P., VAN DEN BENT, M. J., WELLER, M., FISHER, B., TAPHOORN, M. J., BELANGER, K., BRANDES, A. A., MAROSI, C., BOGDAHN, U., CURSCHMANN, J., JANZER, R. C., LUDWIN, S. K., GORLIA, T., ALLGEIER, A., LACOMBE, D., CAIRNCROSS, J. G., EISENHAUER, E. & MIRIMANOFF, R. O. 2005. Radiotherapy plus concomitant and adjuvant temozolomide for glioblastoma. *N Engl J Med,* 352**,** 987-96.

TAKEDA, D. Y., WOHLSCHLEGEL, J. A. & DUTTA, A. 2001. A bipartite substrate recognition motif for cyclin-dependent kinases. *J Biol Chem,* 276**,** 1993-7.

TAN, M. K., LIM, H. J., BENNETT, E. J., SHI, Y. & HARPER, J. W. 2013. Parallel SCF adaptor capture proteomics reveals a role for SCFFBXL17 in NRF2 activation via BACH1 repressor turnover. *Mol Cell,* 52**,** 9-24.

TEKCHAM, D. S., CHEN, D., LIU, Y., LING, T., ZHANG, Y., CHEN, H., WANG, W., OTKUR, W., QI, H., XIA, T., LIU, X., PIAO, H. L. & LIU, H. 2020. F-box proteins and cancer: an update from functional and regulatory mechanism to therapeutic clinical prospects. *Theranostics,* 10**,** 4150-4167.

TOMIMATSU, N., MUKHERJEE, B., HARRIS, J. L., BOFFO, F. L., HARDEBECK, M. C., POTTS, P. R., KHANNA, K. K. & BURMA, S. 2017. DNA-damage-induced degradation of EXO1 exonuclease limits DNA end resection to ensure accurate DNA repair. *J Biol Chem,* 292**,** 10779-10790.

TONG, K. I., KOBAYASHI, A., KATSUOKA, F. & YAMAMOTO, M. 2006. Two-site substrate recognition model for the Keap1-Nrf2 system: a hinge and latch mechanism. *Biol Chem,* 387**,** 1311-20.

TOURE, M. & CREWS, C. M. 2016. Small-Molecule PROTACS: New Approaches to Protein Degradation. *Angew Chem Int Ed Engl,* 55**,** 1966-73.

TRENNER, A. & SARTORI, A. A. 2019. Harnessing DNA Double-Strand Break Repair for Cancer Treatment. *Front Oncol,* 9**,** 1388.

UDESHI, N. D., MANI, D. C., SATPATHY, S., FERESHETIAN, S., GASSER, J. A., SVINKINA, T., OLIVE, M. E., EBERT, B. L., MERTINS, P. & CARR, S. A. 2020. Rapid and deep-scale ubiquitylation profiling for biology and translational research. *Nat Commun,* 11**,** 359.

UNK, I., HAJDÚ, I., FÁTYOL, K., HURWITZ, J., YOON, J. H., PRAKASH, L., PRAKASH, S. & HARACSKA, L. 2008. Human HLTF functions as a ubiquitin ligase for proliferating cell nuclear antigen polyubiquitination. *Proc Natl Acad Sci U S A,* 105**,** 3768-73.

VAN RECHEM, C., BLACK, J. C., ABBAS, T., ALLEN, A., RINEHART, C. A., YUAN, G. C., DUTTA, A. & WHETSTINE, J. R. 2011. The SKP1-Cul1-F-box and leucine-rich repeat protein 4 (SCF-FbxL4) ubiquitin ligase regulates lysine demethylase 4A (KDM4A)/Jumonji domain-containing 2A (JMJD2A) protein. *J Biol Chem,* 286**,** 30462-30470.

VARSHAVSKY, A. 1991. Naming a targeting signal. *Cell,* 64**,** 13-5.

VENABLE, J. D., DONG, M. Q., WOHLSCHLEGEL, J., DILLIN, A. & YATES, J. R. 2004. Automated approach for quantitative analysis of complex peptide mixtures from tandem mass spectra. *Nat Methods,* 1**,** 39-45.

VIÑAS-CASTELLS, R., BELTRAN, M., VALLS, G., GÓMEZ, I., GARCÍA, J. M., MONTSERRAT-SENTÍS, B., BAULIDA, J., BONILLA, F., DE HERREROS, A. G. & DÍAZ, V. M. 2010. The hypoxia-controlled FBXL14 ubiquitin ligase targets SNAIL1 for proteasome degradation. *J Biol Chem,* 285**,** 3794-3805.

VIÑAS-CASTELLS, R., FRÍAS, Á., ROBLES-LANUZA, E., ZHANG, K., LONGMORE, G. D., GARCÍA DE HERREROS, A. & DÍAZ, V. M. 2014. Nuclear ubiquitination by FBXL5 modulates Snail1 DNA binding and stability. *Nucleic Acids Res,* 42**,** 1079-94.

VON DER LEHR, N., JOHANSSON, S., WU, S., BAHRAM, F., CASTELL, A., CETINKAYA, C., HYDBRING, P., WEIDUNG, I., NAKAYAMA, K., NAKAYAMA, K. I., SÖDERBERG, O., KERPPOLA, T. K. & LARSSON, L. G. 2003. The F-box protein Skp2 participates in c-Myc proteosomal degradation and acts as a cofactor for c-Myc-regulated transcription. *Mol Cell,* 11**,** 1189-200.

VON WILLEBRAND, M., ZACKSENHAUS, E., CHENG, E., GLAZER, P. & HALABAN, R. 2003. The tyrphostin AG1024 accelerates the degradation of phosphorylated forms of retinoblastoma protein (pRb) and restores pRb tumor suppressive function in melanoma cells. *Cancer Res,* 63**,** 1420-9.

WALTER, D., HOFFMANN, S., KOMSELI, E. S., RAPPSILBER, J., GORGOULIS, V. & SORENSEN, C. S. 2016. SCF(Cyclin F)-dependent degradation of CDC6 suppresses DNA re-replication. *Nat Commun,* 7**,** 10530.

WARD, P. S., PATEL, J., WISE, D. R., ABDEL-WAHAB, O., BENNETT, B. D., COLLER, H. A., CROSS, J. R., FANTIN, V. R., HEDVAT, C. V., PERL, A. E., RABINOWITZ, J. D., CARROLL, M., SU, S. M., SHARP, K. A., LEVINE, R. L. & THOMPSON, C. B. 2010. The common feature of leukemia-associated IDH1 and IDH2 mutations is a neomorphic enzyme activity converting alpha-ketoglutarate to 2-hydroxyglutarate. *Cancer Cell,* 17**,** 225-34.

WATANABE, N., ARAI, H., NISHIHARA, Y., TANIGUCHI, M., WATANABE, N., HUNTER, T. & OSADA, H. 2004. M-phase kinases induce phospho-dependent ubiquitination of somatic Wee1 by SCFbeta-TrCP. *Proc Natl Acad Sci U S A,* 101**,** 4419-24.

WATANABE, N., BROOME, M. & HUNTER, T. 1995. Regulation of the human WEE1Hu CDK tyrosine 15-kinase during the cell cycle. *Embo j,* 14**,** 1878-91.

WEI, J., MIALKI, R. K., DONG, S., KHOO, A., MALLAMPALLI, R. K., ZHAO, Y. & ZHAO, J. 2013. A new mechanism of RhoA ubiquitination and degradation: roles of SCF(FBXL19) E3 ligase and Erk2. *Biochim Biophys Acta,* 1833**,** 2757-2764.

WELCKER, M. & CLURMAN, B. E. 2008. FBW7 ubiquitin ligase: a tumour suppressor at the crossroads of cell division, growth and differentiation. *Nat Rev Cancer,* 8**,** 83-93.

WENZEL, D. M., LISSOUNOV, A., BRZOVIC, P. S. & KLEVIT, R. E. 2011. UBCH7 reactivity profile reveals parkin and HHARI to be RING/HECT hybrids. *Nature,* 474**,** 105-108.

WICK, W., WELLER, M., VAN DEN BENT, M., SANSON, M., WEILER, M., VON DEIMLING, A., PLASS, C., HEGI, M., PLATTEN, M. & REIFENBERGER, G. 2014. MGMT testing--the challenges for biomarker-based glioma treatment. *Nat Rev Neurol,* 10**,** 372-85.

WILLIAMSON, A., WICKLIFFE, K. E., MELLONE, B. G., SONG, L., KARPEN, G. H. & RAPE, M. 2009. Identification of a physiological E2 module for the human anaphase-promoting complex. *Proc Natl Acad Sci U S A,* 106**,** 18213-8.

WINSTON, J. T., KOEPP, D. M., ZHU, C., ELLEDGE, S. J. & HARPER, J. W. 1999a. A family of mammalian F-box proteins. *Curr Biol,* 9**,** 1180-2.

WINSTON, J. T., STRACK, P., BEER-ROMERO, P., CHU, C. Y., ELLEDGE, S. J. & HARPER, J. W. 1999b. The SCFbeta-TRCP-ubiquitin ligase complex associates specifically with phosphorylated destruction motifs in IkappaBalpha and beta-catenin and stimulates IkappaBalpha ubiquitination in vitro. *Genes Dev,* 13**,** 270-83.

WINTER, G. E., BUCKLEY, D. L., PAULK, J., ROBERTS, J. M., SOUZA, A., DHE-PAGANON, S. & BRADNER, J. E. 2015. DRUG DEVELOPMENT. Phthalimide conjugation as a strategy for in vivo target protein degradation. *Science,* 348**,** 1376-81.

WITKIEWICZ, A. K., CHUNG, S., BROUGH, R., VAIL, P., FRANCO, J., LORD, C. J. & KNUDSEN, E. S. 2018. Targeting the Vulnerability of RB Tumor Suppressor Loss in Triple-Negative Breast Cancer. *Cell Rep,* 22**,** 1185-1199.

WONG, G. C., LI, K. K., WANG, W. W., LIU, A. P., HUANG, Q. J., CHAN, A. K., POON, M. F., CHUNG, N. Y., WONG, Q. H., CHEN, H., CHAN, D. T. M., LIU, X. Z., MAO, Y., ZHANG, Z. Y., SHI, Z. F. & NG, H. K. 2020. Clinical and mutational profiles of adult medulloblastoma groups. *Acta Neuropathol Commun,* 8**,** 191.

WU, L., BACHRATI, C. Z., OU, J., XU, C., YIN, J., CHANG, M., WANG, W., LI, L., BROWN, G. W. & HICKSON, I. D. 2006. BLAP75/RMI1 promotes the BLM-dependent dissolution of homologous recombination intermediates. *Proc Natl Acad Sci U S A,* 103**,** 4068-73.

WU, T., MERBL, Y., HUO, Y., GALLOP, J. L., TZUR, A. & KIRSCHNER, M. W. 2010. UBE2S drives elongation of K11-linked ubiquitin chains by the anaphase-promoting complex. *Proc Natl Acad Sci U S A,* 107**,** 1355-60.

WYATT, D. W., FENG, W., CONLIN, M. P., YOUSEFZADEH, M. J., ROBERTS, S. A., MIECZKOWSKI, P., WOOD, R. D., GUPTA, G. P. & RAMSDEN, D. A. 2016. Essential Roles for Polymerase θ-Mediated End Joining in the Repair of Chromosome Breaks. *Mol Cell,* 63**,** 662-673.

XIA, Y., PADRE, R. C., DE MENDOZA, T. H., BOTTERO, V., TERGAONKAR, V. B. & VERMA, I. M. 2009. Phosphorylation of p53 by IkappaB kinase 2 promotes its degradation by beta-TrCP. *Proc Natl Acad Sci U S A,* 106**,** 2629-34.

XIAO, J., ZHANG, T., XU, D., WANG, H., CAI, Y., JIN, T., LIU, M., JIN, M., WU, K. & YUAN, J. 2015. FBXL20-mediated Vps34 ubiquitination as a p53 controlled checkpoint in regulating autophagy and receptor degradation. *Genes Dev,* 29**,** 184-96.

XING, W., BUSINO, L., HINDS, T. R., MARIONNI, S. T., SAIFEE, N. H., BUSH, M. F., PAGANO, M. & ZHENG, N. 2013. SCF(FBXL3) ubiquitin ligase targets cryptochromes at their cofactor pocket. *Nature,* 496**,** 64-8.

XU, J., ZHOU, W., YANG, F., CHEN, G., LI, H., ZHAO, Y., LIU, P., LI, H., TAN, M., XIONG, X. & SUN, Y. 2017. The β-TrCP-FBXW2-SKP2 axis regulates lung cancer cell growth with FBXW2 acting as a tumour suppressor. *Nat Commun,* 8**,** 14002.

XU, L., WEI, Y., REBOUL, J., VAGLIO, P., SHIN, T. H., VIDAL, M., ELLEDGE, S. J. & HARPER, J. W. 2003. BTB proteins are substrate-specific adaptors in an SCF-like modular ubiquitin ligase containing CUL-3. *Nature,* 425**,** 316-21.

XU, X., PAGE, J. L., SURTEES, J. A., LIU, H., LAGEDROST, S., LU, Y., BRONSON, R., ALANI, E., NIKITIN, A. Y. & WEISS, R. S. 2008. Broad overexpression of ribonucleotide reductase genes in mice specifically induces lung neoplasms. *Cancer Res,* 68**,** 2652-60.

YADA, M., HATAKEYAMA, S., KAMURA, T., NISHIYAMA, M., TSUNEMATSU, R., IMAKI, H., ISHIDA, N., OKUMURA, F., NAKAYAMA, K. & NAKAYAMA, K. I. 2004. Phosphorylation-dependent degradation of c-Myc is mediated by the F-box protein Fbw7. *Embo j,* 23**,** 2116-25.

YANG, F. & SUN, Y. 2019. FBXW2 suppresses proliferation and invasion of lung cancer cells by targeting SKP2 and β-catenin. *Mol Cell Oncol,* 6**,** 1607458.

YAO, F., ZHOU, Z., KIM, J., HANG, Q., XIAO, Z., TON, B. N., CHANG, L., LIU, N., ZENG, L., WANG, W., WANG, Y., ZHANG, P., HU, X., SU, X., LIANG, H., SUN, Y. & MA, L. 2018. SKP2- and OTUD1-regulated non-proteolytic ubiquitination of YAP promotes YAP nuclear localization and activity. *Nat Commun,* 9**,** 2269.

YAO, T. & COHEN, R. E. 2002. A cryptic protease couples deubiquitination and degradation by the proteasome. *Nature,* 419**,** 403-7.

YAU, R. & RAPE, M. 2016. The increasing complexity of the ubiquitin code. *Nat Cell Biol,* 18**,** 579-86.

YE, Y. & RAPE, M. 2009. Building ubiquitin chains: E2 enzymes at work. *Nature Reviews Molecular Cell Biology,* 10**,** 755.

YEH, K. H., KONDO, T., ZHENG, J., TSVETKOV, L. M., BLAIR, J. & ZHANG, H. 2001. The F-box protein SKP2 binds to the phosphorylated threonine 380 in cyclin E and regulates ubiquitin-dependent degradation of cyclin E. *Biochem Biophys Res Commun,* 281**,** 884-90.

YOO, N. J., KIM, H. R., KIM, Y. R., AN, C. H. & LEE, S. H. 2012. Somatic mutations of the KEAP1 gene in common solid cancers. *Histopathology,* 60**,** 943-52.

YU, H., PETERS, J. M., KING, R. W., PAGE, A. M., HIETER, P. & KIRSCHNER, M. W. 1998. Identification of a cullin homology region in a subunit of the anaphase-promoting complex. *Science,* 279**,** 1219-22.

YUAN, R., LIU, Q., SEGEREN, H. A., YUNIATI, L., GUARDAVACCARO, D., LEBBINK, R. J., WESTENDORP, B. & DE BRUIN, A. 2019. Cyclin F-dependent degradation of E2F7 is critical for DNA repair and G2-phase progression. *Embo j,* 38**,** e101430.

ZACHARIAE, W., SHEVCHENKO, A., ANDREWS, P. D., CIOSK, R., GALOVA, M., STARK, M. J., MANN, M. & NASMYTH, K. 1998. Mass spectrometric analysis of the anaphase-promoting complex from yeast: identification of a subunit related to cullins. *Science,* 279**,** 1216-9.

ZENGERLE, M., CHAN, K. H. & CIULLI, A. 2015. Selective Small Molecule Induced Degradation of the BET Bromodomain Protein BRD4. *ACS Chem Biol,* 10**,** 1770-7.

ZHANG, D. D., LO, S. C., CROSS, J. V., TEMPLETON, D. J. & HANNINK, M. 2004. Keap1 is a redox-regulated substrate adaptor protein for a Cul3-dependent ubiquitin ligase complex. *Mol Cell Biol,* 24**,** 10941-53.

ZHANG, N., LIU, J., DING, X., AIKHIONBARE, F., JIN, C. & YAO, X. 2007. FBXL5 interacts with p150Glued and regulates its ubiquitination. *Biochem Biophys Res Commun,* 359**,** 34-9.

ZHANG, S., CHEN, Q., LIU, Q., LI, Y., SUN, X., HONG, L., JI, S., LIU, C., GENG, J., ZHANG, W., LU, Z., YIN, Z. Y., ZENG, Y., LIN, K. H., WU, Q., LI, Q., NAKAYAMA, K., NAKAYAMA, K. I., DENG, X., JOHNSON, R. L., ZHU, L., GAO, D., CHEN, L. & ZHOU, D. 2017. Hippo Signaling Suppresses Cell Ploidy and Tumorigenesis through Skp2. *Cancer Cell,* 31**,** 669-684.e7.

ZHAO, B., LI, L., TUMANENG, K., WANG, C. Y. & GUAN, K. L. 2010. A coordinated phosphorylation by Lats and CK1 regulates YAP stability through SCF(beta-TRCP). *Genes Dev,* 24**,** 72-85.

ZHAO, L. & VOGT, P. K. 2008. Class I PI3K in oncogenic cellular transformation. *Oncogene,* 27**,** 5486-96.

ZHENG, H., SHEN, M., ZHA, Y. L., LI, W., WEI, Y., BLANCO, M. A., REN, G., ZHOU, T., STORZ, P., WANG, H. Y. & KANG, Y. 2014. PKD1 phosphorylation-dependent degradation of SNAIL by SCF-FBXO11 regulates epithelial-mesenchymal transition and metastasis. *Cancer Cell,* 26**,** 358-373.

ZHENG, N. & SHABEK, N. 2017. Ubiquitin Ligases: Structure, Function, and Regulation. *Annu Rev Biochem,* 86**,** 129-157.

ZHU, J., LI, K., DONG, L. & CHEN, Y. 2012. Role of FBXL20 in human colorectal adenocarcinoma. *Oncol Rep,* 28**,** 2290-8.

ZHU, Y., ZHOU, Q., ZHU, G., XING, Y., LI, S., REN, N., LIU, T., ZHU, A., BAI, Y. & PIAO, D. 2017. GSK-3β phosphorylation-dependent degradation of ZNF281 by β-TrCP2 suppresses colorectal cancer progression. *Oncotarget,* 8**,** 88599-88612.

ZOU, S., MA, C., YANG, F., XU, X., JIA, J. & LIU, Z. 2018. FBXO31 Suppresses Gastric Cancer EMT by Targeting Snail1 for Proteasomal Degradation. *Mol Cancer Res,* 16**,** 286-295.

ZOU, Y., MI, J., CUI, J., LU, D., ZHANG, X., GUO, C., GAO, G., LIU, Q., CHEN, B., SHAO, C. & GONG, Y. 2009. Characterization of nuclear localization signal in the N terminus of CUL4B and its essential role in cyclin E degradation and cell cycle progression. *J Biol Chem,* 284**,** 33320-32.